The molecular and cellular basis of antigen recognition by unconventional T cells

Michael Nicholas Tod Souter

Submitted in total fulfilment of the requirements of the degree of

Doctor of Philosophy

June 2020

Department of Microbiology and Immunology

The University of Melbourne

Abstract

Unconventional T cells are evolutionarily conserved populations of T cells, many of which recognise non-peptide antigens in the context of monomorphic antigen presentation molecules related to the major histocompatibility complex (MHC). These MHC related molecules, known as CD1 and MR1 present lipid and small metabolite antigens respectively.

Mucosal-associated invariant T (MAIT) cells are a subset of unconventional T cells that are highly abundant in humans and recognise the potent riboflavin biosynthesis derived metabolite 5-OP-RU presented by MR1. The majority of MAIT cells in the peripheral blood of humans express the CD8 co-receptor, a molecule also expressed by other T cells that contributes to antigen recognition and T cell activation. In contrast to other T cells, a role for CD8 on MAIT cells has not been formally tested. The first chapter of results in this thesis examines whether CD8 is able to bind MR1, and if CD8 is important for the activation of MAIT cells and other MR1-reactive T cells. The data revealed that CD8 binds directly to MR1, in a manner concordant with MHC class I, and that this interaction is important for the functional response of MAIT cells. Specifically, both isoforms of CD8 (CD8αα and CD8αβ) bound to MR1 tetramers and the CD8-MR1 interaction could be abrogated by mutating MR1 in the putative CD8 binding site. The effects of the CD8-MR1 interaction were examined on primary MAIT cells, where MR1 tetramers bound more strongly to $CD8^+$ compared $CD8^-$ MAIT cell subsets. Importantly, mutating MR1 tetramers reduced $CD8^+$ MAIT cell engagement to $CD8^-$ MAIT cell levels. To determine the effect of the CD8-MR1 interaction on function, primary MAIT cells were activated in the presence of wild type or mutant MR1. In line with the importance of CD8 on MR1 recognition, the cytokine secretion by $CD8^+$ MAIT cells was decreased in the absence of CD8 binding to MR1. Furthermore, the data here establishes that CD8 is vital for the recognition of MR1 presenting less potent, lower affinity antigens such as folate derivatives. Similarly, low affinity MR1-antigen recognition and cytokine secretion by other MR1-reactive T cells was completely abrogated in the absence of CD8 binding. Thus, CD8 is an important co-receptor for the function of MAIT cells and may expand the diversity of ligands recognised by MAIT and other MR1-reactive T cells.

CD1b-restricted T cells are a subset of unconventional T cells in humans that recognise lipid antigens derived from endogenous and microbial sources that are presented by CD1b. Comparatively little is known about the biology of CD1b-restricted T cells, particularly autoreactive CD1b-restricted T cells that recognise endogenous lipid antigens such as phospholipids. The second chapter of results examines autoreactive TCR recognition of CD1b, including the breadth of permissive endogenous lipid antigens that are bound by mammalian CD1b. Autoreactive CD1b-restricted T cells were identified from healthy blood donors using CD1b tetramers presenting heterogeneous mammalian lipids and the autoreactive T cells expressed distinct T cell receptors (TCRs) which were cloned to generate autoreactive T cell lines. Different CD1b restricted T cell lines exhibited altered staining reactivity with CD1b tetramers loaded with different mammalian phospholipid antigens and strikingly, some autoreactive T cell lines recognised CD1b in an antigen independent manner. An activation assay using the autoreactive T cell lines cocultured with a series of mutant CD1b expressing cell lines revealed several CD1b binding 'hotspots' along the α1 and α2 helices that were critical for TCR-mediated activation. Using soluble proteins, autoreactive TCR permissive ligands were isolated from mammalian CD1b by separating ternary TCR-CD1b-lipid complexes from binary CD1b-lipid complexes that did not bind to the TCR using size-exclusion chromatography. Mass spectra analysis of the fractionated proteins revealed an abundance of phospholipids, particularly phosphatidylcholine as permissive CD1b lipid antigens. These data suggest autoreactive TCR antigen-specificity is more diverse than previously described and that these TCRs may adopt novel docking modes onto CD1b to recognise distinct endogenous antigens.

In the final chapter of results, the phenotype and functional characteristics of *M. tuberculosis*-reactive CD1b-restricted T cells was investigated. Glucose monomycolate (GMM) is a cell wall lipid expressed by pathogenic *Mycobacteria*, including *M. tuberculosis*, that is presented by CD1b to T cells. GMM-reactive T cells were first isolated directly *ex vivo* from the peripheral blood of latent *M. tuberculosis* infected donors using CD1b tetramers. Herein, an optimised CD1b tetramer enrichment was developed to isolate very small frequencies of GMM-reactive T cells from healthy donor

blood directly *ex vivo*. In contrast to *M. tuberculosis* infected patients, GMM-reactive T cells from healthy donors expressed a diverse TCR repertoire. GMM-reactive T cells were exclusively $CD4^{+}CD8^{-}$ and most cells expressed the memory marker CD45RO. Similar to other unconventional T cells, GMM-reactive T cells from healthy donors expressed the transcription factor promyelocytic leukaemia zinc finger (PLZF). *In vitro* stimulation revealed GMM-reactive T cells secrete both TNF and IFNγ, similar to MAIT cells. To characterise these cells further, single-cell transcriptomic analysis was performed on GMM-reactive T cells isolated using CD1b-GMM tetramers. GMM-reactive T cell expressed unique transcriptomic signatures that were accurately distinguishable from the transcriptomes of natural killer T (NKT) cells and $CD4^{+}$ T cells, indicating that these cells may be functionally distinct from other unconventional and conventional T cells populations.

In summary, these data describe a role for the CD8 co-receptor on MAIT and other MR1-reactive T cells and expand on the limited knowledge of CD1b-restricted T cells in healthy blood in regard to TCR repertoire, antigen-specificity and phenotype.

Declaration

This is to certify that:

1. This thesis comprises only my original work towards the PhD except where indicated in the preface
2. Due acknowledgment has been made in the text to all other material used
3. This thesis is less than 100,000 words in length, exclusive of tables, references and appendices

Michael Nicholas Tod Souter

Preface

In accordance with the regulations of the University of Melbourne, I acknowledge that components of the work presented in this thesis were collaborative (percentages refer to the contribution to the thesis overall):

Chapter 3

Shihan Li and Scott Reddiex generated the β_2m deficient SKW-3 cell line (0.5%).

Chapter 4

Shihan Li generated the β_2m deficient Jurkat-76 cell line (0.5%). Fiona Ross isolated and TCR sequenced the donor 1 and donor 4 autoreactive CD1b-restricted T cells (3%). Adam Uldrich performed SPR experiments for 1.27 and NKT15 TCRs with CD1b-endo and CD1d-αGalCer (0.5%). Adam Shahine and Jamie Rossjohn performed X-ray crystallography experiments of prepared 1.27 TCR/CD1b-endo co-complex (0.5%). Tan-Yun Cheng and D. Branch Moody performed mass spectrometry and lipid discovery of prepared 1.27 TCR and 4.17 TCR co-complexes with CD1b-endo (2%).

Chapter 5

Scott Reddiex performed some of the RNA processing and library preparation for RNA sequencing (0.5%). Willem Van Der Byl and Fabio Luciani performed RNA sequencing analysis for GMM-reactive, NKT and $CD4^+$ T cells (2%).

Acknowledgements

Firstly, I'd like to thank my primary supervisor Dr. Daniel Pellicci, who recruited me straight out of Honours to do a PhD with him as part of the Godfrey laboratory. From the very beginning Dan made me feel worthy and instilled in me the confidence to develop as an independent thinker and scientist. Dan has always made time for me both professionally and personally and continues to look out for my best interests. Dan was there when I needed him the most, and I can say with certainty that I wouldn't have made it the end of this journey without his valuable mentorship and friendship. Thanks to my co-supervisor Dr. Sidonia Eckle, who was my Honours supervisor initially, and had the difficult task of teaching me all the fundamentals of lab work. Most of the science skills I have today are a result of Sidonia's dedication and careful teachings that I regard as second to none. Sidonia inspired me in that first year and confirmed my choice to pursue a life in science and for that I am forever grateful. Thank you to my co-supervisor Prof. Jim McCluskey, I remember for about the first six months of lab meetings being stunned by how efficiently and with such clarity Jim could summarise any body of work and direct the discussion to the most important questions. Eventually this is something you get used to, yet is no less impressive. I am grateful for all of Jim's scientific insights and direction with my studies. Thank you to my co-supervisor Prof. Dale Godfrey, whose lab has been home to me over these past years. Dale has constructed a truly world-class team around him and a lab that runs seemingly with ease, which is no small feat. Studying in Dale's lab has been a privilege and has provided me with many opportunities to learn that I do not take for granted. I am also appreciative to Dale for his keen eye and scepticism which are highly respected traits in science.

Thanks to my PhD supervisory committee, Prof. Andrew Brooks, Dr. Melissa Call and Dr. Lars Kjer-Nielsen for their guidance. Thanks to the many external collaborators; Prof. Jamie Rossjohn, Dr. Jérôme Le Nours and Dr. Adam Shahine at Monash University, Prof. Branch Moody, A/Prof. Ildiko Van Rhijn, Dr. Tan-Yun Cheng and Dr. Peter Reinink at Harvard University and Universiteit Utrecht and Prof. George Lovrecz at CSIRO for all of their contributions and guidance. Thank you to the Brooks, Doherty, Wakim, Purcell and Mackay labs and others for their generous lending of reagents and assistance. Thank you to all members past and present of the Godfrey and McCluskey labs who have

contributed immensely to my work and life during the last few years. Special thanks to Bronwyn, Troi, Huimeng, Zhe, John, Zheng, Marc, Chris, Sergio, Marcela and Tian for all of their help and friendship in the lab. Special thanks to Dr. Adam Uldrich for his expertise and assistance with all my troubleshooting queries, Adam is truly the fountain of knowledge. Special thanks to Dr. Zhenjun Chen for all of his guidance and technical assistance. A huge thank you to my close friend and lab contemporary, Tony. A shared passion for science resulting in long working hours together in the lab made our friendship almost inevitable. Tony was always there to support me during the highs and lows of PhD student life, involving countless hours of scientific debate, experimental planning and encouragement during the tough times. Tony is a great scientific thinker and true friend. Thanks to many, many others in the department and institute for their friendship, support, drinks and all-round good times. Special thanks to Fernando, for his friendship, salsa dancing lessons and collegial spirit. Thanks to my 'outside' friends, who have been so understanding and helpful in reminding me put things into perspective once in a while. A big thank you to my parents Marietta and Miles, who have always put me first in life, loved me unconditionally and instilled in me the importance of education and life-long learning. Finally, a big thank you to my girlfriend Kat. Where have you been my entire life? Kat is rarer than one in the theoretical number of unique TCR arrangements possible in a developing thymocyte. In other words, I am beyond lucky that I get to share my life with someone as wonderful as you. Thank you, Kat, for putting up with me throughout my PhD and supporting me always.

List of Abbreviations

αGalCer	α-galactosylceramide
β_2m	β_2-microglobulin
5-A-RU	5-amino-6-D-ribitylaminouracil
5-OE-RU	5-(2-oxoethylideneamino)-6-D-ribitylaminouracil
5-OP-RU	5-(2-oxopropylideneamino)-6-D-ribitylaminouracil
6-FP	6-formylpterin
Ac-6-FP	Acetyl-6-formylpterin
Ag	Antigen
APC	Antigen presenting cell
BCG	Bacillus Calmette–Guérin
BCR	B cell receptor
BSA	Bovine serum albumin/buried surface area
CD	Cluster of differentiation
CTAB	Hexadecyltrimethylammonium bromide
cDNA	Complementary deoxyribonucleic acid
CDR	Complementarity determining region
CLA	Cutaneous lymphocyte antigen
CLIP	Class II-associated invariant chain peptide
CPM	Connecting peptide motif
CTL	Cytotoxic T lymphocyte
DAMP	Danger associated molecular pattern
DC	Dendritic cell
DDM	Dideoxymycobactin
DEAE	Diethylaminoethanol

DN	Double negative
DNA	Deoxyribonucleic acid
DP	Double positive
DTT	Dithiothreitol
EAE	Experimental autoimmune encephalomyelitis
ELISA	Enzyme-linked immunosorbent assay
ER	Endoplasmic reticulum
FACS	Fluorescence activated cell sorter/ing
FCS	Fetal calf serum
FPLC	Fast protein liquid chromatography
G	Glyoxal
GEM	Germline-encoded mycoyl
GFP	Green fluorescent protein
GM1	Monosialotetrahexosylganglioside
GM-CSF	Granulocyte macrophage colony-stimulating factor
GMM	Glucose monomycolate
GNTI	N-acetyl-glucosaminyltransferase I
GroMM	Glycerol monomycolate
HEK	Human embryonic kidney
HIV	Human immunodeficiency virus
HLA	Human leukocyte antigen
HPLC	High performance liquid chromatography
HRP	Horseradish peroxidase

IBP	Inclusion body preparation
IEL	Intra-epithelial lymphocyte
IFN	Interferon
IL	Interleukin
IPTG	Isopropyl β-D-1-thiogalactopyranoside
IS	Immunological synapse
LAM	Lipoarabinomannan
LB	Luria broth
li	MHC-II associated invariant chain
LPA	Lysophosphatidic acid
LPC	Lysophosphatidylcholine
LPE	Lysophosphatidylethanolamine
LTBI	Latent tuberculosis infection
MA	Mycolic acid
MAIT	Mucosal-associated invariant T cell
MFI	Mean fluorescence intensity
MHC	Major histocompatibility complex
MG	Methylglyoxal
MoDC	Monocyte-derived dendritic cell
MS	Mass spectrometry/multiple sclerosis
mRNA	Messenger ribonucleic acid
NK	Natural killer
NKT	Natural killer T

MR1	MHC-I like related protein 1
PA	Phosphatidic acid
PAGE	Polyacrylamide gel electrophoresis
PAMP	Pathogen associated molecular pattern
PBMC	Peripheral blood mononuclear cell
PBS	Phosphate buffered saline
PBS-T	Phosphate-buffered saline tween-20
PC	Phosphatidylcholine
PCA	Principle component analysis
PCR	Polymerase chain reaction
PE	Phosphatidylethanolamine
PG	Phosphatidylglycerol
PI	Phosphatidylinositol
PIM	Phosphatidylmyo-inositol mannoside
PLA	Phospholipase A
PLC	Peptide loading complex
PMA	Phorbol 12-myristate 13-acetate
PS	Phosphatidylserine
RNA	Ribonucleic acid
SAv	Streptavidin
SDS	Sodium dodecyl sulfate
SGL	Sulfoglycolipid
SM	Sphingomyelin

SP	Single positive
SPR	Surface plasmon resonance
TAP	Transporter associated with antigen processing
TBS	Tris-buffered saline
TCR	T cell receptor
TGF-β	Transforming growth factor β
Th	T helper
TL	Thymic leukemia antigen
TNF	Tumour necrosis factor
UV	Ultraviolet
WT	Wild type

List of publications

Michael NT Souter, Sidonia BG Eckle. Biased MAIT TCR usage poised for limited antigen diversity? Frontiers in Immunology. 2020 Jul; Accepted.

Michael NT Souter*, Liyen Loh*, Shihan Li, Bronwyn S Meehan, Jamie Rossjohn, David P Fairlie, Katherine Kedzierska, Daniel G Pellicci, Zhenjun Chen, Lars Kjer-Nielsen, Alexandra J Corbett, James McCluskey, Sidonia BG Eckle. Characterisation of Human MAIT cells (Mucosal Associated Invariant T cells). Current Protocols in Immunology. 2019 Sep;127(1)e90.

Marcela de Lima Moreira*, **Michael NT Souter***, Liyen Loh, James McCluskey, Daniel G Pellicci, Sidonia BG Eckle. Hypersensitivities following allergen antigen recognition by unconventional T cells. Allergy: European Journal of Allergy & Clinical Immunology. 2020 Mar;00:1-14.

Peter Reinink, **Michael NT Souter**, Tan-Yun Cheng, Tamara van Gorkom, Stefanie Lenz, Joanna Kubler-Kielb, Klemen Strle, Kristin Kremer, Steven FT Thijsen, Allen C Steere, Dale I Godfrey, Daniel G Pellicci, D Branch Moody, Ildiko Van Rhijn. CD1b presents self and Borrelia burgdorferi diacylglycerols to human T cells. European Journal of Immunology. 2019 Mar;47:737-746, 2019.

Nicholas A Gherardin, **Michael NT Souter**, Hui-Fern Koay, Kirstie M Mangas, Torsten Seemann, Timothy P Stinear, Sidonia BG Eckle, Stuart P Berzins, Yves d'Udekem, Igor E Konstantinov, David P Fairlie, David S Ritchie, Paul J Neeson, Daniel G Pellicci, Adam P Uldrich, James McCluskey, Dale I Godfrey. Human blood MAIT cell subsets defined using MR1 tetramers. Immunology and Cell Biology. 2018 May;96(5):507-525, 2018.

Jérôme Le Nours*, Nicholas A Gherardin*, Sri H Ramarathinam, Wael Awad, Florian Wiede, Benjamin S Gully, Yogesh Khandokar, T Praveena, Jacinta M Wubben, Jarrod J Sandow, Andrew I Webb, Anouk Von Borstel, Michael T Rice, Sam Redmond, Rebecca Seneviratna, Maria L Sandoval-Romero, Shihan Li, **Michael NT Souter**, Sidonia BG Eckle, Alexandra J Corbett, Hugh H Reid, Ligong Liu, David P Fairlie, Edward M Giles, Glen P Westall, Richard W Tothill, Martin Davey, Richard Berry, Tony Tiganis, James McCluskey, Daniel G. Pellicci, Anthony W Purcell, Adam P Uldrich, Dale I Godfrey#, Jamie Rossjohn#. T cell receptor recognition on the underside of an antigen-presenting molecule. Science. 2019 Dec;366(6472):1522-1527.

Charlotte A James, KQ Krystle, Martine Gilleron, Jacques Prandi, Vijayendar R Yedulla, Zuzanna Z Moleda, Eleonora Diamanti, Momin Khan, Varinder K Aggarwal, Josephine F Reijneveld, Peter Reinink, Stefanie Lenz, Ryan O Emerson, Thomas J Scriba, **Michael NT Souter**, Dale I Godfrey, Daniel G Pellicci, D Branch Moody, Adriaan J Minnaard, Chetan Seshadri, Ildiko Van Rhijn. CD1b Tetramers Identify T Cells that Recognize Natural and Synthetic Diacylated Sulfoglycolipids from Mycobacterium tuberculosis. Cell Chemical Biology. 2018 Apr;25(4):392-402.

*Denotes equal first authors.
#Denotes equal last authors.

Table of Contents

Chapter 1: Literature review

1.1 Introduction

The role of the immune system is to protect the host from disease-causing agents that it may encounter throughout life. This is achieved by detection and elimination of these agents derived both from outside the body as well as agents that arise within the body. These include microbial infections (bacteria, viruses, fungus and parasites), maintaining tolerance to commensal microflora and preventing cells from becoming cancerous (1). In some cases, the immune system becomes mistakenly directed against 'self', referred to as autoimmunity. This process involves immune detection and destruction of host tissue and can manifest from mild to severe diseases depending on the tissues targeted and the immune cells involved. In rare cases, individuals are born with or acquire deficiencies in their immune system that prevent it from functioning properly, often leading to death (1). Thus, the immune system is critically important to the host, maintaining homeostasis within the body and protecting it from disease-causing agents.

The immune system encompasses a broad range of cell types that coordinate to protect the body from disease and maintain homeostasis. It utilises an array of molecular and cellular mechanisms that are segregated by either a rapid or delayed immune response, referred to as the innate or adaptive immunity respectively (1). The innate immune system offers protection from disease in a largely non-specific manner; anatomical barriers such as the outer layers of the skin and various mucous membranes physically prevent the entry of microbes into the body. At the cellular level, a wide range of immune cells that circulate within the blood, including neutrophils, basophils, eosinophils and mast cells, referred to collectively as granulocytes, release chemicals that directly kill or inhibit microbe function and promote inflammation (1). Macrophages and Natural killer (NK) cells are drawn to sites of inflammation where they are involved in directly engulfing microbes and killing infected host cells, respectively (1). Importantly, innate immune cells respond to infection fast and are triggered by recognition of conserved pathogen and danger associated signals, referred to as pathogen associated molecular patterns (PAMPs)

and danger associated molecular patterns (DAMPs) (1). The innate arm of the immune system is able to clear some infections; however, pathogens are often not controlled by innate immunity alone and a more targeted immune response tailored to the infecting pathogen is required (1).

Clearance of pathogens that are not controlled by the innate immune arm is achieved by the adaptive immune system. A cardinal feature of adaptive immunity is the ability for immune cells to recognise pathogens in a highly specific manner. The adaptive immune response is separated into two arms referred to as the humoral and cellular immune responses. These defined immune roles are mediated by two specialised immune cells known collectively as lymphocytes (1).

The humoral immune response is mediated by B lymphocytes (B cells). B cells originate in the bone marrow, however after development, egress to lymphoid organs such as the spleen and lymph nodes, where they reside in waiting to detect infection (1). B cells utilise a highly specialised receptor known as the B cell receptor (BCR) to detect antigen derived from the periphery that drains to the lymphoid organs via the lymphatic system. The BCR is capable of recognising antigen composed of polysaccharides, nucleic acids, and intact or fragmented proteins known as peptides (1). The genes that encode the BCR rearrange during development and enable a theoretical 5×10^{13} (2) of unique BCRs to form, referred to as somatic recombination. Recombination of the BCR causes each B cell to acquire a unique and high specificity for antigen, collectively allowing an individual's pool of B cells to recognise any pathogen-derived antigen that they may encounter throughout life. Upon recognition of their cognate antigen B cells become activated and undergo several stages of differentiation that ultimately lead to the production of soluble BCRs and derivatives, known as antibodies that are directed specifically against the stimulatory antigen (1). Specific to B cells, BCR gene recombination can continue throughout the course of the immune response, leading to an improved antibody response by enhancing the BCR affinity for antigen known as affinity maturation (3). Secreted antibodies are transported through the blood to the periphery where they bind to and directly neutralise pathogens as well as tag pathogens for destruction by other cells via a process known as opsonisation (1).

The cellular immune response is mediated by T lymphocytes (T cells). Similar to B cells, T cells utilize a specialised receptor known as the T cell receptor (TCR) to survey the body for disease (1). The TCR recognises foreign molecules known as antigens, presented by antigen presenting cells (1). Each T cell acquires a unique specificity for antigen during development when the genes that encode the TCR undergo recombination in the thymus (4). Upon recognition of antigen by the TCR, T cells proliferate and undergo specific genetic programs to enable potent effector functions that are exceedingly efficient in controlling or terminating pathogenic disease (1). Most antigen inexperienced T cells, formally known as naïve T cells, require a preparation phase of several days before becoming potent effector T cells, a consequence of generating a specific immune response and largely a defining feature of T cell immunity (1). Upon resolution of infection, the majority of the clonally expanded T cell responders, known as effector T cells, are deleted through a process of programmed cell death known as apoptosis (1). A small (~10%) pool of memory T cells persist that offer prolonged and enhanced protection against pathogen reinfection (5).

1.1.1 MHC restriction

The connection between T cell antigen recognition and the polymorphic molecules known as the major histocompatibility complex (MHC) was first demonstrated by Zinkernagel and Doherty (6). Their elegant series of experiments in the 1970s revealed that T cells from a host were only capable of recognising virus-infected cells from another host if the two shared at least one set of syngeneic MHC (7). This phenomenon was termed MHC restriction and was a major breakthrough in immunology. Later discoveries revealed that the TCR recognised a peptide antigen presented in the cleft on the MHC molecules, formally demonstrating the TCR was capable of recognising an ‘altered self’ (8-10). Although the genes within the MHC locus had been subdivided into regions I, II and III, only the proteins encoded by region I and II, known as MHC-I and -II were responsible for presenting antigen, thus T cells were segregated by their recognition of antigen in the context of these molecules (11).

1.1.2 MHC-I

The MHC-I molecule is composed of a polymorphic heavy chain (H), monomorphic light chain β_2-microglobulin (β_2m) and a short peptide that associates with the H-chain to form a ternary complex (12). The MHC-I-H itself, consists of a single polypeptide organised into three extracellular domains termed α1, α2 and α3 and is anchored into the cell membrane via a transmembrane domain and cytoplasmic tail (13). Upon synthesis in the endoplasmic reticulum (ER), the MHC-I-H preferentially forms a heterodimer by associating with the single domain β_2m, improving the stability of the MHC-I molecule and altering the conformation of the peptide-binding cleft between the α-helical α1 and α2 domains to accommodate peptide loading (13). Peptides that are destined for display on MHC-I are transported from the cytosol to the ER via the transporter associated with antigen processing (TAP), a membrane-bound heterodimer of TAP1/TAP2 that preferentially selects peptides of optimal length (8-16 amino acids) for entry into the ER (14). Once in the ER, peptide loading into MHC-I is facilitated by chaperone proteins calreticulin, tapasin and ERp57, known collectively with TAP and MHC-I as the peptide loading complex (PLC) (14). Upon successful loading of peptide, the PLC disengage and the MHC-I ternary complex (pMHC-I) traffics from the ER, through the Golgi via the secretory pathway to the cell surface (15). The cell surface bound pMHC-I can be subsequently internalised from the membrane for destruction (16). This cycle of antigen capture and presentation is unique to MHC-I and occurs constitutively in all nucleated healthy cells, enabling self- or exogenously-derived protein antigens within the cytosol to become available for survey by patrolling MHC-I-restricted T cells (17). An understanding of the structural features of MHC-I proteins has enabled the generation of soluble MHC-I multivalent complexes (MHC-I tetramers) that are used for the identification of antigen specific T cells with a high precision (18).

1.1.3 MHC-II

The MHC-II molecule is a noncovalent complex composed of two polymorphic polypeptide chains (α-chain and β-chain) that are anchored into the cell membrane via transmembrane domains and cytoplasmic tails {Jardetzky, 1994 #597}. Both the α- and β-chains contribute to the formation of the peptide-binding cleft {Jardetzky, 1994 #597}. Unlike MHC-I, which is loaded with peptides that originate from the cytosol, newly

synthesised MHC-II complexes are protected from binding peptides in the ER by the MHC-II associated invariant chain (Ii), that contains a short peptide sequence known as the class II-associated invariant chain peptide (CLIP) which blocks the peptide binding cleft {Villadangos, 2001 #596}. Immature MHC-II-Ii complexes migrate from the ER to vesicles that fuse with acidified endosomes containing extracellular sampled peptides. Cleavage and dissociation of Ii and CLIP, involving other chaperones, enables the association of MHC-II molecules with extracellular peptide antigens {Villadangos, 2001 #596}. These MHC-II-antigen complexes traffic to the cell surface, thus enabling MHC-II-restricted T cells to survey extracellular derived peptides {Villadangos, 2001 #596}. Importantly, MHC-II presentation is restricted mostly to professional APCs that are efficient at internalising extracellular debris such as DCs, B cells and macrophages {Kambayashi, 2014 #595}.

1.1.4 MHC-I related molecules

In humans and other mammals, a number of antigen presentation molecules exist that resemble MHC-I in sequence and structural homology and arose from genomic duplications of the classical MHC-I (MHC-Ia) (19). They are known as MHC-Ib and MHC-I-like molecules. Identified using anti-human monoclonal antibody, the MHC-I-like molecule CD1a was the first of a family of monomorphic antigen presentation molecules known as CD1 molecules to be discovered (20). Unlike MHC-I and -II, which are polymorphic in nature and can thus vary significantly from one individual to the next, CD1 molecules are largely monomorphic. Further CD1 molecules; CD1b, CD1c, CD1d and CD1e were later identified in humans, however only the ortholog for CD1d is present in mice (21). Like MHC-I, the CD1a-d molecules each consist of the α1-α2-α3 domain polypeptide heavy chain that associates with β_2m and adopts a similar fold as MHC-I molecules, to reveal a cleft between the α1 and α2 helices suitable for antigen presentation (21). Whereas MHC-I provides a constrained, anchored fit for the binding of short peptides that traverse the cleft, CD1 molecules possess a cleft of a greater overall volume with a narrower solvent exposed opening, protecting several hydrophobic channels that are burrowed deep into the molecule, suitable for accommodating the alkyl chains of lipid antigens (22, 23). The cleft of CD1b is the largest by volume, with ~2200Å and consisting of four channels including analogous to MHC A' and F' pockets, a C' channel and a

connecting T' tunnel, providing additional space for presenting lipids with extremely long fatty acid tails (24). Importantly, the unique structural configuration of each CD1 cleft facilitates the capture and presentation of distinct lipid antigens (25, 26).

Similar to MHC-I, the CD1 molecules are synthesized in the ER, where they associate with β_2m and are loaded with endogenous lipids, however upon reaching the cell surface, structural motifs in the cytoplasmic tail of each molecule trigger internalisation and trafficking of CD1 to endosomal vesicles (27). Upon fusion with vesicles, self-lipids in the cleft can be exchanged for lipids sampled from extracellular sources and are returned to the cell surface (28). Each of the CD1 molecules are directed to different endosomal compartments upon internalisation, enabling the capture of unique lipid species (29). For instance, the signalling domain of CD1b binds to the adaptor protein complexes 2 and 3 (AP-2 and AP-3), transporting CD1b specifically to lysosomes where the low pH environment allows for the exchange of lipids in the cleft (30, 31). In addition, several lipid antigens have been identified that are capable of directly loading CD1 molecules at the cell surface (32). In contrast to the other CD1 molecules, CD1e does not present antigen or traffic to the cell surface, instead remaining in the lysosome where a soluble form (sCD1e) acts as a chaperone of extracellular derived lipids for processing and loading into CD1b and CD1c molecules (33). While MHC-I is expressed ubiquitously on all nucleated cells, CD1a-c molecules are resigned to expression on specialised cell populations, similar to MHC-II, however they can be upregulated on other cell types in response to stimulation (34). CD1a is most abundant on Langerhans cells, CD1b and CD1c molecules are expressed mostly on dendritic cells (DCs), CD1c on B cells and all CD1 molecules are expressed on developing thymocytes and sparingly on mature T cells (35, 36). CD1d expression is more pervasive, including many of the specialised cell populations noted above, as well as non-haemopoietic cells such as epithelial cells of the gastrointestinal tract (37), on hepatocytes, keratinocytes and many tissues of the organs such as the kidney, pancreas, breast and conjunctiva of the eye (38).

In addition to the CD1 family, another MHC-I-like molecule was identified in humans by the high sequence homology to the MHC-I (40-50%) and was named the MHC-I related protein 1 (MR1) (39). In a series of crucial experiments, MR1 protein was refolded in the

presence of candidate antigens in an attempt to isolate MR1-antigen (Ag) complex. This approach led to the serendipitous discovery of a novel class of antigens, vitamin B metabolites, as well as defined the structural architecture of MR1 (40). In contrast to the members of the CD1 family, the MR1 antigen binding cleft more closely resembles that of MHC-I. However, while MR1 retains a solvent exposed cleft, it is composed of a mixture of charged, hydrophobic and bulky residues that render it unsuitable for accommodating peptide antigens (40).

Although most cells can express MR1, the amount of MR1 that reaches the cell surface is tightly regulated and expression of cell surface MR1is typically low (41, 42). Recently, key details regarding MR1 trafficking within the cells have been elucidated. The MR1 heavy chain (MR1-H) is synthesised and accumulates in the ER where it remains quiescent in a partially unfolded state, free of β_2m. Only after the MR1-H covalently binds to antigen, it associates with β_2m and efficiently traffics to the cell surface (43). Within one hour of reaching the cell surface, MR1 internalisation begins, where most molecules are degraded, although a small fraction can be recycled to the cell surface (43).

1.1.5 Non-peptide antigens

T cell recognition of antigens presented by CD1 and MR1 is a burgeoning field, as the breadth of antigens that can be presented by these molecules remains elusive. The variation in cleft architecture of the CD1 molecules promotes the presentation of different types of lipid-based antigens derived from both self and bacterial sources. Notably, CD1a has the smallest cleft and shallow pockets and is capable of presenting glycolipids, as well as 'headless' lipids and lipo-peptides (44).

Of particular interest is CD1a-restricted T cell recognition of the microbial antigen dideoxymycobactin (DDM). DDM is a lipo-peptide derived from *Mycobacterium tuberculosis* (*M. tuberculosis*) and consists of a single 20 carbon alkyl chain, acetylated to a central lysine within a peptide backbone, terminating at either end with a cyclic moiety (45, 46). The structure of CD1a bound to a DDM-like analogue reveals how lipo-peptides are accommodated in the cleft, where the single alkyl chain is buried within the A' channel while the peptide backbone folds within the shallow F' pocket, making the

terminal cyclic moieties available for T cell recognition (47). Another *M. tuberculosis* lipid antigen, glucose monomycolate (GMM), is presented by CD1b (48, 49). Unlike DDM, GMM is a glycolipid composed of a sugar head group attached to dual branching alkyl chains, one of which contains more than 50 carbons that burrow into the A' channel, snaking through the T' tunnel and out the F' channel to occupy the entire CD1b cleft, while the other alkyl chain occupies the C' channel (50). Successful stimulation of T cells using a shorter alkyl chain variant of GMM (C:32), highlights a degree of flexibility in putative alkyl chain length as well as the likely dominance of the solvent exposed head group in TCR recognition (51), a property that is consistent with many CD1 antigens. Accordingly, the study of T cells that recognise *M. tuberculosis* derived lipid antigens will provide important insight into the recognition of lipid antigens, the function of these cells and the role they play in the context of *M. tuberculosis* infection.

A range of endogenous lipids have been identified that occupy the cleft of CD1 molecules (52). They include phospholipids such as phosphatidylglcerol (PG) and lysophosphatidylcholine (LPC), as well as triglycerides and even 'headless' wax esters such as squalene (45, 52). While these studies are very limited, phospholipid-reactive T cells have been identified using high order CD1b multimers loaded with PG. Interestingly, these T cells are capable of recognising CD1b-multimers loaded with numerous other phospholipid antigens, indicating a niche in the periphery for T cells that recognize self-lipids with broad reactivity to related antigens (52). Other lipids such as sulfatide, a galactosylceramide sulfate ester, which is a self-lipid, has been shown to bind all antigen presenting CD1 molecules (25, 53). T cell reactivity to sulfatide was initially observed in peripheral blood from multiple sclerosis (MS) patients (54), however these cells have been identified at a lower frequency in healthy donors (53). The recognition of sulfatide demonstrates the possibility for CD1-restricted T cell involvement in autoimmune disease and reveals how a single antigen is capable of stimulating multiple T cells via a conserved antigenic determinant in the context of different CD1 architectures. It is currently unclear why self-lipid reactive T cells exist in the human immune system and how they are regulated to prevent destruction of self-tissues.

A decade after its discovery, MR1 was acknowledged as the restriction element for an evolutionarily conserved T cell population known as mucosal-associated invariant T (MAIT) cells (39, 55, 56). Antimicrobial function was later shown by the activation of MAIT cells using a range of different bacteria- and yeast-infected APCs (57). Refolding of candidate antigens with MR1, including cell culture medium as a control, led to the generation of the first MR1-Ag structural complex (40). Mass spectrometry of MR1-Ag complexes identified 6-formylpterin (6-FP), a photodegradation product of folic acid (vitamin B9) (**Fig. 1.1**), as the antigen presented in the cleft of MR1 (40). This small bicyclic molecule was shown to sit in the A' pocket of MR1, where it formed a Schiff base with a lysine residue (K43) on the base of the α1 helix of MR1 and was surrounded by an aromatic cradle of residues that protected it from solvent exposure (40). Thus, a new class of antigens had been discovered that could bind MR1, although 6-FP and a later discovered synthetic derivative acetyl-6-formylpterin (Ac-6-FP) (**Fig. 1.1**) (58) proved not to be stimulatory to MAIT cells.

In the same study, stimulatory antigens were isolated from *Salmonella enterica* Typhimurium supernatant and suspected to be derived from the riboflavin (vitamin B2) biosynthesis pathway (40). Manipulation of the genes controlling riboflavin biosynthesis in a *Lactococcus* strain and *S. enteria* Typhimurium revealed the existence of a previously predicted intermediary step in the production of riboflavin (59, 60). It was shown that non-enzymatically driven condensation of the riboflavin precursor 5-Amino-6-D-ribitylaminouracil (5-A-RU), by glyoxal (G) and methylglyoxal (MG), produced two unstable monocylic pyrimidine adducts; 5-(2-oxoethylideneamino)-6-D-ribitylaminouracil (5-OE-RU) and 5-(2-oxopropylideneamino)-6-D-ribitylaminouracil (5-OP-RU) respectively (**Fig. 1.1**) (61). These intermediary structures undergo rapid ring closure to form more stable bicyclic ribityllumazines (**Fig. 1.1**) (61). However, these intermediaries can be captured by MR1 and because they share a similar conformation in the cleft as 6-FP, they can position themselves within the A' pocket and form a Schiff base between the open ring and the α1-helix K43 residue, improving chemical stability (58, 61). Strikingly, MR1 presentation of these agonists enables MAIT cells to recognise an unprecedented breadth of microbial species via a single antigenic determinant.

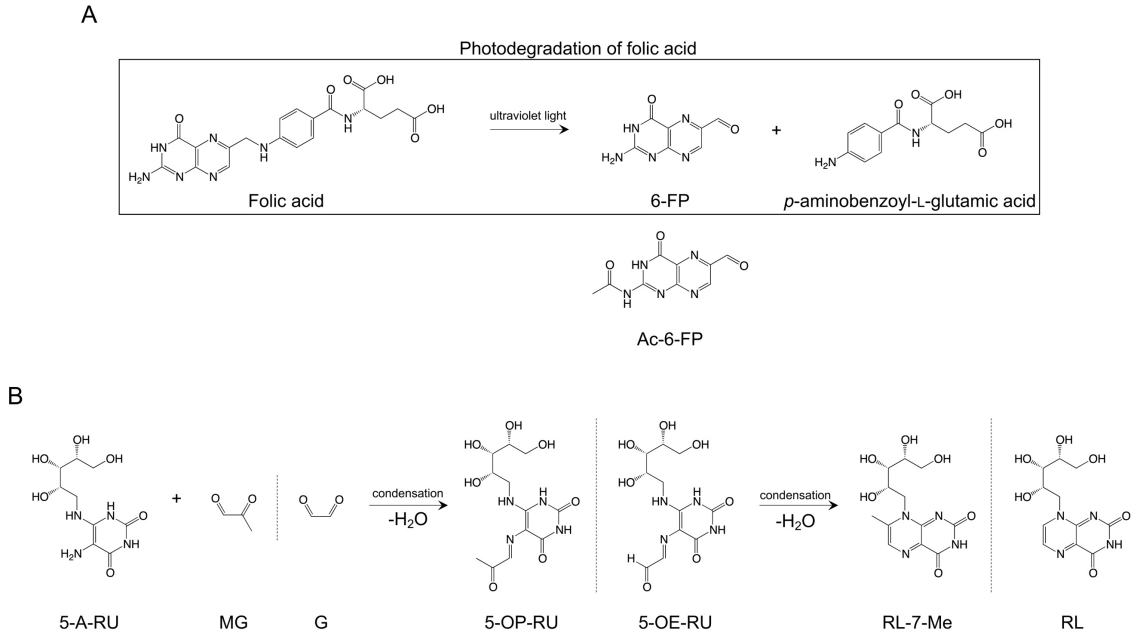

Figure 1.1. Riboflavin- and folate-based ligands presented by MR1. Chemical structures of MR1 ligands and their biosynthetic precursors. **A.** Riboflavin-based ligands; 5-(2-oxopropylideneamino)-6-D-ribitylaminouracil (5-OP-RU) and 5-(2-oxoethylideneamino)-6-D-ribitylaminouracil (5-OE-RU), ribityllumazines RL-7-Me and RL and their biosynthetic precursors 5-amino-6-D-ribitylaminouracil (5-A-RU) and methylglyoxal (MG) or glyoxal (G). **B.** Folate-based ligands; 6-formylpterin (6-FP) and the synthetic derivative form acetyl-6-formylpterin (Ac-6-FP) and the photodegradation pathway of the ligand precursor, folic acid. Chemical structures from *Kjer-Nielsen et al.* (62).

1.1.6 Unconventional T cells

Unconventional T cells comprise various subsets of T cells that are defined by TCR usage, and restriction element and antigen recognition. Unlike conventional MHC-restricted T cells, these cells typically express limited TCR diversity, recognise evolutionary conserved antigens and typically do not require priming upon activation (44, 63). Major subsets of unconventional T cells include natural killer T (NKT) cells and related CD1-restricted T cells that recognize lipid antigens, MAIT cells that recognise small vitamin B derivatives and γδ T cells that recognise phosphoantigens (pAg), lipid molecules and other antigens that are yet to be defined (44). Broadly, unconventional T cells are present at much higher frequencies than antigen specific MHC-restricted T cells and typically localise within non-lymphoid tissues (44, 64). These characteristics enable unconventional T cells to respond rapidly to stimuli at the site of disease, in this way, bridging the gap between the innate immune system and the delayed MHC-restricted adaptive immune response.

1.2 MAIT cells and MR1

1.2.1 Characteristic features of MAIT cells in immunity

MAIT cells were identified as a distinct subset of T cells that are highly conserved in most mammalian species (56, 65). A defining feature of the MAIT cell subset is a restricted αβTCR repertoire. During recombination of the TCR genes in developing T cells, the TCRα chain variable (V) and joining (J) gene segments and TCRβ chain V, diversity (D) and J genes segments each randomly rearrange and then associate to form a unique, functional TCR heterodimer (66). The canonical MAIT TCR in humans consists of an invariant α-chain composed of TRAV1-2 rearranged to TRAJ33, TRAJ20 or TRAJ12 gene segments paired with a less restricted array of β-chains including; TRBV6-1, 6-4 and 20 (56, 67). Early analysis of MAIT cells in the body demonstrated that these cells are localised at mucosal sites; however, MAIT cells are also commonly found throughout the body, including peripheral blood, where they exist at a high precursor frequency of up to 10% of total T cells (61, 68, 69).

The development of soluble MR1-5-OP-RU tetramers has allowed for detailed phenotypic analysis of MAIT cells in humans (40, 61, 67). In the blood of most donors, MAIT cells express the co-receptor CD8 (50-90%), although some MAIT cells lack CD4 and CD8 co-receptors, termed co-receptor double negative (DN) (up to 50%), while a small subset of MAIT cells express the CD4 co-receptor (61, 67). MAIT cells exhibit an effector memory phenotype that is acquired early upon egress from the thymus, expressing CD45RO, the NK marker CD161 and the homing receptor CCR6 (70, 71). Their relative abundance, phenotype and evolutionary conservation, suggest that MAIT cells play an important role in the immune response to microbial infections. Indeed, many studies now suggest a role for MAIT cells in protective immunity, however the exact mechanisms of pathogen control in humans is still unclear (57, 68, 72-74). MAIT cells have been shown to produce effector cytokines such as IFNγ, TNF, IL-17 and granzyme B in response to antigen stimulation by an extensive range of bacterial species (70). In active tuberculosis infection, MAIT cells are found enriched in the lung and depleted from peripheral blood, suggesting MAIT cells are activated during *M. tuberculosis* infection and migrate to the site of infection. *Ex vivo* analysis of MAIT cells sampled

from tuberculosis patients demonstrates how they can detect *M. tuberculosis*-infected lung epithelial cells and secrete IFNγ (72). Interestingly, almost all of the MAIT cells isolated from tuberculosis-infected patients express the CD8 co-receptor. Furthermore, *ex vivo* activation of $CD8^+$ MAIT cells with *M. tuberculosis*-infected cells was prevented by blocking the CD8 co-receptor, suggesting an important role for CD8 ligation by MR1 (71). Pulmonary infection with *Francisella tularensis in* a mouse model of disease showed that MAIT cells can contribute to mucosal immunity by production of IL-17, TNF and IFNγ and, that MAIT cells could significantly reduce the bacterial burden of infected macrophages *ex vivo* (75). Notably, inhibition of bacterial growth was dependent on MR1 as well as the pro-inflammatory molecule IL-12 (75).

In addition to TCR-mediated recognition of antigen, it is now established that Toll-like receptor (TLR) agonists can activate T cells via cytokine stimulation (76). MAIT cells constitute a large portion of these cells and respond to IL-12 and IL-18 cytokine stimulation by secreting IFNγ, TNF, granzyme B and perforin (77-79). Moreover, a recent study examining the requirements for effector function by MAIT cells *ex vivo,* demonstrated that inflammatory stimuli were essential to induce a prolonged effector response (74, 80). Several reports now provide evidence for the involvement of MAIT cells in aberrant disease, including rheumatoid arthritis, MS, inflammatory bowel disease and cancer (70, 81-84). Thus, a greater understanding of the factors involved in MAIT cell activation is required to understand their role in human immunity.

1.2.2 TCR recognition of MR1-Ag

Two events that occur sequentially during TCR rearrangement in the thymus lead to diversity within the T cell population. The translocation, alignment, excision and often revision of V, D and J gene segments within T cell receptor (TR) loci produce an in-frame DNA sequence that encodes a functioning TCR chain (85). Diversity within the TCR chain is imbued through combinations of gene segments and TCR chain pairing, referred to as combinatorial diversity (85). During the joining of gene segments, random nucleotides can be inserted in the junctions between paired gene segments, dramatically increasing the number of unique TCR sequences, referred to as junctional diversity (85). Three hypervariable complementarity-determining regions (CDRs) exist within each

TCR chain that form ‘finger-like’ loops at the distal end of the TCR and interact with pMHC (66, 85). CDR1 and 2 loops are encoded within the germline sequence of the TRAV and TRBV segments, however the CDR3 loop is situated at the highly diverse junction between the V(D)J gene segments and is the major determinant of antigen specificity (66, 85).

To gain a greater understanding of how the MAIT TCR interacts with MR1-Ag, the structure of several MAIT TCRs with MR1-Ag were solved (58, 61, 86) Structural determination revealed that the TCR docks orthogonally across the MR1 cleft whereby the CDR loops are positioned over the A’ pocket of MR1 (61). The prominent feature of the canonical MAIT TCR is its low combinatorial diversity, a consequence of the restricted TCR gene usage. In particular, the highly conserved nature of the TCRα chain (TRAV1-2) provides key molecular contacts to both antigen and the MR1 molecule (61, 67, 86). Specifically, the highly conserved residue (Y95) within the germline TRAJ portion of the CDR3α (either TRAJ33, TRAJ20 or TRAJ12) forms a hydrogen bond with the ribityl moiety of the riboflavin metabolites that is critical for MAIT cell activation by these antigens (61, 67, 86). Notably, heterogeneity does exist within the MAIT TCR repertoire through the broader usage of TCRβ chains consisting of diverse CDR3β regions (58). Although no single molecular determinant within the β-chain is essential for specificity, the junctional diversity within the CDR3β can profoundly modulate the TCR affinity for antigen (58, 67). Interestingly, a degree of flexibility exists within the CDR3β loop when docked on MR1 in the context of riboflavin and folate derived antigens, suggesting a propensity for the TCRβ chain to fine-tune its conformation over MR1 to recognize different antigens (58).

Aside from the TCR, an array of membrane bound molecules are involved in antigen recognition between a T cell and APC. The TCR-pMHC lies at the centre of a tight apposition between interacting cells, surrounded by concentric rings of other membrane receptors that form a framework collectively referred to as the immunological synapse (IS) (87). Within the innermost circle of molecules on the T cell side, is the CD3 complex, a multimeric complex of molecules that associates with each TCR and is responsible for initiating intracellular signals (88). The two co-receptor molecules, CD4 and CD8,

closely associate with the CD3 complex and bind directly to MHC-II and -I respectively. The molecular determinants of co-receptor recognition of MHC and intracellular signalling have been studied in detail on peptide-reactive conventional T cells, clearly demonstrating their importance in T cell activation. Some controversy exists on whether MR1 is equipped with the key molecular determinants required for CD8 ligation (41, 89, 90). However, due to the overwhelming bias for MAIT cells to express the CD8 co-receptor in peripheral blood, it is reasonable to suggest that CD8 may plays a role in the recognition of MR1 (41, 61).

1.3 Structure and function of the CD8 co-receptor

The CD8 co-receptor is a dimer composed of subunit α and β chain glycoproteins, and can be expressed as a CD8αα homodimer or CD8αβ heterodimer isoform (91). The heterodimer is primarily expressed on cytotoxic T lymphocytes (CTLs), whereas the homodimer can be expressed on T cell subsets such as γδ T cells, NKT cells and MAIT cells (67, 92, 93). Each CD8 subunit consists of a single immunoglobulin-like (Ig-like) domain, as well as a long hinge-like extracellular stalk, transmembrane region and a short cytoplasmic tail (94, 95).

The CD8 Ig-like domains form the main contact with the MHC-I via a number of protruding loops homologous to the CDR loops of the TCR. These 'CDR-like' loops contact MHC-I in a highly conserved manner (96), primarily within the α3 domain of MHC-I, but also the α2 domain and β_2m, subject to MHC-I allelic variation (97). In particular, structural analysis revealed that the main interface is at the protruding 'finger-like' CD loop of the α3 domain of MHC-I (92). This region is highly conserved among human and mouse MHC-I and is a major contributor for CD8 recognition of polymorphic antigen presenting molecules (98). In particular, the residue Q226 is a crucial contact required for CD8 ligation and is conserved in all CD8-binding MHC-I molecules (99, 100). CD8 engages with MHC-I independently of other molecules, however it plays a synergistic role by simultaneously engaging MHC-I with the TCR, improving the overall binding avidity of the TCR-MHC interaction (97, 99). The ability for CD8 to interact with various molecules within the synapse is well documented, however the order and relevance of each interaction is unclear. Regarding ligation of MHC-I by CD8, several biochemical features elude to a likely order of events and their importance. The TCR α-chain connecting peptide motif (α-CPM) in conjunction with post-translational palmitoylation of the CD8β chain promote an intimate association between CD8 and the TCR complex at the membrane, even in the absence of cognate pMHC-I (87, 101). This bispecific association enables both the TCR and CD8 to engage the same MHC-I in a coordinated, two step manner (101, 102). The TCR binds cognate pMHC-I first, followed by CD8 (103). Given this proposed order of events, the enhanced avidity afforded to the TCR-MHC interaction via CD8 is only available when the TCR has engaged cognate MHC-I, thereby providing sufficient dwell time for subsequent engagement by CD8.

Upon TCR ligation, the subsequent engagement of MHC-I by CD8 is of relatively low affinity (~200 μM) exhibits rapid kinetics (104), and is reliant on the TCR-MHC interaction for stability. However, this weak interaction is capable of enhancing the association rate of MHC-I with TCR, increasing the number of productively engaged complexes at the membrane and boosting the sensitivity for antigen, critical for the recognition of lower affinity antigens (105-107).

Both CD8αα and CD8αβ bind to soluble MHC-I with a similar affinity, however enhanced activation of primary T cells appears to occur in the presence of CD8αβ (93, 108). This is thought to be due to the contribution of CD8β subunits to signal transduction. Intriguingly, it is the CD8α subunit that associates with the lymphocyte-specific protein tyrosine kinase ($p56^{lck}$), the essential Src family kinase required for initiation of the TCR signalling cascade. The cytoplasmic tail of the CD8α subunit contains a vicinal cysteine motif that interacts with $p56^{lck}$ via a zinc chelate complex. Upon CD8 binding to MHC-I, $p56^{lck}$ is brought into close proximity to the TCR complex, promoting signal transduction by enzymatic phosphorylation of the TCR-CD3 complex (96, 109-111). In contrast, the CD8β subunit does not associate with $p56^{lck}$ directly, but has been hypothesised to increase the association of CD8α with the kinase via several means. The dimerisation of CD8α with CD8β is proposed to enforce a stabilising conformation that favours the association of the α-subunit cytoplasmic tail with $p56^{lck}$ (112). In addition, palmitoylation of the CD8β cytoplasmic tail in mice permits the partitioning of the CD8 co-receptor to lipid rafts (87). Lipid raft microdomains provide a haven for signalling molecules such as $p56^{lck}$ within the IS and exclude negative regulators of signalling such as the protein tyrosine phosphatase, CD45 (113, 114). Therefore, the segregation of CD8αβ into this privileged environment, by way of the β-chain, both increases the association of $p56^{lck}$ with the α-chain cytoplasmic tail as well as prevents negative regulation of signalling by catalysed dephosphorylation.

The process of CD8αα exclusion from membrane lipid rafts has been proposed to have biological consequences for T cells (115). CD8αα expression can be induced both transiently or permanently on T cells upon activation and can be expressed alone or co-

expressed with CD8αβ and CD4. Co-expression of both CD8αα and CD8αβ on T cells in mice has been shown to negatively affect T cell activation, where CD8αα may serve to regulate T cell responses (116). A proposed mechanism of CD8αα suppression is by sequestering $p56^{lck}$ outside lipid rafts thereby reducing the total levels available for signalling upon ligation of productive TCR-pMHC-I-CD8αβ complexes (115). Consistent with this, an increase in CD8αα outside lipid rafts coincided with a decrease in the functional avidity of TCR-CD3 activation (117). Due to the preference for $p56^{lck}$ to bind CD8αβ, it seems likely that other mechanisms are also involved in the observed decrease in T cell activation. CD8αα may interfere directly with the colocalization of CD8αβ with TCR-CD3 complexes by disrupting the organisation of membrane lipid rafts (117). Lipid raft disruption has been described for another suppressive molecule, CTLA-4, that competes with CD28 for ligation with B7 ligands (118). Thus, CD8αα may act as a co-repressor of T cell function, particularly if expressed alongside CD8αβ, and on T cells that rely on CD8 engagement of MHC-I for activation.

Interactions between CD8 and the MHC-like molecules have remained largely speculative. However, intra-epithelial lymphocytes (IELs) have been identified that recognise the mouse thymus leukemia antigen (TL) via CD8αα, demonstrating MHC-like engagement by a co-receptor (94). The CD8αα affinity for TL is exceptionally high (K^d ~12μM), but interestingly, structural determination revealed that the interface was very similar to that of CD8-MHC-I (94, 119). Therefore, small variations within the CD8 binding domain can profoundly alter the affinity with CD8. Due to the disfigured binding groove, peptides are not presented by TL to the TCR (119). Thus, CD8αα does not function as a traditional co-receptor on IELs but rather ligation of TL by CD8αα on IELs appears to coordinate with TCR-MHC interactions to regulate cytotoxic and proliferative responses (94). The majority of CD1-restricted T cells are $CD4^+$ or DN, however some express CD8, including a subset of human CD1d-restricted NKT cells that express CD8αα (120). Recently, a study has determined the CD8 expression does not enhance NKT cell recognition of CD1d (120). However, several studies have examined the contribution of the CD4 co-receptor on NKT cell responses (121, 122). The CD4 co-receptor has been shown to bind to CD1d and enhance signal transduction via

sequestering $p56^{lck}$ (121). Interestingly, the ability for CD4 to enhance NKT cell function is independent of binding CD1d or MHC-II (122), indicating that co-receptors can influence T cell responses non-specifically.

MR1 shares much of the architecture of the CD8 binding α3 domain of MHC-I (41, 123), including residue Q226 within the CD loop of the α3 domain. Moreover, some evidence suggests that CD8 is important for MAIT cell function (124-126). Specifically, a study that examined the $CD8^+$ T cell response to *M. tuberculosis* revealed that $CD8\alpha\beta^+$ MAIT cells were the most abundant unconventional T cell subset identified (71). Moreover, blocking CD8 function using an anti-CD8 antibody prevented MAIT cell detection of *M. tuberculosis* infected cells *in vitro*, suggesting that CD8 was critically important for detection of *M. tuberculosis* by MAIT cells (71). Similarly, a recent study revealed that CD8 blocking of MAIT cells stimulated by *E. coli* treated APCs caused a reduction in cytokine production by $CD8^+$ MAIT cells, but not DN MAIT cells (124). While blocking antibodies are effective at preventing CD8 ligation of MHC-I, these antibodies have been previously demonstrated to affect T cell function non-specifically (127). Therefore, precisely how CD8 may be functioning to enhance T cell responses on MAIT cells has not been addressed, specifically, whether CD8 is capable of engaging MR1 to improve MAIT cell function. Given the importance of the co-receptors in MHC-restricted T cell responses, it is important to understand how CD8 can contribute to CD1- and MR1-reactive immune responses.

1.4 Lipid-reactive T cells

1.4.1 CD1b-restricted T cell responses to microbial antigens

The large cleft of CD1b and the way in which lipids are oriented for presentation permits for a variety of lipids to be accommodated (24). Yet, the number of these lipids that have an immunological significance is unknown. Exogenously derived lipids are the most well characterised antigens presented to CD1b-restricted T cells. Repeated *in vitro* stimulation of PBMCs with *M. tuberculosis* lipid extracts led to the selective expansion of a CD1b-restricted T cell clone (DN1) that could lyse CD1b expressing APCs pulsed with extracts (128). *M. tuberculosis* specific lipids were later identified as antigens presented by CD1b, including mycolic acids (MAs) and related GMM and glycerol-monomycolate (GroMM), mannose linked phosphatidylinositols, such as lipoarabinomannan (LAM) and recently diacylated sulfoglycolipids (AcSGLs) (**Fig. 1.2**) (48, 129-131).

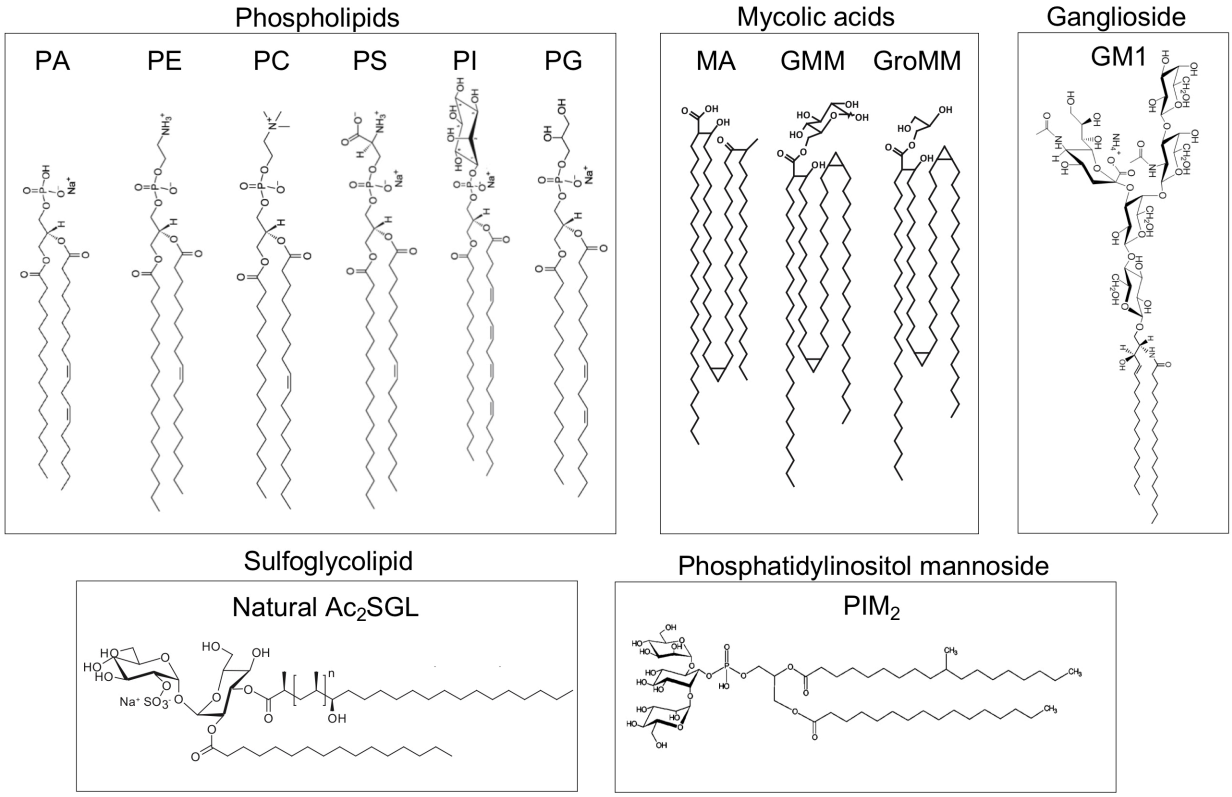

Figure 1.2. Mammalian and microbial lipid antigens presented by CD1b. Different classes of mammalian and microbial lipid antigens are segregated by black borders. Mammalian lipid antigens; phosphatic acid (PA), phosphatidylethanolamine (PE), phosphatidylcholine (PC), phosphatidylserine (PS), phosphatidylinositol (PI), phosphatidylglycerol (PG) and monosialotetrahexosylganglioside (GM1) (structures from Avanti lipids). Microbial lipid antigens; mycolic acid (MA), glucose monomycolate (GMM), glycerol monomycolate (GroMM), naturally occurring diacetylated sulfoglycolipids (Ac_2SGL) and phosphatidylinositol di-mannoside (PIM_2) (structures from *Quemard et al.* (132)*, James et al.* (133)*,* and *Sprott et al.* (134)).

In some cases, recognition of these antigens by T cells is dependent on the bacteria from which they originate. For instance, T cells specific for the cell wall lipid phosphatidylinositol mannoside (PIM) synthesised by *M. tuberculosis* are not cross-reactive to PIMs synthesized by *Mycobacterium leprae*, indicating a fine specificity for antigen and the involvement of both the glycolipid head group and lipid tails in TCR recognition (130). This regulation of specificity by the TCR is exemplified in a subset of CD1b-restricted germline-encoded mycolyl (GEM) T cells. Identified using CD1b-GMM tetramers in latently infected *M. tuberculosis* patients, GEM T cells express an invariant TCRα chain (TRAV1-2) with a short germline encoded CDR3-loop paired to a seemingly restricted number of TCRβ chains, similar to MAIT cells (135). GEM TCR transduced cell lines were shown to recognise GMM but not other related MAs with their native TCRαβ pairs, however the generation of TCR chimeras, where the GEM TCRβ chain was swapped for a MA-specific TCRβ chain, reconstituted recognition of MA at the expense of GMM. Conversely, swapping the TCRα chain with one from a MA-reactive T cell clone ablated recognition of both antigens, indicating that although it is the GEM TCRα that is highly conserved, both TCR chains are critical in surveying the unique molecular determinants of GMM (135).

CD1b-restricted T cells are notoriously hard to identify using tetramers and the majority of the understanding of these cells stems from the limited isolation of T cells with conserved characteristics that are easy to identify, such as for GEM T cells as well as another invariant T cell population (TRBV4-1^{+}), referred to as LDN5-like T cells (136). These early studies support the notion of interdonor TCR conservation among GMM-reactive T cells, yet the extent to which conserved TCR repertoires contribute to the total GMM-reactive T cell pool was not determined. A recent study demonstrated that the TCR repertoire of GMM-reactive T cells is considerably more diverse than expected and composed primarily of private TCR repertoires (137). Further analysis revealed junctional diversity within the CDR3 regions of GEM T cells in all donors, revealing donor specificity that is not strictly germline-encoded. Interestingly, a strong enrichment of both germline and non-germline CDR3α encoded amino acid R107 was observed in GEM T cells, and structural studies verified the importance of this residue in the recognition of GMM (137, 138). Remarkably, a linear discrimination model of the

frequency of T cells with identified TCR motifs accurately diagnosed active tuberculosis from latently infected and control donors in all cases (137). Hence, while the incidence of invariant GMM-reactive T cells among donors is high, the majority of reactive T cells possess private TCR repertoires that contain donor specific motifs. Lastly, clonal expansion of both GEM and other GMM-reactive T cells was detected in active *M. tuberculosis* infected donors, suggesting that CD1b-restricted T cells are active during the course infection (137). These data broaden the known TCR repertoire of GMM-reactive T cells and demonstrate clonal expansion over the course of *M. tuberculosis* infection. However, the low frequency of GMM-reactive T cells in blood and the current approach to obtain them using tetramers is insufficient for in-depth analysis of GMM-reactive T cell phenotype and function *ex vivo*, especially in healthy donors (137).

1.4.2 CD1b-restricted T cell responses to self-lipid antigens

Self-lipids comprise the majority of known lipids that can be presented by CD1b (139). The ganglioside monosialotetrahexosylganglioside (GM1) constitutes a significant portion of lipid content in the brain and is presented by CD1b (54). T cells from the peripheral blood of healthy donors and MS patients were stimulated with gangliosides *in vitro* and demonstrated two patterns of recognition of GM1(54). Two of the three clones identified were strictly reliant on the presence of both the terminal glucose and branched sialic acid of GM1, whereas the sialic acid was dispensable for recognition by the third clone (54). Further investigations into the restrictions on acyl and sphingosine chain length revealed that while it is unlikely that the fatty acid tails are directly recognised by the TCR, their length can profoundly impact TCR recognition by altering the position of the head group within the CD1b cleft (32). These observations align with other studies demonstrating that both acyl chain length and saturation can impact on NKT cell recognition of lipids presented by CD1d (140, 141). Thus, like GMM, TCR recognition of GM1 is dependent on key molecular determinants present on the sugar moiety, yet these precise determinants can vary between cells.

Autoreactive CD1b-restricted T cells do not always exhibit a stringent specificity for antigen. Recently, autoreactive cells have been identified using CD1b multimers loaded with phosphatidylglycerol (PG), a phospholipid found in the mitochondria of mammals

and bacterial cell walls (52). Two clones (PG10 and PG90) were shown to recognise CD1b tetramers loaded with other phospholipid antigens such as phosphatidylinositol (PI), phosphatidylserine (PS) and phosphatidic acid (PA). Recognition of a single molecular determinant shared between these molecules appears unlikely due to the structural variation in the head groups. This is supported by the observation that CD1b tetramers loaded in the antigen vehicle solution without antigen, so called 'mock'-loaded CD1b tetramers, were weakly recognized by the PG-reactive T cell lines. This broad CD1b autoreactivity was largely overlooked by the field due to the relative lack of CD1b autoreactive T cell clones compared to the other CD1 isoforms (142, 143), as well as the high specificity for antigen displayed by microbial CD1b-restricted T cell clones identified so far (135, 138). Consequently, the prevalence of autoreactive T cells and the range of endogenous lipid antigens that they recognise is largely unexplored.

1.4.3 TCR recognition of CD1b-Ag

The first CD1b-TCR ternary structure solved comprised a GMM-reactive GEM TCR (GEM42) ligated to CD1b presenting GMM C:32 (138). The GEM TCR docked centrally over the cleft of CD1b, where the TCRα chain made extensive contacts with both CD1b and GMM (138). In particular, the CDR3α contributed 27% of the total buried surface area (BSA), while both germline-encoded CDR1α and CDR2α loops contributed ~10% BSA each. The CDR3β loop was integral in the recognition of GMM, however the CDR1β and CDR2β played a far lesser role. Visually, the recognition of GMM by GEM42 is described as a tweezer like grip, where the CDR3α and β loops engaged the glucosyl moiety of GMM from above. Due to the constrained fit of GMM by TCR ligation, it is possible to appreciate the full extent to which the antigen headgroup protrudes from the cleft of CD1b and is flattened across the α2 helix by the TCR. The intricate positioning of the CDR3α and CDR3β loops atop of GMM are stabilised by the formation of an interdomain salt bridge between R107α and D113β, enabling the CDR3β chain to contact the glucose moiety. In this way, R107α is vital in both contacting GMM itself and orienting the TCRβ chain. It is no surprise the R107α is conserved among most GEM TCRs identified (137). Comparatively, NKT and MAIT cells express almost universal conservation of TCRα chain elements within their respective TCR repertoires.

Namely, the germline-encoded TRAJ18 region shared among TRAV10^{+} and TRAV10^{-} NKT cells (144) and CDR3α Y95 residue shared among MAIT cells, both of which are crucial for prototypical antigen recognition by the TCR (40, 61, 86).

To establish the importance of the glucose moiety in the recognition by the GEM TCR, the affinity of the GEM42 TCR for CD1b loaded with related glycosylated mycolic acids was measured. The variant antigens included MA, mannose-6-O-monomycolate (ManMM), galactose-6-O-monomycolate (GalMM) and glycerol-6-O-monomycolate (GroMM) and all abolished recognition by GEM42, indicating a stringent specificity for GMM. The structurally imposed intolerance of MA and related glycosylated MAs by the GEM TCR may have important biological consequences. GMM is produced by *M. tuberculosis* from mycolic acids and host derived glucose (145) for which only invasive *Mycobacteria spp*, such as *M. tuberculosis,* can gain access to a sufficient source of host derived glucose (145). Thus, GEM T cells are equipped to specifically recognise an antigen generated by this pathogenic process. While these data reveal the mode of CD1b-GMM recognition by a prototypical GEM TCR, recent studies suggest that in many donors, T cell are able to recognise CD1b-GMM with diverse TCRs (137). Therefore, it may be possible that the high specificity for GMM displayed by GEM T cells is not shared with other GMM-reactive T cells.

In contrast to GEM T cells, autoreactive CD1b-restricted T cells are typically more promiscuous in their antigen recognition (52). PG10 and PG90 are TCRs cloned from CD1b-restricted T cells that strongly recognise CD1b presenting PG (52). PG is of low abundance in mammalian cells and is confined mostly to the mitochondria (146), yet is highly expressed in bacterial cell membranes (147). One hypothesis is that these cells are tuned to detect bacterial infection (52). In this case, the highly antigenic endogenous PG is thought to remain undetected within the mitochondria of healthy cells. Both PG90 and PG90 TCRs are also cross-reactive with more abundant self-phospholipids, including PA, PS and PI (52). However, PG10 and PG90 possess a strong preference for the phospholipid, PG (52). Another possibility is that CD1b-restricted T cells may be permissive to aberrant phospholipids that accumulate or are released from malignant cells. This has been demonstrated in humans by a subset of CD1c-restricted T cells that

recognised a modified phosphatic acid derived from leukaemia cells (148). Similarly, in a mouse model, adoptively transferred CD1b-restricted T cells preferentially recognised phospholipids specifically from tumours and conferred protection from murine T cell lymphoma (149).

Structural analysis of the PG90 TCR ligated to CD1b presenting PG detail the recognition of CD1b and provide insights into the preference for PG specifically. PG90 adopts a similar mode of recognition as GEM42, docking orthogonally over the cleft of CD1b (150). The CDR1α, CDR3α and CDR3β loops of the PG90 TCR contributed most to the recognition of PG and formed a positively charged cup that surrounded the lipid headgroup such that upon ligation the phospholipid is completely buried by the TCR interface. A commonality between PG90 and GEM42 docking is the formation of a tweezer-like grip over the antigen headgroup. This likely explains the high specificity for PG, however the cationic cup of PG90 can accommodate other phospholipids to some degree (150). Furthermore, the amino acid R91α within the CDR3α loop of PG90 performs a similar role as R107α in GEM42, contacting both the phospholipid headgroup as well as the TCRβ chain. To assess whether the strong preference of PG90 for PG loaded CD1b was due to a conformation change induced by the phospholipid itself, a comparison between the binary structures of CD1b-PG, PS and PA was performed. None of the binary structures showed signs of a conformation shift in the CD1b molecule, suggesting that preferences for PG is due to an exquisite recognition of the headgroup moiety.

Novel CD1b-restricted TCRs were recently identified using natural and synthetic AcSGLs. This family of cell wall lipids is found only in *M. tuberculosis* and its abundance is correlated with bacterial virulence (133). An activation assay using CD1b expressing cell lines mutated along the α1 and α2 helices revealed several residues that were important for TCR mediated activation by CD1b presenting AcSGL. Residues located centrally and slightly F' biased (V72, E80, D83 and Y151) moderately or completely abrogated activation when mutated to alanine (133). Interestingly, these residues were also important for the recognition of CD1b presenting GMM to GEM42 and residues E80 and Y151 were involved in the recognition of PG by PG90 (150). Moreover, binary

structures of CD1b loaded with antigens PI, GMM and disialotetrahexosylganglioside (GM2), reveal α1 helix residues R79, E80 and D83 and centrally located residues on the α2 helix contacted the lipid headgroups via hydrogen bonding (24, 50). These data demonstrate that distinct antigen specific repertoires of CD1b-restricted TCRs are sensitive to the same CD1b mutations. Accordingly, it is likely that centrally located residues along the cleft of CD1b stabilise and orient the lipid headgroup moieties for surveillance during TCR engagement.

1.4.4 CD1b-restricted T cells in disease

Few studies have evaluated the importance of CD1b-restricted T cells using disease models as CD1b is not naturally expressed by animals used commonly as laboratory models. However, the generation of CD1b and CD1b-restricted TCR transgenic mice has enabled the study of CD1b-restricted T cells in several models of disease, namely *M. tuberculosis* infection and hyperlipidaemia (151-153).

Using $CD1b^{+}$ MA-reactive TCR (DN1) transgenic mice, *Zhao et al.* demonstrated that adoptively transferred CD1b-restricted T cells were activated by *M. tuberculosis* infection *in vivo* and reduced the bacterial burden in the lungs of $CD1b^{+}Rag2^{-/-}$ mice compared to $CD1b^{+}Rag2^{-/-}$ mice alone (151). Interestingly, DN1 T cells were activated in the mediastinal lymph node 11 days post *M. tuberculosis* inoculation into the lungs, indicating bacteria disseminated from the initial site of infection before being detected by DN1 cells. The absence of DN1 cell activation in the lung and the delayed immune response suggests that these cells do not exhibit an effector memory phenotype at rest, typical of other unconventional T cell subsets (44). However, activation of DN1 cells occurred two days earlier than in an MHC-II-restricted T cell transgenic mouse. Importantly, DN1 cells protected infected animals from disease progression. Adoptive transfer of DN1 cells into a transgenic $CD1b^{+}Rag^{-/-}$ mouse elicited the secretion of IFNγ and TNF and reduced the number of viable bacteria in all organs compared to the $Rag^{-/-}$ alone control (151).

Another study generated $CD1b^{+}$ mice transgenic for an autoreactive CD1b-restricted TCR (H1J) using an ApoE deficient ($ApoE^{-/-}$) background to assess the effects of autoreactive

CD1b-restricted T cells in hyperlipidaemia (153). ApoE$^{-/-}$ mice typically develop aortic root atherosclerotic plaques at 25-30 weeks of age caused by elevated plasma lipids. H1J TCR transgenic mice were generated to examine whether CD1b-restricted T cells contribute to the development of plaques. Surprisingly, H1J T cells did not contribute to atherosclerotic pathology. However, the presence of H1J T cells coincided with spontaneous development of severe psoriasiform dermatitis. By 25 weeks of age, 95% of CD1b^{+} H1J TCR ApoE$^{-/-}$ transgenic mice developed skin disease, compared to 50% of CD1b^{+} ApoE$^{-/-}$ mice and 20% of ApoE$^{-/-}$ mice, suggesting that H1J and endogenous CD1b-restricted T cells contribute to disease.

In contrast to the MA-reactive TCR transgenic model, H1J T cells expressed a preactivated phenotype (CD69^{+}CD44^{+}CD5^{++}) and were enriched in inflamed skin. *In vitro* stimulation of H1J T cells isolated from skin and cervical draining lymph nodes revealed they were potent producers of IL-17, the dominant cytokine associated with psoriatic plaque development in humans (154). To assess the importance of IL-17 in the disease progression, mice were treated with an anti-IL-17 antibody. The severity of disease was dramatically reduced in anti-IL-17 treated mice and correlated with a reduction in infiltrating leukocytes and reduced hyperplasia. The marked response to anti-IL-17 therapy suggests that this model of disease manifests similarly to human psoriasis, where biologic therapy is highly effective for treating moderate to severe skin disease in many patients (155).

In the lipid-enriched environment, CD1b^{+} DCs isolated from the dermis expressed significantly higher levels of the co-stimulatory molecule CD86 and increased secretion of IL-6 than under normal lipid conditions. Furthermore, a disproportionate accumulation of lipids was observed in the skin of ApoE$^{-/-}$ mice, with significantly higher amounts of phospholipids such as PC, SM and PE as well as cholesterol, chol-esters and ceramides (153). Thus, it is likely that the abundance of lipids in the skin provides a source of antigen for autoreactive CD1b-restricted T cells and alters dermal DC maturation to promote pathogenic Th17 differentiation.

Epidemiological studies have identified several comorbidities associated with psoriasis, including obesity, type 2 diabetes and atherosclerosis (156). Accordingly, obese patients are more likely to suffer from severe forms of psoriasis than non-obese patients (157). Although the aetiology of psoriasis is unknown, it is clear that dyslipidaemia contributes to disease severity and possibly onset (158). Therefore, it is likely that the role of lipid-reactive T cells in this mouse model of disease is applicable to humans. Indeed, CD1b expression in lesional skin of psoriasis patients is significantly higher than in control skin and both CD1a- and CD1b-restricted T cells have been identified in the blood of psoriatic patients (153, 159).

In humans, CD1b-restricted T cells have been shown to produce granular proteins such as perforin and granulysin in response to *M. tuberculosis* infection (160, 161). Using a large cohort of latently infected (LTBI) patients, a recent study has indirectly identified a unique population of CD1b-restricted T cells that produce perforin, granzyme B and granulysin in response to the *M. tuberculosis* cell wall lipid and virulence factor LAM (152). The frequency of these polycytotoxic T cells correlated with protection against *M. tuberculosis* reactivation, providing the first example of a role for CD1b-restricted T cells in influencing immune outcomes in humans. LAM-reactive T cells were the most abundant T cell population identified in both healthy donors and LTBI patients and activation was dependent on CD1b. Further, LAM appeared to be the major T cell stimulating antigen in total *M. tuberculosis* lipid extract, illustrating the importance of CD1b-restricted T cells in lipid recognition of *M. tuberculosis*. Most CD1b-restricted T cells identified from the blood of healthy donors express CD4 (52, 135, 136). Interestingly, while the dominant co-receptor expressed by LAM-specific cells was CD4, the polycytotoxic T cells identified from LTBI patients all expressed the CD8 co-receptor (152). The frequency of $CD8^+$ polycytotoxic T cells in healthy donors and their origin remain to be determined, demonstrating the need for a comparative analysis of CD1b-restricted T cell subsets in health and disease settings.

1.5 Summary and Project Aims

Unconventional T cells, such as MAIT and CD1b-restricted T cells, recognise non-peptide antigen, namely small metabolites and lipids presented by monomorphic antigen presenting molecules MR1 and CD1b, respectively. Tetramers loaded with bacterially derived antigens such as the riboflavin metabolite 5-OP-RU and mycobacterial cell wall lipid GMM can be used to identify both MAIT and some CD1b-restricted T cells respectively. Recently, autoreactive CD1b-restricted T cells have been identified using mammalian derived lipid loaded CD1b tetramers. These reagents have become valuable tools to expand our knowledge of unconventional T cell phenotype, function and antigen specificity. However, many important fundamental questions regarding unconventional T cell biology remain, some of which are addressed as part this thesis as outlined in the following:

In human blood, MAIT cells express a variety of different co-receptors, including CD4 single positive (SP), CD8 SP, co-receptor deficient (DN) or CD4/CD8 double positive (DP). On conventional T cells co-receptors have been shown to enhance antigen T cell activation by binding directly to MHC. Using tetramers, it has been determined that the majority of MAIT cells in human blood express the CD8 co-receptor and some data suggest that CD8 may contribute to $CD8^+$ MAIT cell function. It is therefore reasonable to predict that CD8 may be able to interact with MR1 in a similar manner as MHC-I to enhance recognition of antigen and MAIT cell function.

- ***Hypothesis 1:*** *MAIT cells utilise the CD8 co-receptor to engage MR1 and contribute to functional output.*

- ***Aim 1:*** *To determine if CD8 on MAIT cells can bind MR1 directly and to measure the effect of this interaction on the recognition of MR1-Ag by the TCR and the production of cytokines upon MAIT cell activation.*

Recently, autoreactive CD1b-restricted T were identified directly using tetramers for the first time. Using *in vitro* expansion, two T cell clones were enriched from healthy donor blood. Unlike other CD1b-restricted T cell populations, autoreactive CD1b-restricted T cells did not appear to express an invariant TCR, suggesting that these cells represent a novel population of T cells. Autoreactive CD1b-restricted T cells recognised common phospholipids derived from both mammalian and bacterial sources. Specifically, these cells were permissive to different mammalian phospholipid antigens, suggesting a yet undescribed mode of antigen recognition by the TCR. The phenotype of these autoreactive CD1b-restricted T cells and their potential role in immunity is not well understood, nor the breadth of endogenous mammalian lipid antigens that can be recognised by autoreactive CD1b-restricted TCRs.

- ***Hypothesis 2:*** *Mammalian expressed CD1b binds a variety of endogenous lipids that are recognised by autoreactive T cells with unique TCR-specificities.*

- ***Aim 2:*** *To identify and characterise autoreactive CD1b-restricted T cells using CD1b tetramers loaded with endogenous antigens and to determine the permissive and non-permissive mammalian antigens recognised by these cells.*

Using tetramers, CD1b-restricted T cells have been identified in the blood of *M. tuberculosis* infected patients that recognise the CD1b-GMM. However, this population of cells was not identified in healthy blood donors, suggesting that GMM-reactive T cells may be more frequent in *M. tuberculosis* infected patients. In *M. tuberculosis* infected patients, GMM-reactive T cells expressed a semi-invariant TCR and were referred to as GEM T cells. The prevalence of GEM and other GMM-reactive T cells in healthy donors is unknown. Similarly, the phenotype and function of these cells directly *ex vivo* has not been examined. It is likely that GMM-reactive T cells undergo clonal expansion after infection with *M. tuberculosis*, while still being detected in healthy donors at a reduced, precursor frequency.

- ***Hypothesis 3:*** *GMM-reactive T cells are readily identifiable in healthy donors and express a similar phenotype to other innate-like T cells.*

- ***Aim 3:*** *To identify GMM-reactive CD1b-restricted T cells using CD1b tetramers from healthy blood donors and examine their surface phenotype, TCR repertoire, transcriptome and functional potential directly ex vivo.*

Chapter 2: Materials and Methods

2.1 Materials

2.1.1 General reagents

Table 2.1. General reagents and their manufacturer.

Reagent	Manufacturer	Catalogue no.
5-amino-6-D-ribitylaminouracil (5-A-RU)	Dr Ligong Liu, Prof. David Fairlie University of Queensland	N/A
Acetyl-6-formylpterin (Ac-6-FP)	Schircks Laboratories	11.418
6-formylpterin (6-FP)	Schircks Laboratories	N/A
Acetic acid	Chem Supply	AA009-2.5L-P
Ammonium Persulfate (APS)	Bio-Rad	1610700
5M Betaine	Sigma	B0300-1VL
Citric Acid	APC	GPC8017-5X
Sodium deoxycholate	Carbosynth	FS12338
Dithiothreitol (DTT)	ThermoFisher	R0861
DMEM Media	Gibco	10567014
DNAse1	Roche	11284932001
Ethylenediamine-tetraacetic acid (EDTA)	Ajax	AJA180-500G
Foetal bovine serum (FBS)	Thermo Scientific	A31605
Fugene 6	Promega	E2691
Glutathione (oxidized)	Sigma	G4376-10G
Glutathione (reduced)	Sigma	G4251-25G
Horse serum	Media Preparation Unit at the Department of Microbiology & Immunology, The University of Melbourne	N/A
Ionomycin	Sigma	I24222

Table 2.1. (cont.)

Reagent	Manufacturer	Catalogue no.
L-Arginine	Sigma	A5006-1KG
Luria broth	Media Preparation Unit at the Department of Microbiology & Immunology, The University of Melbourne	N/A
Methanol	Merck	1060092511
Methylglyoxal	Sigma	W296902-100G
OptiMEM Media	Gibco	31985-078
Pepstatin A	Sigma	P4265-25MG
Phorbol 12-myristate 13-acetate (PMA)	Sigma	P1585
PMSF	Sigma	P7626
Polybrene	Sigma	H9268
polyethylenimine (PEI)	Sigma	408727-100ML
40% Polyacrylamide solution	Bio-Rad	1610144
RPMI 1640 Media	Gibco	61870036
RNAse inhibitor	Clonetech	2313A
Sodium dodecyl sulfate (SDS)	Aldrich	L5750-500G
Tetramethylethylenediamine (TEMED)	Bio-Rad	1610801
Tris-base	Sigma	T3253-1KG
Triton X-100	Sigma	X100-500ML
Trypan blue	Ajax	AJA3269-10G
Tryptone	Oxoid	LP0042
Tween-20	Sigma	P1379-500ML
Tyloxopol	Sigma	T0307
Urea	Chem Supply	UA001-5KG
Yeast extract	Oxoid	LP0021B

2.1.2 Buffers and solvents

Table 2.2. Preparation of buffers and solvents.

Buffer/solvent	Preparation
ACK lysis buffer	8.02g NH_4Cl final conc. 150mM, 1g $KHCO_3$ final conc. 10mM, 200µL 0.5M EDTA, final conc. 0.1mM in 1L MilliQ H_2O
Biomix buffer A	0.5M Bicine
Biomix buffer B	100mM ATP, 100mM MgOAc. 500µM d-Biotin
Complete RPMI (cRPMI)	60mL pure FBS and 30mL SC in 500mL RPMI 1640
DMEM-10	60mL pure FBS and 30mL SC in 500mL DMEM
0.05% PBS-T	0.05% (w/v) Tween-20 in PBS
Tris running buffer	10mM Tris-HCl pH 8 in MilliQ H_2O
Tris elution buffer	10mM Tris-HCl pH 8, 1M NaCl in MilliQ H_2O
SDS-PAGE destaining solution	250mL methanol, 70mL acetic acid in 1L MilliQ H_2O
FACS buffer	10% FBS in PBS
FACS fix	3.2g glucose, 1% paraformaldehyde in 160mL PBS
FACS wash	2% FBS in PBS
10x G5 buffer	3.87g of sodium citrate in 300mL MilliQ H_2O (50mM sodium citrate), pH adjusted to 5.5
Lower gel buffer (LGB)	182g Tris-base, 0.4% SDS in 1L MilliQ H_2O, pH adjusted to 8.8 with 5M HCl
Upper gel buffer (UGB)	60g Tris-base, 0.4% SDS in 1L MilliQ H_2O, pH adjusted to 6.8 with 5M HCl
Native PAGE loading buffer (2x)	100mM Tris pH 6.8, 0.2% (w/v) bromophenol blue, 20% (v/v) glycerol in MilliQ H_2O

Table 2.2. (cont.)

Buffer/solvent	Preparation
SDS PAGE loading buffer (2x)	100mM Tris pH 6.8, 200mM DTT, 4% SDS, 0.2% (w/v) bromophenol blue, 20% (v/v) glycerol in MilliQ H_2O
IBP lysis buffer	50mM Tris-HCl pH 8, 1% (v/v) Triton X-100, 1% (w/v) NaDeoxycholate, 100mM NaCl, 10mM DTT
3M Imidazole buffer	204.2g of Imidazole in 1L PBS
Refold buffer (MR1/CD8)	100mM Tris-base, 2mM Na_2EDTA pH 8, 400mM L-Arginine, 0.5mM Glutathione oxidized, 5mM Glutathione reduced
Refold buffer (TCR)	100mM Tris-base, 2mM Na_2EDTA pH 8, 400mM L-Arginine, 5M Urea, 0.5mM Glutathione oxidized, 5mM Glutathione reduced
12% Minigel Native-PAGE	Resolving gel: 4mL MilliQ H_2O, 2mL 1.5M Tris pH 8.7, 2mL 40% polyacrylamide, 25µL APS, 10µL TEMED Stacking gel: 4mL MilliQ H_2O, 0.42mL 1.5M Tris pH 8.7, 0.5ml 40% polyacrylamide, 25µL APS, 5µl TEMED
15% Minigel SDS-PAGE	Resolving gel: 3mL MilliQ H_2O, 2mL LGB, 3ml 40% polyacrylamide, 25µL APS, 10µL TEMED
OPD/TMB phosphate-citrate buffer	6.425mL 0.2M Na_2HPO_4, 6.075mL 0.1M citric acid in 25mL MilliQ H_2O
Sucrose resuspension buffer	50mM Tris-HCl pH 8, 25% (w/v) sucrose, 1mM Na_2EDTA pH 8, 10mM DTT, 0.2mM PMSF, 1mg L^{-1} Pepstatin A
10x Native-PAGE running buffer	30.3g Tris-base, 144g glycine in 1L MilliQ H_2O
10x SDS-PAGE running buffer	30.3g Tris-base, 144g glycine, 100mL 20% SDS in 1L MilliQ H_2O

Table 2.2. (cont.)

Buffer/solvent	**Preparation**
Tris buffered saline (TBS)	10mM Tris-HCl pH 8, 150mM NaCl in MilliQ H_2O
Trypan Blue	25% (v/v) Trypan blue in 10mL PBS
Urea Buffer	20mM Tris-HCl pH 8, 8M Urea, 0.5mM Na_2EDTA pH 8, 1mM DTT
Wash Buffer 1	50mM Tris-HCl pH 8, 0.5% (v/v) Triton X-100, 100mM NaCl, 1mM NaEDTA pH 8, 1mM DTT, 0.2mM PMSF, 1mg L^{-1} Pepstatin A
Wash Buffer 2	50mM Tris-HCl pH 8, 100mM NaCl, 1mM NaEDTA pH 8, 1mM DTT, 0.2mM PMSF, 1mg L^{-1} Pepstatin A

2.1.3 Antibodies

Table 2.3. Antibodies manufacturers and particulars.

Immunogen	Clone	Reactivity	Conjugate	Origin	Catalogue no.
CD1a	SK9	Human	N/A	Biolegend	344902
CD1b	SN13	Human	N/A	Biolegend	329102
			APC	Biolegend	329109
CD3	UCHT1	Human	BV421	Biolegend	562426
			BUV805	Biolegend	563546
			APC	BD	555335
CD4	RPA-T4	Human	AF700	BD	557922
			BUV496	BD	564651
	GK1.5	Mouse	APC-Cy7	BD	552051
CD8α	RPA-T8	Human	BV650	Biolegend	301041
	SK1		BUV805	BD	564912
	OKT8		APC	eBioscience	17-0086-42
			PE-Cy7	eBioscience	25-0086-42
	53.6-7	Mouse	BUV395	BD	565968
			BUV805	BD	564920
			PE	BD	561095
	OKT8	Human	N/A	L. Kostenko	N/A
CD8β	2ST8.5H7	Human	APC	BD	641058
	SIDI8BEE		PE-Cy7	eBioscience	25-5273-42
CD14	MΦP9	Human	APC-Cy7	BD	557831
CD19	HIB19	Human	APC-Cy7	BD	557791
			PE/Dazzle™ 594	Biolegend	302252
	1D3	Mouse	PerCP-Cy5.5	BD	551001
CD25	M-A251	Human	FITC	BD	555431
CD27	O323	Human	BV785	Biolegend	302832
CD45.2	104	Mouse	FITC	BD	553772
CD45RO	UCHL1	Human	AF700	Biolegend	304218

Immunogen	Clone	Reactivity	Conjugate	Origin	Catalogue no.
CD69	FN50	Human	APC	BD	555533
			PE	BD	555531
			PEVio770	Miltenyi Biotec	130-099-965
CLA	HECA-452	Human	BV421	BD	563961
MR1	26.5	Human	N/A	T. Hansen **(162)**	N/A
IFNγ	4S.B3	Human	BV650	BD	563416
	XMG1.2	Mouse	PE-Cy7	BD	557649
IL-13	JES10-5A2	Human	APC	BD	562039
IL-17	TC11-18H10.1	Mouse	PE	BD	559502
PLZF	9E12	Human	PE-Cy7	eBioscience	25-9322-80
RORγt	Q21-559	Human	AF647	BD	562620
T-bet	4B10	Human	BV421	Biolegend	644815
TCRβ	H57-597	Mouse	APC	BD	553174
TNF	MAb11	Human	BV421	BD	562783
TRAV1-2	3C10	Human	BV605	Biolegend	351720
			APC	Biolegend	351708
			PE	Biolegend	351706
			FITC	Biolegend	351704

2.2 Methods

2.2.1 Gene cloning for retroviral transduction

DNA strings encoding full length protein genes or variable gene segments for TCR genes were synthesised by ThermoFisher using the restriction sites EcoRI and BamHI or BglII and XhoI. Genes were ligated into pMIG using T4 ligase (Promega, cat no. M1808) and transformed into DH5α *Escherichia coli* (*E. coli*) for amplification and purified via miniprep (Promega, cat no. A1223, Zymo, cat no. D4054). Amplified DNA was verified offsite by the Australian Genome Research Facility (AGRF) using PCR and sanger sequencing. Successful ligations and sequence verified pMIG plasmids were used for transfection of 293T cells.

2.2.2 Transduction of cell lines using retrovirus

Cell lines transduced with proteins of interest were generated using retrovirus raised in 293T cells transfected with the gene of interest. 10^6 293T cells were seeded onto on a $10cm^2$ culture dish in 10mL of cRPMI at 37°C to generate a monolayer. The following day, 4μg gene encoding pMIG plasmid was mixed with Fugene 6 (Promega, cat no. E2691) and OptiMEM media (Gibco, cat no. 31985-078) and incubated for 15 mins. For TCR transfections, 2μg of a human CD3 pMIG was added to 2μg of TCR pMIG to improve cell line TCR levels. The DNA mix was added dropwise to the 293T cells in fresh cRPMI media and gently mixed to ensure even distribution of DNA and incubated overnight. 293T cell supernatant was aspirated the following day and replaced with 10mL of fresh cRPMI. The following day, the virus laden supernatant was carefully removed from the 293T cells, 0.2μm filtered and added to β_2m-deficient SKW-3 cells and 10μL of polybrene (Sigma, cat no. H9268). 10mL of fresh cRPMI was added to the 293T cells and the transduction process was repeated a further four days Gene expression on the SKW-3 cells was verified by flow cytometry by GFP expression and reactivity to monoclonal mAbs. While SKW-3 cells are listed on the database of cross-contaminated or misidentified cell lines, where they are described as being contaminated with the KE-37 line, we have specifically recloned these cells by single cell sorting. Thus, the transduced cell lines are all of a single origin. Following these steps, transduced C1R and Jurkat76 cells were generated similarly by retroviral transduction.

2.2.3 Cloning and expression of soluble proteins in E. coli

DNA strings encoding soluble protein genes were synthesised by ThermoFisher) as described in Table 4 with the restriction sites NdeI and HindIII at the N- and C-termini respectively. Genes were ligated into a pET30 or pET28 plasmids using T4 ligase, transformed into DH5α *Escherichia coli* (*E. coli*) for amplification and purified via miniprep. Successfully ligated pET plasmids were verified offsite by AGRF using PCR and sanger sequencing. Verified plasmids were transformed into BL21 *E. coli* and grown on agar supplemented with 30μg mL^{-1} Kanamycin and 34μg mL^{-1} Chloramphenicol. Single colonies were harvested and grown in 200mL of similarly supplemented LB (Table 2), overnight. 10mL of the turbid culture was aliquoted into an Erlenmeyer flask (12 flasks in total) containing 1L of antibiotic supplemented LB and agitated at 180 RPM at 37°C for approximately 2 h and 20 mins or until an OD600 of 0.6 was reached, measured using an Eppendorf spectrophotometer (Eppendorf, part no. 613100354). Protein synthesis was induced in BL21 *E. coli* by addition of 1M IPTG (Table 1) to a final concentration of 1mM in each flask and agitated for a further 4 h. To harvest, cultured *E. coli* was transferred to 1L centrifuge bottles and centrifuged at 5000 RPM for 10 mins at 4°C in a Beckman Coulter Avanti J26 XPI (Beckman Coulter, part no. B10093AB) using a JLA-8.1000 fixed angle rotor (Beckman Coulter, part no. 969329). Culture medium was separated from the pellet and *E. coli* were resuspended using a sucrose resuspension buffer (Table 2) and stored at -80°C for further processing.

2.2.4 Inclusion body preparation from transformed E. coli

Lysis buffer (2.5x) (Table 2) and 1mg of DNAse1 solution (Table 1) per 1L of expression was added to the harvested *E. coli* and incubated on a RATEK roller (RATEK, cat no. BTR5-5) for 20 mins at room temperature to lyse bacterial pellets. Lysed *E. coli* solution was transferred GSA centrifuge buckets and sheared using a polytron homogeniser (ThermoFisher, part no. 9158167). Lysate was centrifuged in a Beckman Coulter Avanti J-E centrifuge (Beckman Coulter, part no. 369001) using a JLA-16-250 fixed angle rotor (Beckman Coulter, part no. 363934) at 12000 RPM for 15 mins at 4°C. Supernatant was discarded and lysate was resuspended in 150mL of wash buffer 1 per bucket (Table 2), sheared using a polytron homogeniser and centrifuged as described above. Supernatant

was discarded and the procedure was repeated using 120mL wash buffer 2 per bucket (Table 2). Washed lysate was resuspended in 30mL Urea buffer (Table 2) per bucket, sheared and centrifuged for 8000 RPM for 10 mins at 4°C to remove aeration. Lysate was transferred to SS34 centrifuge buckets and centrifuged in a Beckman Coulter Avanti J-E centrifuge using a JA25.50 fixed angle rotor (Beckman Coulter, cat no. 363058) at 17000 RPM for 45 mins at 4°C. Solubilised inclusion bodies were harvested from the lysate and stored at −80°C for subsequent *in vitro* renaturation.

2.2.5 In vitro refolding and purification of soluble proteins from E. coli

Inclusion bodies (24-200mg) were inoculated into a chaotropic refold buffer (Table 2) by rapid dilution at 4°C three times over the course of a day and incubated overnight. Chaotropic agents were slowly removed from the refolding solution by dialysis using a molecularporus membrane tubing with 6-8 kDa protein cut-off (Spectrum Labs, cat no. 132660) submerged in 15L 10mM Tris pH 8 buffer. Dialysing protein was mixed periodically and incubated overnight at 4°C. Purification of soluble protein was achieved using successive anionic exchange, size exclusion and anionic exchange liquid chromatography. In brief, soluble protein was passed over a Diethylaminoethyl (DEAE) sepharose (GE Healthcare, cat no. 17-0709-01) column by gravity and eluted using a 1M NaCl Tris buffer (Table 2) using an AKTA Pure FPLC (GE Healthcare. part no. 29-0211-96 AD). Eluted protein was concentrated and purified further by size exclusion using a HiLoad Superdex 75 pg gel filtration column (GE Healthcare, cat no. 17-1068-01) with an AKTA Pure FPLC. Lastly, eluted protein was buffer exchanged into a 10mM Tris pH 8 buffer and purified further by anion exchange chromatography using a Mono Q 10/100 GL ion exchange column (GE Healthcare, cat no. 17-5167-01) and eluted similarly as for DEAE purification.

For refolding of CD8αα, soluble protein was dialysed into a 25mM morpholine-4-ethanesulfonic acid (MES) pH 6 buffer. Crude purification of CD8αα was achieved by cationic exchange chromatography using a sulphopropyl (SP) sepharose Fast Flow column (GE Healthcare, cat no. 17-0729-01) as similarly described above. For fine purification, CD8αα was buffer exchanged into a 25mM MES pH 6 buffer and purified

by cationic exchange chromatography using a HiTrap SP HP column (GE Healthcare, cat no. 17115101) on an AKTA Pure FPLC.

For refolding soluble peptide-MHC-I heterodimers (NLVPMVATV-HLA-A*02:01, FLRGRAYGL-HLA-B*08:01, TRATKMQVI-HLA-C*06:01 and RIIPRHLQL-HLA-G*01:01), inclusion bodies were prepared similarly to previously described (99, 163, 164) based on *Garboczi et al.* (165). Peptides were purchased from Genscript as follows: HLA-A2: NLV, HLA-B8: FLR, HLA-Cw6: TRAT and HLA-G: RIIPRHLQL. Briefly, 30ug mL^{-1} of peptide, 24μg mL^{-1} of β_2m and 93μg mL^{-1} of HLA heavy chain from *E. coli* inclusion bodies were refolded in buffer containing 10mM Tris pH8, 2mM EDTA pH8, 1M L-Arginine (Sigma A5006), 5mM L-Glutathione reduced (Sigma G4251) and 0.5mM L-Glutathione oxidised (Sigma G4376). Following dialysis, refolded monomers were then purified using sequential anion exchange, size exclusion, anion exchange and hydrophobic interaction chromatography similarly as described above.

2.2.6 Cloning and expression of soluble proteins in mammalian cells

DNA strings encoding soluble protein genes were synthesised by ThermoFisher as described in Table 4 with the restriction sites AgeI and XhoI at the N- and C-termini respectively and included a C-terminal His-tag for purification. Genes were ligated into a pHLsec plasmid using T4 ligase, amplified in DH5α *E. coli*, purified and sequence verified similarly as described above. Gene encoding pHLsec plasmids were amplified further in a 1L LB culture of DH5α *E. coli* and purified using a Gigaprep kit (Zymo, cat no. D4204) as described in the manufacturers protocol. pHLsec plasmid yields were typically 5-10mg per 1L culture. $GNTI^-$ 293S HEK cells were grown in antibiotic deficient supplemented DMEM (Gibco, cat no. 11960-044) (Table 2) using 5x multilayer flasks (BD Biosciences, cat no. 353144) to 40% confluency. Cells were transfected with 137.5μg of gene encoded pHLsec plasmids per flasks using polyethylenimine (PEI) (Sigma, cat no. 408727-100ML). For CD1b expression, a 1:1 ratio of pHLsec plasmids encoding CD1b heavy chain and β_2m was used for transfection. For CD8αα expression, 2x (275μg per flask) CD8αα encoding pHLsec plasmid was used for transfection. Supernatant was harvested twice after four days and eight days in culture, sterile filtered

using a 0.2μm filter (Nalgene, cat no. 5954520) and stored at 4°C for subsequent purification.

2.2.7 Purification of soluble proteins from mammalian cells

Imidazole was added to the protein laden supernatant to a final concentration of 5mM using a 3M Imidazole buffer (Table 2) to reduce non-specific binding during protein purification. Supernatant was passed over a Ni-agarose resin column (ThermoFisher, cat no. 88223) by gravity and purified using a linear gradient of imidazole from 20mM to 1M concentration on a AKTA Pure FPLC. Eluted protein was buffer exchanged into TBS pH 8 (Table 2) and further purified by size exclusion chromatography as described above.

For crystallisation trials, mammalian produced CD1b-endo was deglycosylated to improve protein homogeneity. Endoglycosidase H (Endo H) is an enzyme that can cleave asparagine-linked mannose rich oligosaccharides produced by GNTI$^-$ 293S HEK cells. Purified CD1b-endo was buffer exchanged into 50mM sodium citrate pH 5.5 (Table 2) and concentrated to 1mg mL^{-1}. 1U per 1μg of protein of Endo H (NEB, cat no. P0702S) was added to the protein, thoroughly mixed and incubated at 37°C for 2 h. Deglycosylased CD1b was purified by size exclusion using a HiLoad Superdex 200 pg gel filtration column (GE healthcare, cat no. 28989335) similarly as described above.

2.2.8 Flow cytometry

Cell lines and PBMCs were stained with CD1b or MR1 tetramers for 20 mins at room temperature in the dark in FACS buffer (Table 2). Cells were washed with FACS buffer and resuspended in surface mAb stain outlined in Table 3 including a LIVE/DEAD fixable Near-IR dead cell stain for a further 20 min at 4°C in the dark. Cells were washed twice with FACS buffer and fixed using 2% PFA in PBS for 10 mins. Cells were acquired using on a BD LSR Fortessa (BD Biosciences). Data was analysed using the software Flowjo 10 (Tree Star Inc) and graphs generated with Prism 7 (GraphPad).

2.2.9 Tetramer dissociation assay

SKW-3.$\beta_2m^{-/-}$ cells transduced with CD8αα (SKW-3.$\beta_2m^{-/-}$.CD8αα) or CD8αβ (SKW-3.$\beta_2m^{-/-}$.CD8αβ) were stained with MR1-5-OP-RU or HLA-A*02:01-NLV tetramers

and LIVE/DEAD fixable Near-IR dead cell stain in PBS for 30 mins at 4°C, in the dark. Cells were washed once with PBS and resuspended in PBS containing 10μg mL^{-1} of purified anti-MR1 (26.5) or anti-pan-HLA-A,B,C (W6/32) for MR1-5-OP-RU and HLA-A*02:01-NLV tetramers respectively. Aliquots were taken periodically over 120 mins and fixed using 2% PFA in PBS. Cell data was acquired on a BD LSR Fortessa, analysed using the software Flowjo 10 (Tree Star Inc) and graphs were generated using Prism 7 (GraphPad).

2.2.10 Isolation of human PBMCs from buffy coats

Buffy coat enriched venous blood from healthy blood donors were provided by the Australian Red Cross under agreement numbers 15-05VIC-15, 16-03VIC-16 and 17-08VIC-16. Blood was diluted 1:1 with PBS and lymphocytes isolated by centrifugation at 400 x g for 30 mins with the brake off, overlaid on Ficoll Paque plus (GE Healthcare, cat no. 17-1440-03). Lymphocytes were extracted with a transfer pipette and washed twice with PBS. Platelets were aspirated after centrifugation at 100 x g for 10 mins to pellet cells. Red blood cells were lysed with ACK lysis buffer produced in house (Table 2). Live lymphocytes were diluted 1:1 with 0.1% trypan blue (Sigma, cat no. T6146) and counted using a haemocytometer.

2.2.11 Expansion of primary T cells in vitro

To stimulate primary T cells, a 96 well U-bottom plate (Greiner, cat no. 650180) was coated with 10μg mL^{-1} anti-CD3 (BD Biosciences, cat no. 555329) and 5μg mL^{-1} anti-CD28 (BD Biosciences, cat no. 340975) mAbs in PBS overnight at 4°C. The following day, the plate was washed 3x with PBS and primary T cells isolated using magnetic enrichment or FACS were added to each well resuspended in a 1:1 ratio of AIM-V (Gibco, cat no. 12055083) and cRPMI media supplemented with 200U mL^{-1} recombinant human IL-2 (PeproTech, cat no. 200-02), 25ng mL^{-1} recombinant human IL-15 (PeproTech, cat no. 200-15) and 50ng mL^{-1} recombinant human IL-7 (PeproTech, cat no. 200-07). Primary T cells were counted where possible to ensure a cell density of 10^5 cells per well was not exceeded during stimulation. After 48 h culture stimulated T cells were transferred to a new 96 well U-bottom plate and expanded over 14 days in supplemented AIM-V/cRPMI media.

2.2.12 Magnetic enrichment of CD1b- and MR1-reactive T cells from PBMCs

To enrich for MAIT cells, $5x10^7$ PBMCs were stained in MACS buffer (Table 2) with anti-TRAV1-2-PE (Biolegend, cat no. 351702) for 30 mins at room temperature in the dark, washed once with MACS buffer and resuspended in 1mL of MACS buffer. Cells were incubated with a 1:100 dilution of anti-PE beads (Miltenyi Biotec, cat no. 130-097-054) for 20 mins at 4°C. Cells were washed twice with MACS buffer and resuspended in 3mL for magnetic enrichment. Resuspended cells were passed over a LS column (Miltenyi Biotec, cat no. 130-042-401) under magnetic duress. The column was washed 3x while attached to the magnet. TRAV1-2^+ enriched cells were eluted by plunging 5mL of MACS buffer through the column detached from the magnet. MACS buffer was aspirated from the cells after centrifugation and resuspended in cRPMI for culture overnight.

To enrich for other MR1-reactive T cells or CD1b-restricted T cells, 10^8-10^9 PBMCs were incubated in MACS buffer supplemented with 40% horse serum (Table 2) for 15 mins at 4°C. A concentration of 10μg mL^{-1} cells of PE-conjugated MR1-6-FP or CD1b tetramer was added to the cells resuspended in horse serum and incubated for 30 mins at 4°C. Cells were washed twice with MACS buffer and resuspended in 3mL for magnetic enrichment as described above.

2.2.13 MR1 ligands

6-FP and Ac-6-FP (Schircks Laboratories) were dissolved at 5 mM in water, supplemented with 17 mM NaOH. 5-OP-RU was produced in house as a 1 mM stock solution in DMSO (166). For cellular assays, the stock solutions of 6-FP, Ac-6-FP and 5-OP-RU were diluted into PBS.

2.2.14 Functional analysis of CD1b- and MR1-reactive T cells

CD1b-restricted T cells were isolated using magnetic enrichment as described above and stimulated directly *ex vivo* with PMA (Sigma, cat no. P1585) and Ionomycin (Sigma, cat no. I24222). Cytokine production was assessed by intracellular cytokine staining (ICS). In brief, MACS enriched T cells (>10^3 per well) were cultured in cRPMI media

supplemented with 10ng mL^{-1} PMA, 1µg mL^{-1} Ionomycin and 10µg mL^{-1} Brefeldin A (Sigma, cat no. 20350-15-6) for 2 h at 37°C. Cells were washed and surface stained in 30µL with monoclonal antibodies described in Table 3 for 30 mins in PBS at room temperature. Without washing, 30µL of 2% paraformaldehyde (PFA) (Table 1) was added to each well and incubated for a further 20 mins at room temperature. Fixed cells were washed twice with PBS and resuspended in ICS antibodies (Table 3) supplemented with 0.3% saponin (Sigma, cat no. 8047-15-2) in PBS overnight. Cells were washed the following day with PBS and acquired on a BD LSR Fortessa as described above.

MAIT and other MR1-reactive T cells were isolated by magnetic enrichment with an anti-TRAV1-2-PE mAb or MR1-6-FP tetramer respectively. In stimulation assays, C1R cells deficient in MR1, expressing wild type MR1 or CD8-null MR1 were incubated with 1nM 5-OP-RU or 1µM Ac-6-FP for 2 h and washed three times with PBS. MACS enriched MAIT and MR1-reactive T cells were cultured with the C1R cells in cRPMI at a 1:1 ratio for 6 h. Brefeldin A to a final concentration of 10µg mL^{-1} was added for the final 5 h of culture. Cells were stained with surface antibodies described in Table 3 for 30 mins at room temperature and then without washing, fixed with 2% PFA for 20 min at room temperature. Cells were then washed with PBS twice and stained with intracellular antibodies (Table 3) overnight in PBS supplemented with 0.3% saponin. Cells were washed with PBS the following day and acquired using a BD LSR Fortessa.

2.2.15 Cell line mutant activation assay

SKW-3 or SKW-3.$\beta_2m^{-/-}$ cell lines transduced with autoreactive CD1b-restricted TCRs were cultured at a 2:1 ratio with C1R cell lines expressing wild type or mutant versions of CD1b in 200µL of cRPMI, typically in a 96-well U-bottom plate. Co-cultured cells were incubated for 24 h at 37°C. After the culture period, cells were transferred to a 96-well V-bottom plate and centrifuged to remove culture medium. Cells were washed with PBS and stained as described. Cells were acquired using on a BD LSR Fortessa (BD Biosciences). Data was analysed using the software Flowjo 10 (Tree Star Inc) and graphs generated with Prism 7 (GraphPad).

2.2.16 TCR sequencing

Single cells were sorted into a 96 well PCR plate (Eppendorf, cat no. 951020427) containing 5x VILO (ThermoFisher, cat no. 11754050), 10x Superscript RT (ThermoFisher, cat no. 11754050) and 1% Triton X-100 (Sigma, cat no. T9284-1L) for lysis and reverse transcription (RT). cDNA was synthesized by RT PCR and TCR Vα and Vβ gene segments were further amplified by nested multiplex PCR in a thermocycler (Eppendorf, part no. 6325) using a library of Vα and Vβ gene primers and two Cα and Cβ primers, first described in (167). Purified Vα and Vβ PCR products were sequenced by the Australian Genome Research Facility (AGRF) and analysed using the IMGT database.

2.2.17 Displacement and loading of CD1b with lipid antigens

A low concentration of a non-ionic surfactant such as tyloxapol or tween-20 was used to replace endogenous lipids from the cleft of mammalian produced CD1b molecules with defined lipid antigens. In brief, lyophilised lipid antigens were resuspended to 0.25-1mg mL^{-1} in TBS containing the surfactant tyloxapol to a final concentration of 0.5% (w/v). To ensure lipids were fully dissolved, tubes were sonicated using unisonics sonicator (Unisonics, cat no. FXP8D) for 1 h before use. A 3:1 molar ratio of dissolved lipid antigen to CD1b monomer was incubated at room temperature overnight to promote lipid replacement. Loading efficiency was tested where possible by tetramer reactivity using an antigen specific TCR transduced cell line.

2.2.18 Biotinylation and generation of CD1 and MR1 tetramers

For the generation of biotinylated MR1, a version of soluble MR1 with a C-terminal cysteine was produced (Table 4) and biotinylated using Maleimide-PEG2-biotin (ThermoFischer, cat no. 21901BID), followed by an additional anionic exchange chromatography purification step using MonoQ as described previously. For the generation of biotinylated CD1b, a version of soluble CD1b with a C-terminal BirA tag was produced (Table 4) and biotinylated enzymatically using BirA enzyme produced in house. Briefly, purified CD1b monomers were incubated in equal amounts of biomix buffer A and B (Table 2) and BirA enzyme for 4 h at 30°C, followed by MonoQ purification. Biotinylation efficiency of CD1b and MR1 monomers was assessed by SDS-

PAGE using a 1:1 mass ratio of monomer and unconjugated streptavidin (Sigma, cat no. S0677).

Purified biotinylated monomers were incubated at room temperature with PE or BV421 conjugated streptavidin (BD, cat no. 554061, 563259) for 50 mins in the dark at a mass ratio of 1μg of SAv per 5μg monomer. Specifically, one fifth of SAv was added to monomer every 10 mins to improve multimerization. Tetramers were diluted to 0.25μg mL^{-1} and used at a 1:200 dilution for all assays unless otherwise stated.

2.2.19 Ternary complex formation of TCR with CD1b

Purified soluble CD1b-endo and soluble 1.27 or 4.17 TCRs as described above, were combined in TBS at a 2:3 molar ratio to favour binding of TCR with permissive CD1b-endo monomers. Ternary complex was purified by size exclusion chromatography using a HiLoad Superdex 200 pg gel filtration column at a flow rate of 0.5mL min^{-1}. Complexed protein was eluted earlier than un-complexed TCR and CD1b-endo proteins and permitted sufficient separation to exclude un-complexed protein fractions. Ternary complexes were concentrated for mass spectrometry and crystallisation trials.

2.2.20 Direct and indirect enzyme-linked immunosorbent assays (ELISA)

To verify the conformation of soluble proteins, an indirect ELISA was performed by coating a 96 well U-bottom plate (Microtiter, cat no. 650001) with titrating amounts of the antigen of interest (Table 4), probing with an antigen specific mAb (Table 3) followed by a secondary mAb conjugated to horseradish peroxidase (HRP) (Millipore, cat no. 12-349). Specifically, antigen of interest was added to the plate in 50μL PBS per well and incubated overnight at 4°C. The following day, without washing, the plate was coated 200μL per well of 2% FCS in PBS and incubated at 37°C for 1 h. Excess BSA was removed from the plate by washing 5x with 0.05% tween in PBS (PBS-T) (Table 2). Primary mAb was added to each well in 50μL at a concentration of 2μg mL^{-1} in PBS-T supplemented with 2% FCS and incubated for 1 h at 37°C. Excess primary mAb was removed from the plate by washing with PBS-T as described above. HRP-conjugated secondary mAb was added to each well in 50μL at a 1:1000 dilution in PBS-T supplemented with 2% FCS and incubated for 1 h at 37°C. To examine binding, the

substrate 3,3'5,5'-tetramethylbenzidine (TMB) (Sigma, cat no. T3405-100TAB) buffer was prepared by dissolving two effervescent capsules of TMB in 25mL of a phosphate-citrate buffer (Table 2) and addition of 5µL of a 30% H_2O_2 solution. Secondary mAb was washed off 5x with PBS-T and 50µL of TMB buffer was added simultaneously to each well and incubated for 2-3 mins or until colour develops. Oxidation of substrate was quenched with 50µL 2.25M HCl and absorbance was measured at 450nm and 540nm wavelengths using a Multiskan Ascent multiwell plate reader (Thermo Electron Corporation, part no. 220245).

To examine tetramer binding to plate-bound antigen, a direct ELISA using SAv-HRP tetramers was performed. Specifically, soluble CD8αα was bound to a 96 well U-bottom plate as described above, followed by titrating amounts of MR1 tetramer conjugated with HRP. Detection was achieved using the substrate TMB as described above.

2.2.21 SDS and native polyacrylamide gel electrophoresis

Minigel 15% SDS-PAGE were prepared by pouring resolving gel (Table 2) into a cast (BioRad, cat no. 1658052), overlaid with 0.2% SDS in MilliQ H_2O. Once set, the overlay was discarded and stacking gel (Table 2) was added in addition to a 10-well comb. Protein samples were prepared up to 20µL with SDS loading buffer and 1M DTT (Table 2) and heated at 95°C for 2 mins for denaturation. Set gels were placed into a gel tank (BioRad, cat no. 1658004) with the combs removed and flushed with 1x SDS-PAGE running buffer up to the specified volume before protein sample were loaded, in addition to 5µL of benchmark ladder (Invitrogen, cat no. 10747-012). Electrophoresis was conducted for 45 mins using a current of 25mA per gel. Minigel 12% Native-PAGE gels were prepared in a similar manner, using the buffers specified in Table 2. Samples were prepared to 20µL in the absence of SDS and were not subject to denaturing temperatures. Electrophoresis was conducted for 2 h using a current of 10mA per gel at 4°C. After proteins were sufficiently separated, gels were stained using Coomaisse Brilliant Blue R-250 for 30 mins whilst agitated. Excess dye was removed and the gel by the addition of destain buffer (Table 2) until proteins bands were visible.

2.2.22 RNA sequencing

RNA sequencing was performed using a modified version of the Smartseq2 protocol (168). Standard DNA oligos were synthesized by Sigma and locked nucleic acid (LNA) oligos were synthesized by Exiqon. In brief, single GMM-reactive CD1b-restricted T cells were sorted into a 96 well PCR plate containing RNAse inhibitor (Clonetech, cat no. 2313A), dNTPs (Promega, cat no. U1515) and Vir70 (5'-AAGCAGTGGTATCAACGCAGAGTACT$_{30}$VN-3') in 0.2% Triton X-100 and stored at -80°C immediately after sorting. Lysed cells were thawed and incubated at 72°C for 3 mins to breakdown RNA secondary structures before reverse transcription. A mixture of 100U SuperScript II (ThermoFisher, cat no. 18064-014), 1x SuperScript II buffer (ThermoFisher, cat no. 18064-014) 5U RNAse Inhibitor, 5mM DTT, 1M betaine (Sigma, cat no. B0300-1VL), 6mM $MgCl_2$ (Sigma, cat no. M8266-100G) 1:4x10^8 dilution of ERCC spike-in (ThermoFisher, cat no. 4456740) and Vir54 (5'-AAGCAGTGGTATCAACGCAGAGTACATrGrG+G-3') in nuclease free water was prepared and 3µL was added to each cell and reverse transcription was performed in a thermocycler. A PCR master mix was prepared with 1x KAPA HiFi HotStart ReadyMix (Clonetech, cat no. KP-KK2602), 50nM Vir52 (5'-AAG CAGTGGTATCAACGCAGAGT-3') in nuclease free water and 7.5µL was added to each well for cDNA amplification. An amplification PCR was performed for 28 cycles using an Eppendorf thermal cycler and PCR product was stored at 4°C. Amplified cDNA was purified using Agencourt AMPure XP beads (Beckman Coulter, cat no. A63881) under magnetic duress using a 96 well plate magnetic stand (ThermoFisher, cat no. AM10027). Specifically, 10µL of beads were added to each cDNA sample (0.8:1 ratio) and mixed thoroughly using a pipette to ensure all of the cDNA contacts the beads. The cDNA was incubated for 8 mins at room temperature, then incubated for a further 5 mins on the magnetic stand. The residual RT and PCR master mix was gently aspirated from the cDNA coated beads and discarded. The magnetic beads were washed twice with 150µL 80% ethanol and left to air dry for 2 mins. The PCR plate was removed from the magnetic stand and the cDNA resolubilised in 12.5µL of nuclease free water. The PCR was plate was placed back on the magnet for 2 mins and the cDNA eluate was gently removed from the beads. To verify the integrity of cDNA, gel electrophoresis using a LabChip GX Touch HT (PerkinElmer, part no. CLS137031) was performed. A 1:10

dilution of purified cDNA was prepared in nuclease free water for LabChip analysis. Verified high quality cDNA was further processed as described in SmartSeq2 and sequenced using the Illumina platform.

2.2.23 RNA sequencing data analysis

The single-cell RNA-seq data was analysed using the software R with libraries: *scater, scran, SC3, MAST, data.table* and *pheatmap* available from The Comprehensive R Archive Network (CRAN) (https://cran.r-project.org) and Bioconductor (http://bioconductor.org). Single cell experiment data was loaded into R and genes with no reads were removed from the dataset. Mitochondrial genes and the ERCC spike-ins (ThermoFisher, cat no. 4456740) were used as feature controls. Cell quality control was performed to filter out low quality cells (cells with less than $2x10^5$ reads or 600 genes), high mitochondrial gene content and high ERCC spike-in content (>20% of total gene transcripts). Next, gene quality control was performed to remove highly expressed, non-relevant genes such as long non-coding RNAs (LincRNAs: FP236383.2, FP671120.3, FP236383.3 removed from the dataset). Transcriptome dropouts were managed by comparing mean gene expression and dropout rate, genes with mean expression <5 in less than three cells were filtered out. Normalisation of the filtered dataset was performed using a deconvolution method with *scran*. A batch correction was performed to remove variability in gene expression due experimental design and donor. Clustering of the dataset was performed using *SC3,* where three clusters provided the best separation of the different cell types (CD4, NKT, GMM-reactive). Differential gene expression analysis was performed using the *MAST* package. Gene expression was converted to a factor and the NKT cell type was set as a base to compare each cell type. Differential genes were reported only with an adjusted p-value <0.01 and an absolute log fold change >1.

Chapter 3: The role of the CD8 co-receptor on MAIT and other MR1-reactive T cells

3.1 Introduction

MAIT cells are an unconventional subset of T cells that express a semi-invariant T cell receptor (TCR) comprising the TCRα chain gene segments TRAV1-2 joined to TRAJ33/20/12 and typically paired with a TCRβ chain consisting of TRBV6 or 20 gene segments (56, 67, 169). MAIT TCRs recognise small molecules presented by the monomorphic MHC-related protein 1 (MR1), most notably the riboflavin precursor derivative 5-(2-oxopropylideneamino)-6-D-ribitylaminouracil (5-OP-RU) (61, 62). The MAIT TCR-MR1 axis is highly conserved among mammals, considering MR1 sequence homology, TCR usage (39, 41, 65, 170) and antigen repertoire, such that 5-OP-RU presented by MR1 is shared as a potent microbial antigen across species (61, 80). MAIT cells are identified within most human tissues and constitute around 3% of T cells in the blood yet their frequency varies widely among individuals (171), Moreover, MAIT cells reside at sites where other unconventional T cells are enriched such as human liver, contributing up to half of the T cells at this site (172). Activation of MAIT cells by microbial antigens such as 5-OP-RU drives the rapid secretion of pro-inflammatory cytokines including TNF, IFNγ, IL-17A and IL-21 as well as licencing for cytotoxicity (172, 173). In line with their conservation, abundance and potent effector response, MAIT cells play a key role during immune challenge of various pathogens, as has been demonstrated for *Mycobacterium bovis* BCG, *Klebsiella pneumoniae, Francisella tularensis* and *Legionella longbeachae* (73, 75, 174, 175). To date, considerable work has been carried out to identify MAIT cells in humans, including the use of surrogate markers CD161, TRAV1-2 and CD8 and more recently by generating MR1 tetramers loaded with microbial antigens (40, 61, 67). Analysis of MR1 tetramer$^+$ cells revealed that MAIT cells in peripheral blood can express a variety of co-receptors, including CD4, CD8αα, CD8αβ or both CD4 and CD8 co-receptors, described here as double positive for both co-receptors (DP), as well as being co-receptor deficient, described here as double negative for both co-receptors (DN) (61, 67). In humans, the majority of MAIT cells in peripheral blood express the CD8 co-receptor (61, 67, 126, 171).

The structure of CD8 and its function on T cells has been well elucidated. CD8 is expressed on the surface of some T cells, where it binds to MHC-I concomitantly with the TCR and improves recognition of antigen (99, 104, 176). On conventional $CD8^+$ T cells, CD8 exists as an αβ heterodimer that recognises an invariant region of MHC-I via two immunoglobulin-like ectodomains, one from each CD8 subunit. The highly conserved α3 domain on MHC-I that forms the majority of contacts with CD8 is spatially distinct from the TCR binding site, enabling CD8 and the TCR to engage MHC-I simultaneously (104). It is well established that the CD8-MHC-I interaction can profoundly alter CTL responses (177). Formation of a TCR-pMHC-I-CD8αβ tripartite complex increases the avidity of the complex and stabilises the TCR-pMHC-I complex, increasing T cell sensitivity for antigen (178, 179). CD8 can also exist as a CD8αα homodimer on various T cell subsets, including MAIT cells, as well as non-T cells, yet its role remains ill-defined (67, 94, 180). While both CD8 isoforms bind to MHC-I with a comparable affinity, greater activation of CTLs is observed with the CD8αβ co-receptor, suggesting that CD8β is important for co-receptor function (181, 182). CD8 contributes to signal transduction during activation by co-localising with the early signalling kinase, $p56^{Lck}$ (109). A motif on the cytosolic tail of CD8α is responsible for sequestering $p56^{Lck}$, however dimerisation of CD8α with CD8β is thought to assist the transit of the co-receptor and $p56^{Lck}$ to membrane lipid rapids enriched with CD3 complexes (109, 183). Thus, it has been proposed that CD8αβ, and not CD8αα, facilitate greater CTL function by virtue of access to CD3 signalling domains.

Some indirect evidence in favour of CD8 contributing to MAIT cell function exists, demonstrating that $CD8^+$ MAIT cell activation can be reduced or abrogated with CD8 blocking antibodies (71, 124, 126). However, an interaction between CD8 and MR1 has not been established. Moreover, antibody blocking of CD8 has previously been shown to impact on conventional T cell function indirectly (127). Comparatively, several studies have identified a direct interaction between co-receptors and MHC-like molecules. In mice, a subset of intra-epithelial lymphocytes (IELs) utilise the CD8αα co-receptor to bind the MHC-I related protein murine thymic leukemia antigen (TL) expressed on the intestinal epithelium (94). While TL is conserved in the α3 domain, the peptide binding groove is considerably disfigured, such that TL is unable to present antigen (184).

Consequently, CD8αα does not function as a normal co-receptor on these cells. Ligation of TL by CD8αα on IELs appears to coordinate with TCR-MHC-I interactions to regulate cytotoxic and proliferative responses, thus demonstrating a novel role for CD8αα on T cells (185). NKT cells share many phenotypic and functional characteristics with MAIT cells and are capable of utilising co-receptors (121, 122). Like MAIT cells, NKT cell co-receptor expression is varied, including expression of CD8αα, though most NKT cells express CD4 or are co-receptor deficient and these subsets differ functionally (186, 187). The CD4 co-receptor contributes to NKT cell responses by binding CD1d as well as aiding signal transduction in a $p56^{lck}$ dependent manner (121, 122).

In light of these data and the abundance of $CD8^+$ MAIT cells in peripheral blood, the role of CD8 on these cells was investigated. The data herein formally demonstrate an interaction between CD8 and MR1 and reveal its implications on the function of MAIT and other MR1-reactive T cells.

3.2 Results

3.2.1 The canonical binding site for CD8 is conserved in MR1

Using MR1-5-OP-RU tetramer the frequency of MAIT cells in peripheral blood mononuclear cells (PBMCs) segregated by co-receptor expression was determined from 12 healthy donors. As established in the literature (61, 67, 126, 171), the majority of MAIT cells expressed the CD8 co-receptor (50-95%) (**Fig. 3.1A and B**). In descending order, the next most abundant subsets were $CD4^{-}CD8^{-}$ double negative (DN), $CD4^{+}$ and $CD4^{+}CD8^{+}$ double positive (DP) cells with mean values of 10%, 4% and 4% respectively (**Fig. 3.1B**). As previously shown (171), the CD8 co-receptor usage was split among both CD8 isoforms, CD8αα homodimers or CD8αβ heterodimers, with mean values of 39% and 61% of $CD8^{+}$ MAIT cells respectively (**Fig. 3.1C**). Interestingly, the CD8 isoform usage by DP MAIT cells differed from CD8 single positive (SP) MAIT cells among donors, with mean values of 53% for CD8αα expression and 47% for CD8αβ expression (**Fig. 3.1D**). This is in contrast to non-MAIT $CD8^{+}$ T cells that predominantly express the CD8αβ co-receptor (**Fig. 3.1E**). Furthermore, MAIT cells typically express lower levels of CD8α and CD8β on the cell surface compared to other $CD8\alpha\beta^{+}$ T cells that are defined as MR1-5-OP-RU $tetramer^{-}$ (188) (**Fig. 3.1F and G**).

Because $CD8^{+}$ MAIT cells constitute the majority of MAIT cells in most individuals, it was hypothesised that the CD8 co-receptor may play a role in the recognition of MR1 and aid in MAIT cell function. Based on crystal structures of co-complexes between CD8 co-receptor and human and mouse MHC-I molecules (HLA-A*02:01, HLA-A*24:02, H-$2K^{b}$, H-$2D^{b}$) and the mouse MHC-like molecule TL, it is well established that the primary site of contact between CD8 and MHC-I involves the flexible motif termed the CD-loop located within the α3 domain of the MHC-I heavy chain (96, 99, 189, 190) (**Fig. 3.1H and I**). The CD loop is bound by both CD8 subunits; however, the molecular contacts are unevenly distributed, such that one CD8 subunit dominates the interaction. Designated CD8α1 and positioned proximal to the T cell surface, the CD8α1 subunit makes most of the contacts with the α3 domain of MHC-I, as well as all of the contacts with the α2 domain and β_2m within CD8αα-MHC-I complexes. At the centre of the CD-loop is a highly conserved glutamine residue at position 226 (Q226). This residue forms multiple

side- and main-chain contacts with both CD8 subunits (**Fig. 3.1J and K**), and as such is critically important for CD8 engagement. An alignment of MR1 with various mouse and human MHC-I molecules, as well as the MHC-like molecule TL, for which crystal structures in complex with CD8 have been determined, highlights the conservation between the critically important CD8 contact residues within the CD-loop (Q226 and E227) and neighbouring residues (**Fig. 3.1H and I**). Further, between species, MR1 is highly conserved in this region, although some minor differences do exist for some species (41, 90). The high sequence conservation between MR1 and the various MHC-I molecules examined suggested to us that the CD8 co-receptor may be capable of engaging MR1 in a manner analogous to MHC-I.

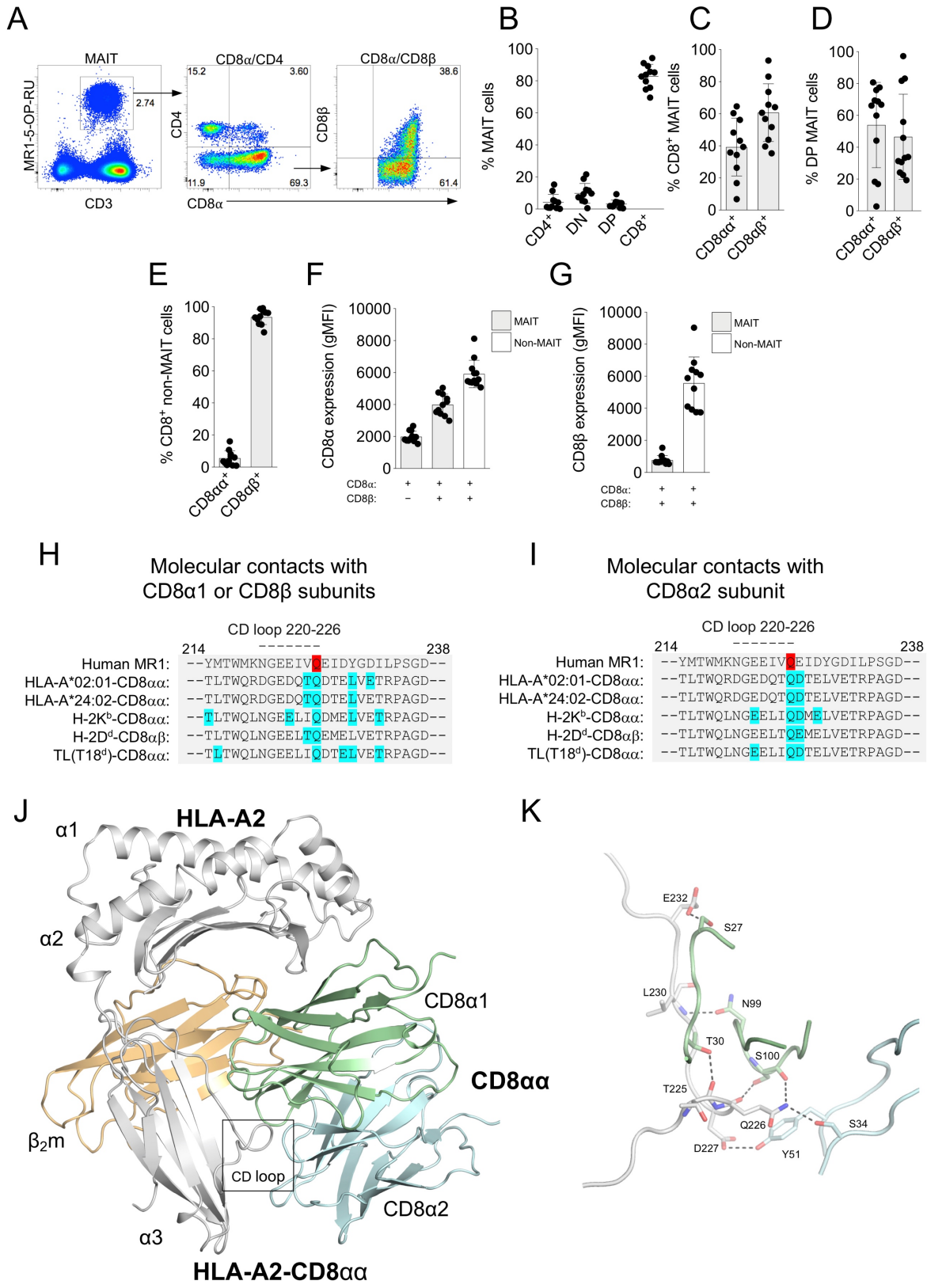

H

Molecular contacts with CD8α1 or CD8β subunits

CD loop 220-226

	214 ------- 238
Human MR1:	--YMTWMKNGEEIVEEIDYGDILPSGD--
HLA-A*02:01-CD8αα:	--TLTWQRDGEDQTQDTELVETRPAGD--
HLA-A*24:02-CD8αα:	--TLTWQRDGEDQTQDTELVETRPAGD--
H-2K^{b}-CD8αα:	--TLTWQLNGEELIQDMELVETRPAGD--
H-2D^{d}-CD8αβ:	--TLTWQLNGEELTQEMELVETRPAGD--
TL(T18^{d})-CD8αα:	--TLTWQLNGEELIQDTELVETRPAGD--

I

Molecular contacts with CD8α2 subunit

CD loop 220-226

	214 ------- 238
Human MR1:	--YMTWMKNGEEIVEEIDYGDILPSGD--
HLA-A*02:01-CD8αα:	--TLTWQRDGEDQTQDTELVETRPAGD--
HLA-A*24:02-CD8αα:	--TLTWQRDGEDQTQDTELVETRPAGD--
H-2K^{b}-CD8αα:	--TLTWQLNGEELIQDMELVETRPAGD--
H-2D^{d}-CD8αβ:	--TLTWQLNGEELTQEMELVETRPAGD--
TL(T18^{d})-CD8αα:	--TLTWQLNGEELIQDTELVETRPAGD--

Figure 3.1. Blood MAIT cells predominately express CD8 and the canonical CD8 binding site is conserved in MR1. **A.** Gating strategy for co-receptor usage by MAIT cells from peripheral blood identified using MR1-5-OP-RU tetramer; viable lymphocytes were gated based on forward and side scatter area, followed by forward and side scatter height to remove doublets, and finally a live/dead discriminator dye to exclude dead cells. **B.** Peripheral blood MAIT cell co-receptor usage showing the frequency of each subset (CD4, DN, DP and CD8) as a percentage of total MAIT cells. **C, D and E.** The frequency of CD8αα and CD8αβ usage as a percentage of $CD8^+$ SP MAIT cells, DP MAIT cells or non-MAIT T cells. **F and G.** Geometric mean fluorescence intensity (gMFI) of CD8α and CD8β expressed on $CD8\alpha\alpha^+$ and $CD8\alpha\beta^+$ MAIT cells compared to other $CD8\alpha\beta^+$ T cells (non-MAIT). **B to G.** Accumulated data from the same 11 healthy blood donors, assessed in two experiments, showing mean and SD. **H and I.** Alignment of a section of the α3 domains of human and mouse MHC-I molecules with human MR1, annotated with the hydrogen bonds (highlighted in blue) between both the T cell proximal and distal CD8 subunits respectively. CD8 interactions were identified with PDBsum (191) using entries with PDB IDs; 1AKJ (99), 3QZW (189), 1BQH (96), 3DMM (190) and 1NEZ (119). **(J)** Schematic representation of the CD8-MHC-I interaction based on the crystal structure of the complex between HLA-A*02:01 and CD8αα (PDB ID 1AKJ (99)), highlighting the CD loop, the primary site of engagement between MHC-I and CD8. **(K)** A schematic of the hydrogen bonds between CD8 and MHC-I within the region 214-238, including the CD loop, based on the crystal structure of the complex between HLA-A*02:01 and CD8αα (PDB ID 1AKJ (99)).

3.2.2 The CD8 co-receptor binds MR1 in a similar manner as MHC-I

To examine whether the CD8 co-receptor can engage MR1, staining of CD8 expressing T cell lines with MR1 and MHC-I tetramers was assessed. For this purpose, β_2m-deficient SKW-3 cells (SKW-3.$\beta_2m^{-/-}$), generated previously from parental SKW-3 cells, were transduced with either CD8αα (SKW-3.$\beta_2m^{-/-}$.CD8αα) or CD8αβ (SKW-3.$\beta_2m^{-/-}$.CD8αβ) (**Fig. 3.2A**) and parental and CD8 transduced cell lines were stained with MR1 tetramers refolded with 5-OP-RU, 6-FP and Ac-6-FP (**Fig. 3.2B, data not shown**). Intriguingly, despite being deficient in cognate TCR, MR1-Ac-6-FP and -5-OP-RU tetramers were capable of staining the CD8αα and CD8αβ expressing cell lines (**Fig. 3.2B and C**). The ability of other MHC-I and MHC-I-like tetramers to stain the CD8 expressing cell lines was next investigated, including; HLA-A*02:01-NLV, a mutant (Q115E) HLA-A*02:01-NLV that binds more strongly to CD8, HLA-B*08:01-FLR, HLA-C*06:02-TRAT and HLA-G*01:01-RII (**Fig. 3.2C**). It was noted that all tetramers were capable of engaging both CD8αα and CD8αβ expressing cell lines to varying degrees in the absence of TCR. Interestingly, the hierarchy of fluorescence intensity between the labelled tetramers was different when engaging CD8αα or CD8αβ (**Fig. 3.2C**). Substantially greater staining was observed across all tetramers binding to the CD8αα expressing cell line compared to the CD8αβ expressing cell line (**Fig. 3.2C**), possibly due to the disparate expression of CD8α between the cell lines (**Fig. 3.2A**). While MR1 tetramers stained the CD8αα expressing cell line comparatively weakly compared to wild type HLA-A*02:01 tetramers, they stained the CD8αβ expressing cell line more strongly than wild type HLA-A*02:01 tetramers (**Fig. 3.2C**). Similarly, both HLA-B*08:01 and HLA-C*06:02 tetramers stained the CD8αβ cell line more strongly than the HLA-A2 tetramer (**Fig. 3.2C**). Thus, although largely conserved in the CD8 binding domain, different MHC-I and related molecules appear to engage CD8 isoforms distinctly. Nevertheless, it was observed that both isoforms of CD8, if overexpressed, could bind to MR1 in the absence of TCR and that this interaction likely occurs independently of antigen. To further elucidate differences in CD8 binding, the CD8αα and CD8αβ cell lines were stained with wild type MR1-5-OP-RU or HLA-A*02:01-NLV tetramers and the dissociation of tetramers over time was examined (**Fig. 3.2D**). Despite the MR1 tetramers staining the CD8αβ cell line more strongly than the HLA-A*02:01

tetramers, MR1 tetramers dissociated faster from both cell lines, and reached a state of equilibrium of ~60% and ~45% of the fluorescence at time zero for the CD8αα and CD8αβ cell lines respectively (**Fig. 3.2D**). Comparatively, the HLA-A*02:01-NLV tetramers reached a state of equilibrium of ~80% and ~60% of the fluorescence at time zero for the CD8αα and CD8αβ cell lines respectively, dissociating substantially slower than MR1 tetramers from the CD8αα cell line (**Fig. 3.2D**).

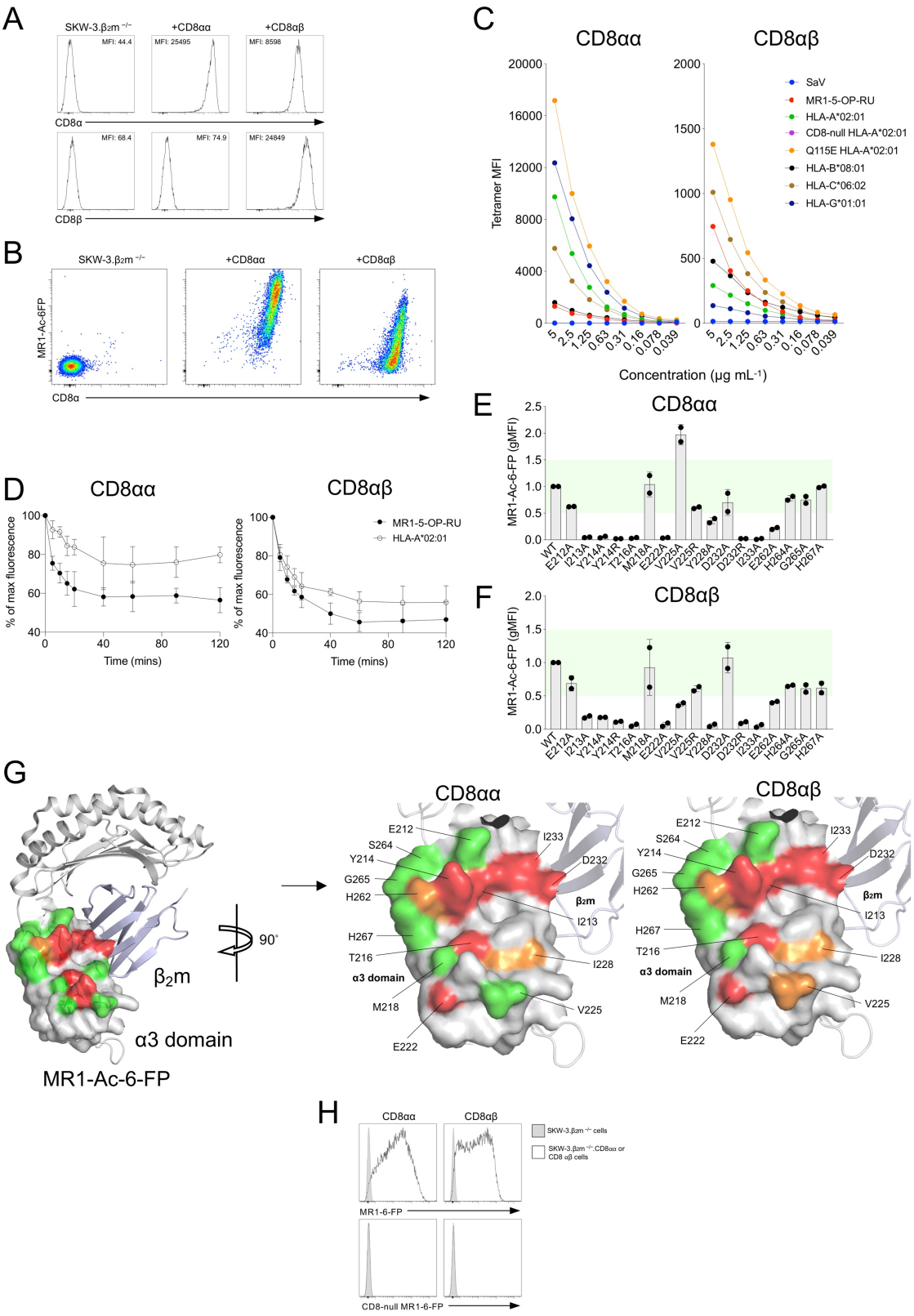
A
SKW-3.β2m −/−
+CD8αα
+CD8αβ
MFI: 44.4
MFI: 25495
MFI: 8598
CD8α
MFI: 68.4
MFI: 74.9
MFI: 24849
CD8β
B
SKW-3.β2m −/−
+CD8αα
+CD8αβ
MR1-Ac-6FP
CD8α
C
CD8αα
CD8αβ
Tetramer MFI
SaV
MR1-5-OP-RU
HLA-A*02:01
CD8-null HLA-A*02:01
Q115E HLA-A*02:01
HLA-B*08:01
HLA-C*06:02
HLA-G*01:01
Concentration (μg mL-1)
D
CD8αα
CD8αβ
% of max fluorescence
MR1-5-OP-RU
HLA-A*02:01
Time (mins)
E
CD8αα
MR1-Ac-6-FP (gMFI)
WT
E212A
I213A
Y214A
Y214R
T216A
M218A
E222A
V225A
V225R
Y228A
D232A
D232R
I233A
E262A
H264A
G265A
H267A
F
CD8αβ
MR1-Ac-6-FP (gMFI)
G
β2m
α3 domain
MR1-Ac-6-FP
90˚
CD8αα
CD8αβ
E212
S264
Y214
G265
H262
H267
T216
α3 domain
M218
E222
I233
D232
β2m
I213
I228
V225
H
CD8αα
CD8αβ
SKW-3.β2m −/− cells
SKW-3.β2m −/−.CD8αα or CD8 αβ cells
MR1-6-FP
CD8-null MR1-6-FP

Figure 3.2. MR1 binds to both isoforms of CD8 and MR1 α3 domain mutations abrogate binding. **A.** Histograms displaying CD8α and CD8β expression on SKW-3.$\beta_2m^{-/-}$, SKW-3.$\beta_2m^{-/-}$.CD8αα and SKW-3.$\beta_2m^{-/-}$.CD8αβ cell lines. **B.** Comparison of MR1-Ac-6-FP tetramer binding to SKW-3.$\beta_2m^{-/-}$, SKW-3.$\beta_2m^{-/-}$.CD8αα and SKW-3.$\beta_2m^{-/-}$.CD8αβ cell lines. **C.** Fluorescence staining (gMFI) of SKW-3.$\beta_2m^{-/-}$.CD8αα and SKW-3.$\beta_2m^{-/-}$.CD8αβ cell lines with serially diluted SAv-fluorochrome, wild type MR1-5-OP-RU and wild type or CD8-null MHC-I tetramers. **D.** Tetramer dissociation of MR1-5-OP-RU (filled dots) and HLA-A*02:01-NLV (clear dots) tetramers from the CD8αα and CD8αβ cell lines over 120 mins. Data points display mean and SD from four independent experiments. **E and F.** Fold change compared to wild type MR1-Ac-6-FP tetramer staining of SKW-3.$\beta_2m^{-/-}$.CD8αα and SKW-3.$\beta_2m^{-/-}$.CD8αβ cell lines with α3 domain mutant MR1-Ac-6-FP tetramers. Green section marks a ±0.5 change from baseline. **G.** Schematic representation of MR1-Ac-6-FP (PDB ID 4PJ5 (58)) with a colour coded α3 domain Connolly surface overlay. Green, orange and red shading represent α3 domain residues that confer no loss, moderate loss (>0.5 fold reduction) or complete loss of tetramer binding respectively for both SKW-3.$\beta_2m^{-/-}$.CD8αα (left) and SKW-3.$\beta_2m^{-/-}$.CD8αβ cell lines (right). **H.** Histograms for MR1-6-FP (top panel) and CD8-null MR1-6-FP (bottom panel) tetramer staining fluorescence of wild type (grey), CD8αα or CD8αβ (white) SKW-3.$\beta_2m^{-/-}$ cell lines. **A, B, C, E, F, H.** Data are representative of two independent experiments.

To interrogate which residues in the α3 domain of MR1 were contributing to the CD8-MR1 interaction, the CD8 expressing cell lines were stained with a panel of MR1 tetramers mutated at single residues (**Fig. 3.2E and F)**, some of which have previously been shown to abrogate CD8 binding of MHC-I molecules, termed 'CD8-null' mutations (179, 192). Overall, there was a similar pattern of staining of the CD8αα and CD8αβ lines for most mutant MR1 tetramers, suggesting the isoforms engage MR1 in a similar manner. Residue mutations I213A, Y214A, T216A, E222A, D232A and I233A significantly reduced tetramer staining with both CD8 dimer expressing cell lines (**Fig. 3.2E and F**). All of these residues or equivalently positioned residues, with the exception of residue 213, formed contacts within CD8-MHC-I ternary complexes. The mutations E105A, E212A, M218A, V225A, S264A and G265A had no effect on CD8 binding whereas mutation H262A moderately reduced tetramer staining (**Fig. 3.2E and F**). Residue I228 only moderately reduced tetramer staining with the CD8αα expressing cell line when mutated to alanine, yet substantially reduced tetramer staining with the CD8αβ expressing cell line (**Fig. 3.2E and F**). Surprisingly, mutation V225A enhanced tetramer binding by CD8αα and slightly reduced tetramer binding to CD8αβ whereas an arginine mutation at the same position (V225R) only subtly reduced binding by CD8αα and CD8αβ (**Fig. 3.2E and F**). These data suggest that subtle differences in MR1 engagement between CD8αα and CD8αβ exist, however the overall footprint on MR1 is likely comparable as modelled in (**Fig. 3.2G**). Given the large overlap in the residues involved in CD8 binding of MR1 and MHC-I, CD8 likely contacts MR1 in a manner analogous to MHC-I.

Based on the mutational analysis of MR1 and previously described CD8-null MHC-I mutations (179, 192, 193), it was hypothesised that generating an MR1 double mutant would abrogate the CD8-MR1 interaction. 'CD8-null' (Q226A and E227K) MR1-5-OP-RU and MR1-6-FP tetramers (**Fig. 3.3A and B**) were generated and their ability to stain the CD8 expressing cell lines was compared against equivalently produced wild type MR1 tetramers (**Fig. 3.2H**). No staining of either CD8 expressing cell lines was observed using CD8-null MR1 tetramers, indicating complete abrogation of the CD8-MR1 interaction and thereby revealing that CD8 on MAIT cells is capable of engaging MR1 in a manner consistent with MHC-I (96, 99, 178, 189, 190, 194). Importantly, these mutations did not impact recognition by a MAIT TCR transduced cell line that does not express CD8 (**Fig. 3.3C**), validating their use as CD8-null MR1 tetramers. Based on tetramer fluorescence, the affinity of the CD8-MR1 interaction was estimated to be similar to the affinity reported for CD8-HLA-B8 (104, 194-198).

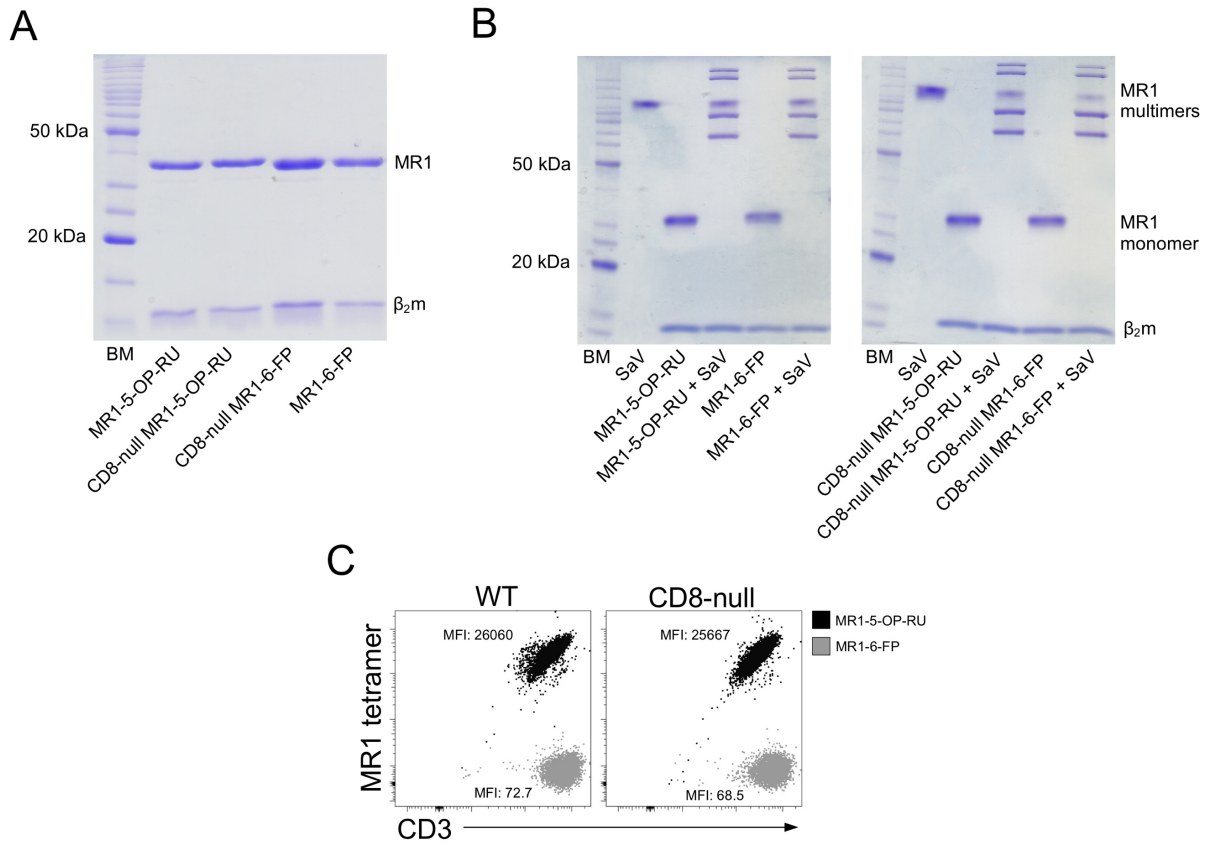

Figure 3.3. In vitro folded wild type and mutant MR1 tetramers are recognized by a prototypic MAIT TCR in an antigen dependent manner. **A.** Wild type and CD8-null MR1 monomers folded with 5-OP-RU or 6-FP (5µg each) were separated on a 15% SDS-PAGE under reducing conditions using 1mM DTT alongside a molecular weight marker (BM) with a protein range of 10-220 kDa. Proteins were identified based on staining with Coomassie Blue R-250 dye. **B.** Wild type and CD8-null MR1 monomers folded with 5-OP-RU or 6-FP (5µg each) were mixed with Streptavidin (SAv) (5µg) and separated on a 12% SDS-PAGE under non-reducing conditions with SAv alone, or MR1-6-FP and MR1-5-OP-RU monomers alone alongside a molecular weight marker (BM) with a protein range of 10-220 kDa. Proteins were identified based on staining with Coomassie Blue R-250 dye. **C.** Dot plots of a MAIT TCR transduced (CD8-deficient) Jurkat-76 cell line stained with wild type and CD8-null MR1 tetramers, assessed by flow cytometry. Data are representative of two independently performed experiments.

3.2.3 CD8 binding enhances MR1 tetramer avidity

Given the experiments described above were performed on cell lines that overexpress CD8, it was next investigated whether CD8 binding to MR1 impacts on MR1 tetramer staining of primary MAIT cells. PBMCs from 12 donors were stained with wild type and CD8-null MR1 tetramer. In most donors, a discernible population of MR1-5-OP-RU tetramer positive cells was identified for all MAIT cell co-receptor subsets (**Fig. 3.4A**). Notably, the $CD8^+$ MAIT cell subsets exhibited the highest level of tetramer staining across all donors stained with wild type MR1-5-OP-RU, with an average mean fluorescence intensity of 20768, 18775 and 20584 for DP, CD8αα and CD8αβ expressing MAIT cells, respectively, compared to 13493 and 13963 for CD4 and DN subsets respectively (**Fig. 3.4A and B**). Notably, differences in tetramer staining of MAIT cell co-receptor subsets cannot be attributed to differences in TCR expression levels, which were consistent based on CD3 expression levels (**Fig. 3.4C**)**.** Within individual donors, $CD8^+$ expressing MAIT cells stained with wild type MR1-5-OP-RU tetramer significantly brighter compared to the other subsets (**Fig. 3.4D**). The amount of surface expressed CD8 was examined to assess whether different CD8 levels correlated with tetramer fluorescence by examining $CD8^+$ MAIT cell populations based on low, intermediate or high CD8 expression (**Fig. 3.4E and F**). A consistent difference in tetramer fluorescence was observed between individual donors, dependent on CD8 expression (**Fig. 3.4F**). These data strongly support the notion that CD8 contributes to MR1 recognition. To verify whether the increase in MR1-5-OP-RU tetramer staining of $CD8^+$ MAIT cells was due to CD8 co-operatively engaging MR1 with the TCR, the level of tetramer staining of wild type and CD8-null MR1-5-OP-RU tetramer staining of each PBMC donor were compared (**Fig. 3.4A and G**). A significant reduction in tetramer fluorescence intensity on all three populations of $CD8^+$ T cell was observed when stained with the CD8-null MR1-5-OP-RU tetramer compared to wild type MR1-5-OP-RU tetramer. In contrast, there was no significant difference between the two tetramers on the CD4 and DN subsets of MAIT cells. Thus, the CD8 co-receptor significantly contributes to the avidity of MR1 tetramer binding by MAIT cells, suggesting that CD8 may function to modulate the activation of MAIT cells.

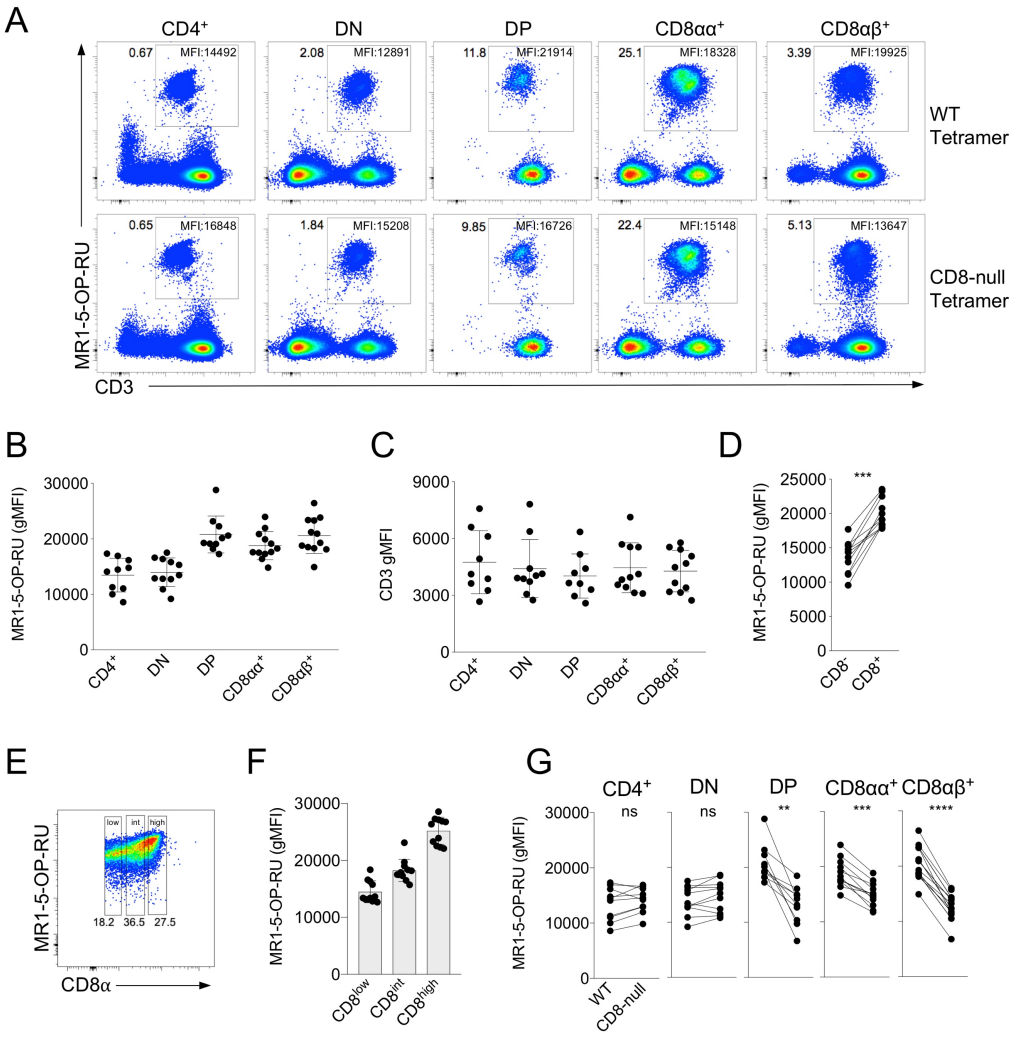

Figure 3.4. CD8⁺ MAIT cells stain brightest with MR1 tetramers and CD8-null MR1 mutations significantly reduce tetramer fluorescence. **A.** MAIT cell subsets pre-gated on co-receptor usage and identified using MR1-5-OP-RU tetramers in human PBMC of healthy donors. The geometric mean fluorescence (gMFI) for each population is displayed in the upper right of each plot. **B.** Pooled (10-12 data points per group) gMFI of MAIT cell co-receptor subsets staining with MR1-5-OP-RU tetramer showing mean and SD. **C.** CD3 expression (gMFI) of MAIT cell co-receptor subsets from 11 donors identified using MR1-5-OP-RU tetramer, analysed as part of experiments shown in Figures 1 and 3. Mean and SD is displayed. **D.** Comparison of $CD8^-$ and $CD8^+$ MAIT cells wild type MR1-5-OP-RU tetramer gMFI. **E.** Gating strategy for defining $CD8^+$ MAIT cells as low, intermediate and high for CD8α expression. **F.** Comparison of wild type MR1-5-OP-RU tetramer gMFI between low, intermediate and high CD8α expressing MAIT cells, showing mean and SD. **G.** Comparison of wild type and CD8-null MR1-5-OP-RU tetramer gMFI between MAIT cell co-receptor subsets for each donor. **A-G.** Shown is the accumulated data from the same 11 healthy blood donors, assessed in Figure 1. Data are cumulative of two independent experiments. **D and G.** Statistical significance (two-tailed, $P < 0.5$) was evaluated using a Wilcoxon signed-rank test.

3.2.4 CD8 interaction with MR1 augments functional outcome of Ag-recognition by MAIT cells

Having demonstrated that the CD8 co-receptor is capable of binding to MR1 on MAIT cells, it was next addressed whether CD8-MR1 engagement contributes to the functional potential of MAIT cells. To examine the impact of CD8 ligation on MAIT cell activation, the production of IFNγ and TNF cytokines by primary MAIT cells, a reliable measure of MAIT cell activation *in vitro* (40, 172), was assessed. TRAV1-2^{+} cells from 11 healthy PBMC donors were enriched and co-incubated with 5-OP-RU pulsed MR1 deficient C1R cells (C1R.MR1$^{-/-}$) or with C1R cells expressing similar levels of either wild type MR1 (C1R.MR1^{++}) or CD8-null (Q226K, E227A) MR1 (C1R.CD8-null MR1^{++}) (**Fig. 3.5A and B**). As expected, MAIT cells incubated with 5-OP-RU pulsed C1R.MR1$^{-/-}$ cells did not produce any cytokines (**Fig. 3.5C and G**). TRAV1-2^{+} cells cultured in the absence of C1R cells but in the presence of 5-OP-RU antigen, induced TNF production in a small proportion of cells, while no discernible fraction of cells produced IFNγ (**Fig. 3.5C and G**), suggesting that MAIT cells are capable of presenting MR1-antigen at low levels (199, 200). Notably, C1R.MR1^{++} cells pulsed with 5-OP-RU elicited potent cytokine production by MAIT cells from all donors, with ~30% of cells producing IFNγ and ~70% of cells producing TNF (**Fig. 3.5B, C and G**). Both the percentage of IFNγ and TNF producing MAIT cells stimulated with 5-OP-RU pulsed C1R.MR1^{++} cells tended to be greater within the CD8 subset with mean percentages of 49% and 78% respectively (**Fig. 3.5D and H**). In contrast, the fraction of the CD4^{+} subset of MAIT cells that produced IFNγ and TNF was the lowest of all subsets with mean percentages of 9.8% and 25.9% respectively (**Fig. 3.5D and H**). Mean percentages of IFNγ and TNF producing DN MAIT cells were 37.1% and 69.0% respectively (**Fig. 3.5D and H**). Given that there is some variation in cytokine production by CD4^{+}, DN, DP and CD8^{+} MAIT cell subsets, the percentages of IFNγ and TNF producing cells in individual donors were compared. Here it was found that the fraction of CD8αα^{+} cytokine producing MAIT cells was significantly higher for both cytokines compared to DN cytokine producing MAIT cells (**Fig. 3.5E and I**), indicating that CD8αα^{+} MAIT cells are more potent at producing cytokines under these experimental conditions (**Fig. 3.5E and I**).

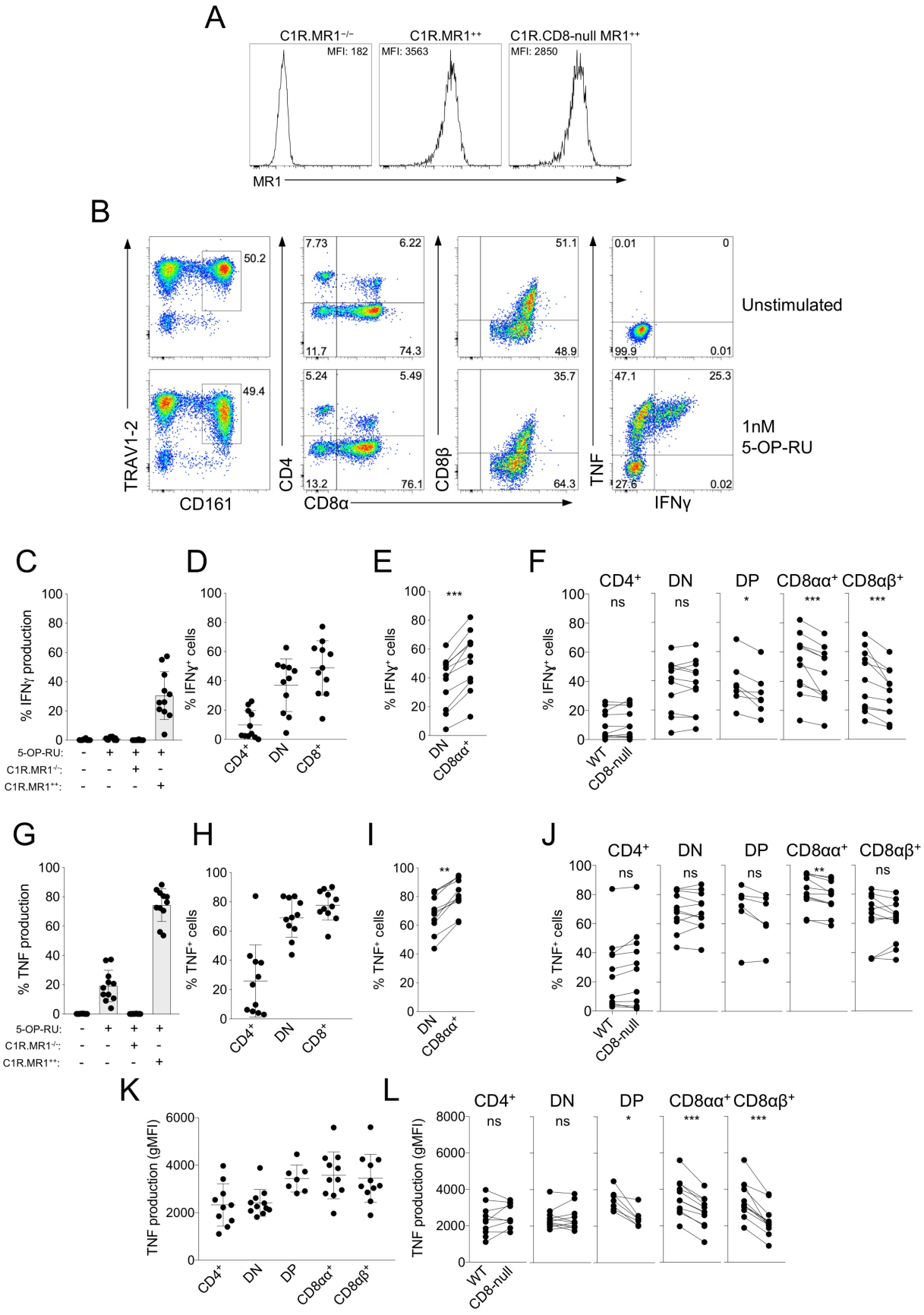
A
C1R.MR1−/−
C1R.MR1++
C1R.CD8-null MR1++
MFI: 182
MFI: 3563
MFI: 2850
MR1
B
TRAV1-2
CD161
CD4
CD8α
CD8β
TNF
IFNγ
Unstimulated
1nM
5-OP-RU
C
% IFNγ production
5-OP-RU:
C1R.MR1-/-:
C1R.MR1++:
D
% IFNγ+ cells
CD4+
DN
CD8+
E
% IFNγ+ cells
DN
CD8αα+
F
CD4+
DN
DP
CD8αα+
CD8αβ+
% IFNγ+ cells
ns
*
***
WT
CD8-null
G
% TNF production
H
% TNF+ cells
I
% TNF+ cells
J
% TNF+ cells
**
K
TNF production (gMFI)
L
TNF production (gMFI)

Figure 3.5. Cytokine production is reduced in CD8$^+$ MAIT cells in the absence of CD8 co-receptor engagement of MR1. **A.** MR1 expression levels on C1R.MR1$^{-/-}$ cells and wild type or CD8-null MR1 overexpressing C1R cells displayed as histograms. **B.** Identification of MAIT cells using surrogate markers CD161 and TRAV1-2 (left plots), and analysis of co-receptor usage and cytokine production of unstimulated and *in vitro* antigen stimulated MAIT cells (middle and right plots). **C.** Percentage of IFNγ production by unstimulated MAIT cells, and MAIT cells stimulated with 1nM 5-OP-RU in the absence of C1R cells, in the presence of C1R.MR1$^{-/-}$ cells or C1R.MR1^{++} cells. **D.** Comparison of IFNγ producing MAIT cells stimulated with 1nM 5-OP-RU in the presence of C1R.MR1^{++} cells segregated by co-receptor subset. **E.** Comparison of IFNγ producing CD8αα$^+$ MAIT and DN MAIT cell among individual donors. **F.** Comparison of IFNγ producing MAIT cells stimulated with 1nM 5-OP-RU in the presence of C1R.MR1^{++} or C1R.CD8-null MR1^{++} cells. **G, H, I and J.** Same format as C, D, E and F but examining the percentage of TNF producing MAIT cells. **K.** gMFI of TNF produced by MAIT cells in response to 1nM 5-OP-RU in the presence of C1R.MR1^{++} cells, segregated by co-receptor expression. **L.** Comparison of gMFI of TNF produced by MAIT cells in response to 1nM 5-OP-RU in the presence of C1R.MR1^{++} or C1R.CD8-null MR1^{++} cells, segregated by co-receptor expression. **C-L.** Show the accumulated data of 11 individuals, assessed in three independently performed experiments. **C, D, G, H and K.** show mean and SD. **E, F, I, J and L.** Statistical significance (two-tailed, P <0.5) was evaluated using a Wilcoxon signed-rank test.

A comparison of cytokine production by MAIT cell subsets stimulated with 5-OP-RU in the presence of C1R.MR1^{++} or C1R.CD8-null MR1^{++} cells revealed in individual donors a significant reduction in the percentage of IFNγ producing MAIT cells by all three subsets of CD8^{+} MAIT cells (DP, CD8αα and CD8αβ), while CD8^{-} MAIT cells (CD4 and DN) were unaffected (**Fig. 3.5F**). A similar trend was also observed for TNF production by most donors, however a significant difference was only recorded for CD8αα^{+} T cells (**Fig. 3.5J**), suggesting that the CD8αα isoform may engender MAIT cells with a greater functional advantage over other CD8 (DP and CD8αβ) expressing subsets and over CD8^{-} (CD4 and DN) MAIT cell subsets. Similarly, IFNγ expression appeared to be affected greater than TNF by CD8 blockade of TRAV1-2 CD161^{++} cells stimulated using *E. coli* infected monocytic cells (124). While no significant difference was observed in the percentage of TNF producing cells by DP and CD8αβ MAIT cells, possibly due to the maximal stimulation of the MAIT cells, analysis of TNF fluorescence intensity revealed that all subsets of CD8^{+} MAIT cells had a tendency to produce more TNF than CD4 and DN MAIT cells (**Fig. 3.5K**) and furthermore, a significant reduction in TNF fluorescence intensity was recorded with the CD8-null mutant C1R cells (**Fig. 3.5L**). Accordingly, these data closely align with the MR1 tetramer staining, and highlight that the CD8-MR1 interaction contributes to the functional potential of MAIT cells.

3.2.5 MR1-6-FP-reactive T cells are largely dependent on CD8 for MR1-6-FP tetramer recognition

Previous studies have identified MR1-reactive T cells reactive to empty MR1 tetramers (termed MR1 autoreactive) or reactive to antigens other than 5-OP-RU, including the folate derivatives 6-FP and Ac-6-FP (201), drug like metabolites (202), endogenous antigens (203) as well as antigens from a microbe deficient in the riboflavin biosynthesis pathway (204). Curiously, many of these MR1-reactive T cells also express CD8, including almost all folate derivative reactive cells (201). Thus, the role of CD8 in the reactivity to antigens other than 5-OP-RU was examined. The folate derivatives 6-FP and Ac-6-FP, that have been shown to upregulate MR1 surface expression and are recognised by MR1-reactive T cells, were selected as model antigens (40, 58, 201). Using MR1-6-FP tetramer, MR1-6-FP-reactive T cells were enriched from PBMCs of 12 healthy donors and segregated based on TRAV1-2 expression into MR1-6-FP-reactive MAIT cells (TRAV1-2^{+}) and MR1-6-FP-reactive atypical MR1-reactive T cells (TRAV1-2^{-}) and expanded *in vitro* with anti-CD3 and anti-CD28 stimulation (**Fig. 3.6A**). After expansion both subsets of MR1-reactive T cells were stained with wild type MR1-6-FP tetramers and CD8α (**Fig. 3.6B, C and D**).

Within the TRAV1-2^{-} subset, amongst donors a mean average of 85% of cells were CD8α^{+} and 6-FP reactivity was retained, with a mean average of 64% of cells binding MR1-6-FP tetramer, and a proportion of these cells displaying cross-reactivity to MR1-5-OP-RU tetramer with a mean average of 37% amongst donors (**Fig. 3.6B and C**), akin to a previously published study (201). Strikingly, when the TRAV1-2^{-} subset was stained with CD8-null MR1 tetramers, the majority of cells in all donors could not recognise either MR1-6-FP or MR1-5-OP-RU tetramers (**Fig. 3.6E and G**), indicating that these cells required CD8 binding for recognition of MR1 tetramers, regardless of antigen specificity.

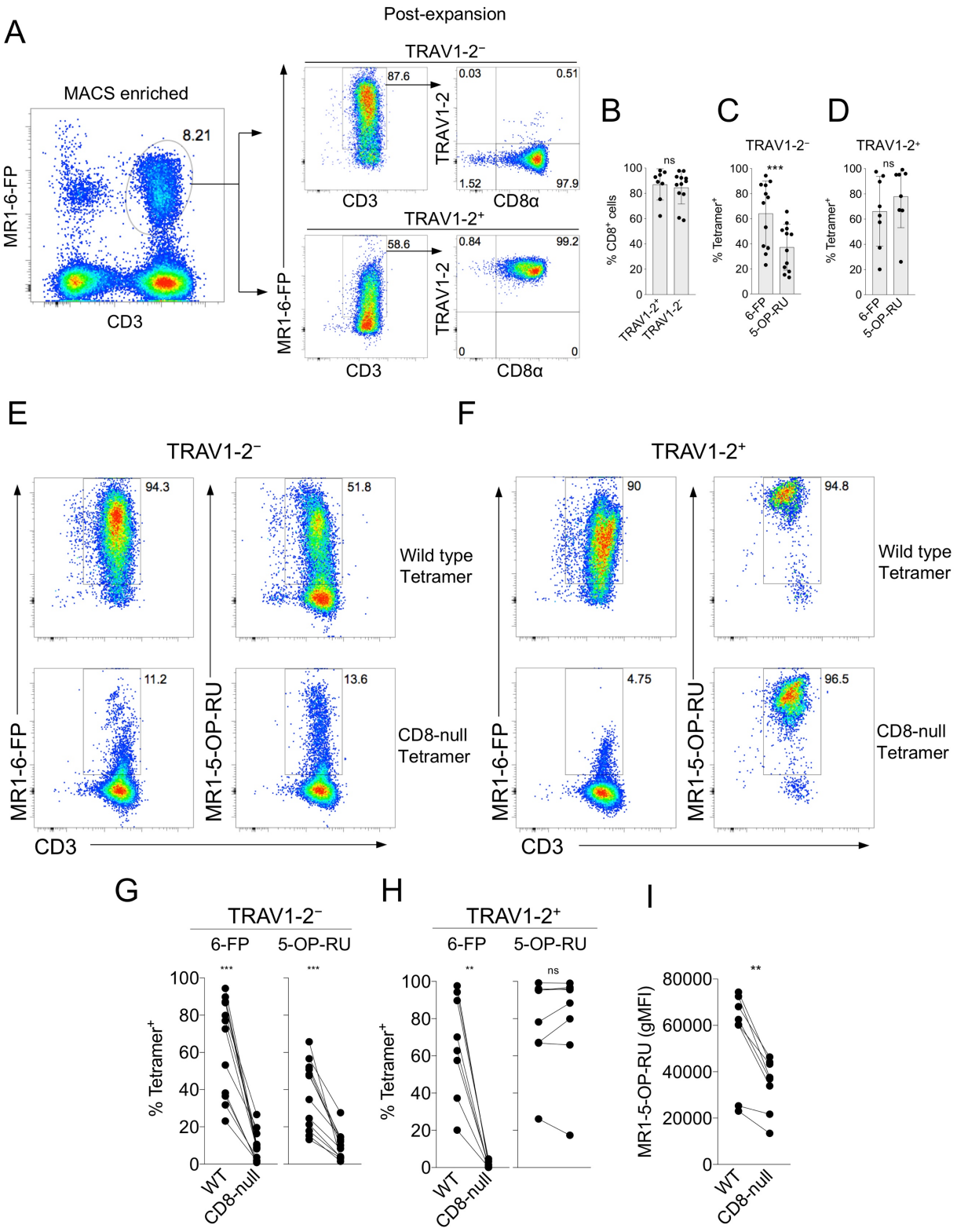
A
Post-expansion
MACS enriched
8.21
MR1-6-FP
CD3
TRAV1-2⁻
87.6
0.03
0.51
TRAV1-2
CD3
CD8α
1.52
97.9
TRAV1-2⁺
58.6
0.84
99.2
MR1-6-FP
0
0
B
% CD8⁺ cells
ns
TRAV1-2⁺
TRAV1-2⁻
C
TRAV1-2⁻
% Tetramer⁺
***
6-FP
5-OP-RU
D
TRAV1-2⁺
% Tetramer⁺
ns
6-FP
5-OP-RU
E
TRAV1-2⁻
94.3
51.8
Wild type Tetramer
11.2
13.6
CD8-null Tetramer
MR1-6-FP
MR1-5-OP-RU
CD3
F
TRAV1-2⁺
90
94.8
Wild type Tetramer
4.75
96.5
CD8-null Tetramer
MR1-6-FP
MR1-5-OP-RU
CD3
G
TRAV1-2⁻
6-FP
5-OP-RU
***
***
% Tetramer⁺
WT
CD8-null
H
TRAV1-2⁺
6-FP
5-OP-RU
**
ns
% Tetramer⁺
WT
CD8-null
I
**
MR1-5-OP-RU (gMFI)
WT
CD8-null

Figure 3.6. MR1-6-FP-reactive T cells are largely dependent on CD8 for MR1-6-FP tetramer recognition. **A.** Identification of MR1-6-FP tetramer enriched T cells from peripheral blood directly *ex vivo* and surface phenotype after 14 days of expansion *in vitro,* segregated by TRAV1-2 expression. **B.** Percentage of expanded TRAV1-2^{+} and TRAV1-2^{-} cell CD8α expression, showing mean and SD. **C and D.** Percentage of TRAV1-2^{-} or TRAV1-2^{+} T cells that are reactive to MR1-6-FP or 5-OP-RU tetramers after expansion from 12 healthy donors, showing mean and SD. **E and F.** Expanded TRAV1-2^{-} or TRAV1-2^{+} T cells stained with wild type (WT) MR1-6-FP or CD8-null MR1-6-FP and MR1-5-OP-RU tetramers. **G and H.** Comparison of WT and CD8-null MR1-6-FP and MR1-5-OP-RU tetramer staining of expanded TRAV1-2^{-} or TRAV1-2^{+} cells for 12 or 8 donors respectively. **I.** Comparison of WT and CD8-null MR1-5-OP-RU tetramer gMFI of expanded TRAV1-2^{+} cells. **B, C, D, G, H and I.** Show the accumulated data of 8-12 individuals, assessed in three independently performed experiments. **G-I**. Statistical significance (two-tailed, P <0.5) was evaluated using a Wilcoxon signed-rank test.

Within the TRAV1-2$^+$ subset, amongst donors a mean average of 87% of cells were CD8α^+ and 6-FP reactivity was retained with a mean average of 66% of cells that bound to MR1-6-FP tetramer (**Fig. 3.6B and D**). Consistent with the expression of TRAV1-2 by these cells, the preferred TCR for MAIT cells, more of these cells recognised MR1-5-OP-RU compared to the TRAV1-2$^-$ cells, with a mean average of 78% of cells amongst donors binding to MR1-5-OP-RU tetramer (**Fig. 3.6D**). Similar to the TRAV1-2$^-$ subset, most TRAV1-2$^+$ cells failed to bind the CD8-null MR1-6-FP tetramer but interestingly retained the ability to bind the CD8-null MR1-5-OP-RU tetramer suggesting that a component of the interaction is intrinsically due to weak Ag cross-reactivity and/or autoreactivity to MR1 of these MAIT TCRs (**Fig. 3.6F and H**). Closer analysis of the MR1-5-OP-RU tetramer staining revealed a reduction in fluorescence intensity of the CD8-null tetramer compared to wild type tetramer (**Fig. 3.6I**), indicating that CD8 plays a role in MR1-5-OP-RU recognition for this subset of cross-reactive MR1-reactive T cells.

3.2.6 MR1-6-FP/Ac-6-FP-reactive T cells are largely dependent on CD8 for cytokine production

To examine whether the interaction between CD8 and MR1 also impacted on their function, the cytokine potential of these cells following activation was assessed. Enriched MR1-6-FP tetramer reactive T cells from four healthy PBMC donors were expanded *in vitro* as described above and their reactivity to MR1-6-FP tetramers was confirmed (**Fig. 3.7A**). Due to the heterogeneous phenotype of TRAV1-2$^-$ MR1-reactive T cells (201), the dominant cytokines produced by these cells were determined by measuring the production of various Th1, Th2 and Th17 cytokines upon PMA/Ionomycin stimulation (**Fig. 3.7B**). IFNγ, followed by TNF as well as IL-13 were identified as the most abundant cytokines secreted in all donors (**Fig. 3.7B**), and were included as activation markers in subsequent assays.

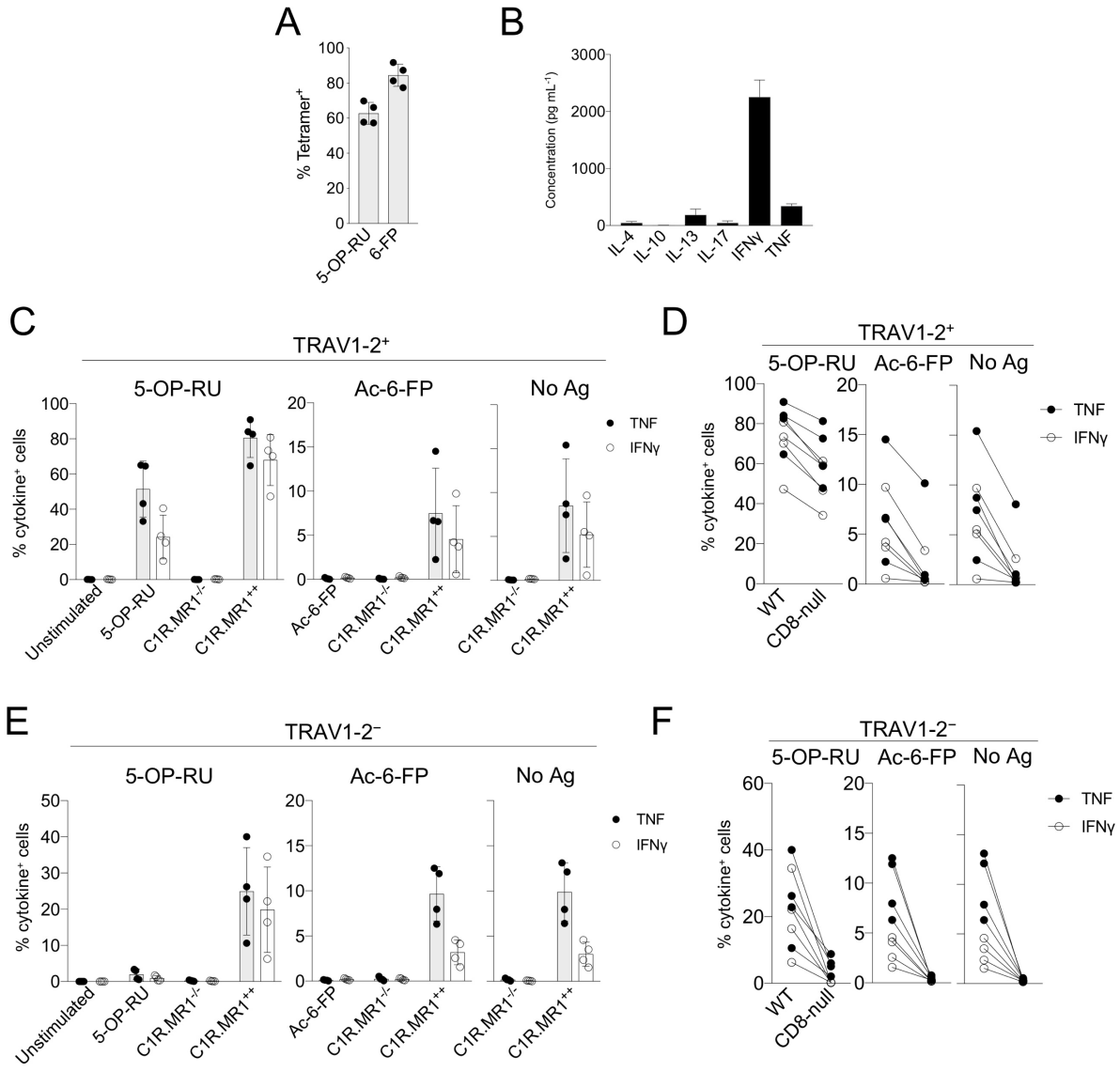

Figure 3.7. MR1-6-FP/Ac-6-FP-reactive T cells are largely dependent on CD8 for cytokine production. **A.** Percentage of MR1-5-OP-RU^{+} and MR1-6-FP^{+} cells after *in vitro* expansion. **B.** Concentration of common Th1, Th2 and Th17 cytokines in the supernatant of cultured MR1-6-FP-reactive expanded T cells after 24 h stimulation with PMA and Ionomycin. **C.** Percentage of TNF (black) and IFNγ (white) producing expanded TRAV1-2^{+} cells cultured without C1R cells or with C1R.MR1$^{-/-}$ or C1R.MR1^{++} cells in the presence of 1nM 5-OP-RU, 1μM Ac-6-FP or in the absence of antigen. **D.** Comparison of TNF and IFNγ producing expanded TRAV1-2^{+} cells cultured with wild type or CD8-null C1R.MR1^{++} cells in the presence of 1nM 5-OP-RU, 1μM Ac-6-FP or in the absence of antigen. **E and F.** Same format as C and D but examining TNF and IFNγ producing expanded TRAV1-2^{-} cells. Statistical significance was evaluated using a two-tailed Wilcoxon signed-rank test ($P < 0.5$). **A-F.** Data is representative of two independent experiments performed using the same four donors in each experiment. **A, B, C and E.** Mean and SD is displayed.

Expanded MR1-6-FP-reactive T cells were stimulated in the presence or absence of MR1 deficient, wild type or CD8-null MR1 expressing C1R cells pulsed with 5-OP-RU, Ac-6-FP or no antigen and the IFNγ, TNF and IL-13 production was examined. Both TRAV1-2$^+$ and TRAV1-2$^-$ subsets were most responsive to 5-OP-RU pulsed MR1 expressing C1R cells as compared to all other conditions, with mean percentages of TNF, IFNγ and IL-13 cytokine producing TRAV1-2$^+$ cells of 80.6%, 68.0% and 15.4% respectively, and cytokine producing TRAV1-2$^-$ cells and 24.9%, 19.8% and 4.5% respectively (**Fig. 3.7C, E and 3.8A, B and D**). In line with the bright staining observed using MR1-5-OP-RU tetramer, and indicative of a predisposition for TRAV1-2 to recognise MR1-5-OP-RU, substantially more TRAV1-2$^+$ cells produced cytokines in response to 5-OP-RU than TRAV1-2$^-$ cells. The cytokine production by cells stimulated with MR1 expressing C1R cells pulsed with Ac-6-FP or no antigen in both subsets was largely reduced compared to 5-OP-RU conditions, suggesting that although these cells bind MR1 tetramers presenting folate derivatives, 5-OP-RU is a more potent activating antigen for these T cells under these conditions (**Fig. 3.7C, E and 3.8A, B and D**). Similar fractions of cells producing cytokine in the presence of Ac-6-FP were observed as compared to in the absence of antigen for both TRAV1-2$^+$ and TRAV1-2$^-$ subsets, demonstrating that both subsets did not discriminate between MR1 presenting exogenous folate derivatives or endogenous antigens (**Fig. 3.7C, E and 3.8B and D**). Notably, a previous study has demonstrated that TCR reactivity to MR1 can be modulated by folate derivatives in some cases (201).

The percentage of cytokine producing cells in both subsets stimulated by wild type or CD8-null MR1 expressing C1R cells was subsequently examined (**Fig. 3.7D, F and 3.8C and E**). within the TRAV1-2$^+$ subset, the fraction of cytokine producing cells was largely reduced in response to CD8-null MR1 presenting C1R cells pulsed with Ac-6-FP or no antigen, except in one donor, demonstrating a spectrum of reliance on CD8 binding (**Fig. 3.7D and 3.8C**). In accordance with the tetramer staining, a substantial percentage of TRAV1-2$^+$ cells produced TNF and IFNγ in response to 5-OP-RU, however the percentage of cytokine producing cells was reduced in the absence of CD8 binding, similarly as observed for IFNγ production by CD8$^+$ MAIT cells (**Fig. 3.5F**). Similarly, for the TRAV1-2$^-$ subset, cytokine production in response to all conditions was almost completely reliant on CD8 binding, as only a modest number of cells retained the ability

to produce cytokines in response to CD8-null MR1 expressing C1R cells (**Fig. 3.7F and 3.8E**). It is clear that the CD8-MR1 interaction impacts greatly on the production of cytokines by these MR1-reactive T cells, contributing to the recognition of a potent antigen and more strikingly, permitting recognition of weaker stimulating MR1-Ag complexes.

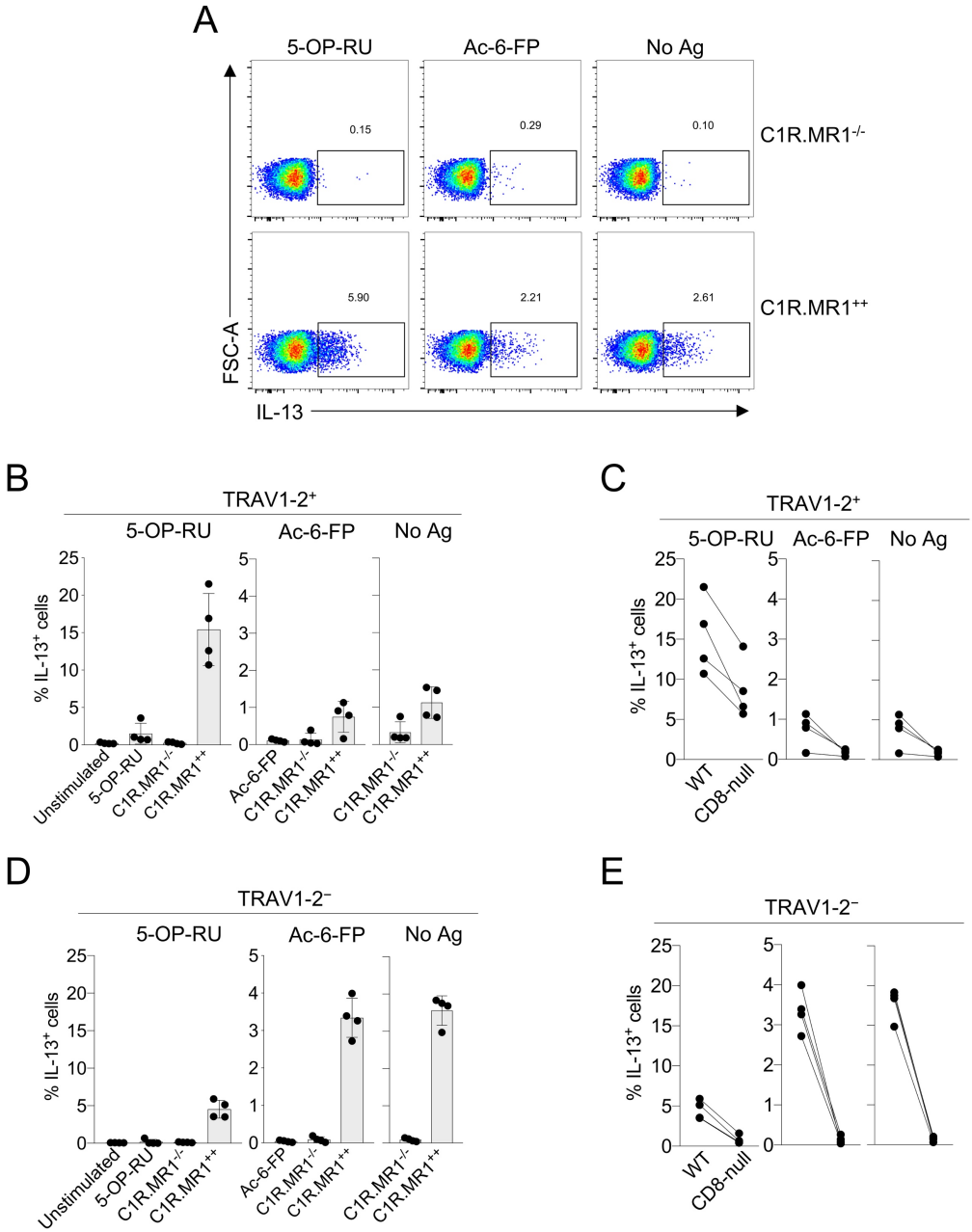

Figure 3.8. MR1-6-FP/Ac-6-FP-reactive T cells produce IL-13 after stimulation in vitro. **A.** IL-13 production by expanded T cells in the context of C1R.MR1$^{-/-}$ or C1R.MR1^{++} cells in the presence of 1nM 5-OP-RU, 1µM Ac-6-FP or in the absence of antigen. **B and C.** Percentage of IL-13 producing expanded TRAV1-2^{+} or TRAV1-2^{-} cells, respectively, cultured as described above. **D and E.** Comparison of IL-13 producing expanded TRAV1-2^{+} or TRAV1-2^{-}cells, respectively, cultured with wild type or CD8-null C1R.MR1^{++} cells in the presence of 1nM 5-OP-RU, 1µM Ac-6-FP or in the absence of antigen. **B-D.** PBMCs of 4 healthy donors were assessed. Data is representative of two independent experiments performed using the same four donors in each experiment. **B and D.** Mean and SD is displayed.

3.3 Discussion

Conflicting analysis on whether MR1 features a CD8 binding site (41, 89, 90) affirm that the MR1-CD8 interaction cannot be predicted based on sequence homology within a putative binding site on the α3 domain of MR1. The potential for a CD8-MR1 interaction was examined herein by interrogating CD8 binding to MR1 directly using MR1 mutant tetramers and MR1 mutant cell lines. In addition, the functional consequences of this interaction were assessed directly for MAIT cells and other MR1-reactive T cells. The data here describes a semi-conserved CD8 binding site on MR1 and a role for both paralogues of CD8 in the recognition of MR1.

CD8αα$^+$ MAIT cells were consistently the greatest cytokine producers among subsets in response to stimulation with 5-OP-RU. This was at least in part facilitated by CD8αα engagement of MR1, where its loss was detrimental to MR1-Ag recognition and cytokine production. CD8αα expression on T cells is limited largely to unconventional T cells and IELs (205). However, in patients with chronic viral infections, terminally differentiated CD8αα$^+$ (CD8α$^+$CD8β^{low}) CTLs are found that produce greater amounts of pro-inflammatory cytokines and cytotoxic granules compared to CD8αβ$^+$ CTLs counterparts (206). Although it has been shown, in principle, that CD8αα can also recognise MHC-I with a similar affinity to CD8αβ (181, 182), CD8αα does not appear to be a functional co-receptor for conventional T cells (183) and might even repress T cell activation (reviewed in (115)). In contrast to conventional T cells, for MAIT cells and other MR1-reactive T cells, the data here suggest CD8αα has a functional role similar to CD8αβ, whereby membrane-bound TCR and both CD8 isoforms can engage MR1 co-operatively and contribute to T cell activation.

The cytokines produced by activated MAIT cells stimulated non-specifically or in the context of infection, are largely concordant among subsets, and typically include Th1 and Th17 cytokines (124, 125, 171-173, 207). Nevertheless, several studies have identified variations in the cytokine response. Consistently, it is reported that CD4$^+$ MAIT cells have a lower capacity to secrete TNF and IFNγ and degranulate compared to other MAIT cells (124, 171), however retain the capacity to produce IL-4 and IL-13 under some circumstances (124, 208). The pattern of cytokine production by the co-receptor subsets

is consistent with their transcription factor expression, whereby lower levels of transcription factors PLZF, RORγt, T-bet, Eomes and Helios were found in $CD4^+$ MAIT cells compared to other MAIT cell subsets (124, 171, 209). DN and $CD8^+$ MAIT cells appeared to express these transcription factors similarly in blood and mucosal tissue (74, 124, 209). A similarly reduced cytokine output was observed by $CD4^+$ MAIT cells in response to 5-OP-RU compared to the other MAIT cell subsets in this study. Interestingly, the lower cytokine production did not correlate with tetramer binding, as $CD4^+$ and DN MAIT cells were capable of recognising MR1-5-OP-RU with equal tetramer fluorescence. It is therefore likely that the reduced functional response by $CD4^+$ MAIT cells is not due to a lower affinity TCR interaction with MR1. Curiously, $CD4^+$ MAIT cells were the dominant population identified in blood of one donor and secreted similar amounts of TNF as $CD8^+$ or DN MAIT cells from other donors (included in **Figure 3.4G**). Thus, while factors influencing the cytokine response of $CD4^+$ MAIT cells are unclear, $CD4^+$ MAIT cells are capable of producing cytokine responses comparable to other MAIT cell subsets in some donors.

Consistent with others (124-126, 171, 210), modest differences were noted between DN and $CD8^+$ MAIT cells that produced cytokines upon stimulation. This included a consistent reduction in the proportion of cytokine producing cells within DN as compared to $CD8^+$ MAIT cells, as noted previously for *E. coli* (124, 126) and *Helicobacter pylori* (210). Importantly, the differences observed in response to the antigen 5-OP-RU were reduced in the absence of CD8 binding. Thus, CD8 appears to enhance functional capacity rather than compensating for a potential subset-specific lower functional capacity such as a reduced affinity of $CD8^+$ MAIT TCRs for MR1. One could speculate that the additive effect of CD8 on MR1 recognition is a means to tune MAIT cell responsiveness whereby co-receptor expression is modulated over time, in response to stimulation or the microenvironment as has been described for CD8 on $CD4^+$ ILCs (211). In support of CD8 fine-tuning, Dias *et al.*(126) revealed that the TCR repertoire of DN MAIT cells is less diverse and shared with the TCR repertoire of $CD8^+$ MAIT cells, suggesting that DN MAIT cells may be derived from the more diverse $CD8^+$ subset. In the context of a natural infection, a low concentration of MR1 ligand (5-OP-RU or other riboflavin-based MAIT antigen), in addition to the minimal surface expression of

endogenous MR1 may further accentuate the role for CD8 in enhancing MAIT cell activation. Comparatively, T cells that recognised folate-derived antigens typically expressed high levels of CD8 (201), similar to CTLs and were mostly reliant on CD8 for recognition of MR1, thus CD8 downregulation would likely impair MR1 recognition.

In the absence of CD8 binding, a large population of $CD8^+$ MAIT cells remained clearly identifiable in blood with MR1 tetramer. Consequently, for most $CD8^+$ MAIT cells, CD8 engagement is not a strict requirement for recognition of MR1 presenting the strongly agonistic antigen 5-OP-RU, to which prototypic human MAIT TCRs bind with high affinity (K^d ~1-10 μM) (58, 86). The importance of CD8 became quickly apparent in the recognition of TCR-MR1 interactions that are characterised by lower affinity. As exemplified here, these include recognition of folate derived antigens recognised by some MAIT cells and other MR1-reactive T cells and are likely applicable to other weakly agonistic antigens such as the ribityllumazines and interactions involving autoreactive MR1-reactive T cells. Thus, the dependence on CD8 for TCR recognition of MR1 is similar to that observed for TCR recognition of pMHC-I by CTLs, where TCR-pMHC-I interactions of sufficiently high affinity do not require CD8, while low affinity TCR-pMHC-I interactions are reduced or ameliorated by interfering with CD8 binding of MHC-I (179, 212). CD8 might also be important for MR1-reactive T cells to recognise the more recently identified novel molecules, both related and unrelated to the riboflavin biosynthesis pathway (201-204, 213). Accordingly, the MAIT cells responding to both *Mycobacterium tuberculosis* and *M. smegmatis* appear to be largely $CD8^+$, and CD8 was indispensable for detection of *M. tuberculosis* infection *in vitro* (71, 214). It is likely that CD8 will play a crucial role in expanding the antigen repertoire of MAIT and other MR1-reactive T cells and this way grant greater antigenic promiscuity. Considering the accumulating diversity within the MR1-reactive TCR repertoire and the discovery of novel antigens for MR1, the importance of CD8 will become increasingly evident. Staining with CD8-null MR1 tetramers, that are described here, alongside wild type MR1 tetramers, will serve as a powerful experimental approach to assess CD8 dependence and distinguish between TCR mediated interactions with MR1 of high and low affinity.

Chapter 4: Autoreactive CD1b-restricted T cell responses to lipid antigens

4.1 Introduction

Several recent studies have identified autoreactive CD1b-restricted T cells in healthy human blood as well as in the context of autoimmune disease (52, 149, 153, 215). It is therefore likely that these cells recognise lipid antigens presented by CD1b in the context of human immunity. For instance, in a transgenic mouse model of autoimmune disease, CD1b-restricted T cells were shown to be the sole mediators of severe skin inflammation by reacting to an accumulation of endogenous lipids in the tissues (153). Thus, some autoreactive CD1b-restricted T cells may have the capacity to initiate and sustain an inflammatory response and may be currently underappreciated in the study of inflammatory diseases.

Despite these recent advances, our understanding of the phenotype, TCR repertoire and lipid binding characteristics of autoreactive CD1b restricted T cells is limited to a few T cell clones derived from *in vitro* expansion (52, 149). These pioneering studies revealed that autoreactive T cells can recognise lipid antigens shared by both mammals and bacteria (52) as well as lipids that are enriched in certain tissues, such as the gangliosides in the brain and other nervous tissue (54). Recent crystallographic data have improved our understanding of how lipid antigens are both presented to and recognised by the TCR, revealing variable modes of lipid antigen recognition. TCR recognition was either dominated by the lipid head group and demonstrated high specificity for antigen (138, 150), while other TCRs recognised conserved structural motifs in related lipid species (216). However, the diversity of lipids that can be presented by CD1b, including phospholipids, cholesterol based lipids and ceramides, suggested a variety of TCR docking modes or greater TCR plasticity are required to mediate the broad lipid reactivity observed by CD1b-restricted T cells (25, 52, 54, 153). In agreement with this, preliminary experiments have identified autoreactive TCRs that recognise a profound number of different lipid antigens in the context of CD1b.

To examine their prevalence, frequency, phenotype and antigen specificity, autoreactive CD1b-restricted T cells from healthy peripheral blood were identified using CD1b tetramers loaded with mixed endogenous lipids. Autoreactive T cells were isolated by cell sorting and *in vitro* expansion, as has been described previously (52), as well as directly *ex vivo* with tetramer enrichment, following optimisation of this novel technique. The TCR usage of several autoreactive T cells was determined, revealing a largely diverse TCR repertoire. Reporter cell lines were produced to characterise their TCR antigen specificity. These data support previous studies that showed autoreactive T cells recognise common phospholipid antigens. However, clear differences in phospholipid preference were noted for the autoreactive cell lines. Soluble TCRs were produced from two autoreactive T cell clones that displayed unique antigen specificity. For each TCR permissive endogenous lipids were identified, providing insights into how they are recognised.

4.2 Results

4.2.1 Production of CD1b tetramers in the presence of endogenous mammalian lipids

To generate CD1b tetramers, mammalian GNTI HEK293S cells were transfected with a soluble CD1b heavy chain gene fused to a BirA-tag and His-tag encoding plasmid concurrently with a β_2m gene encoding plasmid (**Table AI.1**). Fully-folded CD1b monomers were collected from the supernatant of cultured cells. Using a mammalian expression system implied that CD1b monomers were produced in the presence of mammalian endogenous lipids that might be presented in the cleft of CD1b, thus referred to as 'CD1b-endo', for 'endogenous-loaded'. CD1b from the supernatant was purified by subsequent affinity chromatography and size exclusion chromatography. His-tag affinity chromatography using nickel-coated resin beads and eluting with imidazole resulted in two distinct UV absorbance peaks on the chromatogram (**Fig. 4.1A**), corresponding to aggregated protein and CD1b monomers respectively, as evaluated by sodium dodecyl sulphate polyacrylamide gel electrophoresis (SDS-PAGE) of selected fractions under non-reducing conditions (**Fig. 4.1B**). Highly purified proteins that corresponded to CD1b heavy chain of approximately 35 kDa in size, and β_2m of approximately 12 kDa in size, were observed in equal proportion. The multiple CD1b heavy chain protein bands resolved by SDS-PAGE likely represented CD1b species that varied in types of posttranslational glycosylation, as previously reported (217). In addition, some higher order aggregates were present across all fractions corresponding to protein smears greater than 100 kDa in size, likely CD1b heavy chain that was translated incorrectly or misfolded, due to its persistence after affinity chromatography suggesting the presence of His-tags.

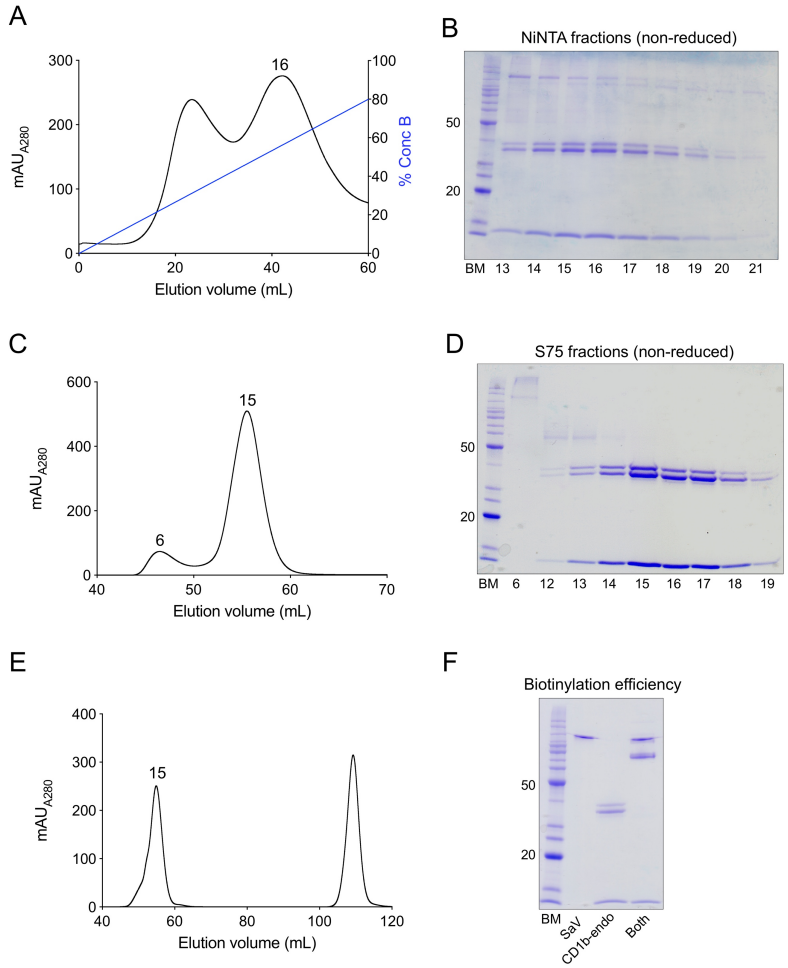

Figure 4.1. Purification of CD1b-endo by liquid chromatography and subsequent biotinylation

CD1b-endo monomers were purified from supernatant of mammalian cells using affinity and size exclusion chromatography and then biotinylated enzymatically. **A.** Chromatogram showing UV absorbance of eluted protein from NiNTA column run using an imidazole gradient (% ConcB). Number annotation corresponds to the protein fraction (16) containing purified CD1b-endo monomers as determined by SDS-PAGE. Each fraction contained 6 mL of elution volume, numbered from the start of the elution. **B.** 12% SDS-PAGE under non-reducing conditions of key fractions eluted from the NiNTA column run alongside a benchmark protein ladder (BM), annotated are the 50k Da and 20k Da size standards. **C.** Chromatogram showing UV absorbance of the protein eluted by size exclusion chromatography using Superdex 75pg column, number annotations correspond to aggregated protein (fraction 6) and CD1b-endo monomers (fraction 15). Each fraction contained 1 mL of elution volume, starting from 40 mL. **D.** 12% SDS-PAGE under non-reducing conditions of key fractions eluted from the Superdex 75pg column, annotated as described above. **E.** Chromatogram shows UV absorbance of purified CD1b-endo monomers and impurities after 4 h biotinylation using BirA enzyme. Each fraction contained 1 mL of elution volume, starting from 40 mL. **F.** 12% SDS-PAGE of native SAv, reduced CD1b-endo using 0.1M DTT or a mixture of both, as indicated, alongside a benchmark protein ladder (BM) with annotated 50 kDa and 20 kDa size standards. These data represent at least two independently performed experiments.

In order to remove higher order aggregates, the CD1b monomers were further purified using size-exclusion chromatography (**Fig. 4.1C**). In principle, size-exclusion chromatography allows for the separation of differently sized proteins by impeding passage through a bead matrix consisting of pores. Larger proteins elute faster than smaller proteins that are slowed down by transit through the pores. CD1b monomers were separated from residual higher order aggregate proteins of much greater size (**Fig. 4.1C**), as well as from contaminating free β_2m that is much smaller than correctly folded CD1b monomers. Two UV absorbance peaks were present on the chromatogram (**Fig. 4.1C**) and an SDS-PAGE was performed to reveal the identity of each peak (**Fig. 4.1D**). As expected, higher order protein aggregates were eluted first, present in the peak fraction 6 (**Fig. 4.1D**), followed by CD1b monomer in the peak fraction 15. Purified CD1b monomer was collected from fractions 14-19 for biotinylation.

CD1b monomers were biotinylated enzymatically using the BirA enzyme as previously described (218) and further purified by size-exclusion chromatography (**Fig. 4.1E**). Two prominent peaks were apparent on the chromatogram, the first peak at elution volume 45-60 mL confirmed by SDS-PAGE as pure CD1b-endo (**Fig. 4.1E**). The second peak at elution volume 105-115mL, was not identified by SDS-PAGE, suggesting that no protein was present in the fractions and that the UV absorbance measured was due to other constituents within the biotinylation buffers (**Table 2.2**). Efficiency of CD1b-endo biotinylation was examined by SDS-PAGE using Streptavidin (SAv) under non-reducing conditions (**Fig. 4.1F**). CD1b-endo mixed at a molar 4:1 ratio with SAv to produce multimeric complexes migrated more slowly through the polyacrylamide gel due to its larger size, as visualised by the distinct protein bands at >90 kDa compared to CD1b-endo alone. These data indicate that full biotinylation of mammalian expressed CD1b was achieved.

4.2.2 Identification and expansion of autoreactive CD1b-restricted T cells

Previous studies on autoreactive CD1b-restricted T cells used T cell clones cultured for prolonged periods, which may have affected their phenotype and function (52). Thus, to identify and characterise autoreactive CD1b-restricted T cells directly *ex vivo*, PBMCs from healthy blood were stained using CD1b-endo tetramers. In all donors, less than 1%

of $CD3^+$ lymphocytes stained positive for CD1b-endo tetramers and the $tetramer^+$ cells varied widely in fluorescence intensity from very dim to exceptionally bright (**Fig. 4.2A**). The frequency of autoreactive CD1b-restricted T cells has been estimated previously as approximately 1% of αβ T cells by culturing cloned cells from PBMCs or cord blood with $CD1^+$ APCs (219). Moreover, microbial reactive CD1b-restricted T cells have been identified using tetramers and have a reported frequency similar to naïve αβ T cells of 1 in 10^5 (52). Thus, while the percentage of $tetramer^+$ cells we observed was within the limits of previous studies, the lack of a clear $tetramer^+$ population (**Fig. 4.2A**) and the wide variation in tetramer binding strength suggested that tetramer binding may not be solely TCR dependent.

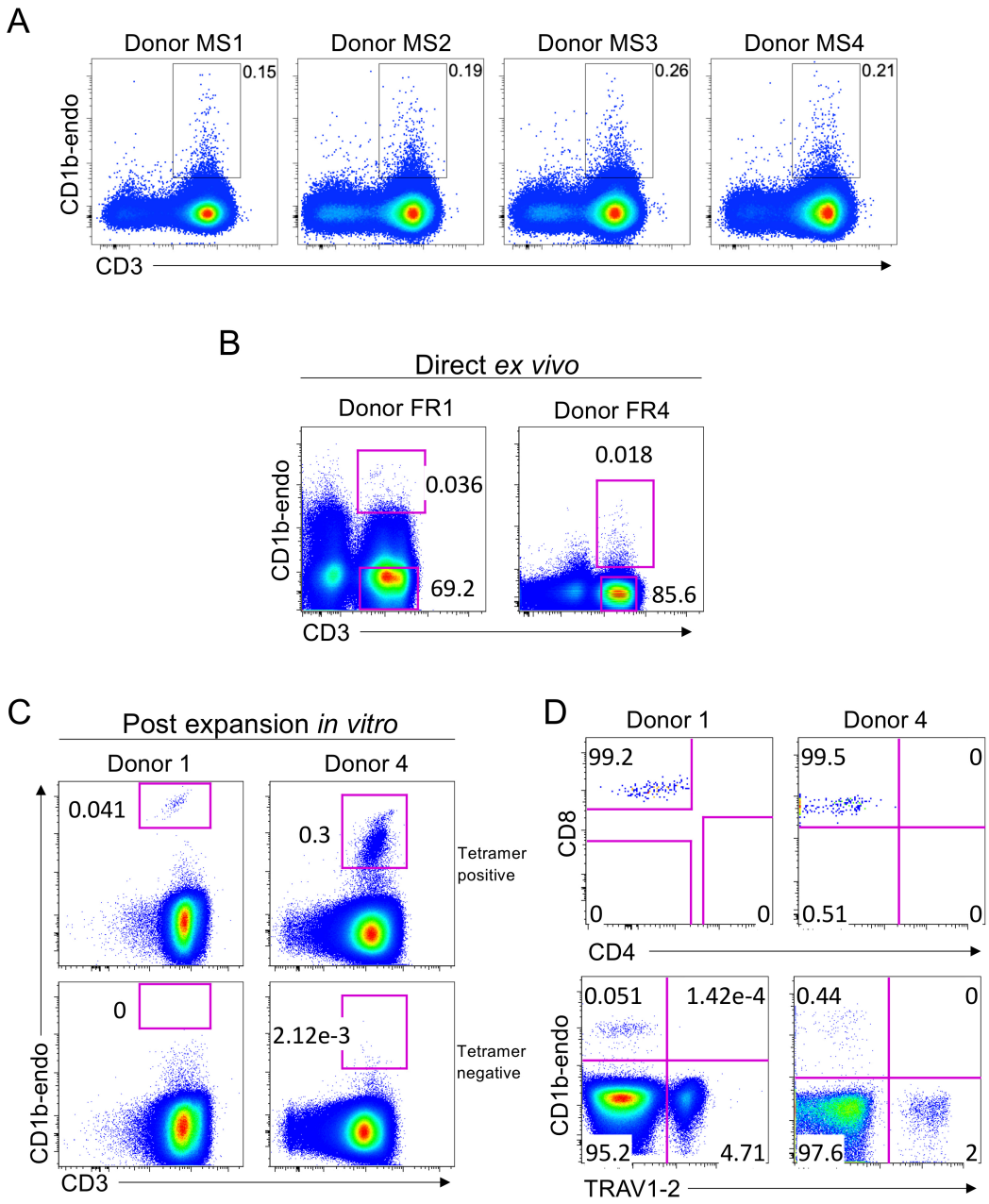

Figure 4.2. CD1b-endo tetramer staining of PBMCs from healthy donors. PBMCs were purified from buffy coats donated by the Australian Red Cross and stained with CD1b-endo tetramers, followed by an antibody cocktail outlined in **Table 2.3**. Tetramer$^+$ cells from donor FR1 and FR4 were sorted expanded *in vitro*. **A.** CD1b-endo tetramer$^+$ cells that previously gated to remove doublets, dead cells, CD14$^+$ and CD19$^+$ cells. **B.** Tetramer$^+$ and tetramer$^-$ cells from donors FR1 and FR4 were sorted based on high or negative tetramer fluorescence and expanded *in vitro* for three weeks with cytokines. **C.** Expanded cells from FR1 and FR4 were stained with CD1b-endo tetramers and CD3 to assess reactivity of tetramer$^+$ and tetramer$^-$ cells. **D.** Staining of key surface markers expressed by tetramer$^+$ cells expanded from FR1 (donor 1) and FR4 (donor 4), including TRAV1-2, CD4 and CD8α. The data and figure were prepared by Fiona Ross.

To determine whether the specificity observed for CD1b-endo was due to TCR binding, both tetramer$^+$ and tetramer$^-$ CD3$^+$ cells from donors 1 and 4 were sorted (**Fig. 4.2B**) and expanded non-specifically for three weeks by crosslinking CD3 and CD28 molecules using antibodies in the presence of 100U/mL of soluble IL-2. After expansion, rested cells from donors 1 and 4 were stained with CD1b-endo tetramer. A distinct population of tetramer$^+$ cells was observed from both donor 1 and 4 in the tetramer$^+$ expanded cells and tetramer intensity correlated with CD3 expression (**Fig. 4.2C**). Within the same expanded population, there was a large number of CD3$^+$ T cells that failed to stain with tetramer suggesting that a large proportion of cells that originally stained with CD1b tetramer bound to CD1b independently of TCR, that efficient sort gates included tetramer$^-$ CD3$^+$ cells, or that *in vitro* activation resulted in TCR downregulation. As expected, there were very few cells from the tetramer$^-$ CD3$^+$ population that stained with CD1b tetramer post expansion in culture (**Fig. 4.2C**). Expanded CD1b-restricted T cells from donors 1 and 4 were exclusively CD4$^+$ (**Fig. 4.2D, upper panel**), and unlike CD1b-restricted GEM T cells, autoreactive cells did not express TRAV1-2 (**Fig. 4.2D, lower panel**), suggesting that these cells were distinct from the GMM-reactive GEM T cells. In support of this, CD1b-endo tetramers were unable to detect GEM T cells from peripheral blood from *M. tuberculosis*-infected patients (135).

4.2.3 Determination of TCR usage by CD1b-restricted T cell clones

To evaluate the number of expanded clones from donor 1 and 4, and to determine the precise TCR gene usage, CD1b-endo tetramer$^+$ single cells were isolated by FACS for TCR sequencing. mRNA from cells was reverse transcribed and TCR Vα and Vβ domain genes were amplified using multiplex nested PCR and the subsequent cDNA was amplified as previously described (220). Amplified cDNA was recovered from 13 cells from donor 1 and from 46 cells from donor 4. Interestingly, a single clone was identified from donor 1 as determined by the identical TCR nucleotide sequence recovered from 13/13 cells (**Table 4.1**). This clone, termed 1.27, expressed a TCR comprised of TRAV27, TRAJ53 α-chain genes, paired with TRBV5-8 and TRBJ1-4 β-chain genes (**Table 4.1**). Four clones were identified from donor 4, of which one expressed TRAV27 and TRAJ53 genes, with an almost identical CDR3α region as that observed from clone 1.27, however this TRAV27 clone from donor 4, termed 4.27, expressed TRBV5-4 and

TRBJ2-4 β-chain genes (**Table 4.1**). Other clones from donor 4 included: clone 4.13-2, which expressed TRAV13-2 and TRAJ52 α-chain genes paired with TRBV19 and TRBJ2-7 β-chain genes; clone 4.17, which expressed TRAV17 and TRAJ11 α-chain genes paired with TRBV6-6 and TBJ2-7 and; clone 4.41, which expressed TRAV41 and TRAJ22 α-chain genes paired with either TRBV6-2 or TRBV6-3 and TRBJ2-7 β-chain genes (**Table 4.1**). Due to the limited amplification of the Vβ gene segment from 4.41 and the similarities between TRBV6-2 and TRBV6-3 germline encoded gene segments near the CDR3 region, the precise Vβ gene usage could not be determined, and for subsequent experiments TRBV6-2 gene usage was assumed. Thus, five novel CD1b restricted T cell clones from two separate donors were identified, suggesting that the TCR repertoire of autoreactive T cell clones may be distinct from the GMM-reactive TCR repertoire previously reported (135, 136).

Donor	TRAV	CDR3α	TRAJ	TRBV	CDR3β	TRBJ	Frequency	I.D.
1	27	CAGPRLSGGSNYKLTF	53	5-8	CASSSGHSTNEKLFF	1-4	13/13	1.27
4	13-2	CAENRYAGGTSYGKLTF	52	19	CASSLTSVAKNIQYF	2-4	3/47	4.13.2
4	17	CAAQMGYSTLTF	11	6-6	CASSQNRGRGDHYEQYF	2-7	19/47	4.17
4	27	CAGPRYSGGSNYKLTF	53	5-4	CASSDRDIAKNIQYF	2-4	6/47	4.27
4	41	CAVLSGSARQLTF	22	6-2/6-3	CASSYLRGRSYEQYF	2-7	18/47	4.41

Table 4.1. TCR sequences derived from CD1b-endo reactive primary T cells. Expanded tetramer^{+} cells from donors FR1 (donor 1) and FR4 (donor 4) were single-cell sorted. TCR Vα and Vβ domain gene segments were amplified by multiplex nested PCR and TCR genes were determined by Sanger sequencing. TCR sequences were analysed using the IMGT database.

4.2.4 Generation of autoreactive CD1b-restricted T cell lines

To confirm that the TCRs identified from donor 1 and 4 were CD1b-restricted following *in vitro* expansion and re-staining with CD1b-endo tetramer, TCR reporter cell lines expressing each of the 1.27, 4.13-2, 4.17, 4.27 and 4.41 TCRs were generated (**Table 4.1**). Jurkat-76 cells deficient in TCR were transduced with retrovirus containing CD3 complex and each of the CD1b-restricted TCRs. Transduced cell lines were sorted for high CD3 expression to ensure high levels of TCR expression in order to differentiate subtle differences in tetramer binding between the cell lines. All of the cell lines maintained high levels of CD3, indicating the TCRs were folded correctly and stably expressed at the cell surface (**Fig. 4.3**). The cell lines were stained with CD1b-endo tetramers and tetramer binding was observed (**Fig. 4.3**), confirming reactivity to CD1b for all TCRs. In particular, the 1.27 TCR-transduced cell line recognised CD1b-endo comparatively strongly, likely due to a high affinity interaction between the TCR and CD1b-endo and was concordant with the expanded T cell staining (**Fig. 4.2 and 4.3**). In comparison, the 4.13-2 TCR-transduced cell line weakly bound to CD1b-endo tetramers, where staining was only observed for cells that expressed very high levels of CD3, suggesting a lower affinity interaction between TCR and CD1b-endo (**Fig. 4.3**). It is possible that altering the endogenous lipids presented by CD1b may modulate tetramer binding by the cell lines and reveal permissive and non-permissive lipid antigens.

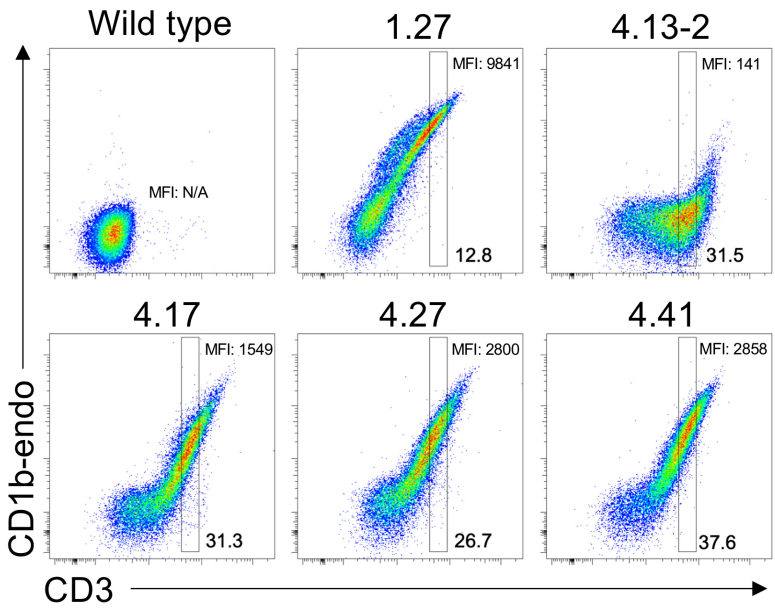

Figure 4.3. CD1b-endo tetramer reactivity of autoreactive TCR transduced cell lines Jurkat-76 cells were transduced with TCRs derived from FR1 and FR4 to verify their reactivity to CD1b-endo tetramers. Transduced 1.27, 4.13-2, 4.17, 4.27 and 4.41 cells were sorted for high CD3 expression and rested for two weeks before experiments were performed. Cell lines were stained with CD1b-endo tetramers in conjunction with CD3 and a live/dead marker. Plots display tetramer reactivity and CD3 expression of viable cells. Geometric MFI (MFI) of gated CD3 expression displayed for each cell line, except for wild type SKW-3.$\beta_2m^{-/-}$ cells. These data are representative of two independently performed experiments.

4.2.5 Refolding of CD1b monomers without endogenous mammalian lipids

The diversity of lipid antigens bound by CD1b-endo tetramers is not well understood including the lipids bound by CD1 molecules produced in a mammalian expression system. Thus, it is possible that a single CD1b tetramer will bind up to four different lipids, limiting their potential avidity. One attempt to resolve this involved staining T cells using CD1b dextramers, large multivalent structures that contained >10 CD1b molecules (52). In principle, increasing the number of CD1b molecules in a single multimer also increases the chances of repeated permissive or non-permissive lipids that are presented to T cells. However, given the huge diversity in possible lipids that may bind to CD1 molecules (221) this method does not guarantee homogenous presentation of lipid species by CD1b. To provide more control of the lipid antigens presented by CD1b tetramers, CD1b monomers were refolded *in vitro*, in the absence of endogenous mammalian derived lipids, and loaded with defined lipid species *post hoc*.

A CD1b heavy chain gene was order and cloned for expression in bacteria (**Table AI.1**) comprised of the native CD1b heavy chain, with a C-terminus BirA-tag and His-tag and a β_2m construct used previously (58). The gene construct was successfully cloned into pET30 vector, expressed and purified from bacterial inclusion bodies as depicted by SDS-PAGE (**Fig. 4.4A**). The CD1b heavy chain protein was extremely pure and expressed at a high concentration (~15 mg/mL^{-1}) (**Fig. 4.4A**). As expected, even though the protein sequences were identical the bacteria-derived CD1b heavy chain was smaller than the CD1b-endo heavy chain, in line with the lack of glycosylation during bacterial as compared to mammalian expression (**Fig. 4.4A**).

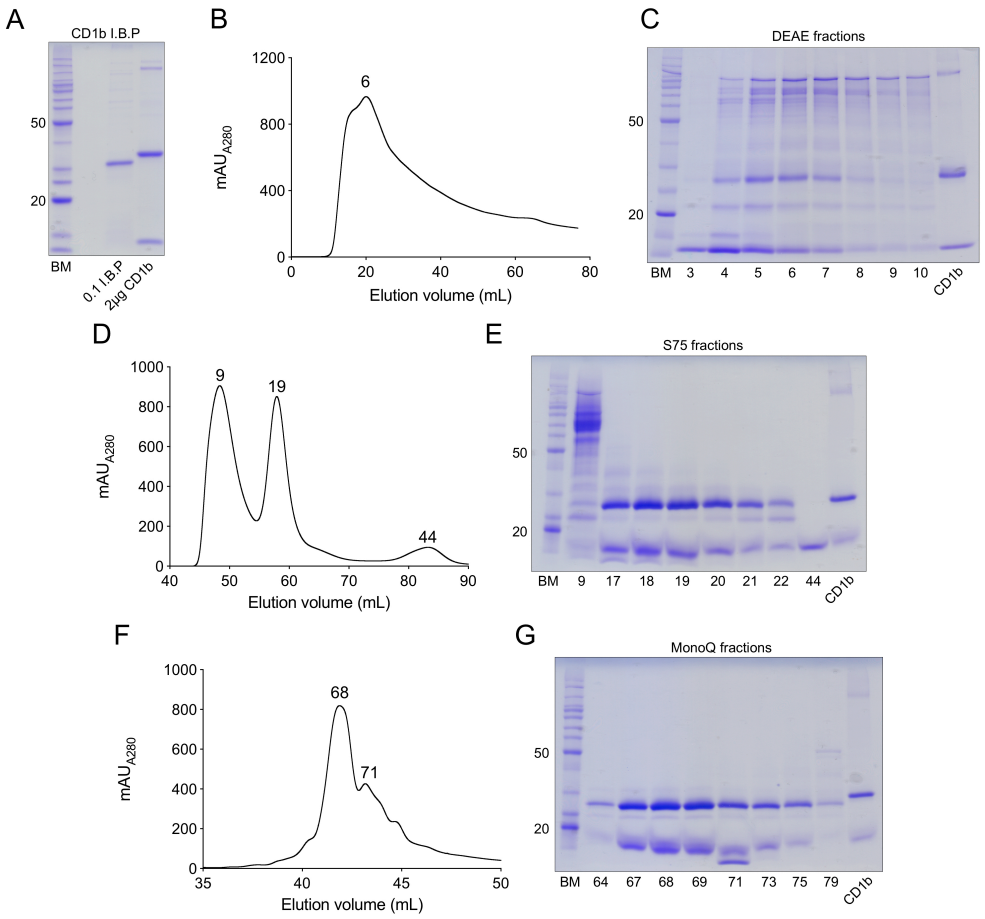

Figure 4.4. Purification of refolded CD1b derived from bacterial inclusion bodies. CD1b was refolded from bacterial inclusion bodies in the absence of defined antigen *in vitro* and purified by successive liquid chromatography. **A.** 12% SDS-PAGE of CD1b heavy chain IBP under reducing conditions, 0.1µL of CD1b heavy chain (0.1 IBP) was examined alongside 2µg of mammalian CD1b-endo monomer (2µg CD1b) to estimate protein concentration. CD1b heavy chain was highly pure and estimated as 15 mg mL^{-1} within the preparation. **B.** Chromatogram showing UV absorbance of eluted CD1b/β_2m protein from DEAE column. Number annotation refers to peak fraction containing refolded CD1b monomers. **C.** 12% SDS-PAGE under non-reducing conditions of key fractions eluted from DEAE column alongside a benchmark (BM) protein ladder annotated at the 50 kDa and 20 kDa protein standards and a CD1b-endo reference. **D.** Chromatogram showing UV absorbance of eluted protein from Superdex 75pg column. Fraction 9, 19 and 44, correspond to peak fractions containing high order aggregate, CD1b monomer and free β_2m respectively. **E.** 12% SDS-PAGE under non-reducing conditions of key protein fractions eluted from the Superdex 75pg column. **F.** Chromatogram showing UV absorbance of eluted CD1b/β_2m protein from MonoQ column. Fraction 68 and 71 (annotated on the chromatogram) correspond to peak fractions containing the two species of CD1b monomers identified. **G.** 12% SDS-PAGE under non-reducing conditions of key fractions eluted from MonoQ column. These data are representative of two independently performed experiments.

It has previously been shown that refolding CD1 molecules *in vitro* requires the presence of a chaperone to stabilise CD1b and prevent misfolding (24, 222), likely due to the large hydrophobic clefts of CD1 molecules that are exposed during folding. To refold CD1b, both CD1b IBP and β_2m IBP were injected into a chaotrophic refolding buffer (**Table 2.2**). A single alkyl chain detergent, hexadecyltrimethyl ammonium bromide (CTAB), was used as an artificial chaperone to stabilize the partially folded CD1b monomers. After two days of continuous refolding, methyl-β-cyclodextrin (MβCD) was added to capture the CTAB molecules, liberating the partially folded CD1b monomers and enabling them to fold completely as described previously (24).

Refolded CD1b monomers were purified by anionic exchange chromatography with diethylaminoethyl (DEAE) resin beads and a constant concentration of 200mM NaCl. Two overlapping peaks were registered early on the chromatogram during elution (**Fig. 4.4B**), which corresponded to CD1b monomers and higher order aggregates as assessed by SDS-PAGE under non-reducing conditions (**Fig. 4.4C**). A protein band corresponding to CD1b heavy chain was apparent in fractions 3-7 at ~35k Da (**Fig. 4.4C**) and a protein band corresponding to β_2m at ~12k Da in size was also observed, suggesting the expression of some CD1b monomers, some higher order aggregates and two protein species of undetermined identity at ~21k Da and ~15k Da (**Fig. 4.4C**).

To further enrich CD1b monomers, fractions 3-7 were collected and purified using size-exclusion chromatography (**Fig. 4.4D**). Three prominent UV absorbance peaks were apparent on the chromatogram, which were analysed by SDS-PAGE under non-reducing conditions (**Fig. 4.4E**). The first peak (fraction 9) corresponded to mostly aggregated protein, the second peak (fractions 17-22) contained both CD1b monomer and β_2m as well as small amounts of two unknown species at ~21k Da and <15k Da in size and the third peak (fraction 44) was comprised entirely of free β_2m (**Fig. 4.4E**).

In an attempt to further purify monomeric CD1b from residual contaminants, fractions 17-22 were collected and subjected to further purification using a MonoQ anionic exchange column with a shallow salt gradient to enhance the resolution of protein spearation. A prominent UV absorbance peak was detected in fraction 68, although a

shoulder peak was observed in fraction 71 (**Fig. 4.4F**). SDS-PAGE under non-reducing conditions revealed protein fractions 67-69 were primarily composed of CD1b heavy chain and β_2m, although small amounts of contaminating protein were still observed (**Fig. 4.4G**). Curiously, the protein band corresponding to β_2m at ~12 kDa in size appeared less defined and across a wider size range within the gel (**Fig. 4.4G**). This was also visible in the CD1b-endo control protein, perhaps a consequence of experimental variation on the day (**Fig. 4.4G**). Fraction 71 appeared to CD1b and β_2m of two distinct sizes and thus this was excluded from further use. Fractions 67-69 were collected for further characterisation of CD1b conformation and biological activity.

4.2.6 Validation of refolded CD1b monomers

To establish whether the CD1b monomers were folded in their native conformation, a direct enzyme-linked immunosorbent assay (ELISA) was performed using an anti-CD1b monoclonal antibody. Refolded CD1b monomers or mammalian CD1b-endo monomers were coupled directly to an ELISA plate at serial doubling dilutions starting at a concentration of 10μg mL^{-1} (**Fig. 4.5A**). As a control, 10μg mL^{-1} of CD1a-endo was coupled to the ELISA plate for detection by anti-CD1a or anti-CD1b antibodies. Both types of CD1b monomers (refolded CD1b monomers or mammalian CD1b-endo) were detected using the anti-CD1b antibody (**Fig. 4.5A and B**). Mammalian CD1b-endo appeared to bind the anti-CD1b antibody greater than refolded CD1b at all monomer concentrations and a titrating effect was not visible until a concentration of 0.31μg mL^{-1} was reached (**Fig. 4.5B**). It is possible that the glycosylated form of CD1b may be more antigenic than the refolded CD1b, however it is more likely that the concentrations of the two CD1b monomers were not equal, in part due to the glycosylation of CD1b-endo impacting the accuracy of determining the protein absorbance, as well as the inability to completely remove protein impurities from the refolded CD1b (**Fig. 4.4G**). Nevertheless, recognition by the anti-CD1b antibody strongly indicated that the refolded CD1b had adopted the native conformation. As expected, CD1a-endo monomer was detected by an anti-CD1a antibody (**Fig. 4.5C**) but not by the anti-CD1b antibody, supporting the antibody specificity for CD1b.

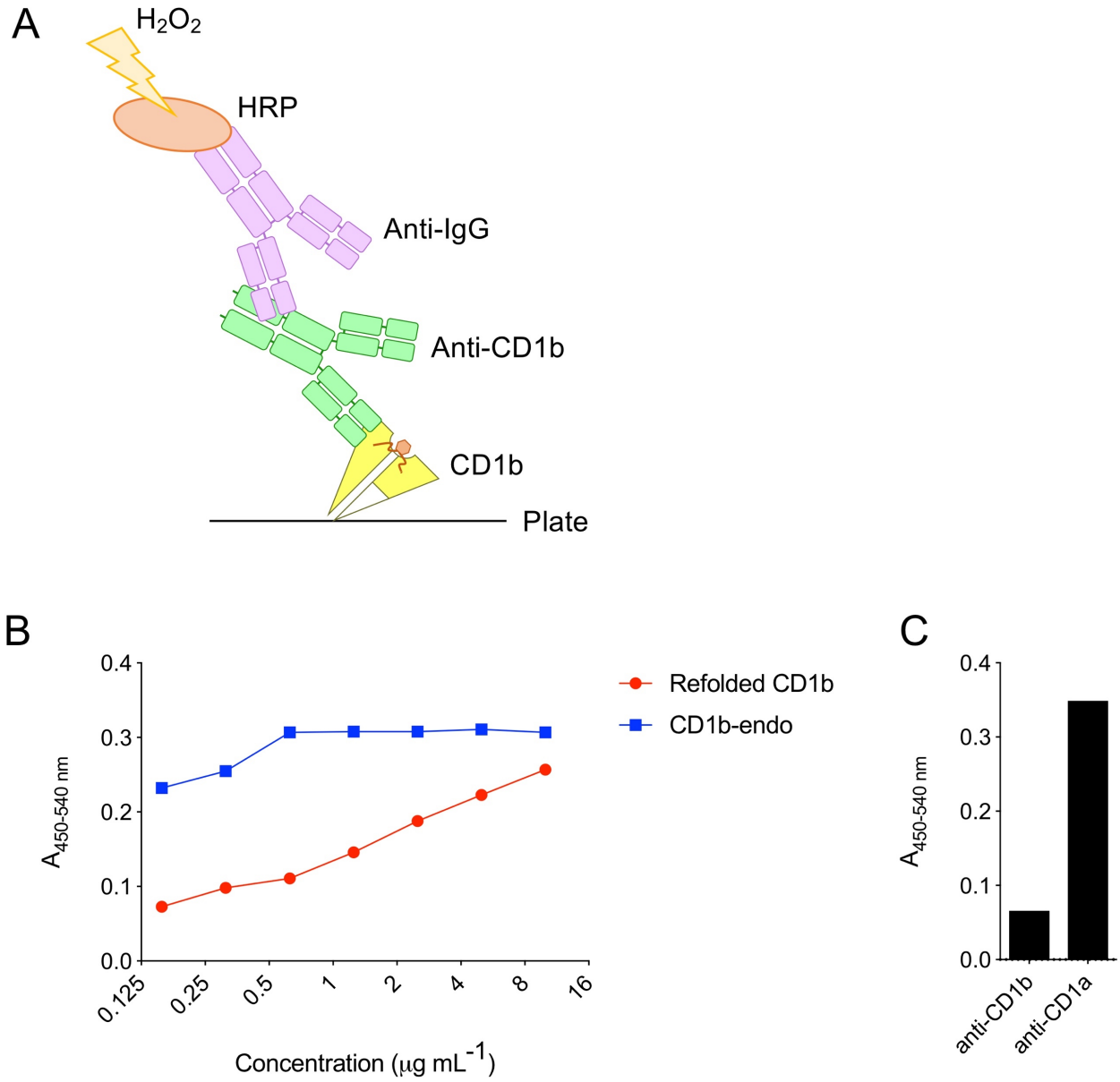

Figure 4.5. Validation of refolded CD1b conformation by indirect ELISA. Purified refolded CD1b, CD1b-endo or CD1a-endo monomers were coupled to an ELISA plate at a serial dilution starting at a concentration of 10μg mL^{-1} and incubated overnight. Remaining binding sites on the ELISA plate were blocked using a BSA solution and soluble CD1b and CD1a was probed using an anti-CD1b monoclonal antibody (SN13) or anti-CD1a monoclonal antibody (HI149) and HRP- conjugated anti-IgG1 secondary monoclonal antibody (Genscript). **A.** Schematic representation of sequential steps in indirect ELISA from binding monomers to plate to detection of HRP fluorescence using H_2O_2. **B.** Absorbance at 450nm minus absorbance at 540nm of serially diluted refolded CD1b and CD1b-endo proteins. **C.** Absorbance at 450nm minus absorbance at 540nm of control CD1a-endo protein at 10μg mL^{-1} bound by anti-CD1a or anti-CD1b antibodies. Data are from one experiment.

To assess the biological activity of refolded CD1b, biotinylated monomers were prepared as described for CD1b-endo and the biotinylation efficiency was verified by SDS-PAGE (data not shown). Refolded CD1b tetramers were prepared and used to stain 1.27 TCR transduced cells or untransduced cells alongside mammalian CD1b-endo. Refolded CD1b tetramers stained the 1.27 TCR expressing cells to a similar degree as CD1b-endo tetramers (**Fig. 4.6**), even in the absence of exogenous antigen, highlighting that the refolded CD1b had adopted the correct conformation. Interestingly, structural studies revealed that refolding CD1b in the presence of single alkyl chain detergents, such as CTAB, not only supports CD1b folding, but these detergents can be found captured deep within the antigen binding cleft, occupying the solvent-protected F' and T' channels (24). The single alkyl chain detergents stabilise the CD1b monomer, while leaving the A' and C' channels available for loading with exogenous antigen. Thus, in the absence of exogenous antigen, refolded CD1b monomers may have an empty antigen-binding cleft.

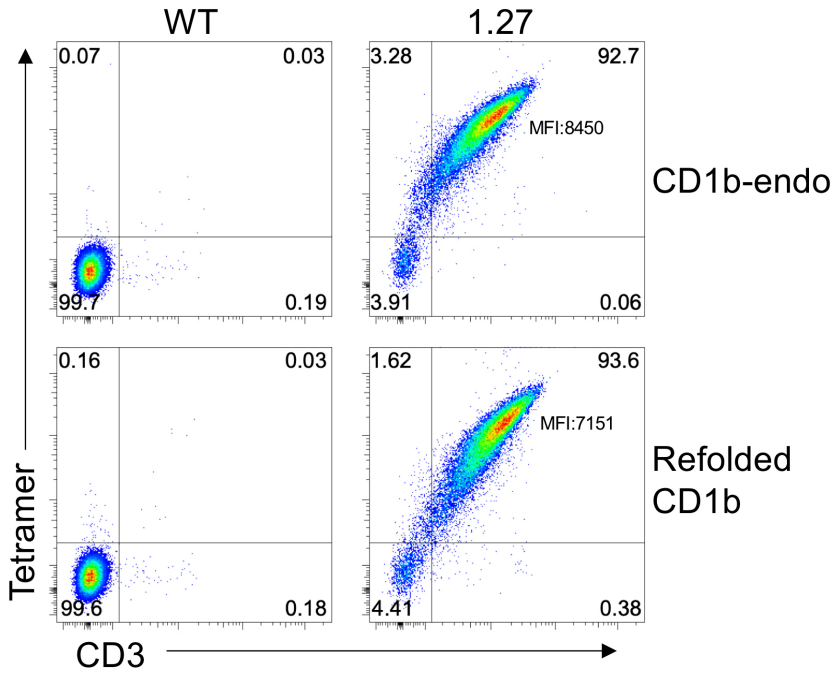

Figure 4.6. Comparative reactivity of 1.27 cell line to refolded CD1b and CD1b-endo tetramers. Wild type Jurkat-76 cells (untransduced) or 1.27 cells were stained with tetramers to assess the biological activity of refolded CD1b and CD1b-endo. The cell lines were stained with the CD1b-endo (top panel) or refolded CD1b (bottom panel) tetramers in conjunction with CD3 and a live/dead marker. Plots display tetramer reactivity and CD3 expression of viable cells. Data are representative of three independently performed experiments.

4.2.7 Differential recognition of antigens by autoreactive T cell lines

To interrogate whether the reactivity of the autoreactive T cell lines to refolded CD1b could be enhanced and to identify potential lipid specificities by the autoreactive TCRs, refolded CD1b monomers were loaded with a suite of different lipid antigens, including phosphatidic acid (PA), phosphatidylserine (PC), phosphatidylcholine (PC), lysophosphatidylcholine (LPC), phosphatidylethanolamine (PE), phosphatidylglycerol (PG), phosphatidylinositol (PI), phosphatidylserine (PS), glucose monomycolate (GMM) or monosialotetrahexosylganglioside (GM1) which were subsequently tetramerised for cell line staining (**Fig. 4.7A**). A similar hierarchy in tetramer staining intensity was observed for refolded CD1b tetramers as for CD1b-endo tetramers among all autoreactive T cell lines, however in some cases, refolded CD1b tetramers stained the autoreactive T cell lines considerably weaker (**Fig. 4.7B**). Despite a wide variation in the lipids' headgroup complexity, the 1.27 cell line recognised all tetramers with similar intensity, suggesting that the 1.27 TCR did not discriminate between these antigens presented by CD1b, although subtle fluctuations were present between lipid loaded tetramers (**Fig. 4.7C**). The 4.27 cell line stained with all lipid loaded tetramers (**Fig. 4.7C**), however this line exhibited a clear preference for CD1b-endo tetramers that could not be simulated by loading refolded CD1b with lipid antigen. Due to the near identical TCRα chains between these two cell lines and similar TCRβ chains, TRBV5-8 and TRBV5-4 respectively, it is possible that the 1.27 and 4.27 TCRs may engage the CD1b-Ag cleft in a similar manner, albeit with a seemingly wide variance in binding affinity (**Fig. 4.7B and C**).

Interestingly, while the 4.13-2 cell line was only weakly CD1b-reactive and recognised both the CD1b-endo and refolded CD1b tetramers comparably, by cells that had very high surface expressed CD3, the staining intensity was marginally increased when these cells were stained with the PA-loaded refolded CD1b tetramers (**Fig. 4.7C**). Thus, it is possible that the 4.13-2 TCR recognises the CD1b protein itself and may be hindered sterically by non-permissive lipids, including CD1b-endo binding lipids. Disruption of TCR autoreactivity by non-permissive antigens has previously been demonstrated for CD1a-restricted T cells (223).

Interestingly, the 4.41 cell line stained strongly with mammalian CD1b-endo tetramers but substantially weaker with refolded CD1b tetramers (**Fig. 4.7C**). These data suggest that antigen is important for 4.41 TCR recognition. In support of this, the addition of a variety of diacylated lipid antigens, including the structurally diverse GMM and GM1, to refolded CD1b partially or fully restored staining intensity to a similar level as CD1b-endo (**Fig. 4.7C**). Furthermore, loading of refolded CD1b with PG caused a large increase in tetramer staining of the 4.41 cell line compared to both mock loaded CD1b-endo and mock loaded refolded CD1b, suggesting the 4.41 TCR may be strongly reactive to this phospholipid, similar to two cell lines identified using CD1b dextramers in a previous study (52) (**Fig. 4.7C**). In contrast, refolded CD1b loaded with LPC was unable to restore CD1b-endo levels of tetramer binding by the 4.41 cell line (**Fig. 4.7C**). These data support that the 4.41 TCR is sensitive to changes at the TCR/CD1b interface caused by presence of different antigens.

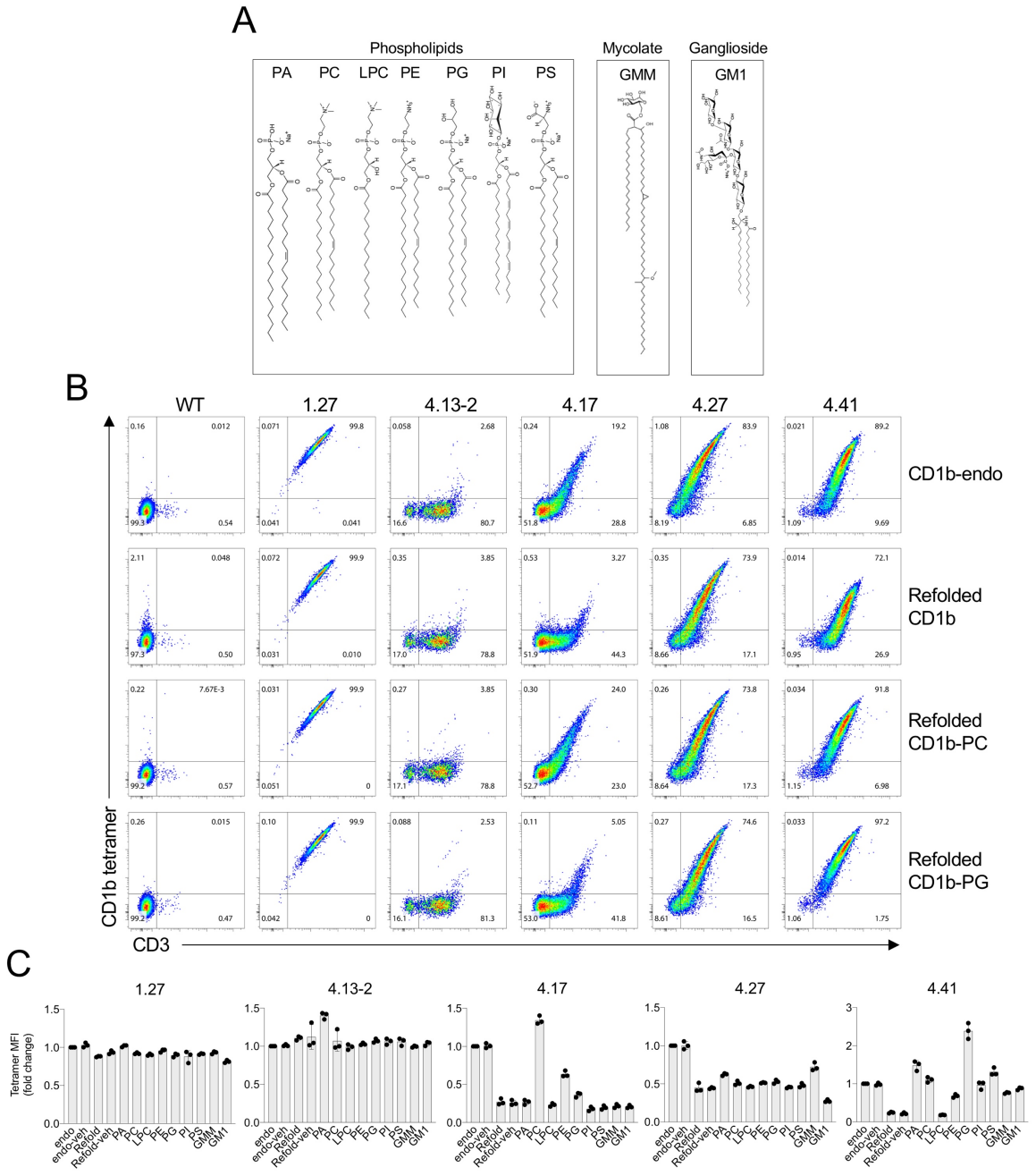

Figure 4.7. Autoreactive T cell line recognition of exogenous lipid loaded CD1b tetramers. Refolded CD1b monomers were loaded with the phospholipids PA, PC, LPC, PE, PG, PI, PS, the mycolate GMM or ganglioside GM1 and tetramerised for staining the Jurkat-76 cell lines transduced with autoreactive TCRs. **A.** Schematic of lipid antigens used to load into refolded CD1b. **B.** Autoreactive T cell lines stained with either mammalian CD1b-endo, refolded CD1b, refolded CD1b loaded with PC or refolded CD1b loaded with PG. **C.** Tetramer geometric MFI (relative to CD1b-endo) of autoreactive T cell lines stained with mammalian CD1b tetramers; CD1b-endo, mock loaded CD1b-endo (endo-veh) and refolded CD1b tetramers; refolded CD1b (Refold), mock loaded refolded CD1b (Refold-veh) and refolded CD1b loaded with various lipid antigens. Data are from three independently performed experiments.

The 4.17 cell line stained strongly with CD1b-endo and only very weakly with refolded CD1b, suggesting this line was also sensitive to changes in antigen at the TCR/CD1b interface (**Fig. 4.7C**). However, many of the lipid antigens, including; PA, LPC, PG, PI, PS, GMM and GM1 loaded into refolded CD1b did not increase tetramer reactivity by the 4.17 TCR (**Fig. 4.7C**). In contrast, PC and to a lesser extent PE and PG, loaded refolded CD1b tetramers were recognised by the 4.17 TCR suggesting these phospholipids were favoured by the 4.17 TCR (**Fig. 4.7C**). Notably, the headgroups of PC and PE are structurally similar and both possess a net positive charge compared to the other phospholipid antigens that may influence TCR recognition.

Taken together, differences in lipid antigen resulted in changes in TCR recognition by our T cell clones, despite the original cells these TCRs were derived from being identified using CD1b-endo tetramers. These results suggest that the mode of CD1b-endo tetramer recognition by the TCR is not conserved among autoreactive CD1b-restricted T cells. Clones 4.17, 4.27 and 4.41 all stained substantially brighter with CD1b-endo tetramers than refolded CD1b tetramers (**Fig. 4.7B and C**), and in some cases, loading with lipid antigens could not restore CD1b-endo level staining intensity, indicating that the precise endogenous lipid or lipids that are recognised most strongly by these autoreactive TCRs are yet to be elucidated. Moreover, different autoreactive TCRs conferred a broad range of antigen specificities, conceivably permitting these cells to respond to a variety of different immune challenges based on the lipid antigens present.

4.2.8 Generation of mutant CD1b expressing cell lines

To gain greater insight into how the different autoreactive TCRs interact with CD1b, a panel of 17 CD1b-expressing cell lines was produced that each contained a single site mutation, with the exception of one line that possessed wild type CD1b (**Table AII.1**). Solvent-exposed amino acids in the cleft of CD1b were selected for mutation as these would most likely contact TCR (**Fig. 4.8A**). Constructs containing the full length CD1b heavy chain gene were designed with mutations corresponding to single alanine substitutions along the α1 and α2 helices of CD1b. The antigen presenting C1R cell line was transduced with each of the CD1b mutant heavy chain gene with retrovirus. C1R cells were sorted using an anti-CD1b monoclonal antibody to ensure cells expressed similar levels of CD1b (**Table 2.3**). All of the CD1b expressing C1R cells stained with

the anti-CD1b antibody with a similar intensity (**Fig. 4.8B**), suggesting that the mutations did not impair CD1b expression appreciably.

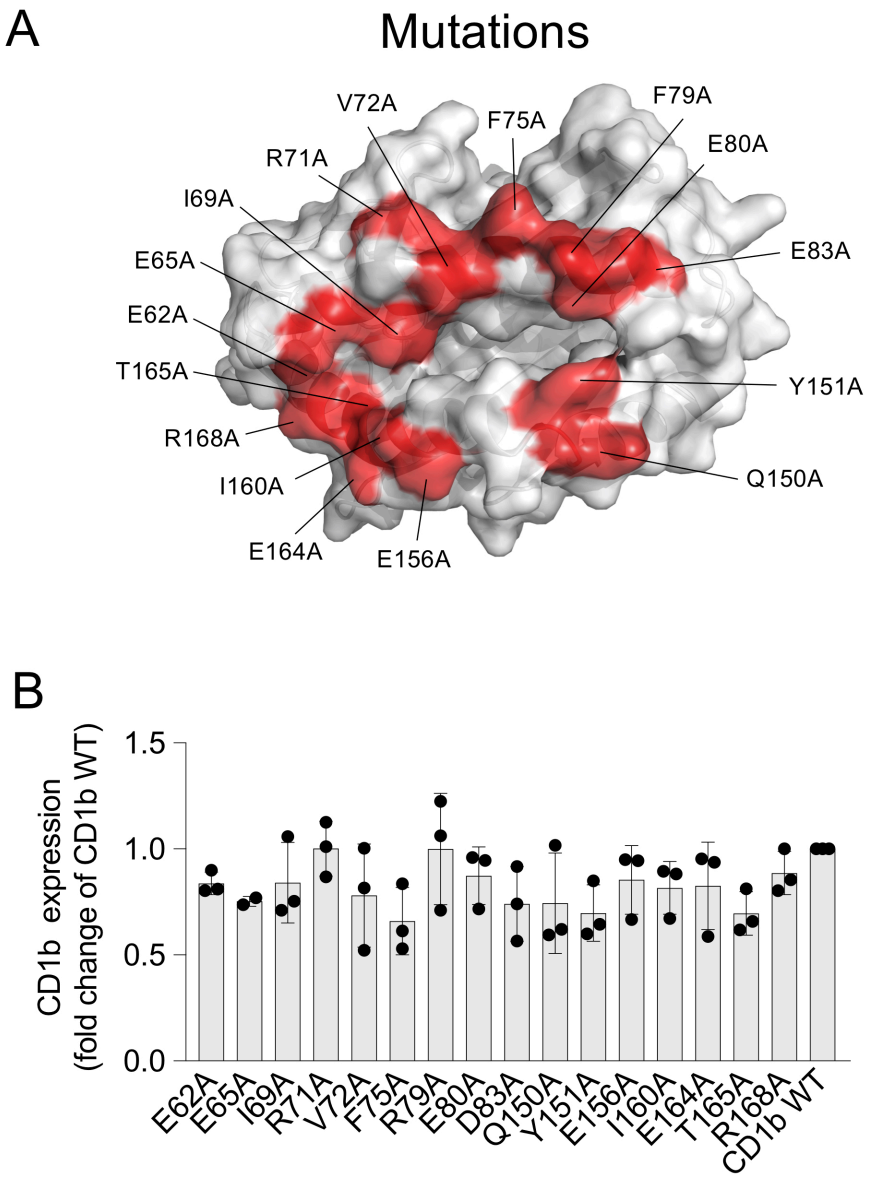

Figure 4.8. CD1b expression levels of mutant CD1b transduced cell lines. C1R cells were transduced with 16 mutant full-length CD1b genes or unmutated CD1b for cell line activation assays. CD1b expression was verified using an anti-CD1b monoclonal antibody (SN13) **A.** Schematic of CD1b structure showing the α1 and α2 helices of the CD1b antigen binding cleft, annotated in red are the amino acid residues that were mutated to alanine. CD1b schematic was prepared using the CD1b-GM2 structure deposited as 1GZP in the protein databank (PDB) **B.** Bar chart displays CD1b antibody fluorescence of mutant CD1b and wild type CD1b (CD1b WT) expressing cell lines after transduction and cell sorting. Data are representative of at least two independently performed experiments.

4.2.9 The effects of CD1b mutagenesis on autoreactive T cell line activation

To test whether autoreactive TCRs were reactive to the mutant CD1b-expressing cell lines, SKW-3 cells deficient in TCR as well as β_2m, referred to as SKW-3.$\beta_2m^{-/-}$ cells were generated for the 1.27 and 4.17 TCRs as well as two previously published CD1b/PG-reactive TCRs, PG90 and PG10 (52). Autoreactive TCR transduced SKW-3.$\beta_2m^{-/-}$ cells were co-cultured with each of the mutant CD1b-expressing cell lines or a wild type CD1b expressing cell line and CD69 expression was examined, a marker that is strongly upregulated in SKW-3 cells following TCR ligation. Hence in this assay, reactivity to mammalian endogenous lipids was assessed, whereby C1R derived lipids may be similar or identical to those presented by CD1b-endo tetramers from HEK culture. After 24 hours in culture, the T cell lines were analysed for CD69 expression.

The 1.27 cell line upregulated CD69 in response to wild-type CD1b expressing C1Rs to a greater extent than wild type C1R cells, providing a baseline for comparing the mutant CD1b expressing C1R cells (**Fig. 4.9A**). Even though CD69 expression by the 1.27 cell line in response to wild type CD1b was only ~2-fold higher than wild type C1R cells it was possible to accurately measure the effects of the CD1b mutations on activation by the 1.27 cell line. Residues R71 and R79 appeared to be critical for activation, as mutating these residues to alanine abrogated CD69 expression entirely (**Fig. 4.9B**). Similarly, flanking residues F75 and D83 moderately impaired CD69 upregulation when mutated to alanine. Strikingly, residue E65, that is positioned over the A' roof on the α1 helix (**Fig. 4.9C**) enhanced CD69 upregulation considerably (**Fig. 4.9B**). Charged residues across the A' roof have been known to control lipid loading in response to pH change or when mutated (224). It is possible that E65A may alter the lipid repertoire presented by CD1b. However, due to the limited antigen discrimination exhibited by the cell line, it is more likely that the enhanced activation is due to a conformational change in the CD1b protein that is more favourable for 1.27 TCR recognition. Moreover, only residues along the lateral part of the α1 helix impaired CD69 expression (**Fig. 4.9C**), supporting an off-axis TCR docking mode with limited surveillance of antigen.

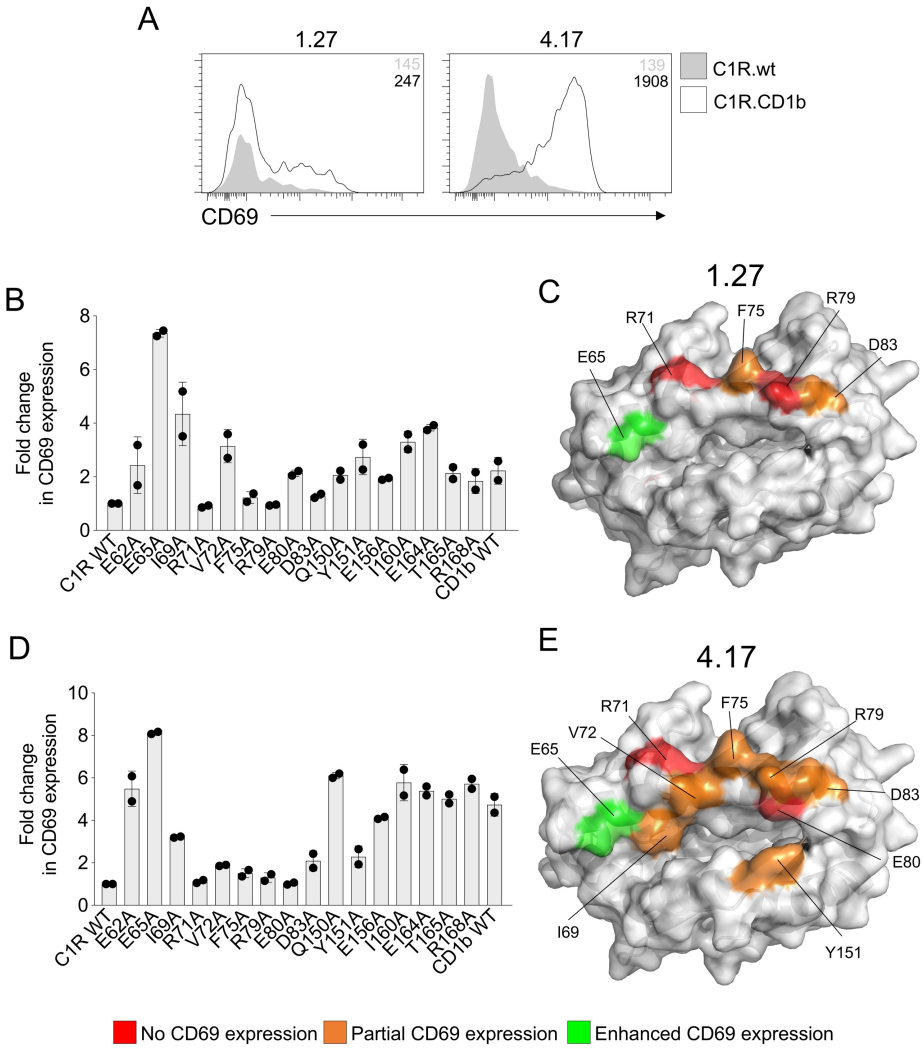

Figure 4.9. Mutant CD1b activation assay with autoreactive T cell lines. 1.27 or 4.17 SKW-3.$\beta_2m^{-/-}$ cells were cultured 1:1 with mutant or wild type CD1b expressing C1R cells for 24 hours. After the culture period, cells were stained with anti-CD69, anti-CD19 and anti-CD3 monoclonal antibodies to assess T cell activation. C1R cells were removed using CD19, and CD69 expression was examined on viable $CD3^+$ cells. **A.** Histograms display CD69 upregulation of 1.27 and 4.17 cell lines cultured with either wild type C1Rs that lack CD1b (C1R.wt) or CD1b expressing C1Rs (C1R.CD1b). Geometric mean fluorescence intensities are displayed in the top right corner of each plot. **B.** Fold change in CD69 expression by 1.27 cells cultured with mutant or wild type CD1b expressing C1R cells, compared to wild type C1R cells (C1R wt). **C.** CD1b structure depicting mutations at residues that impacted CD69 expression by the 1.27 cell line. Residue mutations in red completely abrogated CD69 expression and mutations in green enhanced CD69 expression. **D.** Fold change in CD69 expression by 4.17 cells cultured with C1R cell lines as described above. **E.** CD1b structure depicting mutations that impacted CD69 expression by the 4.17 cell line. Residues in red abrogated CD69 expression (No CD69 expression), residues in orange reduced CD69 expression (Partial CD69 expression) and residues in green enhanced CD69 expression (Enhanced CD69 expression). Data are representative of two independent experiments.

The 4.17 cell line was significantly more sensitive to CD69 upregulation (**Fig. 4.9A**), with a ~5-fold increase in CD69 expression when 4.17 cells were cultured with CD1b expressing C1R cells compared to parental C1R cells that lack CD1b expression (**Fig. 4.9A and D**). Similar to the 1.27 cell line residues R71, R75, R79 and E83 mutations severely reduced or abrogated CD69 expression and E65A enhanced CD69 expression but had less of an effect compared to the 1.27 cell line (**Fig. 4.9D**). Additional residues along the α1 helix, specifically V72 and E80, were also critical for CD69 expression (**Fig. 4.9E**), suggesting that the 4.17 TCR makes extensive contacts with the α1 helix. Residue mutation I69A, positioned next to the CD1b cleft opening, moderately reduced CD69 expression (**Fig. 4.9D and E**) and mutation Y151A, on the α2 helix substantially reduced CD69 expression (**Fig. 4.9D and E**). In contrast to the 1.27 cell line, the 4.17 cell line relied on residues along both the α1 and α2 helices of CD1b for activation, particularly surrounding the lipid exposed cleft of CD1b, likely due to the observed role of the lipid antigen in shaping TCR reactivity (**Fig. 4.7B**).

Both the PG90 and PG10 cell lines expressed CD69 in response to wild type CD1b expressing C1R cells (**Fig. 4.10A**), even in the absence of PG, likely due to a broader reactivity to other phospholipids demonstrated with CD1b tetramers or possibly by the presence of PG in C1R cells (52). In contrast to the CD1b-endo reactive 1.27 and 4.17 cell lines, PG90 activation was not affected by residue mutations along the α1 helix with the exception of residue E80A that completely abrogated CD69 expression (**Fig. 4.10B**). Mutations Y151A and I160A on the α2 helix also abrogated CD69 expression (**Fig. 4.10B**). Notably, the ternary complex of PG90 and CD1b-PG reveals that both E80 and Y151 residues are contacted directly by the TCR and reactivity to mutant CD1b-PG tetramers at these sites validates their involvement in TCR recognition (150).

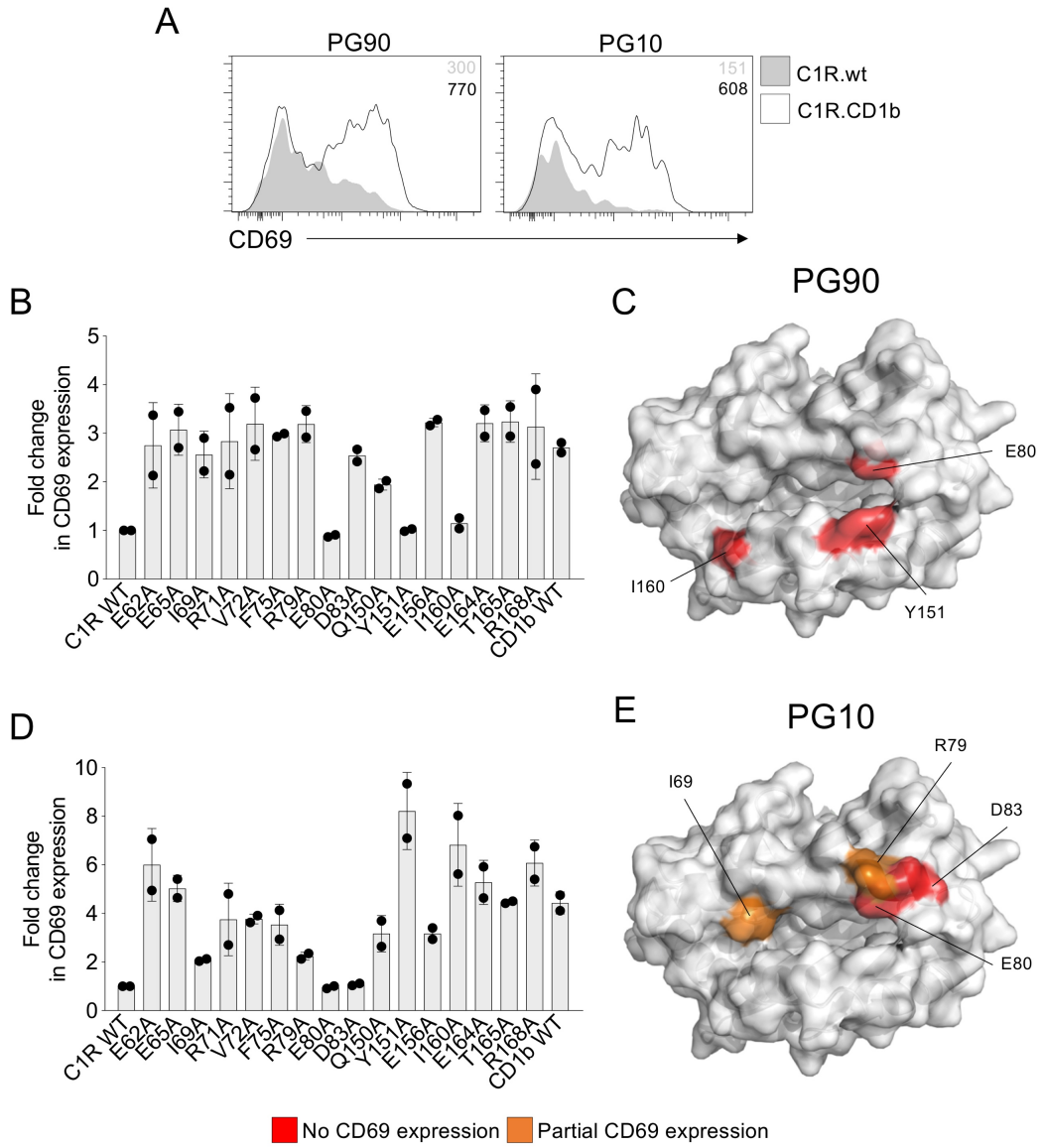

Figure 4.10. Mutant CD1b activation assay with PG-reactive cell lines. PG90 or PG10 SKW-3.$\beta_2m^{-/-}$ cells were cultured 1:1 with mutant or wild type CD1b expressing C1R cells for 24 hours. After the culture period, cells were stained with anti-CD69, anti-CD19 and anti-CD3 monoclonal antibodies to assess T cell activation. **A.** Histograms display CD69 upregulation of PG90 and PG10 cell lines cultured with either wild type C1Rs that lack CD1b (C1R.wt) or CD1b expressing C1Rs (C1R.CD1b). Geometric mean fluorescence intensities are displayed in the top right corner of each plot. **B.** Fold change in CD69 expression by PG90 cells cultured with mutant or wild type CD1b expressing C1R cells, compared to wild type C1R cells (C1R wt). **C.** CD1b structure depicting mutations at residues that impacted CD69 expression by the PG90 cell line, residues in red completely abrogated CD69 expression. **D.** Fold change in CD69 expression by PG10 cells cultured with C1R cells as described above. **E.** CD1b structure depicting mutations at residues that impacted CD69 expression by the 4.17 cell line. Residues in red abrogated CD69 expression (No CD69 expression) and residues in orange reduced CD69 expression (Partial CD69 expression). Data are representative of two independent experiments.

The PG10 cell line was most affected by residue mutations on the F' side of the α1 helix, including R79A, E80A and E83A as well as residue I69A on the A' side (**Fig. 4.10D and E**) that all significantly reduced or abrogated CD69 expression. Notably, E80A which is centrally located within the CD1b cleft, appeared to be a hotspot on CD1b, impairing activation by 4.17, PG90 and PG10 cell lines when mutated to alanine (**Fig. 4.9E, 4.10C and E**). Notably, while PG90 and PG10 TCRs strongly recognise CD1b-PG (52), the 4.17 cell line was not reactive to CD1b-PG tetramers (**Fig. 4.7B**). Therefore, E80 might play a role in orienting the phospholipid backbone for TCR recognition and is itself a contact made by the PG90 TCR (150). Interestingly, while E80 is contacted directly by the GEM42 TCR, an E80A mutation had no appreciable impact on TCR recognition of CD1b-GMM based on affinity studies (138).

4.2.10 Production of autoreactive TCRs reactive to CD1b

The autoreactivity observed with CD1b-restricted reporter cell lines suggests that autoreactive TCRs adopt a variety of docking modes and considerable plasticity to survey CD1b-Ag (**Fig. 4.7, 4.9 and 4.10**). However, the lipids presented by mammalian expressed CD1b-endo that are permissive to autoreactive TCR recognition remain speculative. To help elucidate the precise lipid antigens presented by CD1b, TCR-trap experiments were carried out. Hereby soluble 1.27 and 4.17 TCRs were used to capture permissive lipid antigens presented by CD1b, akin to previous studies using the CD1a and CD1d systems (223, 225). TCR-trap allows distinguishing soluble CD1b bound to TCR permissive lipids from CD1b bound to TCR non-permissive lipids. This is achieved by the separation of larger TCR-CD1b ternary complexes from unbound TCR and CD1b using size-exclusion chromatography.

Genes encoding the extracellular portions of the 1.27 or 4.17 TCRα and TCRβ chains were designed with Avidex tags (**Table 2.4**). Avidex tags are repurposed leucine zipper proteins, modified from the Fos and Jun transcription factor subunits, and are added to the C-terminus of each TCR subunit to specifically promote binding and stability of TCRαβ heterodimers through paired Fos-Jun dimerisation (226). Synthesised TCR chain genes were cloned into separate pET30 constructs using the 5' and 3' restriction sites NdeI and HindIII respectively and transformed into *E. coli* bacteria for expression. All

TCR chains were expressed and recovered from bacterial inclusion bodies at approximately 10-20 mg mL^{-1} concentrations (**Fig. 4.11A and B**). As expected, both the 1.27 and 4.17 TCRβ chain IBPs appeared larger on the SDS-PAGE than the paired TCRα chains, due to their greater molecular weight (**Fig. 4.11A and B**). Matching TCR chains were injected into a refolding buffer (**Table 2.2**) at a 2:1 ratio of α to β chain to reduce TCRβ chain homodimer formation during refolding.

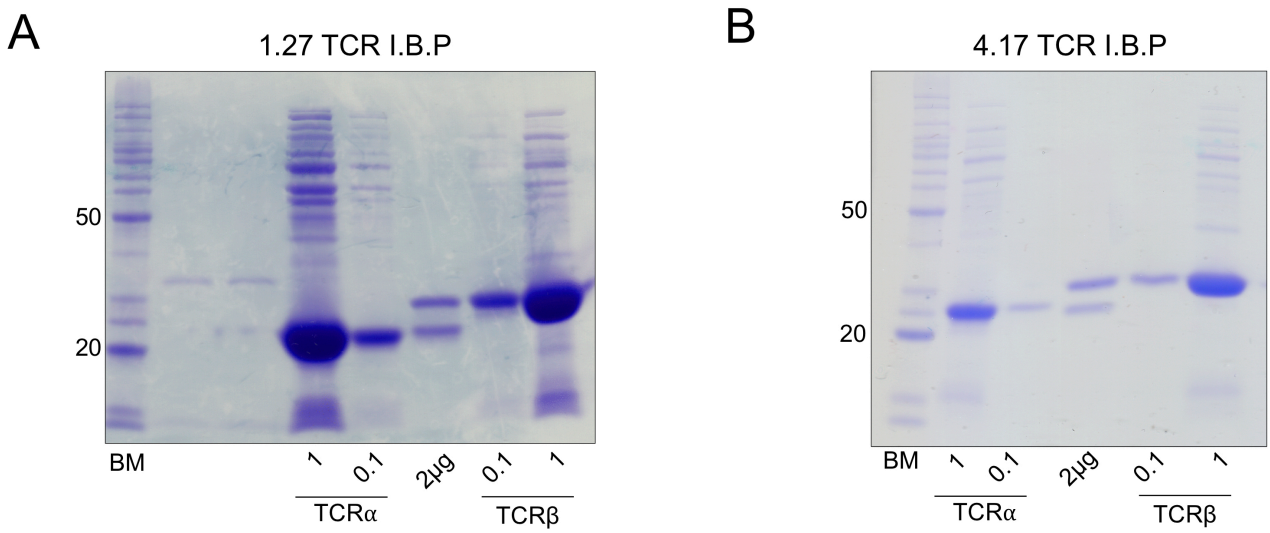

Figure 4.11. SDS-PAGE of 1.27 and 4.17 TCR chain I.B.Ps. *E. coli* bacteria were transformed with soluble gene constructs containing the TCRα and TCRβ chains from the 1.27 and 4.17 TCRs. Soluble TCR chains were expressed and purified from bacterial inclusion bodies. **A.** 12% SDS-PAGE of 1.27 TCR α and β chains (1 µL and 0.1 µL) under reducing conditions alongside a benchmark protein ladder (BM) and 2 µg of a control TCR. Left annotations refer to the 50 kDa and 20 kDa protein standards. **B.** 12% SDS-PAGE of 4.17 TCR α and β chains (1 µL and 0.1 µL) under reducing conditions alongside a benchmark protein ladder (BM) and 2 µg of a control TCR, annotated as described above. These data are representative of at least two independently performed expressions of each TCR chain.

Both the 1.27 and 4.17 TCRs were purified by DEAE anionic exchange chromatography followed by size-exclusion chromatography using a Superdex 75 pg column and a subsequent MonoQ anionic exchange chromatography to isolate TCR homodimers from all impurities. Similar to refolding CD1b, the 1.27 and 4.17 TCRs were purified first with DEAE resin beads exposed to a constant NaCl concentration of 200 mM. A broad UV absorbance peak visible from volumes 30-40 mL was detected for both TCRs (**Fig. 4.12A and 13A**). An SDS-PAGE of the eluted fractions from the 1.27 TCR, under reducing conditions, revealed two protein bands that corresponded to TCRα and TCRβ chains at 25 kDa and 30 kDa respectively, across fractions 4-11 (**Fig. 4.12B**). Due to the presence of an interchain disulfide bond, TCR dimers are only separated with a reducing agent (227). SDS-PAGE performed under non-reducing conditions revealed several protein bands corresponding to intact TCR dimer of ~50 kDa in fraction 7 (**Fig. 4.12B**), likely TCRαβ and TCRββ dimers as there was more TCRβ protein relative to TCRα under reducing conditions. Within all fractions, faint protein bands of low and high molecular weight were visible, likely due to larger misfolded TCR aggregates and endogenous bacterial impurities (**Fig. 4.12B**). A reducing SDS-PAGE of the eluted fractions from the 4.17 TCR revealed two protein bands, corresponding to TCRα and TCRβ chains (**Fig. 4.13B**). Similarly, the amounts of TCRβ to TCRα as discerned by the thickness of the protein bands, particularly in fraction 5, suggests that far more TCRβ has refolded compared to TCRα (**Fig. 4.13B**) albeit having invested a 2-fold excess of TCRα compared to TCRβ for folding. For both TCRs, fractions 4-11 were collected for further purification.

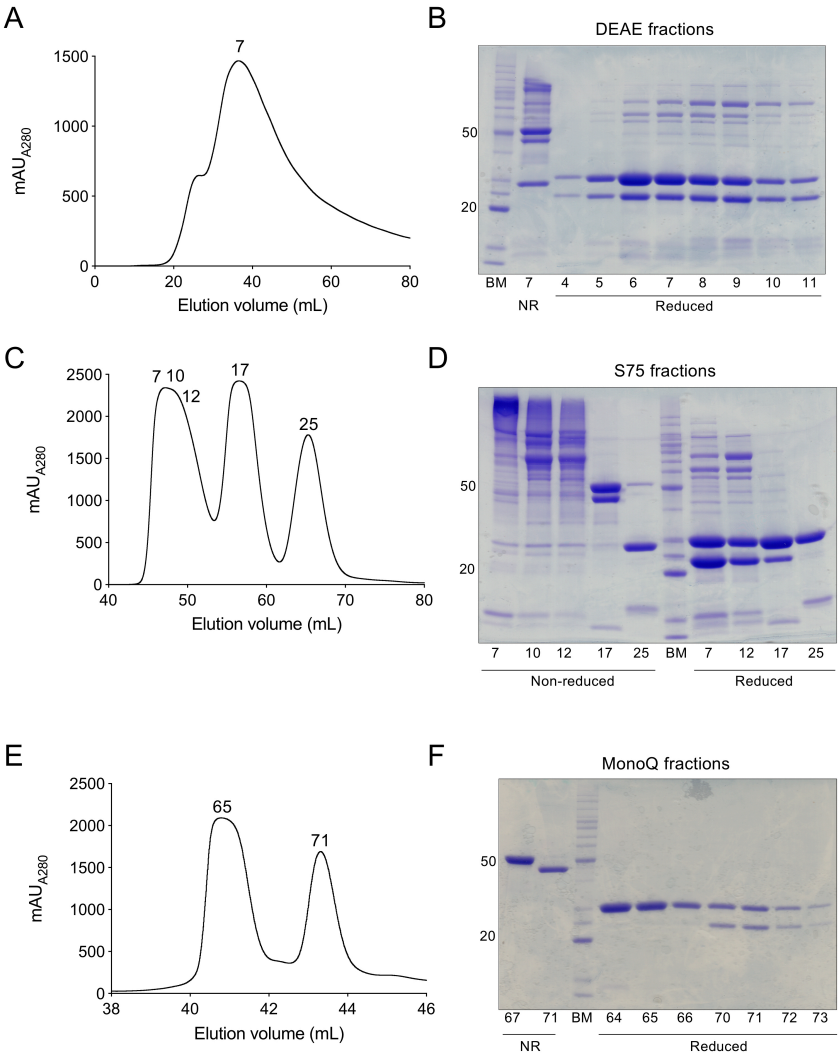

Figure 4.12. Purification of the 1.27 TCR by liquid chromatography. Refolded 1.27 TCR was purified after dialysis by successive anionic exchange and size exclusion chromatography. **A.** Chromatogram of UV absorbance after 1.27 TCR purification from DEAE beads using a constant NaCl concentration. Number annotation 7 refers to the peak fraction containing TCRα and TCR chains. **B.** 12% SDS-PAGE of key fractions eluted from DEAE purification under non-reducing (NR) and reducing conditions alongside a benchmark protein ladder (BM) annotated with the 50 kDa and 20 kDa protein standards. **C.** Chromatogram of UV absorbance after 1.27 TCR purification from a Superdex 75 pg column. Number annotations refer to fractions containing high order aggregate (7, 10 and 12) TCR dimers (17) and free TCR chain monomers (25). **D.** 12% SDS-PAGE of key fractions eluted from Superdex 75 pg column under reducing and non-reducing conditions, next to a benchmark protein ladder described above. **E.** Chromatogram of UV absorbance after 1.27 TCR purification from MonoQ column using a linear NaCl gradient. Number annotations 66 and 71 refer to purified TCRββ and TCRαβ dimers respectively. **F.** 12% SDS-PAGE of key fractions eluted from MonoQ column under non-reducing and reducing conditions, separated by a benchmark protein ladder as described above. These data are representative of at least three independently performed experiments.

To separate the TCR dimers from higher molecular weight aggregates and smaller proteins, both TCRs were passed over a size-exclusion Superdex 75 pg column. Three UV absorbance peaks were detected from 40-70 mL of eluted volume from the 1.27 TCR column run that corresponded to fractions 10, 17 and 25 (**Fig. 4.12C**), suggestive of three species of protein with significant size differences. An SDS-PAGE of the peak fractions from the UV absorbance chromatogram revealed protein bands corresponding to TCRβ and TCRα chains in fractions corresponding to each of the UV absorbance peaks under reducing conditions (**Fig. 4.12D**). However, under non-reducing conditions, only the UV absorbance peak in fraction 17 contained a protein band corresponding to correctly refolded TCR dimers at ~50 kDa in size (**Fig. 4.12D**). Fractions 7-12 also contained both TCRα and TCRβ chains, but under non-reducing conditions these TCR chains formed aggregates that were of greater molecular weight than TCR dimers (**Fig. 4.12D**). Fraction 25 contained TCRβ but TCRα under both reducing and non-reducing conditions, indicative of free TCRβ in this fraction (**Fig. 4.12D**). According to these observations, fractions 14-21 were pooled for further purification.

Three UV absorbance peaks were detected from 45-75 mL of eluted volume from the 4.17 TCR column run and corresponded to fractions 8, 18 and 27 (**Fig. 4.13C**). An SDS-PAGE revealed that fraction 8 contained both TCRα and TCRβ chains, as well as high order aggregates under reducing conditions, however substantially more TCRβ was present based on both the thickness and intensity of the protein band on the gel (**Fig. 4.13D**). Fraction 18 contained mostly TCRβ and TCRα chains, of which there was much more TCRβ than TCRα, suggestive of a mix of TCRαβ and TCRββ dimers, while fraction 27 consisted entirely of TCRβ chain (**Fig. 4.13D**), similar to fraction 25 from the 1.27 TCR purification (**Fig. 4.12D**). Fractions 15-21, containing both TCRαβ and TCRββ dimers were pooled for further purification.

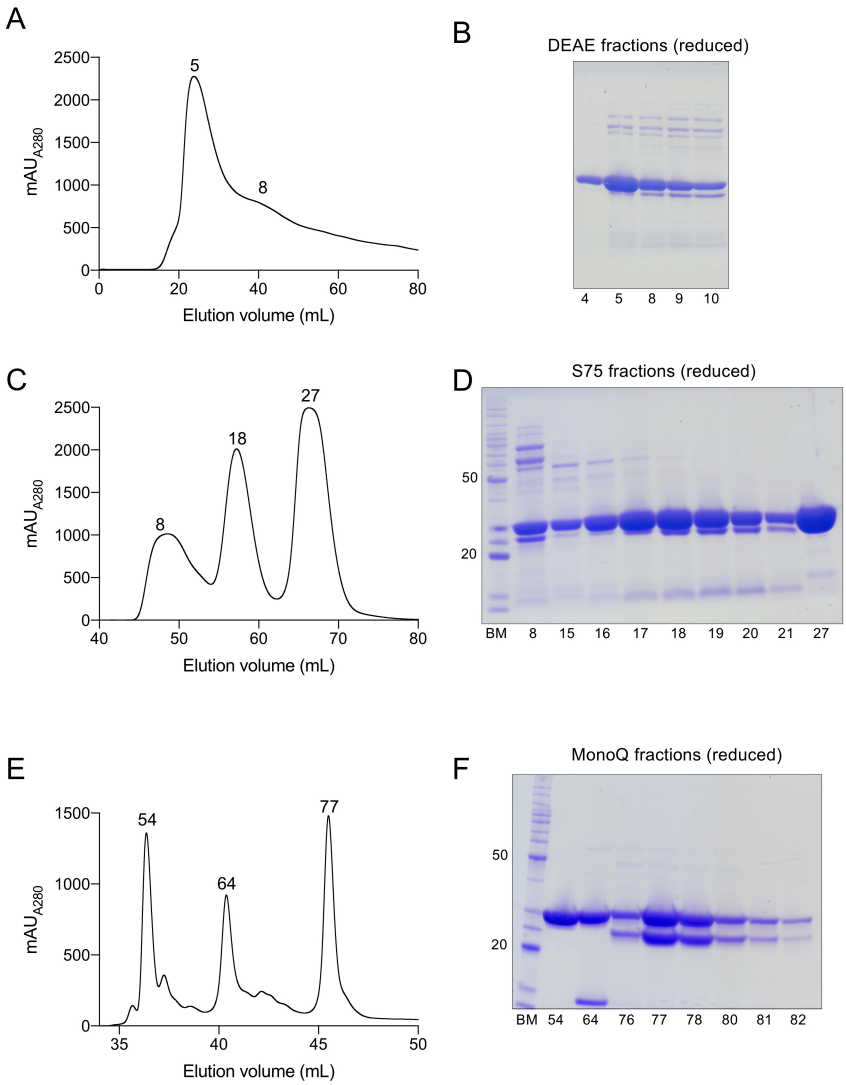

Figure 4.13. Purification of the 4.17 TCR by liquid chromatography. Refolded 4.17 TCR was purified after dialysis by successive anionic exchange and size exclusion chromatography. **A.** Chromatogram of UV absorbance after 4.17 TCR purification from DEAE beads using a constant NaCl concentration. Number annotations refer to the peak fractions identified on the chromatogram. **B.** 12% SDS-PAGE of key fractions eluted from DEAE purification under reducing conditions. **C.** Chromatogram of UV absorbance after 4.17 TCR purification from a Superdex 75 pg column. Number annotations refer to fractions containing high order aggregate (8), TCR dimers (18), and free TCR chain monomers (27). **D.** 12% SDS-PAGE of key fractions eluted from Superdex 75 pg column under non-reducing conditions alongside a benchmark protein ladder (BM) annotated with the 50 kDa and 20 kDa protein standards. **E.** Chromatogram of UV absorbance after 4.17 TCR purification from MonoQ column using a linear NaCl gradient. Number annotations 54, 64 and 77 refer to purified TCRββ dimers, TCRββ dimers and impurity and TCRαβ dimers respectively. **F.** 12% SDS-PAGE of key fractions eluted from MonoQ column under non-reducing and reducing conditions, alongside a benchmark protein ladder as described above. These data are representative of at least three independently performed experiments.

Due to the similar size of TCRαβ and TCRββ dimers, a further anionic exchange chromatography was performed using a shallow gradient from 0 M to 1 M NaCl over 72 mL, to separate the TCR dimer species from the 1.27 and 4.17 TCR protein preparations. For the 1.27 TCR purification, two clear UV absorbance peaks were detected during the elution from the MonoQ column (**Fig. 4.12E**). The maximal absorbance peaks were detected in fractions 65 and 71 respectively. SDS-PAGE under non-reducing conditions revealed clearly two separate protein bands in fraction 67 and 71 of different sizes, corresponding to TCRββ dimers and TCRαβ dimers, respectively (**Fig. 4.12F**). Thus, fractions 70-73, containing purified 1.27 TCRαβ were collected for ternary complexation.

Three UV absorbance peaks were identified on the chromatogram after anionic exchange chromatography of the pooled 4.17 TCR, with peak absorbance contained in fractions 54, 64 and 77 respectively (**Fig. 4.13E**). An SDS-PAGE under non-reducing conditions revealed the identity of the three protein species as TCRβ alone in fraction 54, TCRβ that co-eluted with an unknown species of ~10 kDa in fraction 64 and TCRα and TCRβ chains in fraction 77 that appeared visually in a 1:1 ratio (**Fig. 4.13F**). Thus fractions 76-78, containing purified 4.17 TCRαβ were collected for ternary complexation.

4.2.11 Ternary complexation of autoreactive TCRs with CD1b-endo

To capture antigens presented by CD1b-endo, a 3:2 molar ratio of purified 1.27 TCR or 4.17 TCR was mixed with purified CD1b-endo monomers and eluted complexed proteins by size exclusion chromatography. Slightly more TCR was added than CD1b to maximise the capture of permissive antigens from CD1b. This method of antigen isolation relies on the soluble TCR engaging CD1b-endo with sufficient affinity that complexed proteins migrate through the column more quickly than their monomeric counterparts. Based on the tetramer staining exhibited by the 1.27 and 4.17 cell lines (**Fig. 4.7B**), both TCRs were expected to be capable of co-complexation with CD1b-endo. To establish a baseline elution profile for the TCRs as well as CD1b-endo, all of the proteins were repurified using the same size-exclusion column. As expected, both TCRs as well as CD1b-endo eluted at a similar volume due to their similar size (**purple and blue line, respectively Fig. 4.14A**).

A clear peak in UV absorbance profile was observed during purification of the 1.27 TCR-CD1b-endo co-complex (**red line, Fig. 4.14A**). The co-complex appeared to be eluted much earlier than either 1.27 TCR or CD1b alone (**purple and blue line, respectively Fig. 4.14A**). A small peak was present at the same elution volume as TCR or CD1b-endo alone, presumably excess TCR. Due to the large shift in the elution profile, it was assumed that the 1.27 TCR had an exceptionally high affinity for CD1b-endo (**Fig. 4.14A**). To identify the constituents of the co-complex and un-complexed fractions, an SDS-PAGE was performed under reducing conditions (**Fig. 4.14B and C**). In the fractions containing the early elution, four protein species were observed in equal proportions, corresponding to the 1.27 TCR α and β chains, CD1b heavy chain and β_2m as determined by the reference lanes (**Fig. 4.14B**). In the fractions that contained the late elution, only two protein species were observed, corresponding to excess 1.27 TCRα and TCRβ chains (**Fig. 4.14C**). Thus, in agreement with the CD1b tetramer and activation assays (**Fig 4.7B and 4.9A**), the 1.27 TCR was capable of engaging all the CD1b-endo monomers, irrespective of lipid antigen.

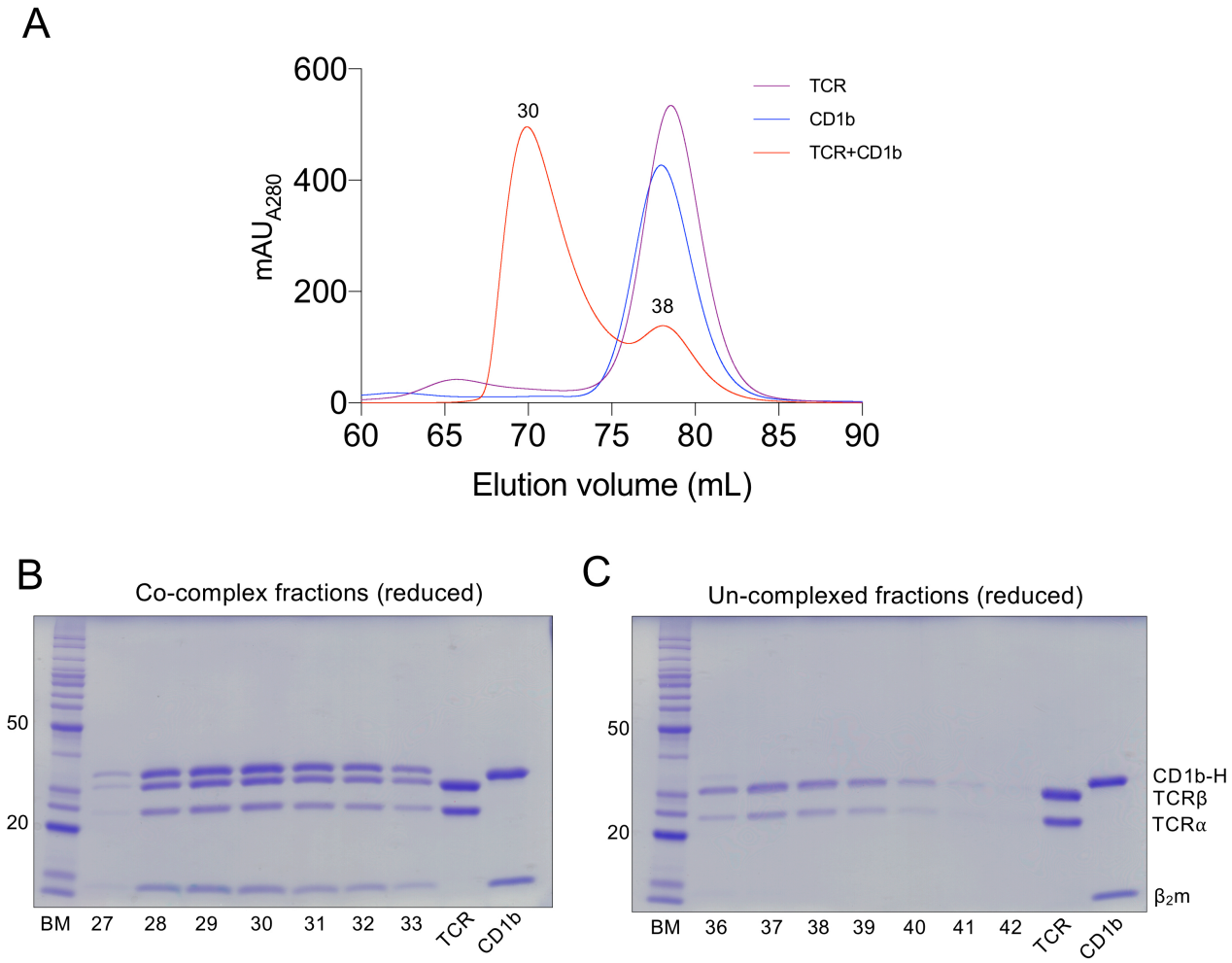

Figure 4.14. Complexation of the 1.27 TCR with CD1b-endo. Soluble 1.27 TCR and CD1b-endo monomers were purified by size-exclusion chromatography to remove any impurities and to establish a baseline elution volume for each protein. TCR was added to CD1b-endo at a saturating 3:2 ratio in favour of TCR. Complexed proteins were purified by size exclusion chromatography. **A.** Chromatogram overlay of UV absorbances for 1.27 TCR alone (TCR) in purple, CD1b-endo alone (CD1b) in blue, or 1.27 TCR and CD1b-endo together (TCR+CD1b) in red after purification using a Superdex 200 pg column. **B.** 12% SDS-PAGE of protein fractions containing complexed 1.27 TCR with CD1b-endo under reducing conditions, alongside a benchmark protein ladder (BM) annotated with 50 kDa and 20 kDa protein standards (left) and 2 µg 1.27 TCR or CD1b-endo alone (right). **C.** 12% SDS-PAGE of protein fractions containing uncomplexed 1.27 TCR and CD1b-endo under reducing conditions, alongside a benchmark protein ladder (left) and 2 µg 1.27 TCR or CD1b-endo alone (right). These data are representative of three independently performed experiments.

A similar shift was observed in the UV absorbance on the chromatogram for the 4.17 TCR-CD1b-endo co-complex (**Fig. 4.15A**). However, the separation between the co-complex and uncomplexed proteins was less apparent compared to the 1.27 TCR, most likely due to a lower affinity for CD1b-endo. Moreover, the UV absorbance peak corresponding to the uncomplexed proteins was larger than the peak corresponding to the complexed proteins, indicating that the much of the 4.17 TCR did not complex with CD1b-endo (**Fig. 4.15A**). SDS-PAGE under non-reducing conditions of the co-complex fractions revealed three protein bands, corresponding to 4.17 TCR, CD1b heavy chain and β_2m in equal quantities as visualised on the gel (**Fig. 4.15B**). However, in the uncomplexed fractions eluted later from the column, an increase in the amount of protein species corresponding to TCR was observed, while the CD1b-endo protein species remained constant, particularly evident in fractions 37-40 (**Fig. 4.15B**). It is likely that only a proportion of the CD1b-endo contained lipid antigens permissive to recognition by the 4.17 TCR, while excess TCR was unable to co-complex with CD1b containing non-permissive antigens which eluted later.

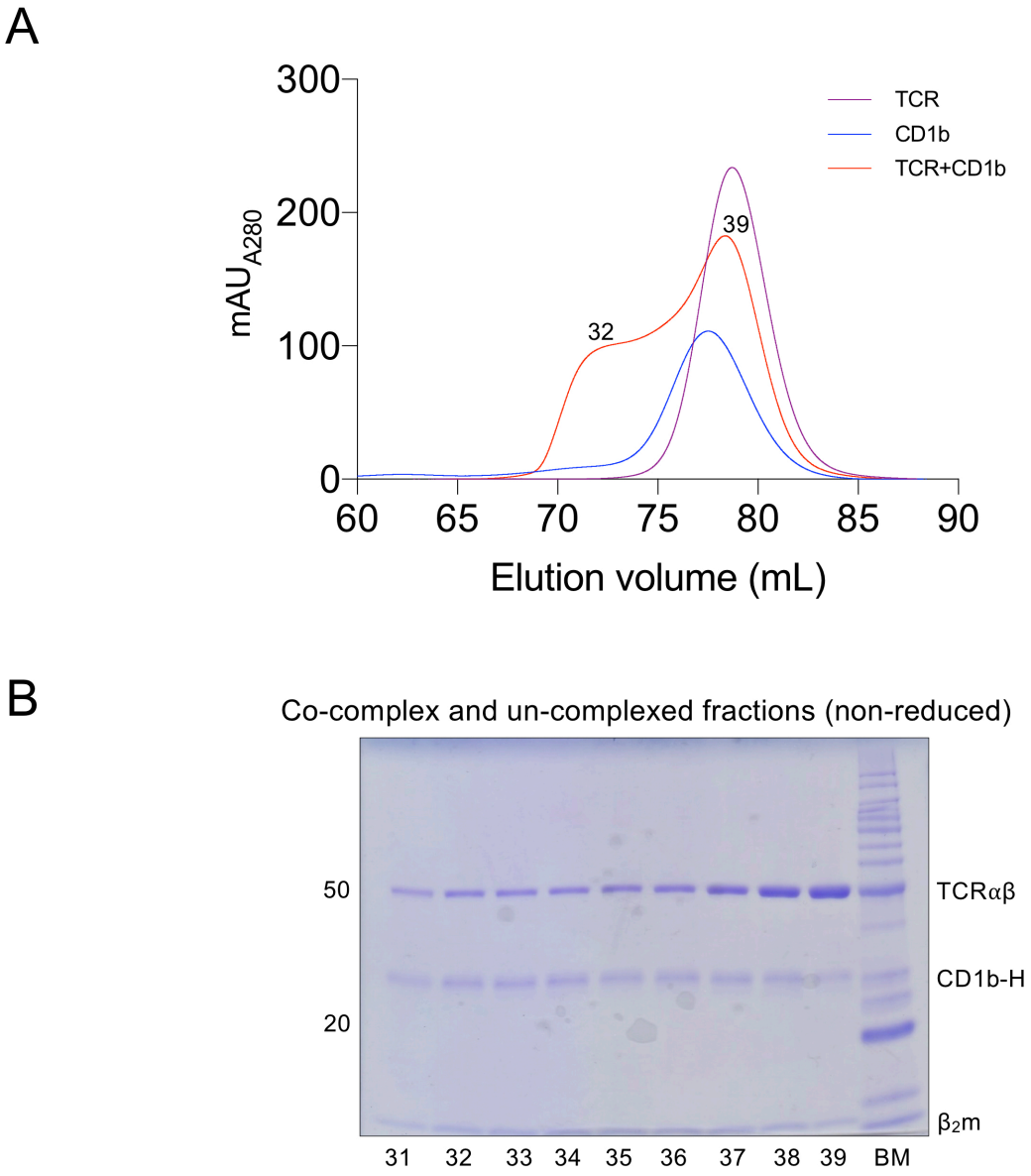

Figure 4.15. Complexation of the 4.17 TCR with CD1b-endo. Soluble 4.17 TCR and CD1b-endo monomers were purified by size-exclusion chromatography to remove any impurities and to establish a baseline for each protein. TCR was added to CD1b-endo at a saturating 3:2 ratio in favour of TCR. Complexed proteins were purified by size-exclusion chromatography. **A.** Chromatogram overlay of UV absorbances for the 4.17 TCR alone (TCR) in purple, CD1b-endo alone (CD1b) in blue, or 4.17 TCR and CD1b-endo together (TCR+CD1b) in red after purification using a Superdex 200 pg column. **B.** 12% SDS-PAGE of protein fractions containing complexed and uncomplexed 4.17 TCR and CD1b-endo under non-reducing conditions, alongside a benchmark protein ladder (BM) annotated with 50 kDa and 20 kDa protein standards (right). These data are representative of three independently performed experiments.

4.2.12 Identification of permissive lipid antigens from CD1b-endo

To determine the identity of the isolated permissive antigens presented in the CD1b-endo co-complexes, these were sent to collaborators at Harvard University (Branch Moody and Tan-Yun Cheng) who carried out high performance liquid chromatography (HPLC) mass spectrometry (MS) of the 1.27 and 4.17 TCR/CD1b ternary complexes. The TCR/CD1b ternary complex fractions, uncomplexed fractions and CD1b-endo protein alone, were purified by HPLC, nebulised by nanospray ionisation and analysed by MS in negative mode. Lipids antigens that are common in mammalian cells were the focus of the MS analysis. Ions were detected from CD1b-endo alone with a mass to charge ratio (m/z) specific to common phospholipids such as sphingomyelin (SM), PC, PA, PS and PI of various acyl chain lengths, as well as an unknown species with a m/z of 715.2 (**Fig. 4.16A**). Importantly, PC was the most abundant and diverse of the phospholipids presented by CD1b (**Fig. 4.16A**).

Notably, all of the lipids identified from CD1b-endo alone were also identified from the 1.27 TCR co-complex fractions, except for the single species of PA detected at 673.6 m/z (**Fig. 4.16B**). Given the indiscriminate recognition of CD1b-endo by the 1.27 TCR, it is interesting that the TCR did not form ternary complexes with CD1b presenting PA. It is unclear what happened to the PA as it was not detected in the uncomplexed fractions, which only contained few lipid species, of 715.2, 766.5, 794.6 and 822.6 m/z that were identified as PC of different lipid tail length and the unknown species also detected in the complex fractions (**Fig. 4.16C**). Regardless, these data support the tetramer binding experiments that show that the 1.27 TCR is capable of recognising CD1b presenting a broad range of phospholipid antigens, of differing class and acyl chain length.

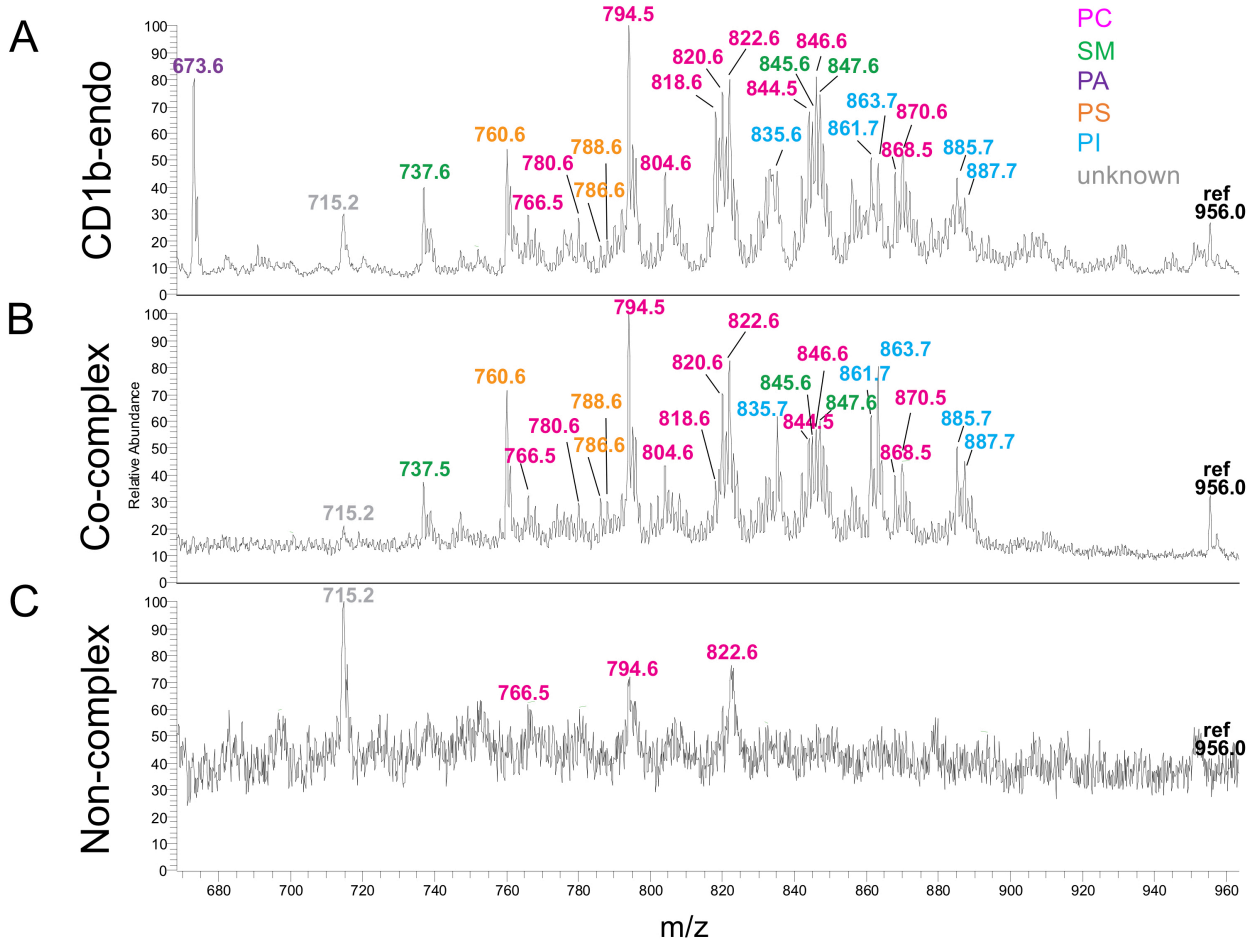

Figure 4.16. Mass spectrometry analysis of the 1.27 TCR co-complex. CD1b-endo alone, 1.27 TCR-CD1b-endo (co-complex) or uncomplexed 1.27 TCR and CD1b-endo (non-complex) fractions isolated by size exclusion chromatography were analysed by mass spectrometry to identify the permissive and non-permissive lipid antigens presented by CD1b. Each histogram displays the relative abundance of isolated lipid ions and their mass/charge ratio (m/z). The top, middle and bottom panels refer to lipid antigens isolated from CD1b-endo alone, complexed 1.27 TCR-CD1b-endo fractions or uncomplexed fractions respectively. The annotations on the histogram indicate the m/z ratio of defined species that are colour coded. The colour-coded key refers to the class of lipid species identified, including from top to bottom; phosphatidylcholine (PC), sphingomyelin (SM), phosphatidic acid (PA), phosphatidylserine (PS), phosphatidylinositol (PI) and unknown lipid species. Experiment was performed and analysed by Tan-Yun Cheng. Data are from one experiment.

The 4.17 TCR/CD1b ternary co-complex fractions displayed far less diversity of lipid species than the 1.27 TCR fractions (**Fig. 4.17B**). Based on our tetramer staining of the 4.17 cell line, we expected the 4.17 TCR to display considerable discrimination of the common phospholipids, with a bias for PC (**Fig. 4.7B**). Consistent with our findings, the dominant ions enriched within the 4.17 TCR co-complex were, 766.5, 780.6, 794.5, 808.6, 820.6, 822.6, 844.5, 846.6, 868.5 and 870.6 m/z, identified as PC of various tail lengths as well as 737.6 m/z, a species of SM (**Fig. 4.17B**). The 4.17 TCR favours the choline headgroup, and many variations in lipid tail length appear to be well tolerated as well as the more diverse SM. The uncomplexed fractions contained non-permissive phospholipids, such as PI and PS and several of the SM species (**Fig. 4.17C**) and a PC species that was identified with a m/z of 818.6, that was not enriched in the co-complex (**Fig. 4.17B and C**).

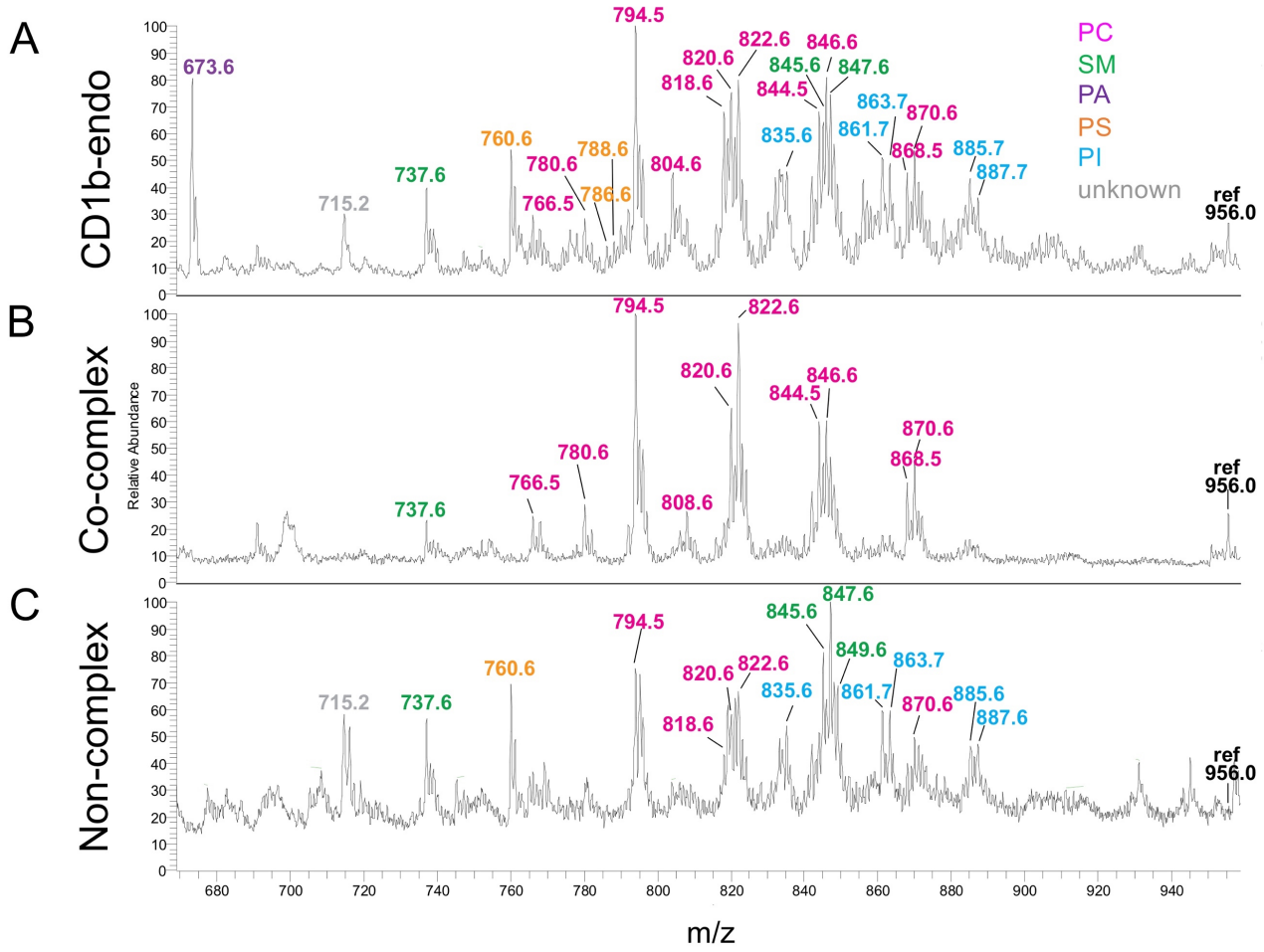

Figure 4.17. Mass spectrometry analysis of the 4.17 TCR co-complex. CD1b-endo alone, 4.17 TCR-CD1b-endo (co-complex) or uncomplexed 4.17 TCR and CD1b-endo (non-complex) fractions isolated by size-exclusion chromatography were analysed by mass spectrometry to identify the permissive and non-permissive lipid antigens presented by CD1b. Each histogram displays the relative abundance of isolated lipid ions and their mass/charge ratio (m/z). The top, middle and bottom panels refer to lipid antigens isolated from CD1b-endo alone, complexed 4.17 TCR-CD1b-endo fractions or uncomplexed fractions respectively. The annotations on the histogram indicate the m/z ratio of defined species that are colour coded. The colour coded key refers to the class of lipid species identified, including from top to bottom; phosphatidylcholine (PC), sphingomyelin (SM), phosphatidic acid (PA), phosphatidylserine (PS), phosphatidylinositol (PI) and unknown lipid species. Experiment was performed and analysed by Tan-Yun Cheng. Data are from one experiment.

4.2.13 Affinity of the 1.27 TCR for CD1b-endo

It was hypothesised that the 1.27 TCR had a high affinity for CD1b due to its ability to readily form ternary complexes with CD1b-endo (**Fig. 4.14A**), and the bright CD1b tetramer staining exhibited by the 1.27 cell line (**Fig. 4.7B**). Using the soluble 1.27 TCR, we measured its precise affinity for CD1b-endo using surface plasmon resonance (SPR).

Biotinylated CD1b-endo and control biotinylated CD1d-α-galactosylceramide (α-GalCer) were coupled to the SPR chip interface indirectly, by first coating the interface with unconjugated SAv by amide coupling, then passing over the biotinylated CD1 monomers separately. 1.27 TCR and a control NKT15 TCR (228) proteins were prepared, by size-exclusion chromatography to remove any impurities (data not shown) and serially diluted. TCR was injected over the interface and the affinities for CD1b and CD1d monomers were measured (**Fig. 4.18A and B**). The response units (RU) were calculated for interactions between 1.27 and CD1b and the NKT15 TCR and CD1d-α-GalCer. TCRs 1.27 and NKT15 only bound to their cognate antigens, CD1b-endo and CD1d-α-GalCer, respectively (**Fig. 4.18A and B**). The saturation plots verified the affinity of the NKT15 TCR for CD1d-α-GalCer as ~0.24μM (**Fig. 4.18D**) (228) and revealed that the 1.27 TCR recognised CD1b-endo with an affinity of 2μM (**Fig. 4.18C**), a remarkably high affinity for an autoreactive αβ TCR (229, 230). The high affinity of the 1.27 TCR suggests it makes extensive electrostatic contacts with CD1b (**Fig. 4.9B**) and yet is able to do so independently of antigen (**Fig 4.7B**). Therefore, it was hypothesised that the 1.27 TCR may adopt a novel docking mode atop of CD1b, favouring lipid independent molecular contacts. Thus, we set out to elucidate the crystal structure of the 1.27/CD1b ternary complex.

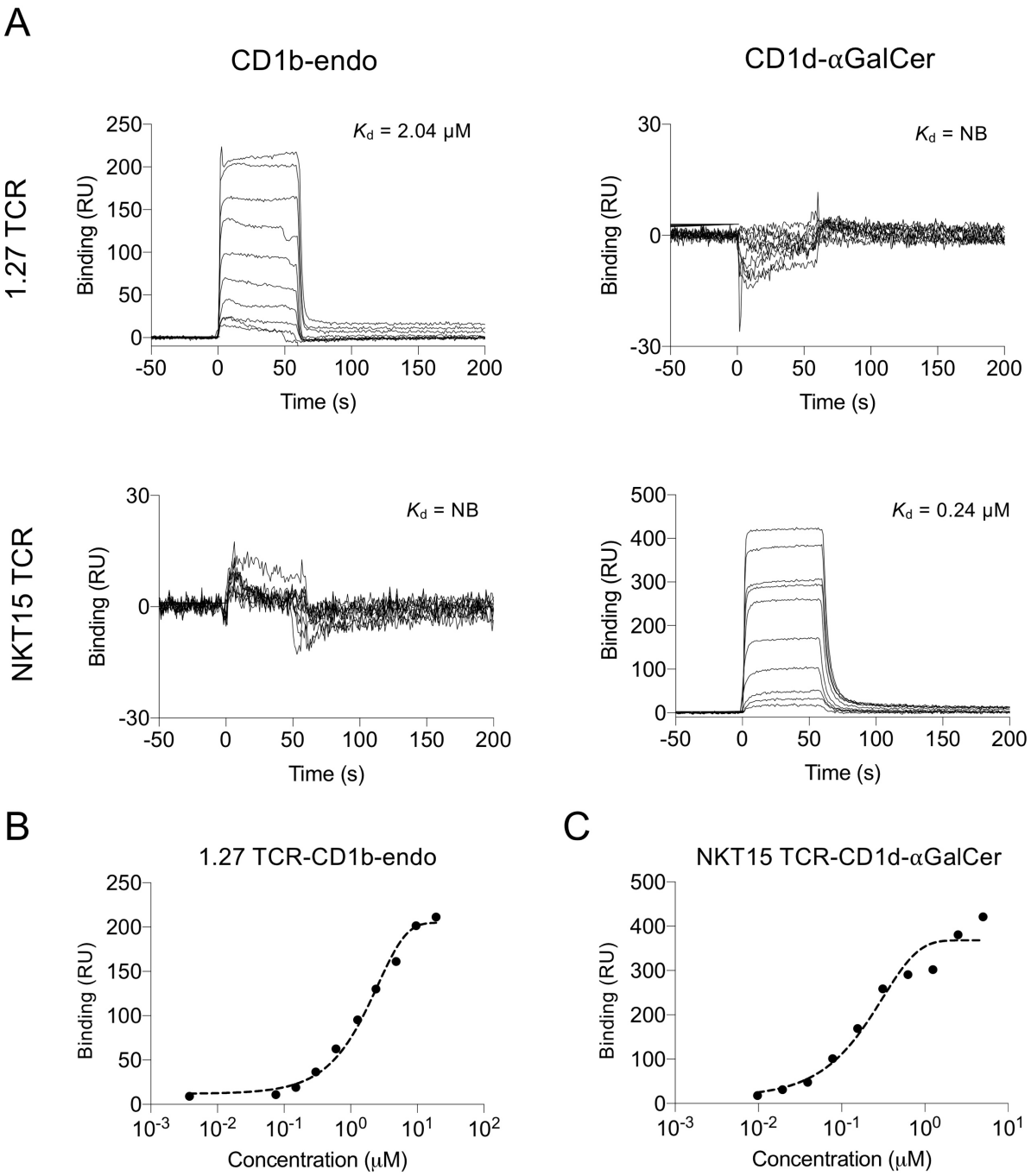

Figure 4.18. Affinity measurements of the 1.27 TCR interaction with CD1b-endo. Biotinylated CD1b-endo or control CD1d-α-GalCer were coupled to an SPR chip that was precoated with SAv. Serially diluted 1.27 TCR or control NKT15 TCR were passed over the chip to measure the interactions between proteins. **A.** Left panels display the response units (RU) measured over time (s) of 1.27 TCR or NKT 15 TCR binding to CD1b-endo. Similarly, the right panels display the RU measured over time of 1.27 TCR or NKT 15 TCR binding to CD1d-αGalCer. **B and C.** Saturation plot displaying RU achieved over the concentration range (μM) of injected protein for the 1.27 TCR and NKT15 TCRs respectively. K_d refers to the dissociation constant calculated for each interaction from the IC50 determined by fitting a four-parameter logistic curve. NB refers to no binding. Experiment performed with Adam Uldrich. Data are from one experiment.

4.2.14 Structure of the unliganded 1.27 TCR

The TCR-trap experiments had previously demonstrated that the 1.27 TCR was capable of forming a ternary complex with CD1b-endo and was readily isolated by size-exclusion chromatography (**Fig. 4.14A**). 1.27 TCR-CD1b-endo ternary complexes were prepared similarly as described as well as purified 1.27 TCR alone (data not shown) for broad crystallisation screens using a robotic nanolitre seeding system. Despite preparing enough ternary complex for the Monash Molecular Crystallisation Facility (MMCF) to set up an extensive screen involving approximately 2000 different crystallization condition, no crystals of the 1.27 TCR-CD1b-endo ternary complex were observed. However, several conditions were identified that produced crystals for the unliganded 1.27 TCR, including a precipitant that produced large crystals suitable for X-ray diffraction, consisting of 16% (w/v) polyethylene glycol 3350 and 0.1 M citrate-bis-tris-propane (**Fig 4.19A**). The crystals were harvested by Adam Shahine and Jamie Rossjohn (Monash University) and a dataset was produced using the MX2 beamline at the Australian synchrotron. The crystal structure was determined at a resolution of 2.0 Å (**Fig. 4.19B and C**). In the modelled structure the CDR3α loop was only partially resolved, suggesting that this element is highly mobile in the unliganded state (**Fig. 4.19C and D**). The unresolved residues within the CDR3α contained a tandem glycine repeat, of which a single glycine was missing, possibly contributing to the flexibility of the loop. Comparatively, both the 4.13-2 and 4.27 TCRs had similar glycine repeats in the CDR3α loops (**Table 4.1**), as is the case for several CD1b-restricted GEM and LDN5 TCRs (135, 136). A surface representation of the 1.27 TCR antigen-binding interface revealed that the CDR2β loop packed closely alongside the CDR3β and CDR1β loops, adopting a sharp hairpin loop and maximising the overall binding interface with the CDR3β loop (**Fig. 4.19E**). Moreover, the CDR2α loop was extended towards the CDR3 loops (**Fig. 4.19E**) in comparison to other published CD1b-restricted TCR structures (135). Together, the germline-encoded CDR loops were tightly packed against the CDR3α-CDR3β interface, where the CDR3α forming a focal point of contact primarily involving the TCRα chain and the mobile CDR3α loop (**Fig. 4.19D and E**). Further work is required to obtain the crystal structure of the 1.27 TCR-CD1b-endo ternary complex.

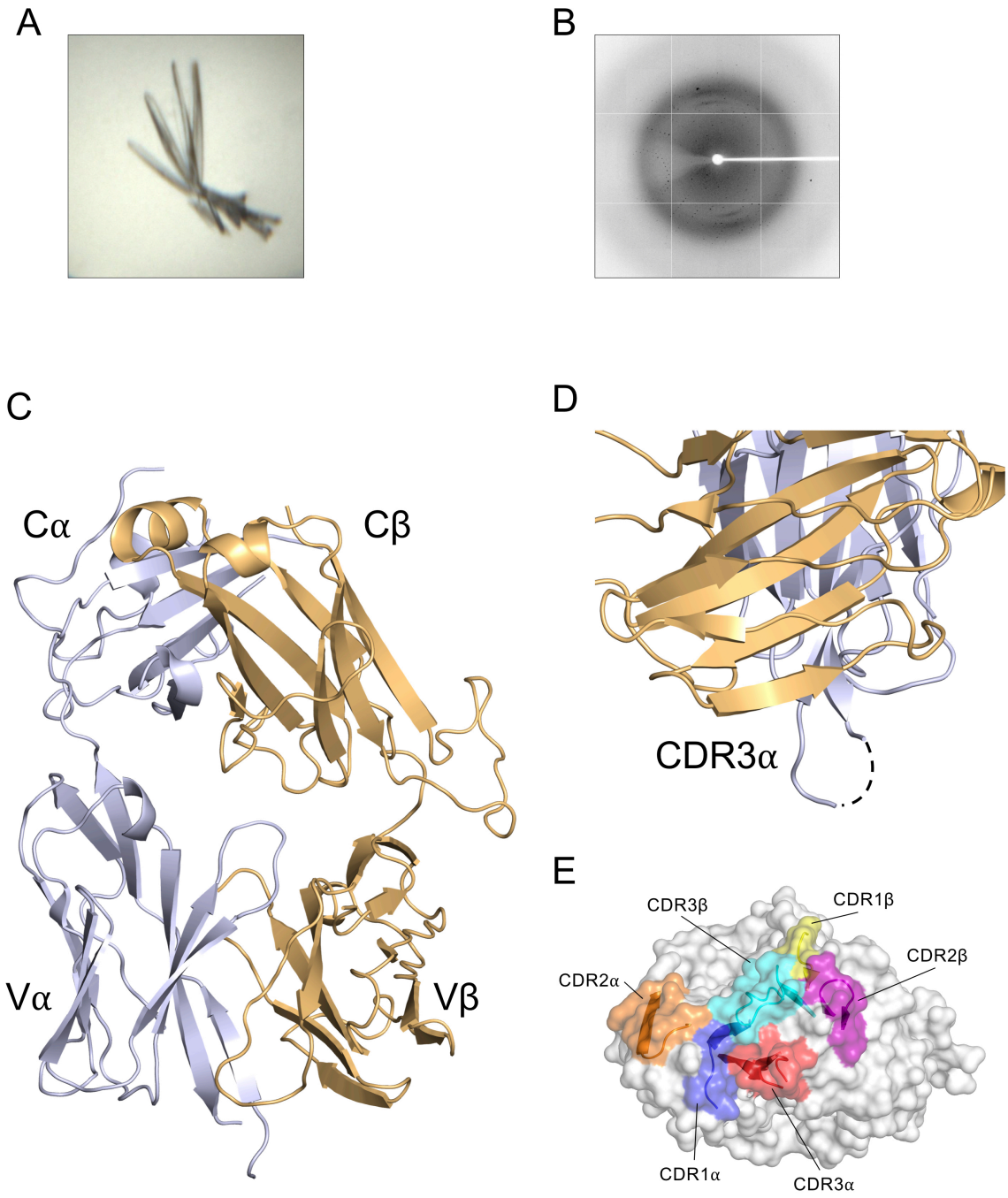

Figure 4.19. Structure of the unliganded 1.27 TCR. Purified 1.27 TCR alone was prepared for crystallisation trials using a robotic seeding system. Crystals of promising morphology and size were harvested by Adam Shahine for X-ray diffraction at the Australian synchrotron. **A.** Image of drop conditions that produced large crystals of the 1.27 TCR using the precipitate 16% (w/v) polyethylene glycol 3350 and 0.1 M citrate-bis-tris-propane that were harvested. **B.** Image of X-ray diffraction pattern of the 1.27 TCR measured by the MX2 beamline detector. **C.** Structural model of the 1.27 TCR built using the X-ray diffraction data by Adam Shahine. **D.** Close up of the unresolved residues within the CDRα loop. Missing residues are denoted by the dashed line. **E.** Surface model of the 1.27 TCR highlighting the CDRα and CDRβ loop locations.

4.2.15 Identification of autoreactive CD1b-restricted T cells directly ex vivo

Autoreactive T cells were successfully identified from healthy human blood by cell sorting CD1b-endo tetramer$^+$ cells, followed by *in vitro* expansion and re-staining with tetramer (**Fig. 4.2B and C**), however many phenotypic and functional characteristics are likely altered during cell culture (231). To try to identify autoreactive T cells without altering their phenotype, PBMCs were stained with CD1b-endo tetramers and magnetically enriched to separate highly reactive cells from lower affinity and unreactive cells directly *ex vivo*. Using this method, small numbers of CD1b-endo tetramer$^+$ cells were identified in 3/24 donors examined (**Fig. 4.20**). Autoreactive T cells were exceedingly rare, both in prevalence within the blood donor cohort and in cell frequency, typically 10-100 tetramer$^+$ cells were retained after magnetic enrichment of 10^7 PBMCs from healthy donors (**Fig. 4.20**). It is likely that these highly tetramer reactive cells constitute a very small fraction of circulating T cells in the blood of healthy individuals. All of the CD1b tetramer$^+$ cells identified from the three healthy donors expressed CD4 and were negative for TRAV1-2, (**Fig. 4.20**), indicating that these cells do not share the TCR repertoire of GEM T cells (135). These data highlight that magnetic enrichment can be used to isolate a small but discrete population of autoreactive CD1b-restricted T cells from healthy human blood. Further work is required to validate the specificity of the enriched cells, as well as to elucidate their phenotype and function and to determine their role in the human immune system.

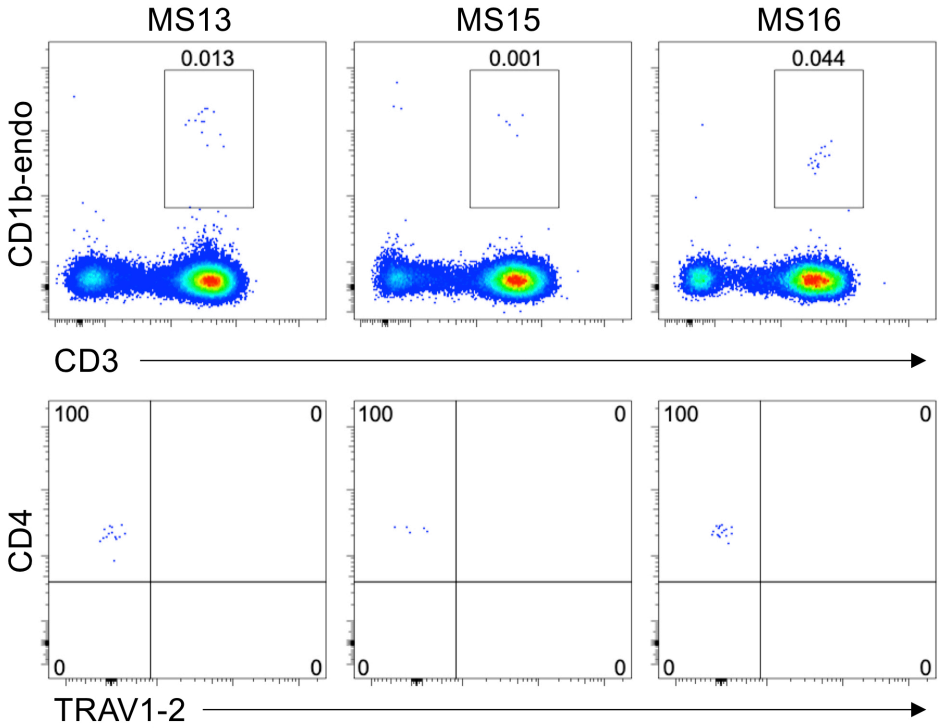

Figure 4.20. Magnetic enrichment of T cells using CD1b-endo tetramers. PBMCs from healthy blood donors were stained with CD1b-endo tetramers, followed by tetramer specific microbeads that were enriched using a magnetic column. Enriched tetramer$^+$ cells were stained with monoclonal antibodies outlined in **Table 2.3**. Top panel of plots depict tetramer positive cells isolated from three donors (MS13, MS15 and MS16), gating previously to remove CD19$^+$ and dead cells. Bottom panel plots depict CD4 and TRAV1-2 expression of tetramer$^+$ cells from donors MS13, MS15 and MS16. Cumulative data from two independently performed experiments.

4.3 Discussion

Autoreactive CD1b-restricted T cells are rare (52) and difficult to identify. While not much is known about their function, recent evidence suggests that these cells respond to immune challenge (54) and contribute to autoimmune disease (153). Herein, CD1b-endo tetramers were used to identify and characterise CD1b-restricted autoreactive T cells, to examine their lipid antigen specificity and to understand how they interact with CD1b-Ag. Similar to recent studies, which used CD1b dextramers (52), the data here showed that autoreactive CD1b restricted T cells are exceeding rare. It is possible that these cells are more abundant in the tissues, however unlike some other unconventional T cells that acquire a memory phenotype early after development and egress to the periphery in larger numbers, some CD1b-restricted T cells do not appear to expand after thymic maturation, suggesting that these cells might be more akin to naïve conventional T cells (137). It is likely that in healthy people, autoreactive CD1b-restricted T cells remain quiescent in the absence of stimulatory conditions. It is also possible that autoreactive CD1b-restricted T cells expand in response to microbial infection. The T cell clones PG10 and PG90, identified using CD1b dextramers from a healthy donor, were strongly reactive to PG loaded CD1b, a common phospholipid component of bacterial cell walls and minor constituent of mammalian mitochondria (150). However, both cell lines displayed moderate cross-reactivity to more abundant mammalian phospholipids such as PA, PS and PE (52). Autoreactive T cells that are primed by CD1b in the context of infection, may expand and become sensitive to related mammalian lipids due to cross-reactivity, possibly by molecular mimicry. Thus, while rare in healthy donor blood, autoreactive CD1b-restricted T cells may be more frequent in autoimmunity or following an immune response to an infectious pathogen that expresses similar endogenous antigens.

All of the autoreactive T cells that were identified directly *ex vivo* and after *in vitro* expansion, expressed the CD4 co-receptor. Similarly, both GEM and autoreactive CD1b-restricted T cells typically express solely the CD4 co-receptor (52, 135). It is possible that CD4 may contribute to the recognition of CD1b by T cells, as CD4 has been shown to influence NKT cell responses (121, 122). Moreover, a protein alignment of CD1 molecules with the β-chain of HLA-DR1, the primary contact chain between CD4 and

MHC-II, reveals several CD4 contact residues that are conserved in CD1, particularly CD1b and CD1c (**Fig 4.21**). However, early evidence using a blocking antibody suggests that CD4 is not involved in the functional response of CD1b-restricted T cells (232) and more recently, novel subsets of CD1b-restricted T cells have been identified that do not express CD4, such as a subset of LAM-reactive polycytotoxic CD1b-restricted T cells that almost exclusively express the CD8 co-receptor (152). Therefore, the strong bias and persistence of CD4 by our autoreactive T cells may not have any functional significance, but rather a vestige from a preceding development or differentiation event.

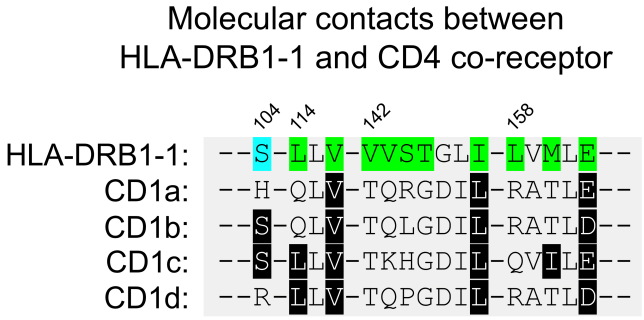

Figure 4.21. Alignment of the putative CD4 binding site on HLA-DRB1 with CD1 molecules. Schematic of amino acids spanning from 104 to 162 of the HLA-DRB1 that contact the CD4 co-receptor, aligned with the conserved residues in each of the CD1 molecules. Residues coloured in blue indicate hydrogen bonding between HLA-DR1 and CD4 and residues coloured in green indicate van der Waals interactions. CD1 residues coloured in black indicate amino acids with conserved chemical properties with the corresponding HLA-DRB1-1 residues. The amino acid alignment was performed with Uniprot and the HLA-DRB1-CD4 interaction was analysed with PDBsum using data from the entry 3T0E in the PDB repository.

In contrast to most studies examining CD1b-restricted T cells, that focussed on identifying T cells using defined antigens (51, 52, 133, 135, 137, 152, 233), the experiments performed in this study used CD1b-endo tetramers presenting heterogeneous and undefined lipid antigens. Using this approach, T cell clones with a broad range of antigen specificities were identified that have not yet been described. Of particular interest are two T cell clones (1.27 and 4.27) that recognised CD1b presenting a variety of phospholipid antigens, microbial derived GMM and refolded CD1b loaded with a non-physiologically relevant detergent molecule. Both 1.27 and 4.27 TCRs displayed considerable TCR degeneracy by strongly recognising CD1b presenting structurally diverse antigens with relatively minimal perturbations. Most MHC-I-restricted TCRs

dock in an orthogonal manner where the TCR Vα and Vβ chains are positioned over the α2 and α1 helices of MHC-I respectively (85). In addition to this, MHC-I-restricted TCRs exhibit a remarkably conserved docking footprint with only a few exceptions (85). Thus, degeneracy of MHC-I-restricted TCRs relies heavily on the flexibility of the CDR3 loops that conform to cognate peptide whilst maintaining an approximately orthogonal docking mode (234). Comparatively, CD1-restricted TCRs utilise a variety of docking modes to recognise structurally diverse lipid antigens (138, 150, 216, 223, 228). For instance, type I NKT TCRs typically dock parallel to the lipid binding groove, on the F' side of CD1d where the conserved TCRα chain is positioned atop the lipid headgroup (228). In contrast to this, a type II NKT TCR identified in mice, recognises the self-lipid sulfatide by docking orthogonally across the A' roof of CD1d and contacting the antigen solely with the CDR3β loop (235). In both these instances, and in all cases described for TCR recognition of MHC/peptide, the TCR always makes contact with the antigen (lipid or peptide). However, a recent paper which described an autoreactive CD1a-restricted TCR showed that TCR recognition did not involve contacts with the antigen (223). In this instance, the TCR engaged CD1a presenting a variety of lipids, providing the lipid head group did not interfere with A' roof of the CD1a molecule. The data herein suggests that the 1.27 TCR may bind CD1b using a similar approach, although structural studies are required for validation. Further, the 4.27 TCR reporter cell line was capable of recognising all CD1b-Ag tetramers examined, suggesting a shared or similar mode of TCR recognition. Both the 1.27 and 4.27 TCRs share the Vα domain TRAV27, which only differ within the CDR3α loops by a single amino acid residue. One explanation for why we were able to identify these cells could be due to the heterogeneous lipids presented by CD1b-endo tetramers. In the absence of a consistent antigen, it was challenging to identify T cells that expressed TCRs with high antigen specificity. Thus, it was more likely to identify cells capable of forming multiple TCR-CD1b interactions with tetramers, independent of antigen. In this way, these data were biased for identifying autoreactive T cells with a high cross-reactivity for CD1b-Ag. Whether these particular TCR binding characteristics are widespread among autoreactive CD1b-restricted T cells requires further investigation.

A single T cell (4.17) was identified that displayed a preference for CD1b-endo tetramers but was able to recognise CD1b loaded with some exogenous phospholipid antigens. The 4.17 cell line displayed a finer specificity for antigen than the other cell lines, capable of differentiating minor details between CD1b loaded with common phospholipids and recognising CD1b presenting PC and to a lesser extent PE and PG. Analysis of lipid antigens presented by CD1b-endo to the 4.17 TCR confirmed this, revealing that almost all of the lipids presented by CD1b-endo were PC species of varying acyl tail length. However, PC was also the most abundant lipid species occupying the cleft of mammalian expressed CD1b-endo molecules. Although CD1b-endo tetramers contained heterogeneous lipids, it is probable that any four CD1b-endo molecules, once multimerised, would contain proportionally more PC than any other lipid species and therefore favour recognition by PC-reactive T cells tolerant of variations in acyl tail length. Notably, the 4.17 cell line was also responsive to the myeloid C1R cells transduced with CD1b that likely exhibit an altered lipid profile compared to epithelial HEK cells (236), suggesting a broad tolerance to mammalian lipids from different cell origins.

PC and PE together are the most abundant phospholipids present in mammals (237). PC is synthesised by all nucleated cells via the Kennedy pathway (238) and is found in all lipid membranes in the cell. In contrast PE is highly enriched in the inner membrane of the mitochondria and in the brain, where it comprises ~40% of total phospholipid content (239). A small amount of PE is produced from PS in the ER, while the majority of PE is synthesised from an ethanolamine precursor lipid in the mitochondria (237). Thus, PC is ubiquitous, and PE is mostly confined to organelles. Although varied in location and function, the structures of PC and PE are highly similar, differing only by terminating in a methylated or unmethylated primary amide respectively. From an immune perspective, possessing T cells with a specific reactivity to common phospholipids does not seem conducive for good health. Yet no evidence exists that these cells are harmful in healthy individuals.

In a dysregulated metabolic state however, such as uncontrolled cell proliferation, ubiquitous phospholipids may be useful targets for detection of malignant cells.

Consistent with this, clinical screening of PC and PE metabolites in urine, serum and plasma have been used as a biomarker for the progression of breast cancer (240). In a transgenic mouse model, CD1b-restricted T cells recognised phospholipids produced by adoptively transferred lymphoma cells (149). CD1b-restricted T cells were capable of lysing $CD1b^+$ lymphoma cells and the anti-tumour response was increased in the presence of TLR stimulation (149). Interestingly, IL-2 production was enhanced in response to tumour-derived lipids, including PE and lysophosphatidylethanolamine (LPE) species, compared to normal T cell lipids, suggesting that tumour-derived phospholipids may be more antigenic. In particular, lysophospholipids produced by malignant cells contribute to tumour growth, angiogenesis and immune modulation (241) and would be an attractive target for T cell-based immunotherapy. Similarly, a related CD1c-restricted T cell subset was identified that recognised specifically methyl-lysophosphatidic acids (LPAs) presented by $CD1c^+$ leukemia cells and monocyte-derived DCs (MoDCs) and these lipids seemed to accumulate specifically in malignant cells (148). Thus, lysophospholipids may be physiologically relevant target lipids for autoreactive CD1-restricted T cells. Typically, the acyl tails of lipid antigens fill the A' and F' pockets of CD1 molecules, leaving the lipid headgroup exposed for TCR recognition (reviewed in (221)). In the case of exogenous lysophosphatidylcholine (LPC) presentation by CD1d, the single acyl chain was shown to occupy the F' pocket of CD1d while the A' pocket contained two small scaffold lipids derived from an insect cell expression system (242). Interestingly, the LPC headgroup was oriented 180° compared to the headgroup of PC presented by CD1d, likely impinging on TCR cross-reactivity between antigens. CD1b also contains scaffold lipids deep within channels of the lipid binding groove, that aid specifically in the presentation of smaller lipid antigens that themselves cannot occupy the entire cleft of CD1b (243). It is conceivable that CD1b would be well suited to presenting diverse tumour-derived lipids, including lysophospholipids, by virtue of its voluminous lipid binding cleft, and the ability to bolster lipid antigens of varying size using non-agonistic scaffold lipids. In this study however, we were unable to identify an autoreactive T cell with enhanced recognition of CD1b presenting a lysophospholipid species. For the 4.17 TCR, in the context of refolded CD1b, it appears as though the use of a non-physiological detergent molecule in place of a scaffold lipid did not appreciably alter antigen reactivity compared to CD1b-endo. In fact, we were able to predict the preferred phospholipid species

presented by CD1b-endo using refolded CD1b tetramers loaded with exogenous phospholipids.

Autoreactive T cells may also encounter altered lipid repertoires in inflammatory disease states, including neuroinflammatory diseases such as Alzheimer's disease and MS (244). In Alzheimer's disease, dysregulated neuronal metabolism affects the function of both secreted and cytosolic phospholipase A2 (PLA_2), enzymes that catalyses the cleavage of the sn-2 fatty acid from phospholipids, releasing lysophospholipids and fatty acids such as arachidonic acid that contribute to the inflammatory response (244). Cytosolic PLA_2 digests membrane phospholipids, liberating lysophopholipids that accumulate within the cell and preventing their conversion back into diacyl chained lipids (244). Consequently, autoreactive T cells may detect lysophospholipids or other lipids produced during inflammation and help restore immune homeostasis in the brain. Comparably, it was shown that PLA_2 enzymes from bee and wasp venom, upon breach of host cells, were capable of digesting host membrane phospholipids from antigen presenting Langerhans cells (245). The resulting neo-antigens, including antigenic fatty acids and lysophospholipids, were presented by CD1a to autoreactive T cells and stimulated the secretion of IFNγ (245). Interestingly, neo-antigen formation from endogenous lipids can occur in the absence of exogenous stimuli. In psoriatic disease, cytosolic PLA_2G2D is produced in high quantities by infiltrating mast cells and keratinocytes in inflamed skin plaques (246). In particular, mast cells release exosomes, some of which contain neo-antigens produced by cytosolic PLA_2 and are captured by nearby Langerhans cells that are presented to CD1a-restricted T cells (246).

Immunogenic phospholipids are also derived from bacterial sources, some which are shared between bacteria and mammals, while others are unique to bacteria (247). For instance, PG is the most dominant phospholipid in *Staphylococcus aureus* and *Salmonella typhimurium* (52), whereas it is relatively scarce in mammals (239). However, some common phospholipids in mammals are also highly enriched in bacteria, including PE and PC (247, 248). It is now estimated that 15% of bacteria and archaea are capable of producing PC by converting the ethanolamine moiety of PE to choline via enzymatic N-methylation (248) and PC is a virulence factor for *Legionella pneumophila*, *Pseudomonas*

aeruginosa and *Brucella* species (248). Thus, the 4.17 TCR may cross-react to PC and PE derived from bacterial sources. The utility of phospholipids among even highly divergent evolutionary species is well preserved and suggests that phospholipids from the host or microbes may be difficult to distinguish by the TCR. It is possible that CD1-restricted TCRs rely on differences in lipid acyl chain length to subtly orient the headgroup and fine-tune TCR reactivity, however substantial tolerance of the 4.17 TCR in recognising PC species was observed. Further, a structure of the BC8B TCR bound to CD1b-PC revealed that the TCR was capable of forcefully orienting the lipid headgroup to the desired position for TCR recognition (216). Therefore, it is likely that recognition of phospholipid antigen alone, whether host or microbe derived, is insufficient to elicit an immune response, and that in the context of cellular stress or infection, the presence of DAMPs and PAMPs, inflammatory cytokines and other signals are integral in regulating T cell responses.

The data presented in this chapter is consistent with many recent studies examining CD1-restricted T cell frequency and phenotype (52, 63, 142, 249) but also provides new insights into endogenous lipid reactivity that have not been reported in the literature. Specifically, autoreactive TCRs were identified that recognise CD1b in a manner that is discordant with models of TCR recognition reported previously (138, 150, 216). Additionally, a TCR with a high specificity for phospholipid antigens presented by CD1b was identified. It is likely that the method of identifying autoreactive CD1b-restricted T cells in this study was influenced by using CD1b tetramers loaded with a mixture of endogenous lipids. This phenomenon was explored by identifying the lipid antigens presented by mammalian produced CD1b-endo as well as isolating the specific lipid antigens recognised by the autoreactive TCRs. The role of these T cells in humans is largely unknown and further investigations will facilitate greater understanding of the role of autoreactive CD1-restricted T cells in the human immune system. The development of lipid specific CD1b tetramers will aid in the identification of these autoreactive T cells, allowing for greater characterisation of their phenotype and function.

Chapter 5: Characterisation of *M. tuberculosis*-specific CD1b-restricted T cells

5.1 Introduction

M. tuberculosis is a highly prevalent pathogen in humans and is estimated to infect approximately one quarter of all humans globally (250). In most cases, after a period of acute disease, *M. tuberculosis* is controlled by the immune system and confined to a latent state within the lungs (251). However, both infants and young children are often unable to contain *M. tuberculosis* in the lungs and are at risk of developing severe systemic disease, responsible for the high mortality associated with *M. tuberculosis* in these populations (252). As expected, the burden of disease is greatest in areas where *M. tuberculosis* is endemic; such as Southeast Asia and parts of Africa (253). In immunocompromised adults, *M. tuberculosis* often reactivates thereby increasing the infectivity of *M. tuberculosis* and causing high morbidity, particularly among HIV^+ patients (254). Consequently, there have been many efforts to prevent and treat *M. tuberculosis* infection and reduce its disease burden. To date, the most effective vaccine developed against *M. tuberculosis* is a live attenuated strain of *M. bovis*, known as Bacillus Calmette Guérin (BCG) which is avirulent in humans (255). The BCG vaccine contains a largely complete set of Mycobacterial antigens; including highly immunogenic cell wall lipids that are absent from recently developed, less effective subunit vaccines (255, 256). Vaccination with BCG has been shown to protect children from the life-threatening systemic *M. tuberculosis* dissemination (257, 258), however, is not effective at preventing local pulmonary infection in adults (255). Thus, a large reservoir of *M. tuberculosis* persists in latently infected carriers, contributing to the incidence of infection in endemic regions each year.

Since the introduction of the BCG vaccine, research has established that effective clearance of *M. tuberculosis* relies on the adaptive immune response, specifically $CD4^+$ T cells and their secretion of effector cytokines, including IFNγ (259). Interestingly, $CD4^+$ T cell responses that elicit polyfunctional effector responses, defined by the simultaneous production of IFNγ, TNF and GM-CSF, confer greater protection against *M. tuberculosis* challenge than monofunctional T cell responses (260, 261). Thus, stimulating T cells that

are known to induce polyfunctional responses against *M. tuberculosis* may lead to greater protection from or clearance of disease. Unconventional T cells are rapid effectors and secrete multiple Th1, Th2 and Th17 cytokines that may contribute to the clearance of *M. tuberculosis* (44). However, targeted attempts to develop T cell stimulating *M. tuberculosis* vaccines have only focussed on the conventional peptide-reactive T cell pool (262). Glucose monomycolate (GMM) is one of several known immunogenic glycolipids derived from the cell wall of pathogenic Mycobacteria, including *M. tuberculosis* (145). Comprising a host derived glucose headgroup, fused to a long (C32-C100) mycolic acid backbone (263), GMM is a non-peptide antigen that is presented to unconventional T cells via CD1b (49, 50, 264). Thus, utilising non-peptide antigens to target CD1b-restricted T cells in *M. tuberculosis* vaccines may be a suitable strategy to stimulate a polyfunctional T cell response. The phenotype and function of GMM-reactive CD1b-restricted T cells is poorly understood at this point, as these cells have only recently been isolated *ex vivo*, made possible by the development of CD1b tetramers (51, 135, 137).

Studies of GMM-reactive T cells from *M. tuberculosis* patients reveal consistent phenotypic traits that are shared between donors, including: CD4 co-receptor expression, low or lack of CD161 expression and an increased frequency in the blood of *M. tuberculosis* infected patients compared to healthy controls (135). Moreover, some donors present with GMM-reactive T cells that express a highly conserved TCRα chain that is shared between genetically unrelated donors, comprising the TRAV1-2/TRAJ9 gene segments (135). How pervasive this conserved TCR repertoire is at the population level is unclear (137). Importantly, GMM-reactive T cells appear to be clonally expanded in response to *M. tuberculosis* infection (137), likely explaining their observed higher frequency in tuberculosis patients. If GMM-reactive T cells are actively involved in the immune response during *M. tuberculosis* infection, then developing a greater understanding of their phenotype and function may provide a useful biomarker to delineate patients for diagnostic purposes (137), advise therapeutic interventions and aid in the development of vaccines that specifically target unconventional T cell responses.

To evaluate the phenotype of GMM-reactive T cells in healthy blood donors, an enrichment strategy using CD1b tetramers was developed which allowed isolating GMM-reactive T cells with high accuracy. Using this approach, the surface phenotype, TCR

repertoire, gene expression and functional response of GMM-reactive T cells from multiple healthy donors were determined and compared to other unconventional T cell subsets.

5.2 Results

5.2.1 Validation of GMM lipid loaded CD1b tetramers using cell lines and PBMCs

CD1b-endo monomers were prepared as described in chapter 4 (**Fig. 4.1**) and loaded with GMM at a 3:1 molar ratio (lipid antigen to CD1b), using the detergent tyloxapol, to liberate endogenous lipid antigens from the cleft of CD1b. This lipid antigen to CD1b ratio was determined to provide the optimal CD1b-GMM tetramer fluorescence (data not shown). To confirm that the GMM has been loaded into the cleft of CD1b, GMM loaded CD1b molecules were tetramerised and the staining of GMM-loaded CD1b tetramers and CD1b-endo tetramers was examined on wild type SKW-3 cells and SKW-3 cell line expressing TCR42, a TCR derived from a GMM-reactive TCR isolated from a patient latently infected with *M. tuberculosis* (135) or an SKW-3 cell line expressing the autoreactive 1.27 TCR described in chapter 4. The amino acid sequence for the TCR42 can be found in **Table AII.1**. No staining of the SKW-3 wild type cell line (WT) with either of the CD1b tetramers was observed, indicating that loading with GMM did not cause non-specific binding of CD1b to the SKW-3 cell line **(Fig. 5.1A)**. Clear staining of the TCR42 expressing cell line was observed only with CD1b-GMM tetramer, but not CD1b-endo tetramer confirming the specificity of the TCR42 cell line. Moreover, CD1b-GMM tetramer fluorescence intensity correlated with CD3 expression, further confirming TCR specificity for the CD1b-GMM tetramer. As expected, the 1.27 cell line stained with both CD1b-endo and CD1b-GMM tetramers.

Next, the ability of CD1b-GMM tetramers to identify GMM-reactive T cells from healthy blood donors was examined **(Fig. 5.1B)**. A relatively large number of T cells were identified that appeared to be positive when stained with CD1b tetramers, inconsistent with previous studies demonstrating a low frequency of GMM-reactive T cells in healthy blood (135, 137). Moreover, the CD1b-GMM tetramer reactive T cells did not appear oligoclonal or to correlate with CD3 expression (51, 135, 137) (data not shown) (**Fig. 5.1B**). Although these cells stained with CD1b-GMM tetramers, whether these data represented true TCR-reactivity was not determined. To increase the specificity of the approach, the surface markers CD4 and TRAV1-2 were used to specifically identify the GEM T cell subset. A defined population of cells was observed where tetramer

fluorescence appeared to correlate with TRAV1-2 expression and comprised 0.57% of total $CD4^+TRAV1\text{-}2^+$ cells (**Fig. 5.1B**). Thus, using this approach, CD1b-GMM tetramers were validated on GEM T cells isolated from healthy donor PBMCs, however the very low frequency of cells obtained was not sufficient for extensive phenotypic analysis. Furthermore, this approach skewed the analysis towards CD1b-GMM $tetramer^+$ cells that expressed both CD4 and TRAV1-2 and therefore potentially excluded GMM-reactive T cells that lacked these molecules.

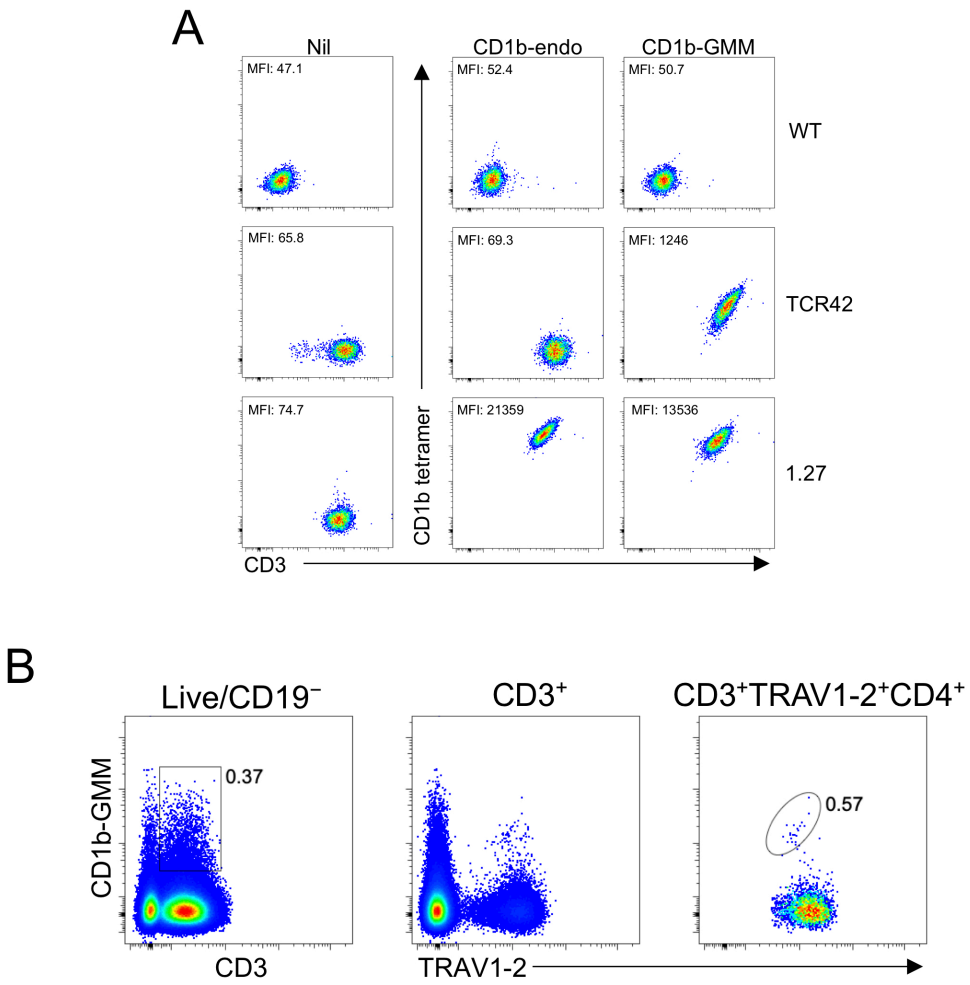

Figure 5.1. Validation of CD1b-GMM tetramers using cell lines and PBMCs. CD1b monomers prepared using a mammalian expression system were purified and loaded with GMM C:32 lipid and subsequently tetramerised. CD1b-GMM tetramers were used to stain both autoreactive and GMM-reactive T cell lines and PBMCs. **A.** Wild type (top row) or transduced SKW-3 cell lines expressing TCR42 (middle row) or 1.27 TCR (bottom row) were stained with a live/dead discriminator dye, anti-CD3 antibody and CD1b-endo or CD1b-GMM tetramers. Plots are gated to represent viable single cells. **B.** PBMCs from a healthy blood donor were stained with a panel of monoclonal antibodies (**Table 2.3**) and CD1b-GMM tetramers. The left and middle plots display live, $CD19^-$ CD1b-GMM $tetramer^+$ cells, some of which co-stain with anti-CD3 or anti-TRAV1-2 antibodies respectively, while the right plot displays only $CD3^+$ GEM T cells (defined as $CD4^+TRAV1\text{-}2^+$ CD1b-GMM $tetramer^+$ cells). These data are representative of at least two independent experiments.

5.2.2 Surface phenotyping of CD1b-GMM-reactive T cells from healthy donor blood

To isolate greater numbers of GMM-reactive T cells and enhance the fluorescence intensity of the CD1b-GMM tetramers and this way the staining resolution, CD1b-GMM tetramer$^+$ cells from PBMCs were isolated using tetramer magnetic enrichment, as previously described (265). Similar to the process of identifying CD1b autoreactive T cells directly from blood, large numbers of PBMCs were subjected to CD1b-GMM tetramer magnetic enrichment to increase the recovery of tetramer$^+$ cells (**Fig. 5.2A**). The CD1b-GMM tetramer staining of enriched cells (Enrichment) was compared to unenriched cells (Pre-enrichment), and cells that had passed through the magnetic column but were not captured (Flow through) (**Fig. 5.2A**). As expected, very few tetramer$^+$ cells were observed in the flow through (**Fig. 5.2A**). In a few donors, a population of CD1b-GMM tetramer-reactive T cells were observed in the unenriched fraction that substantially increased in both tetramer fluorescence intensity and in frequency (**Fig. 5.2A**). However, the ability to resolve CD1b-GMM tetramer-reactive T cells directly in the unenriched fraction was highly donor dependent. In most donors, a discernible population of tetramer$^+$ cells were only visible among enriched cells (data not shown). By enriching with CD1b-GMM tetramer, the fluorescence intensity and frequency of defined tetramer$^+$ cells were increased over *ex vivo* staining of PBMCs, while simultaneously reducing the number of cells with less defined, lower tetramer fluorescence. Whether these lower affinity cells represent a legitimate subset of GMM-reactive T cells restricted to CD1b is unclear. Nevertheless, it is possible that the tetramer magnetic enrichment may bias for T cells that express TCRs with higher affinity towards CD1b-GMM. Accordingly, the use of CD1b-GMM tetramers in combination with magnetic enrichment allows for the clearer identification of CD1b-GMM-reactive T cells directly *ex vivo* from healthy human blood.

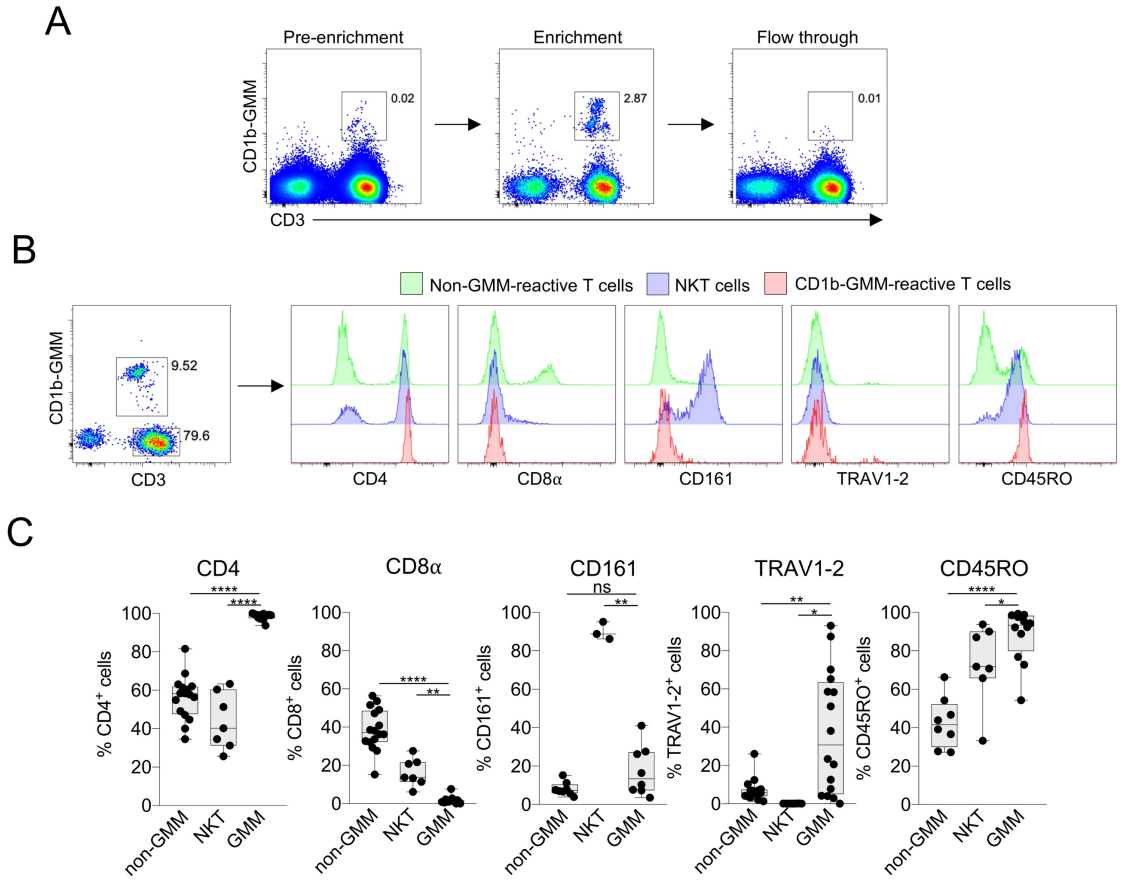

Figure 5.2. Enrichment and surface phenotype of CD1b-GMM-reactive T cells from healthy blood donors. GMM-reactive T cells or NKT cells were magnetically enriched from healthy donor PBMCs using CD1b-GMM or CD1d-α-GalCer tetramers respectively and stained with a panel of surface marker-specific monoclonal antibodies outlined in **Table 2.3**. The surface phenotype of CD1b-GMM-reactive T cells was compared to NKT cells and tetramer$^-$ CD3$^+$ (non-GMM) T cells. **A.** CD1b-GMM tetramer staining and CD3 expression of PBMCs from a healthy blood donor before magnetic enrichment (Pre-enrichment), after enrichment (Enrichment) and of the PBMCs that did not bind to the magnetic column (Flow through). **B.** The cell surface phenotype (right histograms) of CD1b-GMM-reactive T cells from a donor (left plot) compared to CD1d-α-GalCer tetramer enriched NKT cells and non-GMM T cells from the same donor, comparing cell surface expression of CD4, CD8α, TRAV1-2 and CD45RO. Non-GMM T cells, NKT cells and CD1b-GMM-reactive T cells are represented by green, blue and red histograms respectively. **C.** Cumulative data for surface marker expression displaying the percentage of cells that express the surface marker from up to 16 healthy donors for CD1b-GMM-reactive and non-GMM T cells and up to 7 healthy donors for NKT cells. All data are overlaid on box and whisker plots that display quartiles, median and min to max values. Statistical significance was evaluated using Tukey's multiple comparison test with a Geisser-Greenhouse correction. Data are accumulated from at least three independent experiments.

CD1b-GMM tetramer$^+$ cells were examined for the expression of conventional and unconventional T cell surface markers such as CD4, CD8α, CD161, TRAV1-2 and CD45RO. As a comparison, tetramer$^-$ CD3$^+$ T cells (non-GMM-reactive T cells) and CD1d-α-GalCer tetramer$^+$ T cells (NKT cells) were also analysed (**Fig. 5.2B and C**). High expression of CD4 was observed among all CD1b-GMM tetramer$^+$ cells, akin to that recently described (135), while very few of these cells expressed CD8α (**Fig. 5.2B and C**). In comparison, a large proportion of NKT cells (20-60%) and non-GMM-reactive T cells (35-80%) expressed CD4$^+$. Interestingly, CD1b-GMM tetramer$^+$ cells from most donors were predominantly CD161$^-$ compared to the high expression of CD161 observed for NKT cells (135) (**Fig. 5.2B**), however in some donors a portion of CD1b-GMM tetramer$^+$ cells (10-40%) expressed low to intermediate surface levels of CD161 (**Fig. 5.2C**). As expected very few non-GMM-reactive T cells expressed CD161 (**Fig. 5.2B and C**). Moreover, most CD1b-GMM tetramer$^+$ cells also expressed the T cell memory marker CD45RO, similar to NKT cells, but different to non-GMM-reactive T cells, which were heterogeneous for CD45RO expression. These data suggest that CD1b-GMM tetramer$^+$ cells may have had prior exposure to GMM, or express a mature phenotype following development within the thymus, as observed for NKT cells (266, 267).

Notably, TRAV1-2 TCR expression, which is typically associated with GMM reactive T cells, varied greatly among donors, ranging from 0% to 93% of CD1b-GMM tetramer$^+$ cells with a mean value of 37% (**Fig. 5.2C**), demonstrating that the frequency of GEM T cells in healthy donors is highly variable compared to *M. tuberculosis* infected patients (135). Surprisingly, TRAV1-2$^+$ cells typically stained with CD1b-GMM tetramer with a lower tetramer fluorescence compared to TRAV1-2$^-$ cells, in contrast to initial observations (135). It should be noted that no correlation between the overall frequency of CD1b-GMM-reactive T cells and TRAV1-2$^+$ expression was observed.

5.2.3 TCR usage of GMM-reactive T cells from healthy blood donors

Given that TCR usage based on TRAV1-2 expression was highly variable between donors, the TCR repertoire of CD1b-GMM reactive T cells was examined. To further validate the enrichment approach and to elucidate the precise TCR gene usage by the TRAV1-2$^-$ and TRAV1-2$^+$ tetramer$^+$ cells, CD1b-GMM-reactive T cells from six healthy blood donors were isolated for single cell TCR sequencing (**Fig. 5.3A**).

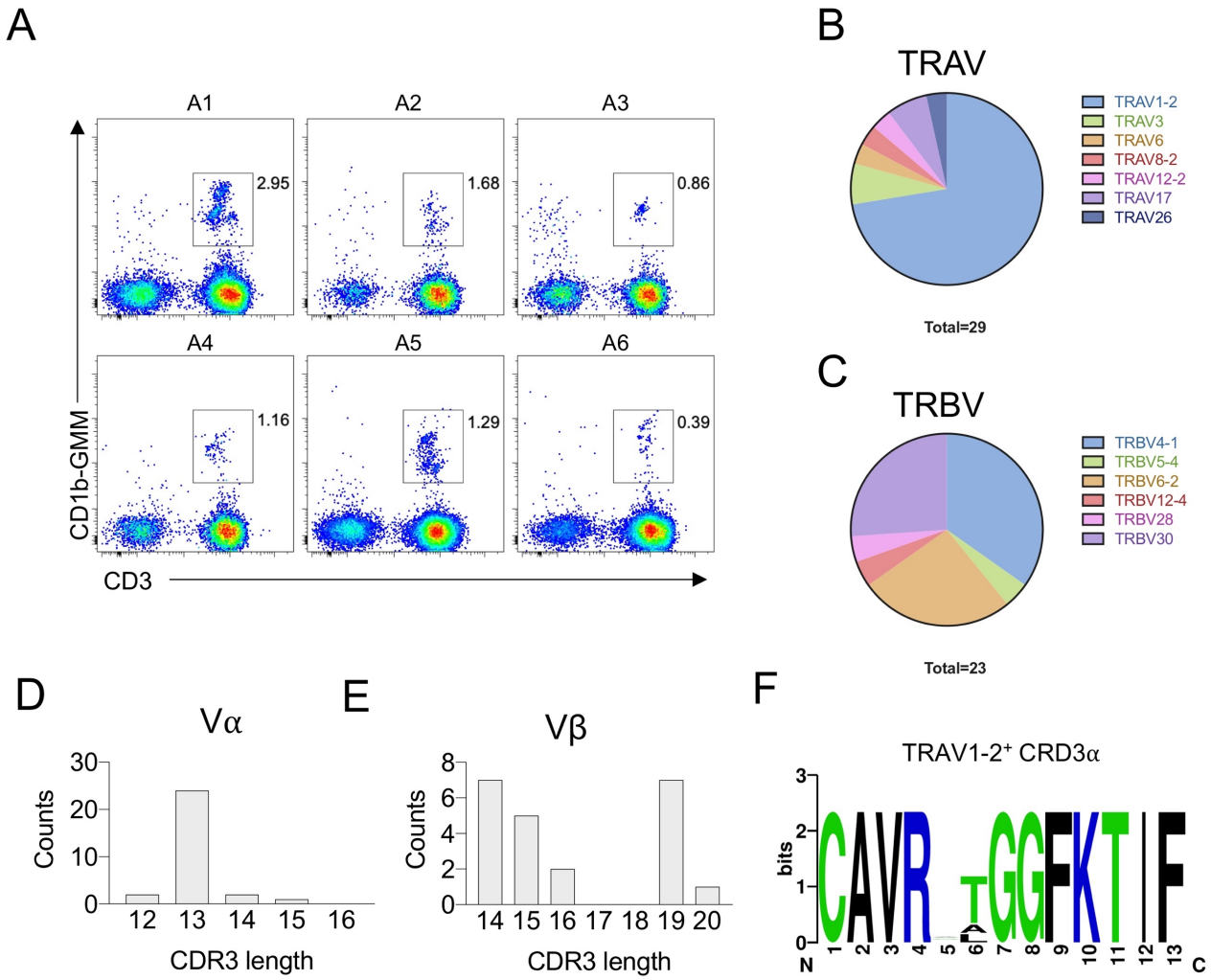

Figure 5.3. CD1b-GMM-reactive T cell TCR repertoire from six healthy donors. CD1b-GMM-reactive T cells were enriched from PBMCs of six healthy donors and single-cell sorted to derive TCR sequences. **A.** Plots display gating strategy used to isolate CD1b-GMM-reactive T cells from donors A1-A6 using CD1b-GMM tetramers after magnetic enrichment. **B and C.** Pie charts display the TRAV and TRBV gene segment usage (colour coded) of unpaired TCRα and TCRβ sequences derived from CD1b-GMM tetramer positive single sorted cells. **D and E.** Comparison of the CDR3α and CDR3β amino acid length of unpaired TCRα (n=29) and TCRβ (n=23). **F.** Sequence logo displaying consensus amino acid sequence between all unpaired TRAV1-2^{+} TCRα chains identified from donors A1-A6. Polar, basic and hydrophobic residues are colour coded in green, blue and black respectively. Data from **A** are representative of two experiment. Data from **B-F** are from one experiment.

In some donors, such as donor A1 and A5, discreet populations of CD1b-GMM tetramer$^+$ cells were visible within the tetramer$^+$ gate, possibly a consequence of clonal expansion of these cells. TCR sequencing revealed 13 unique TCR pairs from the 29 TCRα and 23 TCRβ unpaired sequences amplified from five donors **(Table 5.1, AIII.1, AIII.2, Fig. 5.3B and C**). No cDNA was successfully amplified from donor A6 single sorted cells. Interestingly, in these donors, ~75% of cells TCRs comprised the Vα domain gene segment TRAV1-2/TRAVJ9 (**Fig. 5.3B)** and expressed the canonical CDR3α of GEM T cells (**Table 5.1**). Among the ~25% of TRAV1-2$^-$ TCRα chains, the variable gene usage was diverse, including TRAV3, 6, 8-2, 9-2, 12-2, 17 and 26 (**Table AIII.1**, **Fig. 5.3B**), of which only TRAV17 expression has been previously reported (136). One third of the variable TCRβ genes identified were TRBV4-1, followed by TRBV6-2 and TRBV30 (**Fig. 5.3C**), all three of which commonly pair with the canonical GEM TCRα chain (135, 136) (**Fig. 5.3C**). Two of the TRBV4-1 gene segments were paired with non-GEM TCRα chains and a previously described TCRα chain from a CD1b-restricted T cell clone called LDN5 (**Table 5.1**) (135, 136). Notably, cells from two donors expressed identical GEM TCRα chains paired to different TCRβ chains (**Table 5.1**), in one donor composed of TRBV6-2 with unique CDR3β sequences, while in the other donor, composed of two unique TCRβ chains; TRBV4-1 and TRBV5-4. Additionally, TRBV12-4 and 28 were identified among unpaired TCRβ sequences (**Fig. 5.3C**), indicating that greater diversity exists among GMM-reactive TCRs than has been previously reported. The CDR3α regions, especially among TRAV1-2$^+$ sequences were short (**Fig. 5.3D**), typically 13 amino acids in length and only two CDR3α were identified that were greater in length, with14 and 16 amino acids. Similarly, the length of the CDR3β regions were consistently short, yet less constrained than CDR3α regions, where most sequences were of 16 amino acids length or less (**Fig. 5.3E**), while the TCRβ chains paired to GEM TCRα chains were more variable in CDR3β length, ranging from 13-16 amino acids (**Table 5.1**). In one donor, CDR3β sequences from both TRAV1-2$^+$ and TRAV1-2$^-$ cells were far longer than in other donors, at 19 amino acids long (**Fig. 5.3E**). A sequence logos analysis (**Fig. 5.3F**) corroborated the known high amino acid conservation in the CDR3α region of TRAV1-2$^+$ GMM-reactive T cells (135). Among the six donors examined, TRAV1-2$^+$ CDR3α sequences varied only at positions 5 and 6, for which a bias was detected for threonine,

alanine and leucine residues at position 6 (**Fig. 5.3F**). The detection of TRAV1-2$^+$ CD1b-GMM-reactive T cells that shared the conserved GEM CDR3α further confirmed that the enrichment approach was suitable for identifying GMM-reactive T cells directly *ex vivo*.

Table 5.1. Paired TCRαβ sequences derived from TCR-sequencing of CD1b-GMM-reactive T cells.

Donor	TRAV	CDR3α	TRAJ	TRBV	CDR3β	TRBJ	Count
A1	1-2*01	CAVRLTGGFKTIF	9*01	30*01	CAWSYSGLTTNEKLFF	1-4*01	1
A1	1-2*01	CAVRALGGFKTIF	9*01	6-2*01	CASSSRVGGDEAFF	1-1*01	1
A1	1-2*01	CAVRATGGFKTIF	9*01	30*01	CAWSKTGLGADTQYF	2-3*01	1
A1	12-2*01	CAVKNFGNEKLTF	48*01	4-1*01	CASSHVGLAGGHYYNEQFF	2-1*01	1
A2	26-1*01	CIVRGRGGADGLTF	45*01	12-4*02	CASSFRQTYSNQPQHF	1-5*01	1
A3	3*01	CAVRDLRHKLTF	10*01	4-1*01	CASSQPGLARPQDDPDTQYF	2-3*01	1
A4	1-2*01	CAVRGAGGFKTIF	9*01	6-2*01	CASTPRLGGDEQFF	2-1*01	1
A5	1-2*01	CAVRSTGGFKTIF	9*01	4-1*01	CASSQGGLAGGPRNNEQFF	2-1*01	1
A5	1-2*01	CAVRSTGGFKTIF	9*01	5-4*01	CASTRTGGDGYTF	1-2*01	1
A5	8-2*01	CVVSGWAGTYKYIF	40*01	28*01	CASNKPRGKNIQYF	2-4*01	1
A5	1-2*01	CAVRRTGGFKTIF	9*01	6-2*01	CASSFRVGGEKLFF	1-4*01	1
A5	1-2*01	CAVRRTGGFKTIF	9*01	6-2*01	CASSRRTGGDTQYF	2-3*01	1
A5	6*01	CALDRVTGGGNKLTF	10*01	4-1*01	CASSQPSFRLAGNTDTQYF	2-3*01	1

5.2.4 Transcription factor expression by CD1b-GMM-reactive T cells

To provide insights into the functional potential of CD1b-GMM-reactive T cells, the expression of key transcription factors that are known to regulate the function of other unconventional T cell populations such as MAIT cells and NKT cells were examined (206, 209, 268). CD1b-GMM-reactive T cells were enriched from PBMCs of five healthy donors using CD1b-GMM tetramer and intracellular transcription factor staining for RORγt, T-bet and PLZF was performed. The expression of each transcription factor between naïve (CD4$^+$CD45RO$^-$) CD4$^+$ T cells and MAIT cell (TRAV1-2$^+$CD161$^+$) subsets were compared (**Fig. 5.4A and B**). Naive CD4$^+$ T cells were deficient in RORγt, compared to CD1b-GMM-reactive T cells and MAIT cells, which both expressed high levels of RORγt (**Fig. 5.4B and C**). Interestingly, in some donors, RORγt expression was similar between CD1b-GMM-reactive T cells and MAIT cells, however, MAIT cells typically expressed higher levels of RORγt compared to CD1b-GMM-reactive T cells (**Fig. 5.4C**). Naive CD4$^+$ T cells did not express PLZF, while both CD1b-GMM-reactive T cells and MAIT cells stained with PLZF with a similar intensity (**Fig. 5.4B and C**). PLZF expression by peripheral CD1b-restricted T cells is a strong indicator that these cells undergo thymic development akin to NKT cells and MAIT cells, where PLZF expression is critical to both thymic maturation and innate-like effector differentiation and function (209, 269-271). Naïve CD4$^+$ T cells did not express T-bet, while both CD1b-

GMM-reactive T cells and MAIT cells expressed moderate levels of T-bet, compared to the memory $CD8^+$ T cell subset (**Fig. 5.4B and data not shown**). MAIT cells tended to express higher levels of T-bet in most donors **(Fig. 5.4C**), although greater variation was observed in T-bet staining fluorescence amongst MAIT cells compared to other T cell subsets, possibly indicating a functional disparity among MAIT cells between different donors.

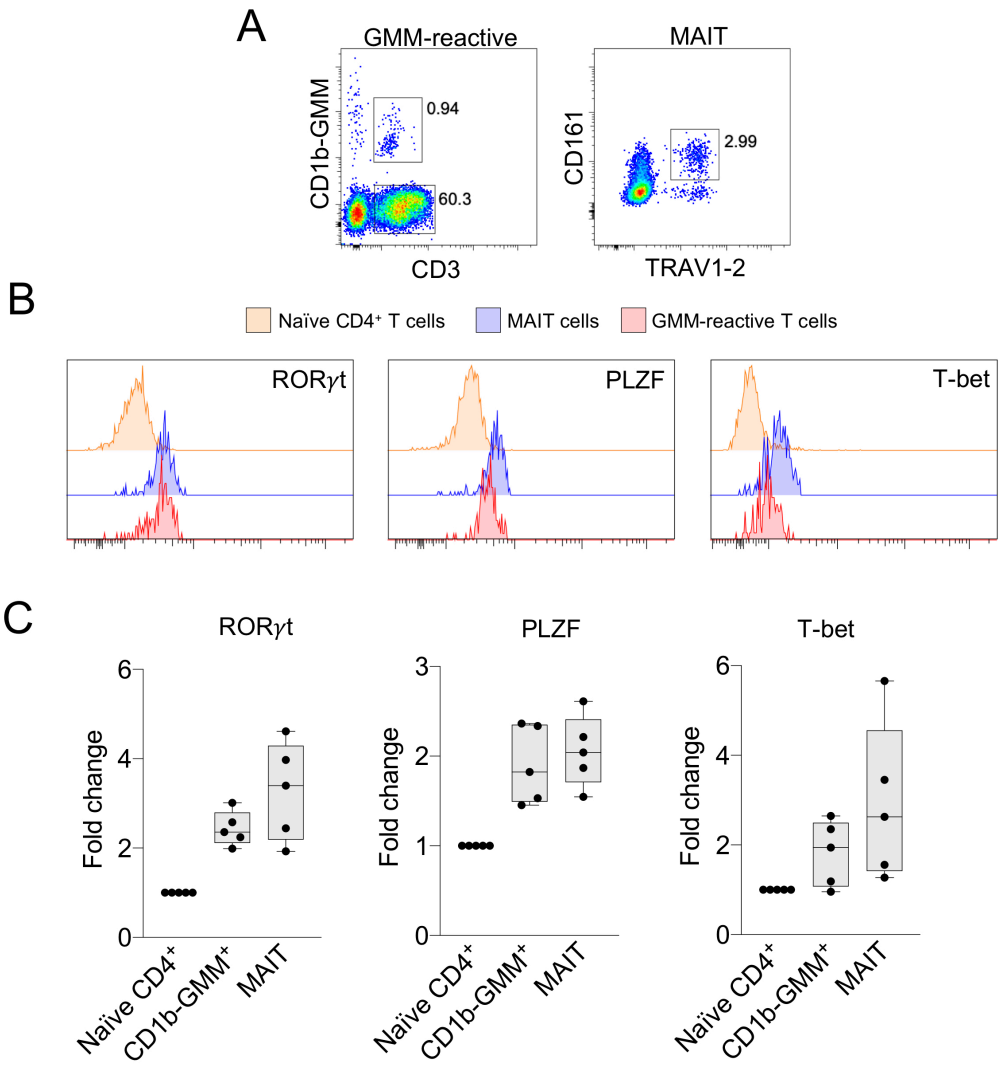

Figure 5.4. Transcription factor expression by CD1b-GMM-reactive T cells. CD1b-GMM-reactive T cells were enriched from healthy donors using CD1b-GMM tetramers stained intracellularly with a panel of anti-transcription factor antibodies outlined in **Table 2.3**. Transcription factor expression was compared between naïve CD4$^+$ T cells (CD45RO$^-$) and MAIT cells (TRAV1-2$^+$CD161$^+$). **A.** Gating strategy for identifying CD1b-GMM-reactive T cells (CD1b-GMM tetramer$^+$) and MAIT cells (TRAV1-2$^+$CD161$^+$) after intracellular staining. **B.** Histograms comparing the fluorescence intensity of RORγt, PLZF and T-bet transcription factor expression between the various T cell subsets. Naïve CD4$^+$ T cells, MAIT cells and CD1b-GMM-reactive T cells are colour coded in orange, green, blue and red respectively. **C.** Cumulative data for transcription factor expression by each T cell subset from five healthy blood donors. All data show the geometric mean fluorescence intensity normalised to the naïve CD4$^+$ T cell population in each donor (fold change) and overlaid on box and whisker plots that display median, quartiles and min to max values. Data are accumulated from three independently performed experiments.

5.2.5 Cytokine production by CD1b-GMM-reactive T cells

Due to the expression of the typical unconventional T cell transcription factor PLZF, as well as RORγt, and T-bet, the capacity for CD1b-GMM-reactive T cells to produce Th1 and Th17 cytokines was examined using the enrichment approach without the need for extended *in vitro* culture that may impact on T cell function. Frozen PBMCs from five healthy blood donors were thawed and rested overnight in culture medium as described in chapter 2. CD1b-GMM-reactive T cells were then enriched from the PBMCs using CD1b-GMM tetramers and cultured with or without PMA/Ionomycin, a non-specific stimulant, to induce cytokine production. Enriched cells were stimulated for 2.5 hours to minimise the loss of CD1b-GMM tetramer fluorescence and TCR downregulation during the culture. The production of TNF and IFNγ by CD1b-GMM-reactive T cells was then examined. The cytokine expression by MAIT cells, identified using the surrogate markers TRAV1-2 and CD161, was also examined (**Fig. 5.5A**). In spite of the short stimulation period, a low fluorescence intensity was observed for CD1b-GMM tetramer staining (**Fig. 5.5A**), possibly due to loss of tetramer binding over the culture period. Nonetheless, a population of CD1b-GMM-reactive T cells could still be identified (**Fig. 5.5A**). TNF or IFNγ production was not detected by unstimulated CD1b-GMM-reactive T cells, however 70-80% of these cells stimulated produced TNF following PMA/Ionomycin stimulation and a large proportion of these cells (~10-50%) produced IFNγ (**Fig. 5.5A and B**). Similarly, MAIT cells produced both cytokines when stimulated with PMA/Ionomycin, similar to previously described (125, 171) (**Fig. 5.5A and B**).

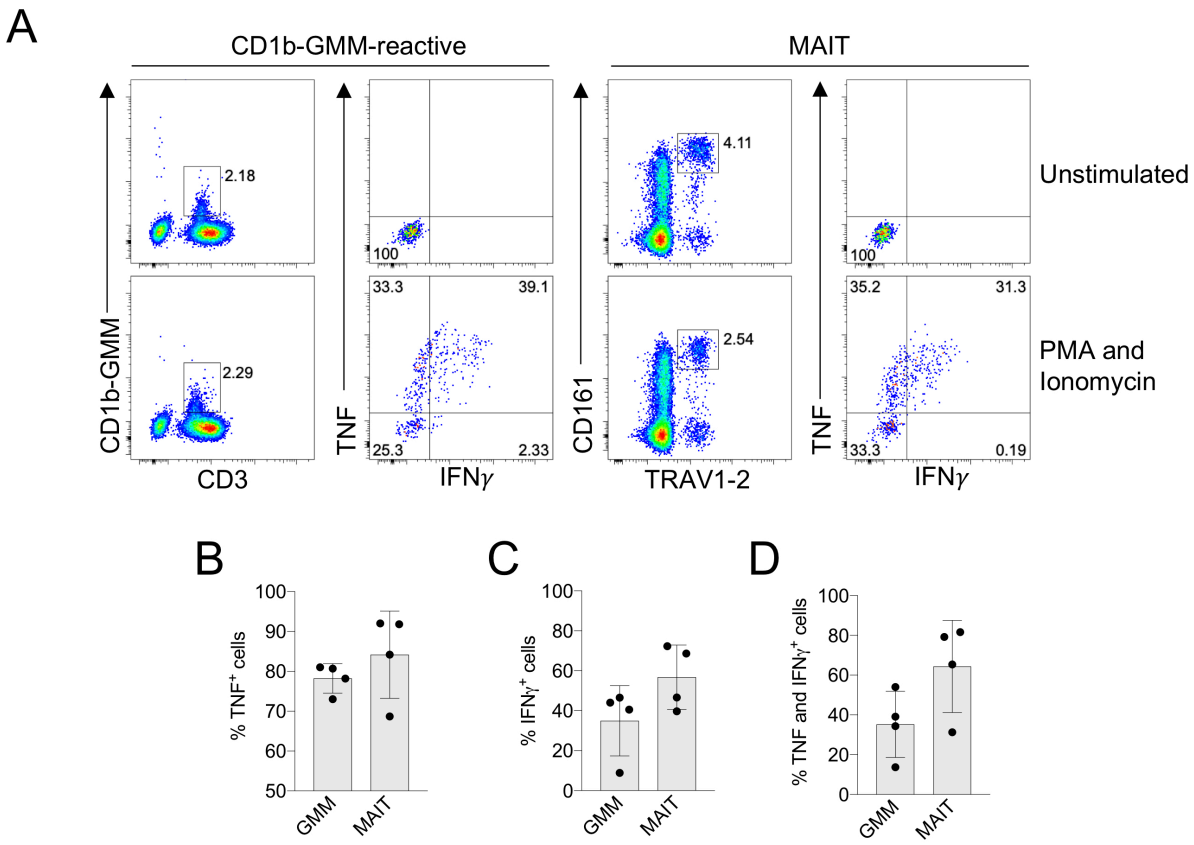

Figure 5.5. Ex vivo cytokine production by CD1b-GMM-reactive T cells after stimulation. CD1b-GMM-reactive T cells were enriched from healthy donors using CD1b-GMM tetramers, stimulated with PMA and Ionomycin and stained intracellularly with anti-cytokine antibodies outlined in **Table 2.3**. **A.** Left plots display CD1b-GMM-reactive T cells or MAIT cells (TRAV1-2^{+}CD161^{+}) unstimulated or stimulated with PMA and Ionomycin. Right plots display cytokine production (TNF and IFNγ) of unstimulated and stimulated cells. **B-D.** Cumulative data of the percentage of TNF, IFNγ and co-producing CD1b-GMM-reactive T cells and MAIT cells from four healthy donors respectively. Data displays mean ± SD. Data are accumulated from three independent experiments.

5.2.6 Isolation of single CD1b-GMM-reactive and NKT cells for transcriptomics analysis

To gain a greater understanding of CD1b-GMM reactive T cells, the transcriptome of CD1b-GMM-reactive T cells was examined using next generation sequencing. In brief, transcriptomic analysis allows for the determination of gene transcripts that are expressed within a cell and can be performed on pooled or single cells, referred to collectively as RNA-sequencing. Using the enrichment approach, CD1b-GMM-reactive T cells were accurately identified from four healthy blood donors for single-cell RNA sequencing to reveal the actively transcribed genes specific to this population for the first time. Given that nearly all CD1b-GMM tetramer$^+$ cells expressed CD4, CD4$^+$ CD1b-GMM tetramer$^-$ cells were sorted as controls. In addition, NKT cells were isolated by enrichment using CD1d-α-GalCer tetramer for comparison (**Fig. 5.6A and B**). Notably, for the same concentration of tetramer, the NKT cells stained with CD1d-α-GalCer significantly brighter than CD1b-GMM-reactive T cells stained with CD1b-GMM, whilst expressing similar levels of CD3 and thus TCR, suggesting that the TCR-CD1d-α-GalCer interaction is of higher affinity than the TCR-CD1b-GMM interaction (**Fig. 5.6A and B**). In support of this, the exceptionally high prototypic NKT TCR-CD1d-α-GalCer interaction affinity of 0.6μM (272, 273), is higher than the affinity recently described for GEM TCR-CD1b-GMM interactions of ~2μM (135).

Single cells were sorted from each donor for RNA-sequencing. Unfortunately, despite large numbers of viable cells sorted from each donor for both CD1b-GMM-reactive and NKT cells (>100 single cells per donor), RNA was only successfully amplified and passed quality control from donors 42, 44 and 63 of which only 31 paired TCRs were determined from CD1b-GMM-reactive and NKT cells collectively (**Fig. 5.6A and B and Table 5.2 and 5.3**). As expected, the phenotype of CD1b-GMM-reactive T cells was similar to that described (**Fig. 5.2C**), although cells from donor 42 were primarily TRAV1-2$^+$, compared to donor 44 which were almost all TRAV1-2$^-$ (**Fig. 5.6A and C**). Interestingly and in contrast to NKT cells (**Fig. 5.6B**), CD1b-GMM-reactive T cells from donors 8, 42, 44 and 46 did not express CD27, a marker that is typically expressed on naïve and memory T cells (274) (**Fig. 5.6C**). Most CD1b-GMM-reactive T cells were CD45RO$^+$, suggesting that these cells are capable of early effector responses after

activation (275) (**Fig. 5.6A and C**). However, there was some heterogeneity in CD45RO expression between individual cells (**Fig. 5.6B and C**). Using index sorting, differences in the surface phenotype of each cell correlate with their transcriptome and TCR expression can be assessed.

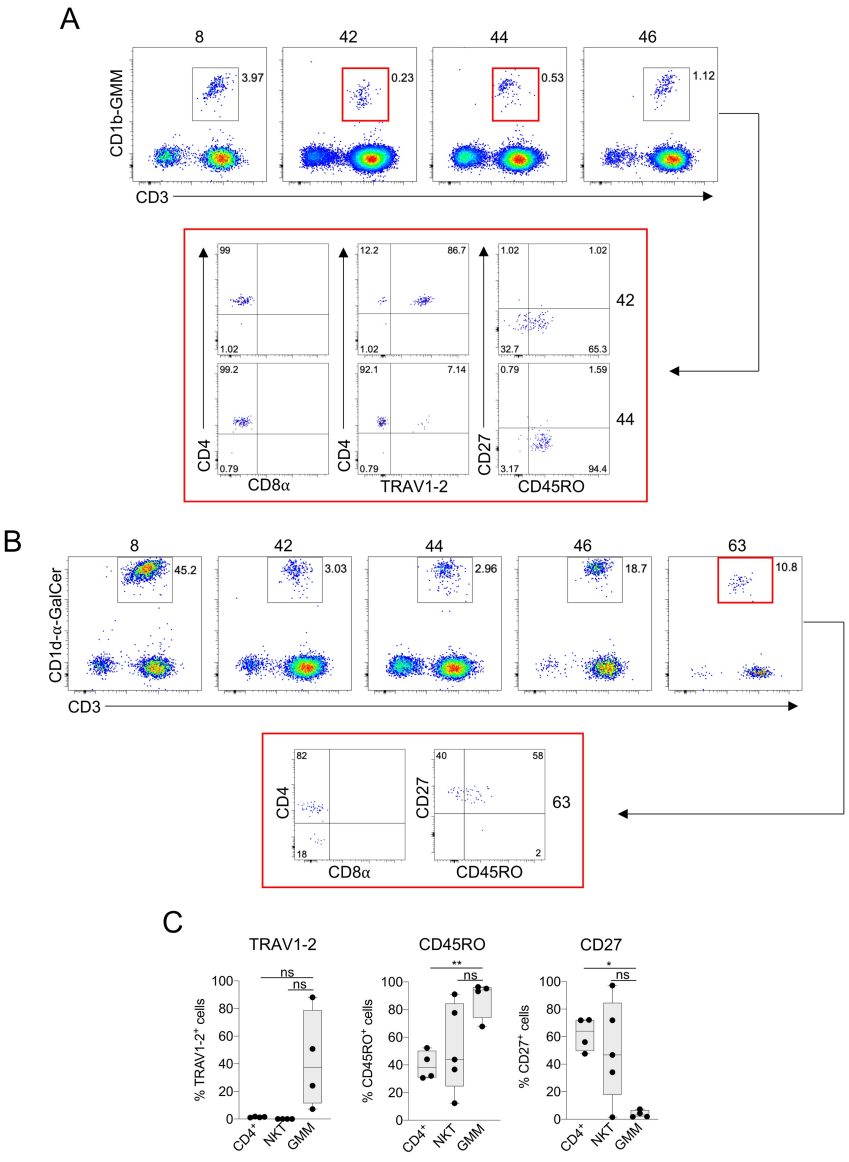

Figure 5.6. Isolation of CD1b-GMM-reactive and NKT cells for RNA-sequencing. *CD1b*-GMM-reactive T cells and NKT cells were enriched from four and five healthy blood donors respectively, and single cell sorted for RNA-sequencing. **A.** Plots depict the CD1b-GMM-reactive T cells enriched using CD1b-GMM tetramer, from donors 8, 42, 44 and 46. Each plot represents viable single cells with the exclusion of $CD19^+$ B cells. The red boxes denote donor cells that provided good quality RNA for sequencing. The large red box shows the surface phenotype, including CD4, CD8α, TRAV1-2, CD27 and CD45RO expression from donors 42 and 44. **B.** Plots depict the NKT cells enriched using CD1d-α-GalCer tetramer, from donors 8, 42, 44, 46 and 63, of which only donor 63 provided good quality RNA for sequencing. The large red box shows CD4, CD8α, CD27 and CD45RO expression from donor 63. **C.** Cumulative data of the percentage of TRAV1-2^+, $CD45RO^+$ and $CD27^+$ CD4+ T cells ($CD4^+$), NKT cells (NKT) and CD1b-GMM-reactive T cells (GMM) from the donors used for single-cell sequencing, representative of one experiment. Statistical significance was evaluated using Tukey's multiple comparison test with a Geisser-Greenhouse correction.

5.2.7 TCR repertoires of CD1b-GMM-reactive, NKT and CD4$^+$ T cells derived from transcriptomics analysis

Using the bioinformatics tool VDJPuzzle (276), full-length TCRα and TCRβ sequences were reconstructed from the transcriptomic data (**Table 5.2-4 and AIII.3-8**) and indexed to each single cell. We obtained 39 unpaired CD1b-GMM-reactive TCRα sequences, of which 48% of the variable gene segments were composed of TRAV1-2, mostly from donor 42, and a single TRAV1-2$^+$ cell was identified from donor 44 (**Table AIII.3 and Fig. 5.7A**). About one third of TCRα variable gene segments were composed of TRAV35 (**Fig. 5.7A**). Interestingly, all TRAV35 sequences were exclusively identified in donor 44, likely derived from clonal expansion of a single cell, as 9/11 of the TRAV35 sequences expressed identical CDR3α regions (**Table AIII.3**). However, three unique TRAV35 sequences were identified in total from donor 44, highlighting a strong TCR bias in this donor. In addition, TRAV2, TRAV8, TRAV17 and TRAV38 variable genes were identified, which further demonstrates a public bias for TRAV17 expression in CD1b-GMM-reactive T cells (136). 33 unpaired TCRβ sequences were reconstructed from the transcriptomic data (**Table AIII.4**), of which 64% of variable gene segments involved TRBV6-2 (**Fig. 5.7B**), akin to the CD1b-GMM-reactive T cells described above (**Fig. 5.3C**) and mostly paired to TCRα chains composed of TRAV1-2 (**Table 5.2 and Fig. 5.7C**). The next most frequent gene usage was TRBV5-4 and TRBV20-1, while very few cells expressed the TRBV4-1 gene segment (**Fig. 5.7B**), which was at odds with the single-cell TCR sequencing data that showed a strong TCR TRBV4-1 bias (**Fig 5.3B**). It is possible that the absence of more extensive TRBV4-1 gene usage was caused by a bias in TCRβ usage in the two donors analysed in these latter experiments. In addition, TRBV7-2 and TRBV14 variable genes were identified in donor 42 (**Table AIII.4**). Similar to the single-cell TCR sequence data described above (**Fig 5.3D**), the CDR3α length determined from the transcriptome data was highly consistent, where all TRAV1-2$^+$ and TRAV17$^+$ CDR3α regions were constrained to 13 amino acids in length (**Fig. 5.7D**), while more diverse TCRα sequences varied from 11-16 amino acids in length. Notably, the clonally expanded TRAV35 TCRα sequence expressed a short CDR3α region of 12 amino acids in length (**Table AIII.3**). Similarly, the CDR3β lengths from the transcriptome data were consistent with the single-cell TCR sequence data described

above (**Table AIII.2 and AIII.4**), where 21/33 sequences had CDR3β regions of 14 amino acids length, while the remaining sequences had a spread of CDR3β lengths ranging from 12 to 17 (**Fig. 5.7E**). A sequence logo of the TRAV1-2^{+} CDR3 sequences revealed high variability in amino acids at position 5 and 6 (**Fig. 5.7F**) as shown previously (**Fig. 5.3F**), as well as a strong bias for arginine or tyrosine at position 4.

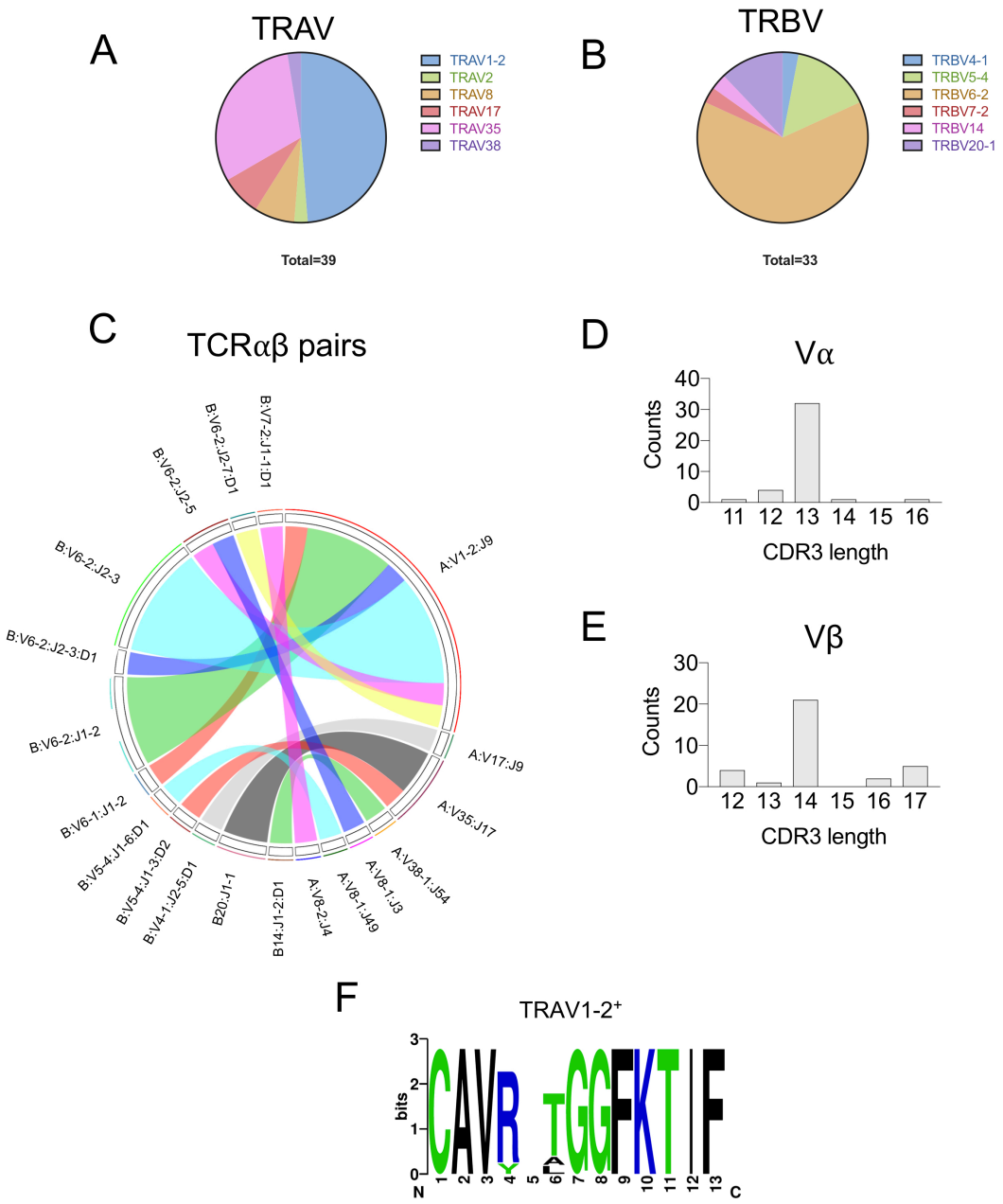

Figure 5.7. CD1b-GMM-reactive T cell TCR repertoire derived from RNA-sequencing. Paired and unpaired TCRα and TCRβ chain sequences were reconstructed from single-cell RNA-sequencing reads using the VDJPuzzle tool (276). **A and B.** Pie chart displays the TRAV and TRBV gene segment usage (colour coded) of unpaired TCRα and TCRβ sequences derived from CD1b-GMM tetramer^{+} cells of donor 42 and 44. **C.** Circos map of TCRαβ dimers from CD1b-GMM-reactive T cells, depicting paired TRAV and TRBV gene segment usage from 10 unique pairs. **D and E.** Comparison of the CDR3α and CDR3β amino acid length of unpaired TCRα (n=39) and TCRβ (n=33) sequences. **F.** Sequence logo displaying consensus amino acid sequence between all unpaired TRAV1-2^{+} TCRα chains identified from donors 42 and 44. Polar, basic and hydrophobic residues are colour coded in green, blue and black respectively. Analysis was performed using a dataset derived from one experiment.

Table 5.2. Paired TCRαβ sequences derived from RNA-sequencing of GMM-reactive T cells.

Donor	TRAV	CDR3α	TRAJ	TRBV	CDR3β	TRBJ	Count
42	1-2*01	CAVRVTGGFKTIF	9*01	6-2*01	CASSFRVGGDTQYF	2-3*01	5
42	8-1*01	CAVHGAGNQFYF	49*01	5-4*01	CASRRTPGDSYNSPLHF	1-6*01	1
42	1-2*01	CAVYSTGGFKTIF	9*01	6-2*01	CASTRRLSNYGYTF	1-2*01	5
42	17*01	CATPGTGGFKTIF	9*01	4-1*01	CASTGLAIETQYF	2-5*01	1
42	38-1*01	CAFMNWRFQGAQKLVF	54*01	14*01	CASSPPWLRGWSGYTF	1-2*01	1
42	8-1*01	CAVSRYSSASKIIF	3*01	6-2*01	CASSSRLGGETQYF	2-5*01	1
42	1-2*01	CAVRKTGGFKTIF	9*01	6-2*01	CASSSRLGGETQYF	2-5*01	2
42	8-2*01	CVVSRGGYNKLIF	4*01	7-2*01	CASGEQGLRQNTEAFF	1-1*01	1
44	1-2*01	CAVRNTGGFKTIF	9*01	6-2*01	CASTLRKGGDEQYF	2-7*01	1
44	35*01	CARRSAGNKLTF	17*01	20-1*01	CSAATWNTEAFF	1-1*01	1

Among NKT cells from donor 63, 42 unpaired TCRα sequences were reconstructed, of which only 62% were composed of the variable gene segment TRAV10 paired to the joining gene segment TRAJ18 (**Fig. 5.8A**), the prototypic variable α-chain of Type I NKT cells (277). The remaining sequences were more diverse, including; TRAV2, 3, 8-2, 9-2, 12, 17, 21, 23, 26-1 and 29, and are derived from atypical NKT cells, as recently described (278). 67 unpaired TCRβ sequences were reconstructed, 70% composed of the variable gene segment TRBV25-1, typical of Type I NKT cells (277) (**Fig. 5.8B**). For paired TCR sequences, TRBV25-1 constituted a greater proportion of total sequences, including all TRAV10 pairs (**Table 5.3 and Fig. 5.8C**). Among the other sequences; TRBV3-1, 5, 6-5, 7, 10, 11-2, 12-3, 18, 19, 20-1, 28 and 29 were identified, a surprisingly diverse and high proportion of atypical NKT TCR gene segments that corresponded with the high proportion of atypical TCRα chains (**Fig. 5.8B**). Given that most NKT cells from humans typically express a semi-invariant TRAV10-TRBV25-1 TCR, it is possible that the NKT TCR repertoire may be biased after magnetic bead enrichment compared to isolating cells directly from PBMCs, however atypical NKT cells have been reported to recognise CD1d-α-GalCer with a lower affinity than Type I NKT cells (278), thus would be less likely retained after enrichment. It seems more probable that the high proportion of atypical TCR sequences that were recovered is due to interdonor variation. The CDR3α regions in 29/42 TCRα chains were 15 amino acids in length (**Fig. 5.8D**), including all TRAV10 chains (**Table AIII.5**) and in total CDR3α regions ranged in length from 12-16 amino acids. In contrast, the CD3β regions were far more varied in length, ranging from 11-21 amino acids (**Fig. 5.8E**), including among TRBV25-1 sequences, which comprised both the shortest and longest CDR3β regions at 11 and 21 amino acids **(Table AIII.6)**. A sequence logo of the TRAV10/TRAJ18^{+} CDR3 regions revealed very high conservation

in all CDR3α residues in most cases, except in three TCRα sequences, that varied at position 4 as well as position 12, that was either an arginine, shown previously (278), or lysine residue (**Fig. 5.8F**).

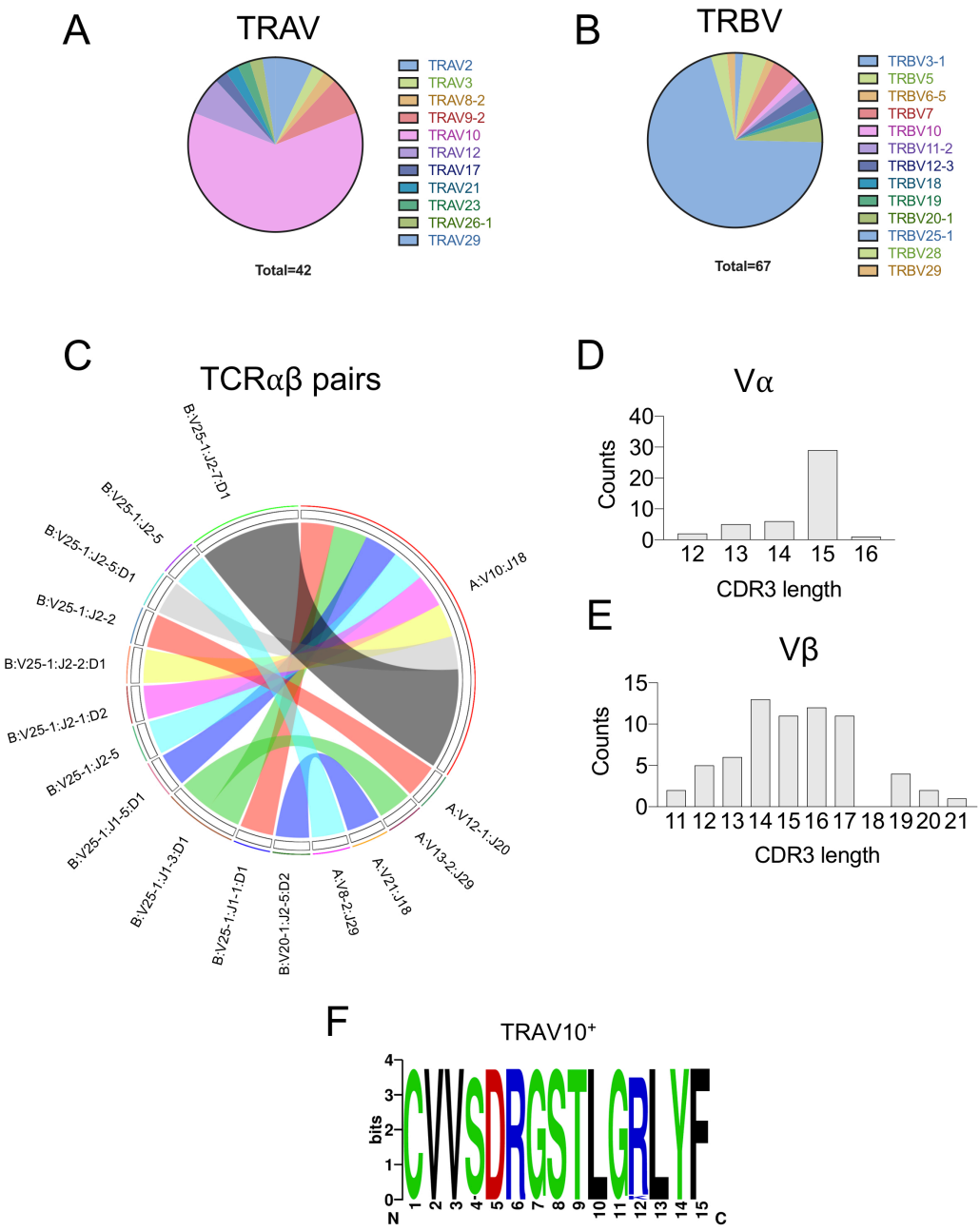

Figure 5.8. NKT cell TCR repertoire derived from RNA-sequencing. Paired and unpaired TCRα and TCRβ chain sequences were reconstructed as described in **Figure 5.7**. **A and B.** Pie chart displays the TRAV and TRBV gene segment usage (colour coded) of unpaired TCRα and TCRβ sequences derived from CD1d-α-GalCer tetramer positive cells of donor 63. **C.** Circos map of TCRαβ dimers from NKT cells, depicting paired TRAV and TRBV gene segment usage from 13 unique pairs. **D and E.** Comparison of the CDR3α and CDR3β amino acid length of unpaired TCRα (n=43) and TCRβ (n=68) sequences. **F.** Sequence logo displaying consensus amino acid sequence between all unpaired TRAV10^{+} TCRα chains identified from donors 63. Polar, basic, acidic and hydrophobic residues are colour coded in green, blue, red and black respectively. Analysis was performed using a dataset derived from one experiment.

Table 5.3. Paired TCRαβ sequences derived from RNA-sequencing of NKT cells.

Donor	TRAV	CDR3a	TRAJ	TRBV	CDR3b	TRBJ	Count
63	10*01	CVVSDRGSTLGRLYF	18*01	25-1*01	CASSEYNTGDTEAFF	1-1*01	1
63	10*01	CVVSDRGSTLGRLYF	18*01	25-1*01	CASSDQRPSGGPGEQFF	2-1*01	1
63	8-2*01	CVVSGGSGNTPLVF	29*01	25-1*01	CASSESRGTQYF	2-5*01	1
63	12-1*01	CVVNLENDYKLSF	20*01	25-1*01	CASSEELRTGELFF	2-2*01	1
63	10*01	CVVSDRGSTLGRLYF	18*01	25-1*01	CASSVTGQVTEAFF	1-1*01	1
63	10*01	CVVSDRGSTLGKLYF	18*01	25-1*01	CASSLTGGGRPNYEQYF	2-7*01	1
63	10*01	CVVSDRGSTLGRLYF	18*01	25-1*01	CASSESGGSGNTIYF	1-3*01	1
63	10*01	CVVSDRGSTLGRLYF	18*01	25-1*01	CASSEKRSTRGTGPKTQYF	2-5*01	1
63	10*01	CVVSDRGSTLGRLYF	18*01	25-1*01	CASSGPDNQPQHF	1-5*01	1
63	10*01	CVVSDRGSTLGRLYF	18*01	25-1*01	CASSDGNWDRGPAEGAQHF	1-5*01	1
63	21*01	CAPDRGSTLGRLYF	18*01	20-1*01	CSARVRLAGTQETQYF	2-5*01	1
8	26-1*01	CIVNGYSGGGADGLTF	45*01	20-1*01	CSARDRGRGHEQYF	2-7*01	1
8	10*01	CVVSDRGSTLGRLYF	18*01	25-1*01	CASTPRGGRADEQYF	2-7*01	1
8	10*01	CVVSDRGSTLGRLYF	18*01	25-1*01	CASSPSGQGLITGELFF	2-2*01	1
8	3*01	CAVRGSSGGSYIPTF	6*01	11-2*01	CASSFSGSLHNEQFF	2-1*01	1
8	9-2*01	CALISGGYQKVTF	13*01	12-3*01	CASSPPKNTEAFF	1-1*01	1
8	12-3*01	CAMSAPRNTDKLIF	34*01	7-3*01	CASSLVAGVTEAFF	1-1*01	1
8	2*01	CAPRKRDDYKLSF	20*01	5-1*01	CASSPGSGTVYEQYF	2-7*01	1
8	10*01	CVVSDRGSTLGRLYF	18*01	25-1*01	CASSESNEQFF	2-1*01	1
8	12-2*01	CAVNIEGGGNKLTF	10*01	5-1*01	CASSLPGGAGTGELFF	2-2*01	1
8	29/DV5*01	CAASATPGANSKLTF	56*01	12-3*01	CASSRRAGEEETQYF	2-5*01	1

As a control population, transcriptome analysis of tetramer$^-$ CD4$^+$ T cells was also performed from donor 63. 15 unpaired TCRα sequences and 22 unpaired TCRβ sequences were reconstructed from the transcriptomic data (**Table AIII.7, AIII.8, Fig. 5.9A and B**). As expected, a high diversity of variable gene segment usage in TCRα chains and an even distribution among TRAV2, 3, 4, 12, 13, 17, 21, 26-2 and 38-2 gene segments was observed, although TRAV8 appeared overrepresented by comprising one third of total TCRα variable gene segments (**Fig. 5.9A**). Among paired TCR sequences (**Table 5.4**), all CD4$^+$ T cells expressed unique TCRs, including variable gene segments, with no two cells sharing the same pairs of variable genes (**Fig. 5.9C**). These data are to be expected based on the indiscriminate method of CD4$^+$ T cell isolation, excluding only CD1b-GMM tetramer$^+$ cells. An even distribution of variable gene segments in TCRβ chains was observed, comprising; TRBV2, 4-1, 5, 6-1, 7-2, 9, 10-3, 12-4, 20-1, 21-1, 24, 28, 29-1 and 30 (**Fig. 5.9B**). The CDR3α length was more variable among CD4$^+$ T cells, than GMM-reactive or NKT cells (**Fig. 5.9D**), ranging from 11-17 amino acids, although 7/15 CDR3α regions were 14 amino acids in length. The CDR3β length among CD4$^+$ T cells was similar in distribution to the NKT cells, ranging from 11-18 (**Fig. 5.9E**), although it tended to be slightly shorter than for NKT cells with a median length of 13 compared to a median length of 15 respectively (**Fig. 5.9E and 5.8E**).

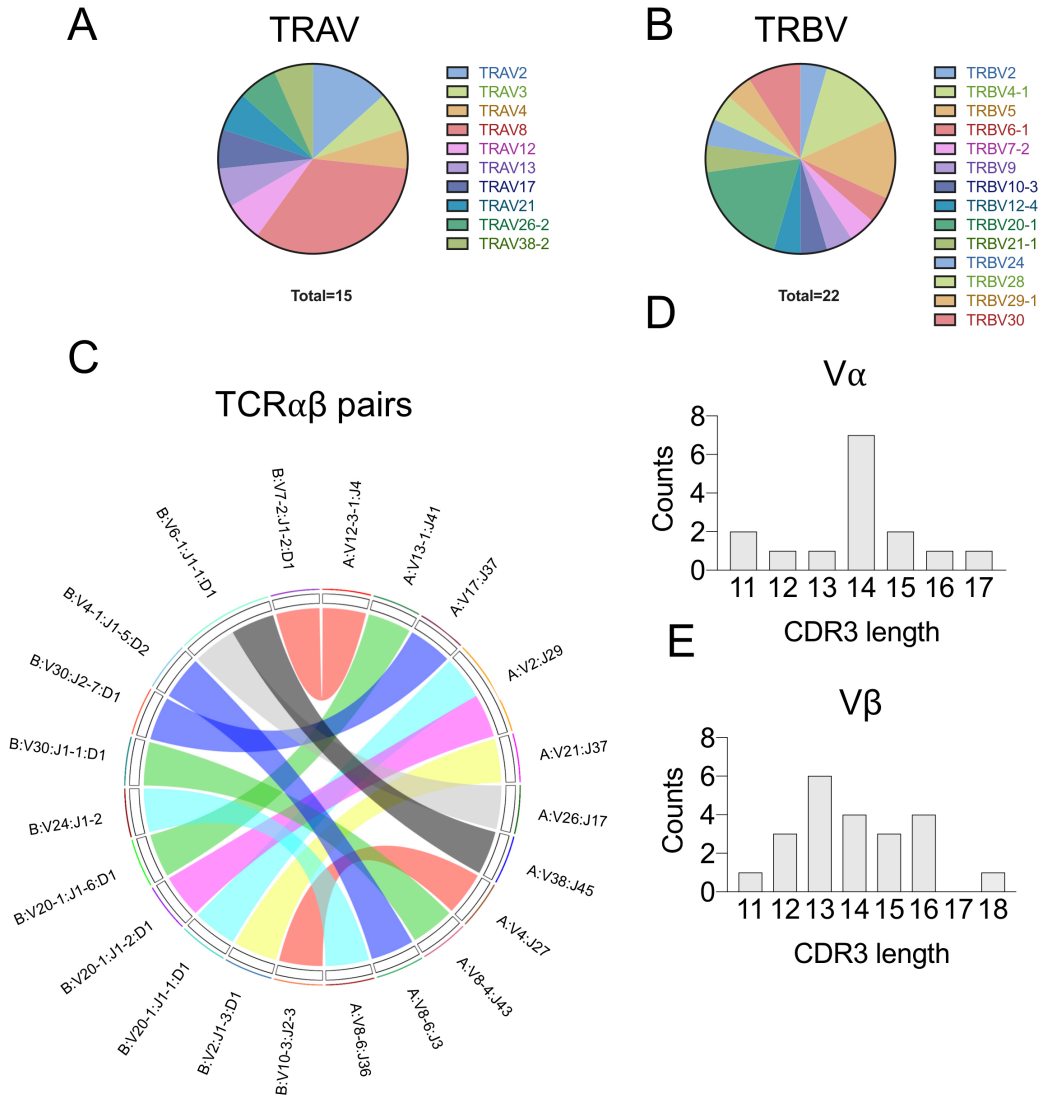

Figure 5.9. CD4⁺ T cell TCR repertoire derived from RNA-sequencing. Paired and unpaired TCRα and TCRβ chain sequences were reconstructed as described in **Figure 5.7**. **A and B.** Pie chart displays the TRAV and TRBV gene segment usage (colour coded) of unpaired TCRα and TCRβ sequences derived from tetramer negative cells of donor 63. **C.** Circos map of TCRαβ dimers from CD4⁺ T cells, depicting paired TRAV and TRBV gene segment usage from 12 unique pairs. **D and E.** Comparison of the CDR3α and CDR3β amino acid length of unpaired TCRα (n=15) and TCRβ (n=22) sequences. Analysis was performing using a dataset derived from one experiment.

Table 5.4. Paired TCRαβ sequences derived from RNA-sequencing of CD4⁺ cells.

Donor	TRAV	CDR3a	TRAJ	TRBV	CDR3b	TRBJ	Count
63	38-2/DV8*01	CAYRFGGSEKLVF	57*01	4-1*01	CASSQGTSEWYNEQFF	2-1*01	1
63	4*01	CLVGSEVDTNAGKSTF	27*01	10-3*01	CAIRSQGTDTQYF	2-3*01	1
63	17*01	CATAGLPSNTGKLIF	37*01	30*01	CAWRRDSTPYEQYF	2-7*01	1
63	2*01	CAVERNTPLVF	29*01	20-1*01	CSARGQRDTEAFF	1-1*01	1
63	26-2*01	CILAMIKAAGNKLTF	17*01	6-1*01	CASSLDRGMNTEAFF	1-1*01	1
63	8-6*01	CAVSRQGGANNLFF	36*01	24/OR9-2*01	CATNDGIGGYTF	1-2*01	1
63	8-6*01	CAVSSYSSASKIIF	3*01	30*01	CASNSDTGPEAFF	1-1*01	1
63	12-3*01	CAMTFSGGYNKLIF	4*01	7-2*01	CASSLGTADGYTF	1-2*01	1
63	2*01	CAVDSNSGNTPLVF	29*01	20-1*01	CSAPGQGVKYGYTF	1-2*01	1
63	21*01	CAVKGSSNTGKLIF	37*01	2*01	CASRGRDRNTIYF	1-3*01	1

5.2.8 Comparison of CD1b-GMM-reactive T cell transcriptome with other T cell subsets

A principle component analysis (PCA) was performed on the transcriptomic data from each of the T cell subsets isolated by magnetic enrichment. Single-cell transcriptomes were normalised to subtract variations between the T cell subsets that were caused by experimental conditions, different donors and features unrelated to cell subset. CD1b-GMM-reactive T cells, NKT cells and CD4⁺ T cells formed separate clusters, each symbol representing a single cell (**Fig. 5.10A**). Some overlap between cells of all three subsets was observed, most notably among NKT cells that either clustered far from the other subsets or overlapped with CD4⁺ T cells (**Fig. 5.10A**). The PCA analysis suggests that three distinct clusters provide a best fit for each of the different cell types. Indeed, the transcriptomes formed almost homogenous clusters containing CD1b-GMM-reactive T cells and most NKT cells when the analysis was restricted to using three clusters only (**Fig. 5.10B**). However, a proportion of NKT cells, as depicted in the PCA plot (**Fig. 5.10A**), as well as several CD1b-GMM-reactive T cells were grouped with the CD4⁺ T cell cluster (**Fig. 5.10B**). Many gene transcripts were detected that were highly expressed by CD1b-GMM-reactive T cells, including; *JUN, TSC22D3, CXCR4* and *KLF6* (**Fig. 5.10B**). The protein encoded by *JUN,* c-Jun, is a leucine zipper that forms part of the AP-1 complex that is critical for cellular proliferation, growth and differentiation (279). Interestingly, *TSC22D3* encodes for another leucine zipper known as GILZ, a transcriptional regulator that is capable of inhibiting T cell proliferation by antagonising AP-1 (280). A proportion of CD1b-GMM-reactive T cells expressed the gene *TRBV6-2*, likely GEM T cells expressing the prototypic TRAV1-2/TRAJ9 TCRα chain that paired with TRBV6-2 expressing TCRβ chains (**Fig. 5.10B**) (135). In addition, *IER2* and *RPSAP58* were expressed by most CD1b-GMM-reactive T cells (**Fig. 5.10B**). NKT cells

were well defined by the gene transcripts *KLRB1*, the gene encoding for CD161, *TGFB1,* the gene encoding for the cytokine TGF-β, *TRBV25-1,* the gene encoding for the prototypical type 1 NKT TCRβ chain, as well as *MTND2P28, MT2A, PDE4B* and *GNLY* (**Fig. 5.10B**). Unsurprisingly, *KLRB1* was also expressed by some CD1b-GMM-reactive T cells, although at lower levels than NKT cells, which is consistent with CD161 being restricted to a minor subset in most donors (**Fig. 5.2B and C**). Unlike CD1b-GMM-reactive T cell transcripts, that were expressed at high levels, some of the NKT cell marker genes were expressed at very low levels, such as *TGFB1*, that was weakly detected among NKT cells and almost completely absent in the other cell types (**Fig. 5.10B**).

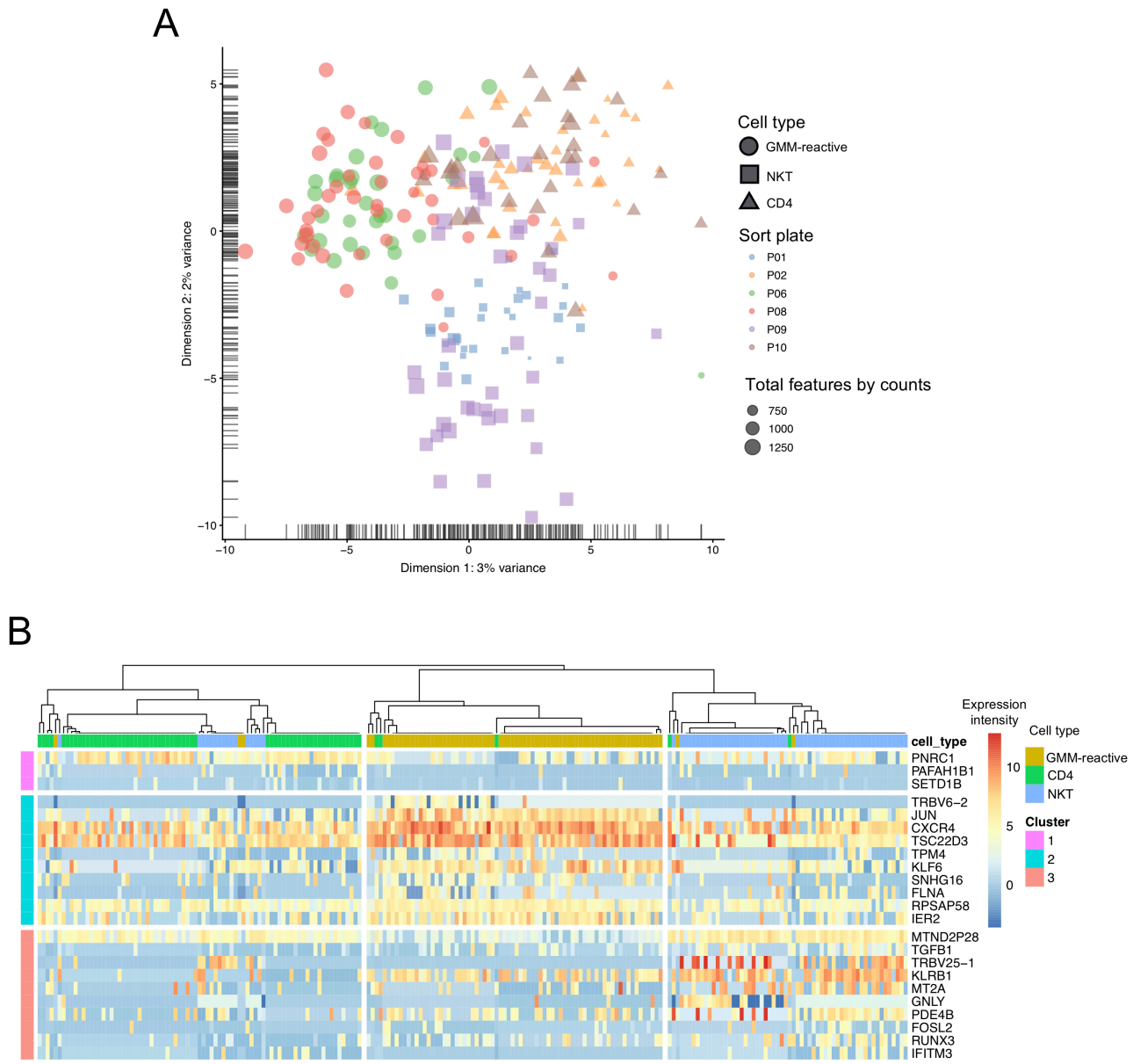

Figure 5.10. CD1b-GMM-reactive T cells are a transcriptionally distinct unconventional T cell subset. Transcriptome variation pre- and post-normalisation and batch correction, principle component analysis (PCA) and heatmap of marker genes for CD1b-GMM-reactive T cells (GMM-reactive), $CD4^+$ T cells (CD4) and NKT cells (NKT). **A.** PCA plot depicting each T cell subset (cell type) annotated with experimental details, including plate number (plate) and total feature count (total features). **B.** A heatmap displaying each T cell subset (cell type) segregated based on unsupervised clustering into three groups (clusters) and displaying the top marker genes for each cluster in mean expression values and ranked using a Wilcoxon signed rank test. Marker genes are defined as having an area under the receiver operating characteristic (AUROC) curve of >0.85 and $p < 0.01$. Analysis was performing using a dataset derived from one experiment.

Subsequently, the genes that were differentially expressed between each cell type were examined, using NKT cells as a reference cell type. A total of 46 differentially expressed genes were identified between CD1b-GMM-reactive T cells and CD1d-α-GalCer-reactive NKT cells of which the top 16 are displayed (**Fig. 5.11A**). Specifically, each gene was categorised with the MAST package (281) using a calculated threshold to distinguish expressed (≥1) or non-expressed (<1) genes. Only expressed genes were compared between the T cell subsets and displayed in log expression. Using this analysis, a number of genes were identified that were downregulated in CD1b-GMM-reactive T cells compared to NKT cells, notably; *GNLY, NKG7* and the pseudogene *MTND2P28* showed substantial differences in expression between the subsets (**Fig. 5.11A and B**). *GNLY* encodes for the cytolytic molecule granulysin, that is typically associated with cytotoxic $CD8^+$ T cells and capable of eliciting antimicrobial activity directly or in concert with perforin (161). Many of the differentially expressed genes were of mitochondrial origin or encoded for ribosomal genes such as; *MT-ND2, MT-ND4L, MT-ND5, MT-ND6, MT-RNR1*, *MTND2P28, RPS26* and *RPS4Y1* (**Fig. 5.11A**), perhaps indicating differences in cell metabolism and protein synthesis between subsets. In general, NKT cells expressed more of these mitochondrial and ribosomal transcripts than CD1b-GMM-reactive T cells, with the exception of *MT-RNR1*, that was highly expressed in both subsets (**Fig. 5.11A**). Genes that were upregulated in CD1b-GMM-reactive T cells compared to NKT cells include; *CXCR4*, encoding for the chemokine receptor of the same name and is involved in T cell migration and co-stimulation during $CD4^+$ T cell activation (282-284), *GAS5*, a non-coding RNA that is highly abundant in growth-arrested cells (285), *PIK3IP1*, encoding for a transmembrane protein that inhibits PI 3-kinases (PI3Ks) function and T cell activation (286), as well as *JUN*, *TSC22D3* and others (**Fig. 5.11B**). A gene set enrichment analysis (GSEA) between CD1b-GMM-reactive T cells and NKT cells was performed to compare the expression of sets of genes known to be enriched in certain cell subsets or that are known to be involved in key functional pathways as defined by the Molecular Signatures Database (MSigDB) (**Fig. 5.11C**). Expectedly, gene sets enriched in NK cells were downregulated in CD1b-GMM-reactive T cells compared to NKT cells, while gene sets associated with signalling in T cells and the AP-1 transcription factor network were upregulated in CD1b-GMM-reactive T cells (**Fig. 5.11C**). Comparing CD1b-GMM-reactive T cells to $CD4^+$ T cells, 55 differentially expressed genes were

identified, of which the top 16 are displayed (**Fig. 5.11C**). Similarly, *CXCR4* as well as some of the mitochondrial and ribosomal genes were differentially expressed between subsets (**Fig. 5.11C**). Genes important for regulating T cell function such as; *BHLHE40, CDKN1A* and *RORA* were also differentially expressed between GMM-reactive T cells and $CD4^+$ T cells (**Fig. 5.11B**). *CDKN1A* encodes for the cyclin dependent kinase inhibitor p21, another regulator of cell proliferation (287). While the transcription factors encoded by *BHLHE40* and *RORA*, Bhlhe40 and RORα respectively, have been shown to influence cytokine production by T cells (288, 289). Thus, high expression of these transcription factors likely influences CD1b-GMM-reactive T cell function upon activation. Additionally, *FKBP11, KLRB1* and *AC004057.1* were highly differentially expressed where *FKBP11* and *KLRB1* were higher in GMM-reactive T cells, while *AC004057.1* was higher expressed in $CD4^+$ T cells (**Fig. 5.11C**). Smaller differences in gene expression were noted for *EEF1A1P6, FTH1, HLA-C.4* and *TMSB10* that were not previously identified as marker genes (**Fig. 5.11C**). Further, some notably genes that were upregulated in CD1b-GMM-reactive T cells compared to $CD4^+$ T cells were *TNFAIP3*, encoding for A20 that regulates TNF receptor and NF-κB signalling (290) and *GADD45B*, encoding for the protein of the same name that helps regulating T cell responses to TCR stimulation and inflammatory cytokines (291), as well as others already described (**Fig. 5.11E**). GSEA revealed relatively few differences in gene expression among gene sets associated with signal transduction, leukocyte differentiation and cell activation (**Fig. 5.11F**). Whereas gene sets associated with the AP-1 transcription factor network, some DC markers and inflammasome related genes were upregulated in CD1b-GMM-reactive T cells (**Fig. 5.11F**). Conversely, some gene sets associated with transcription and cellular division were downregulated in CD1b-GMM-reactive T cells (**Fig. 5.11F**).

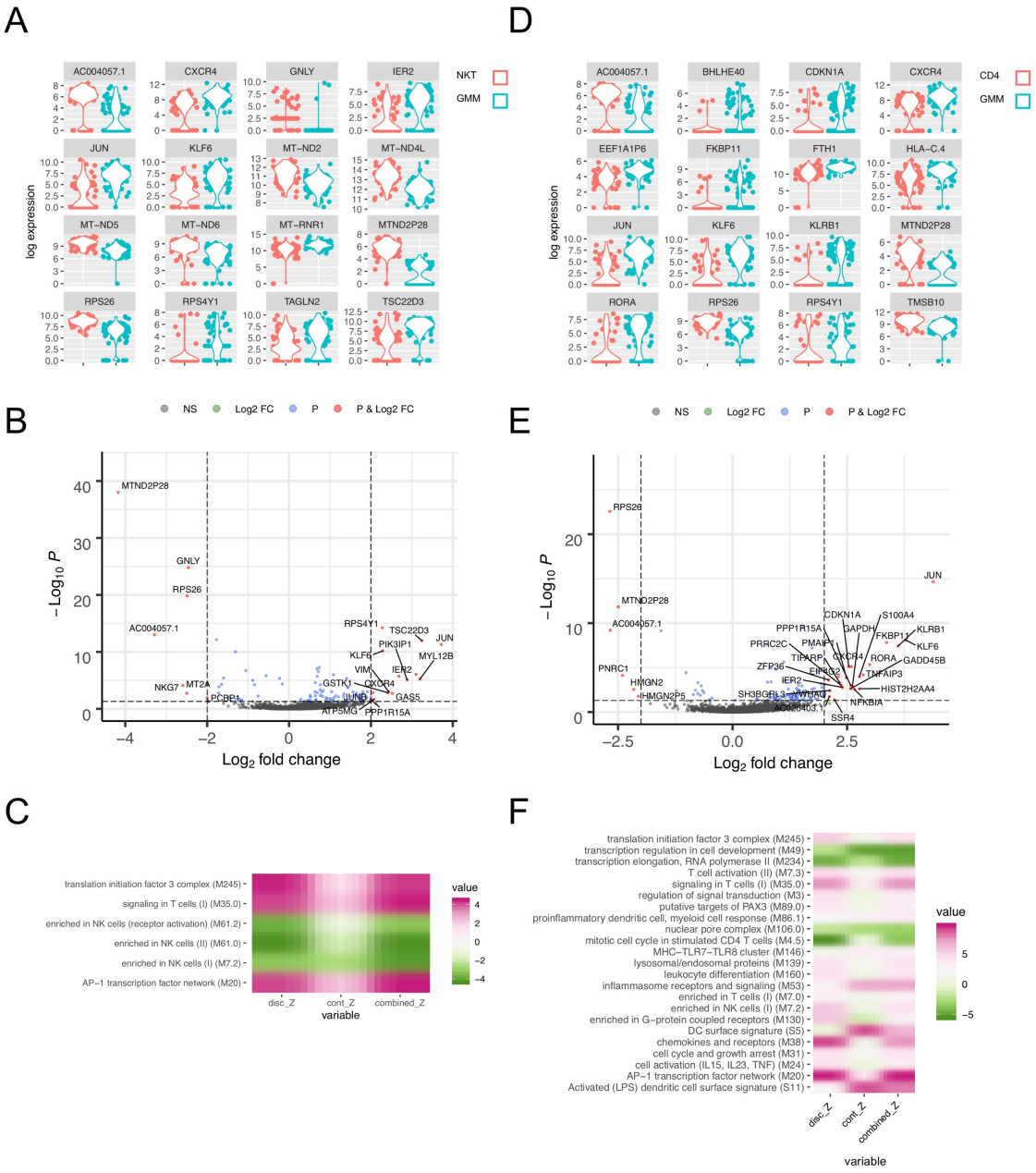

Figure 5.11. Differential gene expression from GMM-reactive T cells with NKT and CD4⁺ T cells. Comparison of the differentially expressed genes between GMM-reactive T cells and NKT cells or CD4⁺ T cells for each single cell measured in absolute log fold change above 1, where <1 are non-detected genes. **A.** Comparison of the top 16 differentially expressed genes between CD1b-GMM-reactive T cells (blue) and NKT cells (red). **B.** Volcano plot displaying differential gene expression labelled as, non-significant (NS), $\log_2$ fold change (Log2FC), significant (P) and significant and > $\log_2$ fold change (P & Log2 FC) between CD1b-GMM-reactive T cells and NKT cells. The horizonal dashed lines show p=0.05 and vertical dashed lines show absolute $\log_2$ fold change of 2. **C.** Gene set enrichment analysis (GSEA) between CD1b-GMM-reactive T cells and NKT cells showing up- (pink) or down-regulated (green) genes in CD1b-GMM-reactive T cells compared to NKT cells. **D-F.** As described in **A-C** between CD1b-GMM-reactive T cells compared to control CD4⁺ T cells. Analysis was performed using a dataset derived from one experiment.

5.3 Discussion

Using CD1b tetramers, CD1b-GMM-reactive T cells were successfully identified in many healthy donors in sufficient numbers to assess their phenotype, without the need for *in vitro* culture and expansion (135, 137). Using single-cell RNA-sequencing, the transcriptome of CD1b-restricted T cells was analysed in depth, identifying transcriptional regulators of CD1b-GMM-reactive T cell function. Interestingly, even using magnetic enrichment, CD1b-GMM-reactive T cells were not identified in all donors, and among donors that possessed CD1b-GMM-reactive T cells, differences were noted in the number of cells recovered after magnetic enrichment, suggesting that the prevalence of these cells in healthy donors is variable. It is likely that in some donors, the frequency of CD1b-GMM-reactive T cells is below the detection threshold of tetramers, similar to what has been described previously for GEM T cells, that were detected by PCR but not *ex vivo* with tetramers (135). The variability in the frequency of enriched CD1b-GMM-reactive T cells from similar starting numbers of PBMCs suggests that other factors may contribute to the abundance of these cells in healthy individuals, such as antigen exposure in the periphery.

MAIT cells are highly abundant in the peripheral blood in humans yet can vary widely in their frequency among donors (124, 171). In contrast to GMM-reactive T cells, MAIT cells recognise a highly prevalent microbial antigen that can be produced by all bacteria and yeasts containing the riboflavin biosynthesis pathway (61). Studies examining the frequency and phenotype of MAIT cells in humans throughout development (269, 292), to maturity (171), demonstrate that they undergo considerable expansion early in life, likely in response to colonisation by the microbiota, and stimulation of MAIT cells directly via MR1 (61). These assumptions translate suitably to mice, where MAIT cells are not readily detected in the periphery from mice raised in germ-free conditions (55, 293), and microbial reconstitution later in life does not induce MAIT cell development (294), (269). Seminal work by *Legoux et al.* recently established that thymic development of MAIT cells is controlled by riboflavin metabolites produced by commensal bacteria at mucosal surfaces (295). These MR1 ligands migrated from mucosal surfaces to the thymus to modulate MAIT cell thymic selection directly. (295). In light of these

advancements, it is perhaps unsurprising that early-life MAIT cell expansion in the periphery is not accompanied by an aberrant immune response or symptomatic disease state (269), rather, MAIT cells that reside in peripheral tissues such as the skin can promote wound healing (294). It is possible that peripheral antigen exposure may also be a significant contributor to GMM-reactive T cells expansion among individuals. Importantly, MAIT cells transition from a naïve phenotype ($CD45RA^+$) to a memory phenotype ($CD45RO^+$) early after egress from the thymus (172), a phenotype that is shared with GMM-reactive T cells isolated from adult blood and indicative of antigen exposure and T cell activation (135). It seems unlikely that CD1b-GMM-reactive T cells isolated from the experimental cohort of healthy blood donors herein had previously been primed by *M. tuberculosis*, or the live-attenuated BCG vaccine strain, especially among younger Australian blood donors (296). It is more likely that the variability in CD1b-GMM-reactive T cell frequency is due to antigen exposure from another source. Other Mycobacterial pathogens such as the skin tropic *M. ulcerans*, are capable of synthesising GMM under optimal conditions (297), however, these infections are rare in the general population (298). Another possibility is that GMM-reactive T cells may recognise antigenic lipids derived from common bacterial symbionts. Other members of Actinobacteria, such as *Corynebacterium* produce MAs (299) that may be antigenic to GMM-reactive T cells. *Corynebacterium*, the causative agent of Diphtheria, is commonly found in the respiratory mucosa and on the skin of humans (300, 301). Interestingly one T cell clone was identified from a *M. tuberculosis* infected patient that recognised MA, but this was not cross-reactive to GMM (135). TCR chimeras with TCRα and TCRβ chains from GEM T cell clones revealed that specificity for MA and GMM were determined by the specificity of the TCRβ chain alone (135). Thus, subtle variations in TCR chain usage among donors may regulate antigen cross-reactivity and T cell expansion. Nevertheless, a wide variation in the frequency of GEM T cells was observed and a more diverse TCR repertoire was identified in most donors. The potential for antigen cross-reactivity among these diverse TCRs is unclear. Thus, the role for other bacterial species, particularly commensals, in influencing both the abundance and TCR repertoire of GMM-reactive T cells requires further investigation.

The data herein reveal that CD1b-GMM-reactive T cells express the transcription factors RORγt and T-bet concurrently, strikingly similar to the transcription factor expression of human MAIT cells (206, 209) and suggests that CD1b-GMM-reactive T cells may produce either Th1 cytokines, Th17 cytokines or perhaps both. This has been described for human MAIT cells isolated from mucosal tissues, that secrete IL-17 as well as IFNγ (188, 302, 303), compared to blood MAIT cells that typically express only TNF and IFNγ (124, 171). The production of TNF and IFNγ cytokines from CD1b-GMM-reactive T cells *ex vivo* was also observed. Early evidence suggests these cells may express a polyfunctional phenotype *in vivo* (137). Polyfunctional CD1b-restricted T cell have been described previously, as another *M. tuberculosis* reactive subset known as LAM-reactive T cells produce both IFNγ and the cytotoxic granules perforin, granulysin and granzyme B (152). Notably, the frequency of polyfunctional LAM-reactive CD1b-restricted T cells in *M. tuberculosis* infected patients correlated with a lower incidence of post-tuberculosis sequalae (152), suggesting that these cells are beneficial in controlling disease. Comparatively, MAIT cells produce TNF and IFNγ directly in response to *M. tuberculosis* infected airway epithelial cells, as well as lyse infected cells by secretion of granulysin (304), demonstrating anti-microbial activity *in vitro*. It would be interesting to evaluate whether GMM-reactive T cells are capable of producing cytotoxic granules, as GMM-reactive T cells typically express the CD4 co-receptor, while the subset of polyfunctional LAM-reactive T cells specifically expressed the CD8 co-receptor (152), as do the majority of human MAIT cells (67). Moreover, our transcriptomic data suggests that CD1b-GMM-reactive T cells from healthy donors do not express *GNLY* transcripts, unlike most of the NKT cells we identified, which have been demonstrated previously to exhibit cytotoxic activity following stimulation with α-GalCer (305, 306). The expression of other cytotoxic granules such as granzyme and perforin were not identified herein, but nonetheless should be investigated.

While the ability for GMM-reactive T cells to produce IL-17 was not examined, production of this cytokine has been observed from expanded CD1b-GMM-reactive T cells (137). Moreover, autoreactive CD1b-restricted T cells in a transgenic mouse model of disease were capable of producing significant amounts of IL-17 in response to auto-antigens presented by CD1b (153). Thus, in agreement with expression of RORγt and

RORA, CD1b-GMM-reactive T cells are likely poised to secrete IL-17 *in vivo*. IL-17 is a protective cytokine in *M. tuberculosis* infection and neutralising IL-17 function *in vivo* increases mouse susceptibility to *M. tuberculosis* (307). Further, IL-17 producing Th17 cells help recruit Th1 cells to the lungs (308) and are critical for the maturation of granulomas that contain infection (309). In humans, their role is less clear, as Th17 cells appear capable of eliciting both anti-microbial (310) and pro-inflammatory responses (311, 312). While most studies examined the role of conventional Th17 cells in *M. tuberculosis* infection, some evidence reveals that unconventional T cell biomarkers also vary in response to *M. tuberculosis* infection. For instance, MAIT cells and γδ T cells were shown to comprise ~12% of all IL-17 producing T cells in latently TB infected (LTBI) patients, and these patients present with a significantly higher frequency of circulating IL-17 producing T cells compared to healthy donors and active TB patients prescribed a standard TB antibiotic regimen (313). In addition, while the percentage of circulating monofunctional IFNγ producing T cells were similar between active TB and LTBI patients, the percentage of polyfunctional IFNγ$^+$IL-17$^+$ T cells, including MAIT cells, was higher in LTBI patients than in active TB patients before receiving treatment (313). These data highlight a possible association between unconventional T cells that exhibit polyfunctionality with infection control and more desirable patient outcomes.

In an effort to assess directly the capacity of CD1b-restricted T cells in the protection against *M. tuberculosis* infection, a mouse model was developed using an MA-reactive T cell clone (DN1) reconstituted into CD1$^+$ mice (CD1$^+$DN1Tg) (151). Upon bacterial challenge, DN1 cells showed faster kinetics than conventional CD4$^+$ T cells, consistent with an innate-like phenotype, and accumulated in lung granulomas (151). Moreover, DN1 cells produced IFNγ, TNF and IL-17 when stimulated with by *M. tuberculosis* infected DCs *in vitro*. However, IL-17 secretion occurred independently of CD1 expression (151). *In vivo*, DN1 cells were active at the site of infection, produced multiple Th1 cytokines and reduced the bacterial burden of immunocompromised mice (151). In sufficient numbers, achievable through targeted vaccination, the functionally akin GMM-reactive T cells may be capable of providing rapid immunity to *M. tuberculosis*, alongside other unconventional T cells.

The data presented in this study show that CD1b-GMM-reactive T cells also express the transcription factor PLZF, the master regulator or innate-like responses (314-316), and an integral transcription factor for thymic maturation of unconventional T cell subsets (269-271). The development of both NKT and MAIT cells has been elucidated in some detail and relies on PLZF expression (269-271), providing a framework on which the development of other subsets can be extrapolated. NKT cells upregulate PLZF immediately after positive selection on DP thymocytes (271), where it is required for NKT cell intrathymic expansion and the acquisition of effector phenotypes (270, 271, 317). Comparatively, PLZF is expressed later during development of mouse MAIT cells yet is equally important for maturation (269). In the absence of PLZF, the frequency of both NKT cells and MAIT cells is significantly reduced and these subsets display altered phenotypes and function (269-271). The importance of PLZF for functional competence is consistent in humans, where late stage developing MAIT cells ($CD161^{+}CD27^{lo}$) express high levels of PLZF and acquire effector function (269). It is likely that GMM-reactive T cells mature like other unconventional T cell subsets, involving selection on DP thymocytes, and acquiring PLZF expression that promotes an innate-like phenotype. Although, unlike other $PLZF^{+}$ innate-like T cells, GMM-reactive T cells expressed low levels of CD161 and were CD27 deficient in the donors examined here. CD27 expression has been associated with changes in both conventional and γδ T cell function. On conventional T cells, CD27 is expressed by both naïve and memory subsets (318); however repeated antigen stimulation can lead to an irreversible downregulation CD27 (319). Loss of CD27 is correlated with greater terminal differentiation, a reduction in IFNγ production and increase in IL-4 production (274, 320). Comparatively, IL-17 production by mouse γδ T cells is restricted to the CD27 deficient subset of cells only (321). Thus, some important distinctions exist among $PLZF^{+}$ innate-like T cells, regarding surface marker expression that may have implications on function and immune outcomes.

Transcriptomic analysis of GMM-reactive T cells revealed several highly expressed genes that differentiated these cells from both NKT cells and $CD4^{+}$ T cells. These included genes encoding for transcription factors *JUN, BHLHE40* and *RORA*, as well as genes encoding for other DNA binding proteins *TSC22D3, KLF6, CDKN1A* and *IER2*,

likely indicating that GMM-reactive T cell phenotype and function are regulated by these gene products. The *JUN* gene encodes for the leucine zipper c-Jun (322), one of the components of the AP-1 transcription factor complex, an important regulator or many cell processes; including differentiation, proliferation and apoptosis (279). Specific to T cells, phosphorylation of AP-1 by the c-Jun N-terminus kinases (JNKs) (323), is critical for the induction of IL-2 and other cytokines upon T cell activation (324) and proliferation (325). *TSC22D3* was expressed at similarly high levels to *JUN* in almost all GMM-reactive T cells that were analysed. *TSC22D3* encodes for the protein GILZ, that associates with c-Jun, c-Fos and NK-κB to promotes both immunosuppressive and anti-inflammatory responses (326). GILZ is transcriptionally induced by the glucocorticoid receptor (GR), stimulated by engagement of potent glucocorticoids (327). Interestingly, many of the therapeutic benefits of glucocorticoid treatment in autoimmune and inflammatory diseases are mediated directly through the actions of GILZ (326). In T cells, GILZ binds transcription factors to regulate T cell activation and differentiation through a range of signalling pathways. GILZ can inhibit IL-2 production, preventing T cell proliferation as well as increase Th2 differentiation in mice, both by inhibition of NK-κB (328, 329). Additionally, GILZ can induce activation of TGF-β signalling to promote regulatory T cell differentiation (330), and negatively regulate Th17 transcriptional programs by binding directly to the promotor regions of *BATF, STAT3, IRF4* and *RORC* (331). In mice, GILZ deficiency was characterised by an increase in Th17 cells, capable of spontaneous IL-17 secretion, suggesting instability, and $GILZ^{-/-}$ mice were significantly more susceptible to imiquimod induced skin inflammation (332). Consequently, for GMM-reactive T cells that express RORγt and produce IL-17 after *in vitro* culture, GILZ could be a key regulator of Th17 programs alongside transcription factors under homeostatic conditions.

KLF6 is another transcription factor that has been shown to antagonise c-Jun function, inhibiting cell proliferation by binding to c-Jun directly (333). Moreover, the suppressive effect of KLF6 on c-Jun function was shown to be dependent on PMA and ionomycin stimulation (333), simulating the same signalling cascade as direct TCR ligation (334). Thus, it is possible that these transcripts were transiently upregulated in response to T cell stimulation via ligation of the TCR by tetramer, a phenomenon that has been observed by

the lab previously in MAIT cells isolated with MR1-5-OP-RU tetramer. However, these transcripts were not upregulated in NKT cells, even though these cells were isolated using tetramers loaded with α-GalCer, a lipid antigen that is recognised by Type I NKT cells with an exceptionally high affinity (272, 273). Alternatively, GMM-reactive T cells may possess high proliferative potential but are tightly regulated by GILZ, KLF6 and $p21^{WAF1/CIP1}$ to prevent aberrant T cell responses. In either case, whether the high expression of these gene transcripts correlates with protein expression has yet to be determined but will be investigated as part of future experiments.

RORA was highly expressed among GMM-reactive T cells and the protein RORα has been demonstrated to function alongside the master regulator RORγt to direct differentiation of Th17 cells in the presence of TGF-β and IL-6 (289, 335-337). In mice, T cells deficient in RORγ were still capable of producing IL-17, albeit at reduced levels due to the presence of RORα (289). However, in the absence of both RORγ and RORα, Th17 cell development was completely blocked and genetically predisposed mice were protected from development of inflammatory disorders (289). Therefore, RORα can act independently of RORγt to permit IL-17 expression yet can function synergistically when RORγt is present (289). Interestingly, other cytokines are capable of polarising $CD4^+$ T cells to differentiate into Th17 cells, although their effects on mRNA expression are varied (338). Both IL-1β and IL-23 induced $CD4^+$ T cells to upregulate *IL17F* and *RORC*, the genes encoding IL-17F and RORγ respectively, but had little effect on the mRNA levels of *RORA* (338). It remains to be determined whether GMM-reactive T cells, or similarly high *RORA* expressing T cell subsets respond differently than conventional Th17 cells to the cytokine milieu, especially if GMM-reactive T cells express high levels of GILZ. To determine whether RORα contributes to GMM-reactive T cell function, RORα expression should be assessed directly using monoclonal antibodies, similar to experiments we performed to show RORγt expression.

None of the gene transcripts for transcription factors expressed by GMM-reactive T cells, PLZF, RORγt and T-bet, were detected during the transcriptome analysis. Additionally, gene transcripts encoding for CD4 and TRAV1-2, highly expressed by GMM-reactive T

cells, were not identified, suggesting that these transcription factor and surface marker gene transcripts may have been expressed below the detection limit for single-cell RNA-sequencing. To address these discrepancies as well as further validate the single-cell transcriptomic data, bulk cell RNA-sequencing could be used providing greater sensitive for the detection of expressed gene transcripts. Using this approach, fewer than 100 GMM-reactive T cells are pooled for transcriptomic analysis, enhancing the sensitivity of the assay by starting with a greater quantity of RNA.

Some GMM-reactive and NKT cells expressed *BHLHE40*, a gene encoding for the transcription factor of the same name. Bhlhe40 is a basic helix-loop-helix transcriptional regulator of the cell cycle, apoptosis and T cell differentiation, and is upregulated upon TCR stimulation (288, 339). In mice, Bhlhe40 was shown to be critical for the function of autoreactive T cells in experimental autoimmune encephalomyelitis (EAE), positively regulating the production of GM-CSF to enhance both Th1 and Th17 responses and exacerbate encephalopathy (288). In the absence of Bhlhe40, autoreactive T cells produced IL-10 and reduced levels of GM-CSF and mice were resistant to disease in an IL-10 dependent manner (288). Specifically, Bhlhe40 was shown to bind within the *IL10* locus, likely inhibiting transcription of *IL10*, as Bhlhe40 deficient cells showed an increase in *IL10* transcripts (288). Consequently, Bhlhe40 may function similarly in GMM-reactive T cells, positively regulating an effector response and suppressing IL-10 production. Bhlhe40 also bound to many other regions within loci shared by transcription factors, including T-bet and RORγt (288), indicating that Bhlhe40 may cooperate with these master transcriptional regulators. In line with this finding, *BHLHE40* expression was shown to correlate directly with *IFNG* expression in NKT cells and affected IFNγ secretion (340). While Bhlhe40 did not bind to the *IFNG* promoter itself, transcription of *IFNG* was facilitated by Bhlhe40 through T-bet, where Bhlhe40 accumulated in the T-box region of the *IFNG* promoter (340). Herein and in other studies (137) robust IFNγ production has been observed by GMM-reactive T cells stimulated *in vitro*, which may be influenced by the expression of *BHLHE40*. In both mouse models, T cells from mice deficient in Bhlhe40 did not shown any defects in T cell development (288, 340), suggesting that while Bhlhe40 may interact with other transcription factors, is not required for thymic maturation and does not impair T cell differentiation programs.

CD1b-GMM-reactive T cells and the majority of NKT cells expressed *CXCR4*, encoding for the chemokine receptor of the same name. CXCR4 is expressed by over 60% of NKT cells and some MAIT cells in humans (172, 341) and may be involved in NKT cell migration in the thymus during development (341). Generally, CXCR4 expression allows T cells to transit along gradients of the chemokine CXCL12 (283) as well as functioning to deliver co-stimulatory signals upon $CD4^+$ T cell activation (283). CD1b-GMM-reactive T cells expressed significantly more *CXCR4* than NKT cells, identified as a differentially expressed gene, and may translate to higher expression levels of this receptor, although surface expression has yet to be examined. If this is the case, it is likely that CD1b-GMM-reactive T cells would be more sensitive to signalling by CXCL12 compared to NKT and MAIT cell subsets. CXCR4 is also utilised by the Human Immunodeficiency Virus (HIV) together with CD4 to infect T cells (342). It is now established that CXCR4-tropic HIV (X4 HIV) arise later in disease course and are associated with a greater reduction in $CD4^+$ T cell count (343). As a consequence, HIV-1 infection is the greatest risk factor for developing active tuberculosis, and co-infection with *M. tuberculosis* can exacerbates HIV-1 replication in blood (344, 345). It is reasonable to propose that if GMM-reactive T cells express high levels of CXCR4, they would likely be more susceptible to depletion by X4 HIV-1 infection (346). Given that GMM-reactive T cells likely co-express CD4 and CXCR4, GMM-reactive T cell immunity in HIV and *M. tuberculosis* co-infection may be compromised to a greater extent than for other CD4 and CXCR4 low or deficient unconventional T cell subsets.

In summary, presented here is the first extensive analysis of *ex vivo* CD1b-GMM reactive T cells from healthy donors, including a transcriptomic analysis of this T cell subset. These analyses were achieved by optimising an enrichment strategy to isolate CD1b-GMM-reactive T cells from peripheral blood at a much greater frequency than in previous studies. The data herein demonstrate that the surface phenotype of CD1b-GMM-reactive T cells from healthy donors corroborates with the published findings from *M. tuberculosis* infected patients (135, 136), however it was noted that the frequency of GEM T cells varied widely in healthy donors (137). The transcriptomes of individual CD1b-GMM-reactive T cells were compared to individual NKT and $CD4^+$ T cells to identify signatures

that differentiate CD1b-GMM-reactive T cells from other T cells as well as support the predicted function of these cells described by others (135, 137). Moreover, GMM-reactive T cells express the crucial innate-like T cell transcription factor PLZF, as well as the Th1 and Th17 master regulators; T-bet and RORγt. In spite of their low frequency, it could be established here that CD1b-GMM-reactive T cells preserve the memory phenotype and polyfunctional characteristics of their antigen experienced counterparts, likely poised to respond rapidly to *M. tuberculosis* infection. These data provide the groundwork for studying CD1b-GMM-reactive T cells in healthy donors and *M. tuberculosis* infected patients alike, and further studies are currently underway to compare these cells in various *M. tuberculosis* disease states.

Chapter 6: General Discussion

Unconventional T cells are an evolutionarily conserved (64) populations of immune cells that together constitute over 10% of total T cells in human blood (44, 142, 171). Yet our understanding of their basic biology and function in the human immune system is still limited. In particular, the persistence of unconventional T cell monomorphic restriction elements and public TCR repertoires suggest that these cells play an important role in mammalian health (64). However, to date most evidence suggests unconventional T cells play a complementary role alongside other immune cells in a broad range of settings; including infectious disease (347-351), cancer (352), homeostasis (353, 354) and are also implicated in autoimmunity (355-357).

One of the barriers to study unconventional T cells effectively has been the lack of reagents to identify these cells. Relying on surrogate markers has allowed researchers to study some unconventional T cell subsets with variable rates of success (171, 358), however a major breakthrough in the field was the development of antigen loaded tetramers (40, 359, 360). Consequently, unconventional T cells are now accurately identified based on antigen specificity alone in both humans and mice, and work is underway to develop and optimise these tools for other mammalian species (361, 362). In spite of these advances, the use of tetramers to isolate unconventional T cells has been met with both technical and functional challenges, some of which were examined herein. MR1 and CD1b tetramers were used extensively in this body of work to examine rare subsets of unconventional T that have been notoriously difficult to identify. In doing so, this thesis expands on the knowledge of how unconventional T cells recognise antigen, their known phenotype, function and possible role in immunity.

The majority of MAIT cells in humans express the CD8 co-receptor (67, 124, 171). By examining the binding of MR1 tetramers to MAIT cells, the data in this study reveal that these cells utilise the CD8 co-receptor to engage MR1 to increase the avidity of TCR-MR1 interaction. These data were consistent with the function of the CD8 co-receptor on conventional T cells to permit or enhance recognition of MHC-I by the TCR (99, 104, 176, 177). Notably, all MAIT cell subsets were able to recognise MR1-5-OP-RU

tetramers, regardless of CD8 expression, indicating that the CD8 co-receptor was not essential for the recognition of the potent ligand 5-OP-RU. These data suggest that the CD8 co-receptor is not necessarily required for MAIT cell recognition of riboflavin synthesising bacteria. However, many variables exist that may affect MAIT cell activation that have not been addressed, including MR1 surface expression *in vivo*, antigen load during natural infection and co-receptor modulation over time (126). For instance, in the context of infections with slow growing microbes such as *M. tuberculosis* (71), the abundance of metabolism-related antigens released for surveillance by MAIT cells are possibly lower than in metabolically active bacterial infections, impacting on MR1 expression and MAIT cell activation (61). In support of this, only $CD8^+$ MAIT cells were capable of detecting and responding to *M. tuberculosis* infection of a monocytic cell line (71, 72). Interestingly, a recent study determined that DN MAIT cells could be generated *in vitro* by TCR-mediated stimulation of $CD8^+$ MAIT cells, suggesting that CD8 levels are dynamic and can be fine-tuned in response to MR1 ligation (126). Moreover, DN MAIT cells were more prone to apoptosis compared to $CD8^+$ MAIT cells (126). One interpretation of these data is that CD8 downregulation precedes resolution of the immune response by preventing overactivation. Transient downregulation of CD8 after TCR ligation of MHC-I has been observed previously for conventional T cells (363). However, in MAIT cells, resolution of the immune response appears to cause preferential apoptosis among cells that have downregulated or lack CD8 expression (126). Thus, the importance of CD8 on MAIT cells is likely underappreciated in the *in vitro* experimental approach and may be more apparent in a physiological environment.

In addition to binding MHC-I and MR1, the CD8 co-receptor enhances T cell activation by bringing $p56^{lck}$ into close proximity to the CD3 complex upon TCR stimulation (109, 183). The role of CD8 as a signalling cascade enhancer was not directly assessed, although it is likely that this contributed to the functional response observed by $CD8^+$ MAIT cells. Curiously, the ability for CD8α to sequester $p56^{lck}$ has also been proposed as a mechanism for T cell repression by segregating CD8αα bound $p56^{lck}$ from the CD3-complex (115). The data herein did not support this proposal, as both CD8αα and CD8αβ isoforms contributed similarly to the recognition of MR1 as well as the induction of

cytokines upon MAIT cell stimulation, suggesting that CD8αα dimers are not excluded from the CD3-complex.

Complementary to the role of CD8 in the recognition of MR1-5-OP-RU, it was shown here that CD8 is critically important for the recognition of weaker antigens presented by MR1, namely folate-derived MR1 antigens (40, 58). In general, MR1-reactive T cells capable of recognising MR1-6-FP/Ac-6-FP, do so with a significantly reduced affinity compared to MR1-5-OP-RU (58, 201). Thus, the importance of CD8 to facilitate recognition of MR1-6-FP was much more apparent; almost all folate-reactive T cells were critically reliant on CD8 to recognise MR1-6-FP tetramers. These findings raise an important question regarding the specificity of MR1 tetramers, especially in light of the discovery of novel MR1-antigens (213) and MR1-reactive T cells (201, 203, 204). Indeed, many of these recently described MR1-reactive T cells express the CD8 co-receptor (201, 203, 204). It is reasonable to predict that many of these MR1 interactions are weakly antigen reactive and possibly autoreactive in nature, and that the CD8 co-receptor contributes to the overall avidity required for antigen recognition and T cell activation (177). In this case, our CD8-null MR1 tetramers serve as a valuable tool in future studies for identifying TCR-MR1 interactions that rely on the CD8-MR1 interaction for antigen recognition.

While the mechanisms driving co-receptor expression of MAIT cells during development are not fully elucidated (269), the data in this study suggest that CD8 may contribute to the selection of $CD8^+$ MAIT cells by boosting recognition of MR1. Interestingly, $CD8^+$ MAIT cells that egress from the thymus almost all express CD8αβ (269, 292), suggesting that CD8β is important for $CD8^+$ MAIT cell development (364, 365). Studies have shown that posttranslational sialyation of CD8β during development fine-tunes the affinity of CD8αβ for MHC-I (366, 367). Accordingly, on immature DP thymocytes in the cortex, CD8αβ is minimally sialylated and possesses a high affinity for MHC-I during, while thymocytes that reach maturity express a highly sialyated glycoform of CD8αβ with a reduced the affinity for MHC-I (366, 367). The various glycoforms of CD8αβ that are expressed throughout T cell development are thought to aid positive selection within the DP thymocyte compartment and more efficiently eliminate autoreactive TCRs during

negative selection (367). If sialyation of CD8β occurs in a similar manner on MAIT cells and also impacts CD8αβ recognition of MR1, it is likely that thymic expression of CD8αβ performs a similar role for developing MAIT thymocytes. In this case, CD8β sialyation might be critical for guiding MAIT cells through negative selection by lowering the affinity of CD8αβ for MR1 during development. After development, CD8αα$^+$ MAIT cells accumulate in the peripheral blood throughout adulthood and share phenotypic and transcriptomic features with CD8αβ$^+$ MAIT cells (368). It seems likely that CD8αα$^+$ MAIT cells are derived from their CD8αβ$^+$ counterparts, perhaps in response to environmental stimuli, however the functional implications of the switch in CD8 isoform expression is largely elusive. The data here suggests that CD8αα$^+$ MAIT cells are the most functionally potent MAIT cell subset, tending to produce more IFNγ and TNF than other MAIT cells and possibly leading to a selective advantage during infection. Additionally, the surface expression of CD8 on MAIT cells can vary widely among cells, most prominently among CD8αα$^+$ MAIT cells. It is therefore possible that CD8$^+$ MAIT cells can fine-tune their responsiveness to antigen in real time. In this way, CD8αα$^+$ MAIT cells may possess greater flexibility and range in modulating CD8α expression only for antigen recognition or functional requirements.

Given the conservation of the putative CD8 binding site in murine MR1 (41), it is plausible that CD8 may contribute to MAIT cell function in mice. Further investigations should examine whether CD8 can engage murine MR1, preferably by measuring direct binding as described in this study for humans. While only a minority of MAIT cells express CD8 in naïve mice (369), the frequency of CD8$^+$ MAIT cells appears to vary throughout development (269) and after infection in some tissues (unpublished data). Thus, modulating CD8 expression on MAIT cells *in vivo* may affect MAIT cell development and the course of MAIT cell mediated immunity and thus disease in some infections. This could be tested by generating an MR1 knock-in mouse that contained mutations in the α3 domain of MR1 that abrogated murine CD8 binding. Alternatively, purified CD8$^+$ or CD8$^-$ MAIT cells could be adoptively transferred into T cell deficient, *RAG2*$^{-/-}$ mice and challenged with a riboflavin-synthesising pathogen. In either case, a

mouse model would provide valuable insights into the role of CD8 during development and in the context of infection or other model disease states.

Almost all of the autoreactive and GMM-reactive CD1b-restricted T cells we identified expressed the CD4 co-receptor, consisted with previous studies (52, 135). However, CD1b-restricted T cells that possess other antigen specificities have been identified that do not express the CD4 co-receptor (152). Nevertheless, the near universal expression of CD4 that was observed here raises the obvious question regarding engagement of CD1b by CD4. Similar to CD8 recognition of MHC-I and MR1, the CD4 co-receptor recognises primarily a conserved region on the MHC-II β-chain that is structurally analogous to the CD loop on the α3 domain of MHC-I as well as recognising a smaller, conserved region on the MHC-II α-chain (370, 371). Some of the structural features of the CD4 binding site on the MHC-II β-chain are conserved on CD1b, however these residues are also shared with the neonatal Fc receptor (FcRn) that does not recognise CD4 (372). Moreover, both the proliferation and cytokine secretion of two $CD4^+$ *M. leprae*-reactive CD1b-restricted T cells were not reduced in the presence of neutralising CD4 antibodies (232). These data suggest the inability of CD4 to engage CD1b directly and influence CD1b-restricted T cell function. Whether CD4 contributes to CD1b-restricted T cell function by off-target engagement of MHC-II, similar to CD4 on NKT cells (121, 122), has yet to be determined. Thus, while the majority of CD1b-restricted T cells express the CD4 co-receptor, there is no clear evidence to suggest it plays a direct role in recognition of antigen or contributes to cell function. To assess whether CD4 is capable of engaging CD1b directly, a panel of cell lines could be generated that express either CD4 or a CD1b-restricted TCR alone, or CD4 and a CD1b-restricted TCR together that are then stained with CD1b tetramers to detect a potential CD4 interaction with CD1b.

We have demonstrated that CD8 is able to boost autoreactive T cell responses in the context of MR1, however these responses are initiated by seemingly weak TCR interactions with MR1-Ag (58, 201), consistent with T cell interactions with MHC-I that are dependent on CD8 (179). Comparatively, strong TCR-mediated autoreactive responses have been reported in the recognition of CD1b-Ag (52) and the molecular features of some of these TCR-CD1b-Ag interactions have been determined (150, 216).

Using CD1b-endo tetramers, several autoreactive T cells from healthy donors were identified and their TCR antigen specificity examined. A spectrum of CD1b autoreactivity among TCRs was observed, where some possessed reactivity to CD1b tetramers that was unabated by the presence of structurally diverse antigens, while others exhibited clear preferences and aversions for lipid species. Moreover, it was demonstrated that some autoreactive TCR interactions with CD1b were of exceptionally high affinity. This spectrum of autoreactivity does not appear entirely compatible with the modes of TCR docking onto CD1b previously described (150, 216). In essence, the two published TCR-CD1b-Ag structures identify a mode of TCR docking that favours the precise recognition of a defined lipid headgroup (150), and a mechanism allowing the recognition of many common phospholipids by virtue of their shared backbone structure (216). At least one TCR was identified here that does not fit these paradigms, displaying considerable TCR degeneracy. These observations align more closely with a TCR interaction with CD1a that did not make contact with lipid but was amenable to lipid-mediated disruptions of the CD1a contact residues (223). Therefore, these specific autoreactive T cell responses likely target the CD1b protein itself, possibly without the need for contact with the antigen.

It is difficult to envision a role for this antigen indiscriminate autoreactivity in a healthy immune system. While these autoreactive T cells were infrequent, we were able to identify them directly *ex vivo* in multiple donors, indicating that they may be permissible in health and are able to progress through thymic maturation with a high affinity self-reactive TCR. This has been reported for other T cell subsets; including natural regulatory T cells (373), NKT cells (374) and CD8$\alpha\alpha^+$ IELs (375). Each of these subsets are diverted from clonal deletion in the thymus, despite inducing strong TCR signals. Thus, evasion of clonal deletion by strongly autoreactive thymocytes can be achieved by commitment to specific T cell lineages. Importantly, most NKT cells are not autoreactive in the periphery (374) and do not typically express a regulatory phenotype (376). In contrast, regulatory T cells maintain their self-reactivity in the periphery to exert immunoregulatory functions upon stimulation with self-antigen (377). It is conceivable that during the course of certain immune responses, CD1b is upregulated (378, 379) to stimulate these autoreactive T cells and dampen the immune response. Further studies

should examine the functional profile of these T cells *ex vivo* and assess whether they possess any immunoregulatory properties. Paradoxically, these autoreactive T cells could function to restore self-tolerance in autoimmunity by indirect means. Activation of NKT cells can alter the cytokine profiles of aberrant autoreactive T cells, inducing IL-4 and IL-10 production, and reducing disease burden in several murine disease models (277, 380). Although this phenotype is highly context dependent, as in some circumstances in mice (381, 382), and in humans (383), NKT cells seemed to exacerbate disease, demonstrating functional plasticity, an attribute likely shared with CD1b-restricted T cells. Indeed, in an $ApoE^{-/-}$ CD1 transgenic mouse model, autoreactive T cells triggered systemic inflammation by recognising self-lipids presented by CD1b (153). It is plausible that these autoreactive T cells could be detrimental to the host and initiate or contribute to disease pathology. Yet, the rarity of these cells in healthy donor blood suggests they would contribute a minor role. Using similar identification techniques established herein, it would be informative to examine the frequency of autoreactive CD1b-restricted T cells in different tissues and in various disease states to provide further insights into their function and possible clinical relevance. Further, due to the likely TCR-specificity bias by using CD1b-endo tetramers, identification techniques should include loading CD1b with rare endogenous lipid antigens such as PG and lysophopholipids that are not readily detected in the mammalian expressed CD1b-endo lipid repertoire.

While the function of autoreactive CD1b-restricted T cells in immunity is mostly speculative, a role for CD1b-restricted T cells in the immune response to *M. tuberculosis* is now emerging (51, 135). Human infection with *M. tuberculosis* remains a persistent global challenge with an incidence of 10.4 million new cases in 2016 and a mortality of 1.7 million lives (384). In light of this, there is an urgent need for better diagnostic and therapeutic intervention. Several unconventional T cells subsets have been identified that specifically recognise antigens derived from *Mycobacteria* (51, 135, 136, 385-387), and their therapeutic potential is largely unexplored. GMM-reactive T cells are present in *M. tuberculosis* infected patients at a higher frequency than in uninfected donors and possess an altered TCR repertoire (51, 135, 137), suggestive of clonal expansion in response to *M. tuberculosis* infection. Accordingly, detection of GMM-reactive T cell TCR repertoire might be used to accurately diagnose active and latent *M. tuberculosis* infected patients

(137). Interestingly, expansion of both MAIT and NKT cells could not be detected in active tuberculosis patients by TCR repertoire analysis (137). Despite expressing the memory marker CD45RO, GMM-reactive T cells seem to be more akin to conventional T cells, exhibiting a low precursor frequency and undergoing expansion in response to antigen stimulation (51, 135, 137).

It is likely that the phenotype of GMM-reactive T cells is influenced by *M. tuberculosis* infection, however there is little phenotypic data on GMM-reactive T cells in healthy donors (137). This is due in part to the challenges in identifying GMM-reactive T cells with tetramers (135). CD1b-GMM-reactive T cells were accurately identified by enrichment from large quantities of peripheral blood from healthy donors. All of the GMM-reactive T cell surface markers identified from *M. tuberculosis* infected donors were also expressed in healthy donors (135, 137). CD1b-GMM-reactive T cells expressed the innate-like T cell transcription factor PLZF (87, 271) as well as RORγt and T-bet, consistent with MAIT cells (171). However, unlike MAIT and NKT cells, only a proportion of CD1b-GMM-reactive T cells expressed CD161 (135), a key difference between GMM-reactive T cells and other innate-like T cells that share transcriptomic signatures (388). While CD1b-GMM-reactive shared many phenotypic features with NKT cells, transcriptomic analysis identified some transcripts, notably of transcription factors, that were highly upregulated in GMM-reactive T cells and may influence T cell function. Validation of these transcription factors and a broad functional analysis of GMM-reactive T cells is needed to determine if these cells are functionally different from NKT cells and MAIT cells. Thus, while many of the core phenotypic markers of unconventional T cells are shared with GMM-reactive T cells, some unique features are identified here that may differentiate these cells functionally from other innate-like T cells. Although CD1b-restricted T cells are not present in mice, the generation of group 1 CD1 expressing mice has facilitated *in vivo* studies on group 1 CD1b-restricted T cells (151). Generating TCR transgenic $CD1^+$ mice using both $TRAV1\text{-}2^+$ and $TRAV1\text{-}2^-$ CD1b-GMM-reactive TCR sequences identified here would enable a comparison to NKT cells and MAIT cells in mice.

To date, whether CD1b-restricted T cells in *M. tuberculosis* infection are harmful or helpful is unclear, largely due to the difficulty in identifying these cells, as well as the absence of a suitable mouse model (389). Development of a $CD1^+$ TCR transgenic mouse has provided some insights (151). MA-reactive CD1b-restricted T cells from mice infected with *M. tuberculosis* expressed a polyfunctional phenotype and responded rapidly upon infection (151). Interestingly, these cells were activated in the mediastinal LN before extravasating to the lungs where they associated closely with granulomas (151). This mode of antigen presentation is consistent with CD1b expression in humans, typically restricted to DCs (390) and further perpetuates the notion that CD1b-restricted T cells are activated similarly to conventional T cells, albeit with faster kinetics (151). In a more physiological model, BCG was administered intradermally to rhesus macaques to measure GMM-reactive T cell responses (391), comparable to vaccination protocols in humans. Interestingly, the GMM-reactive T cell responses were restricted to CD1c, despite the ability for macaque CD1b to present GMM effectively to T cells (392). Nevertheless, GMM-reactive T cells were expanded in response to BCG and produced a polyfunctional response when challenged with GMM *in vitro* (391). Upon re-infection with BCG into the skin, CD1c was significantly upregulated and GMM-reactive T cells migrated from the blood to the site of inoculation (391). Similarly, T cell extravasation to the skin after GMM inoculation has been observed in BCG vaccinated guinea pigs (393). Thus, GMM is a potent immunogen across species, stimulating a CD1-restricted, polyfunctional T cell response and can recall T cells to peripheral sites upon rechallenge and may be a notable contributor in the immune responses to *M. tuberculosis*. The data provided herein validates a strategy for accurately isolating GMM-reactive T cells from blood, providing insights into the phenotype of GMM-reactive T cells in healthy individuals. Further investigations of similar kind in *M. tuberculosis* infected patients would greatly inform the role of GMM-reactive T cells in disease.

MHC-like tetramers are rapidly becoming the gold standard for the identification of unconventional T cells in both humans and mice. The data in this thesis have explored some of the physiological and technical factors that influence tetramer binding by unconventional T cells, delivering some in-depth phenotypic analyses of rare T cell

subsets, their TCR repertoire and antigen specificities. Importantly, these data provide the groundwork for future studies examining unconventional T cells using tetramers.

References

1. Murphy K, Weaver C. Janeway's immunobiology: Garland Science; 2016.

2. Pieper K, Grimbacher B, Eibel H. B-cell biology and development. J Allergy Clin Immunol. 2013;131(4):959-71.

3. Mak TW, Saunders ME. The Humoral Response: B Cell Development and Activation. In: Mak TW, Saunders ME, editors. The Immune Response. Burlington: Academic Press; 2006. p. 209-45.

4. Ciofani M, Zuniga-Pflucker JC. The thymus as an inductive site for T lymphopoiesis. Annu Rev Cell Dev Biol. 2007;23(1):463-93.

5. Van Lier RA, Ten Berge IJ, Gamadia LE. Human CD8+ T-cell differentiation in response to viruses. Nature Reviews Immunology. 2003;3(12):931-9.

6. Zinkernagel RM, Doherty PC. Restriction of in vitro T cell-mediated cytotoxicity in lymphocytic choriomeningitis within a syngeneic or semiallogeneic system. Nature. 1974;248(5450):701-2.

7. Zinkernagel RM, Doherty PC. H-2 compatability requirement for T-cell-mediated lysis of target cells infected with lymphocytic choriomeningitis virus. Different cytotoxic T-cell specificities are associated with structures coded for in H-2K or H-2D. J Exp Med. 1975;141(6):1427-36.

8. Bjorkman PJ, Saper MA, Samraoui B, Bennett WS, Strominger JL, Wiley DC. Structure of the human class I histocompatibility antigen, HLA-A2. Nature. 1987;329(6139):506-12.

9. Babbitt BP, Allen PM, Matsueda G, Haber E, Unanue ER. Binding of immunogenic peptides to Ia histocompatibility molecules. Nature. 1985;317(6035):359-61.

10. Rotzschke O, Falk K, Deres K, Schild H, Norda M, Metzger J, et al. Isolation and analysis of naturally processed viral peptides as recognized by cytotoxic T cells. Nature. 1990;348(6298):252-4.

11. Zinkernagel RM, Doherty PC. MHC-restricted cytotoxic T cells: studies on the biological role of polymorphic major transplantation antigens determining T-cell restriction-specificity, function, and responsiveness. Advances in immunology. 1979;27:51-177.

12. Falk K, Rotzschke O, Stevanovic S, Jung G, Rammensee HG. Allele-specific motifs revealed by sequencing of self-peptides eluted from MHC molecules. Nature. 1991;351(6324):290-6.

13. Madden DR. The three-dimensional structure of peptide-MHC complexes. Annu Rev Immunol. 1995;13(1):587-622.

14. Thomas C, Tampé R. MHC I chaperone complexes shaping immunity. Current opinion in immunology. 2019;58:9-15.

15. Williams A, Peh CA, Elliott T. The cell biology of MHC class I antigen presentation. Tissue Antigens. 2002;59(1):3-17.

16. Neefjes JJ, Smit L, Gehrmann M, Ploegh HL. The fate of the three subunits of major histocompatibility complex class I molecules. Eur J Immunol. 1992;22(6):1609-14.

17. Pamer E, Cresswell P. Mechanisms of MHC class I--restricted antigen processing. Annu Rev Immunol. 1998;16:323-58.

18. Wooldridge L, Lissina A, Cole DK, van den Berg HA, Price DA, Sewell AK. Tricks with tetramers: how to get the most from multimeric peptide-MHC. Immunology. 2009;126(2):147-64.

19. Yu CY, Milstein C. A physical map linking the five CD1 human thymocyte differentiation antigen genes. EMBO J. 1989;8(12):3727-32.

20. McMichael AJ, Pilch JR, Galfre G, Mason DY, Fabre JW, Milstein C. A human thymocyte antigen defined by a hybrid myeloma monoclonal antibody. Eur J Immunol. 1979;9(3):205-10.

21. Porcelli SA, Modlin RL. The CD1 system: antigen-presenting molecules for T cell recognition of lipids and glycolipids. Annu Rev Immunol. 1999;17(1):297-329.

22. Madden DR, Gorga JC, Strominger JL, Cell W-DC. The three-dimensional structure of HLA-B27 at 2.1 Å resolution suggests a general mechanism for tight peptide binding to MHC. Cell. 1992.

23. Zeng Z, Castano AR, Segelke BW, Stura EA, Peterson PA, Wilson IA. Crystal structure of mouse CD1: An MHC-like fold with a large hydrophobic binding groove. Science. 1997;277(5324):339-45.

24. Gadola SD, Zaccai NR, Harlos K, Shepherd D, Castro-Palomino JC, Ritter G, et al. Structure of human CD1b with bound ligands at 2.3 A, a maze for alkyl chains. Nat Immunol. 2002;3(8):721-6.

25. Shamshiev A, Gober HJ, Donda A, Mazorra Z, Mori L, De Libero G. Presentation of the same glycolipid by different CD1 molecules. J Exp Med. 2002;195(8):1013-21.

26. Chancellor A, Gadola SD, Mansour S. The versatility of the CD1 lipid antigen presentation pathway. Immunology. 2018;154(2):196-203.

27. Barral DC, Brenner MB. CD1 antigen presentation: how it works. Nature Reviews Immunology. 2007;7(12):929.

28. van den Elzen P, Garg S, Leon L, Brigl M, Leadbetter EA, Gumperz JE, et al. Apolipoprotein-mediated pathways of lipid antigen presentation. Nature. 2005;437(7060):906-10.

29. Sugita M, Barral DC, Brenner MB. Pathways of CD1 and lipid antigen delivery, trafficking, processing, loading, and presentation. Curr Top Microbiol Immunol. 2007;314:143-64.

30. Sugita M, Cao X, Watts GF, Rogers RA, Bonifacino JS, Brenner MB. Failure of trafficking and antigen presentation by CD1 in AP-3-deficient cells. Immunity. 2002;16(5):697-706.

31. Briken V, Jackman RM, Dasgupta S, Hoening S, Porcelli SA. Intracellular trafficking pathway of newly synthesized CD1b molecules. EMBO J. 2002;21(4):825-34.

32. Shamshiev A, Donda A, Prigozy TI, Mori L, Chigorno V, Benedict CA, et al. The alphabeta T cell response to self-glycolipids shows a novel mechanism of CD1b loading and a requirement for complex oligosaccharides. Immunity. 2000;13(2):255-64.

33. de la Salle H, Mariotti S, Angenieux C, Gilleron M, Garcia-Alles LF, Malm D, et al. Assistance of microbial glycolipid antigen processing by CD1e. Science. 2005;310(5752):1321-4.

34. Roura-Mir C, Wang L, Cheng TY, Matsunaga I, Dascher CC, Peng SL, et al. Mycobacterium tuberculosis regulates CD1 antigen presentation pathways through TLR-2. J Immunol. 2005;175(3):1758-66.

35. Pena-Cruz V, Ito S, Dascher CC, Brenner MB, Sugita M. Epidermal Langerhans cells efficiently mediate CD1a-dependent presentation of microbial lipid antigens to T cells. J Invest Dermatol. 2003;121(3):517-21.

36. Tentori L, Graziani G, Porcelli SA, Sugita M, Brenner MB, Madaio R, et al. Rifampin increases cytokine-induced expression of the CD1b molecule in human peripheral blood monocytes. Antimicrob Agents Chemother. 1998;42(3):550-4.

37. Blumberg RS, Terhorst C, Bleicher P, McDermott FV, Allan CH, Landau SB, et al. Expression of a nonpolymorphic MHC class I-like molecule, CD1D, by human intestinal epithelial cells. J Immunol. 1991;147(8):2518-24.

38. Canchis PW, Bhan AK, Landau SB, Yang L, Balk SP, Blumberg RS. Tissue distribution of the non-polymorphic major histocompatibility complex class I-like molecule, CD1d. Immunology. 1993;80(4):561-5.

39. Hashimoto K, Hirai M, Kurosawa Y. A gene outside the human MHC related to classical HLA class I genes. Science. 1995;269(5224):693-5.

40. Kjer-Nielsen L, Patel O, Corbett AJ, Le Nours J, Meehan B, Liu L, et al. MR1 presents microbial vitamin B metabolites to MAIT cells. Nature. 2012;491(7426):717-23.

41. Riegert P, Wanner V, Bahram S. Genomics, isoforms, expression, and phylogeny of the MHC class I-related MR1 gene. J Immunol. 1998;161(8):4066-77.

42. Huang S, Gilfillan S, Kim S, Thompson B, Wang X, Sant AJ, et al. MR1 uses an endocytic pathway to activate mucosal-associated invariant T cells. J Exp Med. 2008;205(5):1201-11.

43. McWilliam HE, Eckle SB, Theodossis A, Liu L, Chen Z, Wubben JM, et al. The intracellular pathway for the presentation of vitamin B-related antigens by the antigen-presenting molecule MR1. Nat Immunol. 2016;17(5):531-7.

44. Godfrey DI, Uldrich AP, McCluskey J, Rossjohn J, Moody DB. The burgeoning family of unconventional T cells. Nat Immunol. 2015;16(11):1114-23.

45. De Jong A, Cheng T-Y, Huang S, Gras S, Birkinshaw RW, Kasmar AG, et al. CD1a-autoreactive T cells recognize natural skin oils that function as headless antigens. Nature immunology. 2014;15(2):177-85.

46. Moody DB, Young DC, Cheng TY, Rosat JP, Roura-Mir C, O'Connor PB, et al. T cell activation by lipopeptide antigens. Science. 2004;303(5657):527-31.

47. Zajonc DM, Crispin MD, Bowden TA, Young DC, Cheng TY, Hu J, et al. Molecular mechanism of lipopeptide presentation by CD1a. Immunity. 2005;22(2):209-19.

48. Beckman EM, Porcelli SA, Morita CT, Behar SM, Furlong ST, Brenner MB. Recognition of a lipid antigen by CD1-restricted alpha beta+ T cells. Nature. 1994;372(6507):691-4.

49. Moody DB, Reinhold BB, Guy MR, Beckman EM, Frederique DE, Furlong ST, et al. Structural requirements for glycolipid antigen recognition by CD1b-restricted T cells. Science. 1997;278(5336):283-6.

50. Batuwangala T, Shepherd D, Gadola SD, Gibson KJ, Zaccai NR, Fersht AR, et al. The crystal structure of human CD1b with a bound bacterial glycolipid. J Immunol. 2004;172(4):2382-8.

51. Kasmar AG, van Rhijn I, Cheng TY, Turner M, Seshadri C, Schiefner A, et al. CD1b tetramers bind alphabeta T cell receptors to identify a mycobacterial glycolipid-reactive T cell repertoire in humans. J Exp Med. 2011;208(9):1741-7.

52. Van Rhijn I, van Berlo T, Hilmenyuk T, Cheng TY, Wolf BJ, Tatituri RV, et al. Human autoreactive T cells recognize CD1b and phospholipids. Proc Natl Acad Sci U S A. 2016;113(2):380-5.

53. Bai L, Picard D, Anderson B, Chaudhary V, Luoma A, Jabri B, et al. The majority of CD1d-sulfatide-specific T cells in human blood use a semiinvariant Vdelta1 TCR. Eur J Immunol. 2012;42(9):2505-10.

54. Shamshiev A, Donda A, Carena I, Mori L, Kappos L, De Libero G. Self glycolipids as T-cell autoantigens. European Journal of Immunology. 1999;29(5):1667-75.

55. Treiner E, Duban L, Bahram S, Radosavljevic M, Wanner V, Tilloy F, et al. Selection of evolutionarily conserved mucosal-associated invariant T cells by MR1. Nature. 2003;422(6928):164-9.

56. Tilloy F, Treiner E, Park SH, Garcia C, Lemonnier F, de la Salle H, et al. An invariant T cell receptor alpha chain defines a novel TAP-independent major histocompatibility complex class Ib-restricted alpha/beta T cell subpopulation in mammals. J Exp Med. 1999;189(12):1907-21.

57. Le Bourhis L, Martin E, Peguillet I, Guihot A, Froux N, Core M, et al. Antimicrobial activity of mucosal-associated invariant T cells. Nat Immunol. 2010;11(8):701-8.

58. Eckle SB, Birkinshaw RW, Kostenko L, Corbett AJ, McWilliam HE, Reantragoon R, et al. A molecular basis underpinning the T cell receptor heterogeneity of mucosal-associated invariant T cells. J Exp Med. 2014;211(8):1585-600.

59. Bacher A, Eberhardt S, Fischer M, Kis K, Richter G. Biosynthesis of vitamin b2 (riboflavin). Annu Rev Nutr. 2000;20(1):153-67.

60. Kis K, Kugelbrey K, Bacher A. Biosynthesis of riboflavin. The reaction catalyzed by 6, 7-dimethyl-8-ribityllumazine synthase can proceed without enzymatic catalysis under physiological conditions. The Journal of organic chemistry. 2001;66(8):2555-9.

61. Corbett AJ, Eckle SB, Birkinshaw RW, Liu L, Patel O, Mahony J, et al. T-cell activation by transitory neo-antigens derived from distinct microbial pathways. Nature. 2014;509(7500):361-5.

62. Kjer-Nielsen L, Corbett AJ, Chen Z, Liu L, Mak JY, Godfrey DI, et al. An overview on the identification of MAIT cell antigens. Immunol Cell Biol. 2018;96(6):573-87.

63. Van Rhijn I, Moody DB. Donor Unrestricted T Cells: A Shared Human T Cell Response. J Immunol. 2015;195(5):1927-32.

64. Legoux F, Salou M, Lantz O. Unconventional or Preset alphabeta T Cells: Evolutionarily Conserved Tissue-Resident T Cells Recognizing Nonpeptidic Ligands. Annu Rev Cell Dev Biol. 2017;33:511-35.

65. Huang S, Martin E, Kim S, Yu L, Soudais C, Fremont DH, et al. MR1 antigen presentation to mucosal-associated invariant T cells was highly conserved in evolution. Proc Natl Acad Sci U S A. 2009;106(20):8290-5.

66. Davis MM, Bjorkman PJ. T-cell antigen receptor genes and T-cell recognition. Nature. 1988;334(6181):395-402.

67. Reantragoon R, Corbett AJ, Sakala IG, Gherardin NA, Furness JB, Chen Z, et al. Antigen-loaded MR1 tetramers define T cell receptor heterogeneity in mucosal-associated invariant T cells. J Exp Med. 2013;210(11):2305-20.

68. Godfrey DI, Rossjohn J, McCluskey J. Fighting infection with your MAITs. Nat Immunol. 2010;11(8):693-5.

69. Treiner E, Duban L, Moura IC, Hansen T, Gilfillan S, Lantz O. Mucosal-associated invariant T (MAIT) cells: an evolutionarily conserved T cell subset. Microbes and infection. 2005;7(3):552-9.

70. Serriari NE, Eoche M, Lamotte L, Lion J, Fumery M, Marcelo P, et al. Innate mucosal-associated invariant T (MAIT) cells are activated in inflammatory bowel diseases. Clin Exp Immunol. 2014;176(2):266-74.

71. Gold MC, Eid T, Smyk-Pearson S, Eberling Y, Swarbrick GM, Langley SM, et al. Human thymic MR1-reactive MAIT cells are innate pathogen-reactive effectors that adapt following thymic egress. Mucosal Immunol. 2013;6(1):35-44.

72. Gold MC, Cerri S, Smyk-Pearson S, Cansler ME, Vogt TM, Delepine J, et al. Human mucosal associated invariant T cells detect bacterially infected cells. PLoS Biol. 2010;8(6):e1000407.

73. Chua WJ, Truscott SM, Eickhoff CS, Blazevic A, Hoft DF, Hansen TH. Polyclonal mucosa-associated invariant T cells have unique innate functions in bacterial infection. Infect Immun. 2012;80(9):3256-67.

74. Slichter CK, McDavid A, Miller HW, Finak G, Seymour BJ, McNevin JP, et al. Distinct activation thresholds of human conventional and innate-like memory T cells. JCI Insight. 2016;1(8).

75. Meierovics A, Yankelevich WJ, Cowley SC. MAIT cells are critical for optimal mucosal immune responses during in vivo pulmonary bacterial infection. Proc Natl Acad Sci U S A. 2013;110(33):E3119-28.

76. Mills KH. TLR-dependent T cell activation in autoimmunity. Nat Rev Immunol. 2011;11(12):807-22.

77. van Wilgenburg B, Scherwitzl I, Hutchinson EC, Leng T, Kurioka A, Kulicke C, et al. MAIT cells are activated during human viral infections. Nature communications. 2016;7:11653.

78. Ussher JE, Bilton M, Attwod E, Shadwell J, Richardson R, de Lara C, et al. CD 161++ CD 8+ T cells, including the MAIT cell subset, are specifically activated by IL-12+ IL-18 in a TCR-independent manner. European journal of immunology. 2014;44(1):195-203.

79. Godfrey DI, Koay HF, McCluskey J, Gherardin NA. The biology and functional importance of MAIT cells. Nat Immunol. 2019;20(9):1110-28.

80. Chen Z, Wang H, D'Souza C, Sun S, Kostenko L, Eckle SB, et al. Mucosal-associated invariant T-cell activation and accumulation after in vivo infection depends on microbial riboflavin synthesis and co-stimulatory signals. Mucosal Immunol. 2017;10(1):58-68.

81. Chiba A, Tajima R, Tomi C, Miyazaki Y, Yamamura T, Miyake S. Mucosal-associated invariant T cells promote inflammation and exacerbate disease in murine models of arthritis. Arthritis Rheum. 2012;64(1):153-61.

82. Illes Z, Shimamura M, Newcombe J, Oka N, Yamamura T. Accumulation of Valpha7.2-Jalpha33 invariant T cells in human autoimmune inflammatory lesions in the nervous system. Int Immunol. 2004;16(2):223-30.

83. Miyazaki Y, Miyake S, Chiba A, Lantz O, Yamamura T. Mucosal-associated invariant T cells regulate Th1 response in multiple sclerosis. Int Immunol. 2011;23(9):529-35.

84. Peterfalvi A, Gomori E, Magyarlaki T, Pal J, Banati M, Javorhazy A, et al. Invariant Valpha7.2-Jalpha33 TCR is expressed in human kidney and brain tumors indicating infiltration by mucosal-associated invariant T (MAIT) cells. Int Immunol. 2008;20(12):1517-25.

85. Rossjohn J, Gras S, Miles JJ, Turner SJ, Godfrey DI, McCluskey J. T cell antigen receptor recognition of antigen-presenting molecules. Annu Rev Immunol. 2015;33:169-200.

86. Patel O, Kjer-Nielsen L, Le Nours J, Eckle SB, Birkinshaw R, Beddoe T, et al. Recognition of vitamin B metabolites by mucosal-associated invariant T cells. Nature communications. 2013;4:2142.

87. Alarcon B, Mestre D, Martinez-Martin N. The immunological synapse: a cause or consequence of T-cell receptor triggering? Immunology. 2011;133(4):420-5.

88. Guy CS, Vignali DA. Organization of proximal signal initiation at the TCR:CD3 complex. Immunol Rev. 2009;232(1):7-21.

89. Miley MJ, Truscott SM, Yu YY, Gilfillan S, Fremont DH, Hansen TH, et al. Biochemical features of the MHC-related protein 1 consistent with an immunological function. J Immunol. 2003;170(12):6090-8.

90. Walter L, Gunther E. Isolation and molecular characterization of the rat MR1 homologue, a non-MHC-linked class I-related gene. Immunogenetics. 1998;47(6):477-82.

91. Norment AM, Littman DR. A second subunit of CD8 is expressed in human T cells. The EMBO Journal. 1988;7(11):3433-9.

92. Laugel B, Cole DK, Clement M, Wooldridge L, Price DA, Sewell AK. The multiple roles of the CD8 coreceptor in T cell biology: opportunities for the selective modulation of self-reactive cytotoxic T cells. J Leukoc Biol. 2011;90(6):1089-99.

93. Gangadharan D, opinion in immunology C-H. The CD8 isoform CD8αα is not a functional homologue of the TCR co-receptor CD8αβ. Current opinion in immunology. 2004.

94. Leishman AJ, Naidenko OV, Attinger A, Koning F, Lena CJ, Xiong Y, et al. T cell responses modulated through interaction between CD8alphaalpha and the nonclassical MHC class I molecule, TL. Science. 2001;294(5548):1936-9.

95. Classon BJ, Brown MH, Garnett D, Somoza C, Barclay AN, Willis AC, et al. The hinge region of the CD8 alpha chain: structure, antigenicity, and utility in expression of immunoglobulin superfamily domains. Int Immunol. 1992;4(2):215-25.

96. Kern PS, Teng MK, Smolyar A, Liu JH, Liu J, Hussey RE, et al. Structural basis of CD8 coreceptor function revealed by crystallographic analysis of a murine CD8alphaalpha ectodomain fragment in complex with H-2Kb. Immunity. 1998;9(4):519-30.

97. Salter RD, Benjamin RJ, Wesley PK, Buxton SE, Garrett TP, Clayberger C, et al. A binding site for the T-cell co-receptor CD8 on the alpha 3 domain of HLA-A2. Nature. 1990;345(6270):41-6.

98. Connolly JM, Hansen TH, Ingold AL, Potter TA. Recognition by CD8 on cytotoxic T lymphocytes is ablated by several substitutions in the class I alpha 3 domain: CD8 and the T-cell receptor recognize the same class I molecule. Proc Natl Acad Sci U S A. 1990;87(6):2137-41.

99. Gao GF, Tormo J, Gerth UC, Wyer JR, McMichael AJ, Stuart DI, et al. Crystal structure of the complex between human CD8alpha(alpha) and HLA-A2. Nature. 1997;387(6633):630-4.

100. Durairaj M, Sharma R, Varghese JC, Kane KP. Requirement for Q226, but not multiple charged residues, in the class I MHC CD loop/D strand for TCR-activated CD8 accessory function. Eur J Immunol. 2003;33(3):676-84.

101. Mallaun M, Naeher D, Daniels MA, Yachi PP, Hausmann B, Luescher IF, et al. The T cell receptor's alpha-chain connecting peptide motif promotes close approximation of the CD8 coreceptor allowing efficient signal initiation. J Immunol. 2008;180(12):8211-21.

102. Beyers AD, Spruyt LL, Williams AF. Molecular associations between the T-lymphocyte antigen receptor complex and the surface antigens CD2, CD4, or CD8 and CD5. Proc Natl Acad Sci U S A. 1992;89(7):2945-9.

103. Yachi PP, Ampudia J, Zal T, Gascoigne NR. Altered peptide ligands induce delayed CD8-T cell receptor interaction--a role for CD8 in distinguishing antigen quality. Immunity. 2006;25(2):203-11.

104. Wyer JR, Willcox BE, Gao GF, Gerth UC, Davis SJ, Bell JI, et al. T Cell Receptor and Coreceptor CD8αα Bind Peptide-MHC Independently and with Distinct Kinetics. Immunity. 1999;10(2):219-25.

105. Pecht I, Gakamsky DM. Spatial coordination of CD8 and TCR molecules controls antigen recognition by CD8+ T-cells. FEBS Lett. 2005;579(15):3336-41.

106. Gakamsky DM, Luescher IF, Pramanik A, Kopito RB, Lemonnier F, Vogel H, et al. CD8 kinetically promotes ligand binding to the T-cell antigen receptor. Biophys J. 2005;89(3):2121-33.

107. Holler PD, Kranz DM. Quantitative analysis of the contribution of TCR/pepMHC affinity and CD8 to T cell activation. Immunity. 2003;18(2):255-64.

108. Garcia KC, Scott CA, Brunmark A, Carbone FR, Peterson PA, Wilson IA, et al. CD8 enhances formation of stable T-cell receptor/MHC class I molecule complexes. Nature. 1996;384(6609):577-81.

109. Veillette A, Bookman MA, Horak EM, Bolen JB. The CD4 and CD8 T cell surface antigens are associated with the internal membrane tyrosine-protein kinase p56lck. Cell. 1988;55(2):301-8.

110. Zamoyska R. The CD8 coreceptor revisited: one chain good, two chains better. Immunity. 1994;1(4):243-6.

111. Janeway Jr CA. The immune system evolved to discriminate infectious nonself from noninfectious self. Immunology today. 1992;13(1):11-6.

112. Irie HY, Ravichandran KS, Burakoff SJ. CD8 beta chain influences CD8 alpha chain-associated Lck kinase activity. J Exp Med. 1995;181(4):1267-73.

113. Simons K, Toomre D. Lipid rafts and signal transduction. Nat Rev Mol Cell Biol. 2000;1(1):31-9.

114. Altin JG, Sloan EK. The role of CD45 and CD45-associated molecules in T cell activation. Immunol Cell Biol. 1997;75(5):430-45.

115. Cheroutre H, Lambolez F. Doubting the TCR coreceptor function of CD8alphaalpha. Immunity. 2008;28(2):149-59.

116. van Oers NS, Teh SJ, Garvin AM, Forbush KA, Perlmutter RM, Teh HS. CD8 inhibits signal transduction through the T cell receptor in CD4-CD8- thymocytes from T cell receptor transgenic mice reconstituted with a transgenic CD8 alpha molecule. J Immunol. 1993;151(2):777-90.

117. Cawthon AG, Alexander-Miller MA. Optimal colocalization of TCR and CD8 as a novel mechanism for the control of functional avidity. J Immunol. 2002;169(7):3492-8.

118. Rudd CE, Martin M, Schneider H. CTLA-4 negative signaling via lipid rafts: A new perspective. Sci STKE. 2002;2002(128):pe18.

119. Liu Y, Xiong Y, Naidenko OV, Liu J, Immunity Z-R. The crystal structure of a TL/CD8αα complex at 2.1 Å resolution: implications for modulation of T cell activation and memory. Immunity. 2003.

120. Engel I, Hammond K, Sullivan BA, He X, Taniuchi I, Kappes D, et al. Co-receptor choice by V alpha14i NKT cells is driven by Th-POK expression rather than avoidance of CD8-mediated negative selection. J Exp Med. 2010;207(5):1015-29.

121. Thedrez A, de Lalla C, Allain S, Zaccagnino L, Sidobre S, Garavaglia C, et al. CD4 engagement by CD1d potentiates activation of CD4+ invariant NKT cells. Blood. 2007;110(1):251-8.

122. Chen X, Wang X, Besra GS, Gumperz JE. Modulation of CD1d-restricted NKT cell responses by CD4. J Leukoc Biol. 2007;82(6):1455-65.

123. Martin LH, Calabi F, Milstein C. Isolation of CD1 genes: a family of major histocompatibility complex-related differentiation antigens. Proc Natl Acad Sci U S A. 1986;83(23):9154-8.

124. Kurioka A, Jahun AS, Hannaway RF, Walker LJ, Fergusson JR, Sverremark-Ekstrom E, et al. Shared and Distinct Phenotypes and Functions of Human CD161++ Valpha7.2+ T Cell Subsets. Front Immunol. 2017;8:1031.

125. Brozova J, Karlova I, Novak J. Analysis of the Phenotype and Function of the Subpopulations of Mucosal-Associated Invariant T Cells. Scand J Immunol. 2016;84(4):245-51.

126. Dias J, Boulouis C, Gorin JB, van den Biggelaar R, Lal KG, Gibbs A, et al. The CD4(-)CD8(-) MAIT cell subpopulation is a functionally distinct subset developmentally related to the main CD8(+) MAIT cell pool. Proc Natl Acad Sci U S A. 2018;115(49):E11513-E22.

127. Wooldridge L, Hutchinson SL, Choi EM, Lissina A, Jones E, Mirza F, et al. Anti-CD8 antibodies can inhibit or enhance peptide-MHC class I (pMHCI) multimer binding: this is paralleled by their effects on CTL activation and occurs in the absence of an interaction between pMHCI and CD8 on the cell surface. J Immunol. 2003;171(12):6650-60.

128. Porcelli S, Morita CT, Brenner MB. CD1b restricts the response of human CD4-8- T lymphocytes to a microbial antigen. Nature. 1992;360(6404):593-7.

129. De Libero G, Mori L. The T-Cell Response to Lipid Antigens of Mycobacterium tuberculosis. Front Immunol. 2014;5:219.

130. Sieling PA, Chatterjee D, Porcelli SA, Prigozy TI, Mazzaccaro RJ, Soriano T, et al. CD1-restricted T cell recognition of microbial lipoglycan antigens. Science. 1995;269(5221):227-30.

131. Gilleron M, Stenger S, Mazorra Z, Wittke F, Mariotti S, Bohmer G, et al. Diacylated sulfoglycolipids are novel mycobacterial antigens stimulating CD1-restricted

T cells during infection with Mycobacterium tuberculosis. J Exp Med. 2004;199(5):649-59.

132. Quémard A. New insights into the mycolate-containing compound biosynthesis and transport in mycobacteria. Trends in microbiology. 2016;24(9):725-38.

133. James CA, Yu KKQ, Gilleron M, Prandi J, Yedulla VR, Moleda ZZ, et al. CD1b Tetramers Identify T Cells that Recognize Natural and Synthetic Diacylated Sulfoglycolipids from Mycobacterium tuberculosis. Cell Chem Biol. 2018;25(4):392-402 e14.

134. Sprott GD, Dicaire CJ, Gurnani K, Sad S, Krishnan L. Activation of dendritic cells by liposomes prepared from phosphatidylinositol mannosides from Mycobacterium bovis bacillus Calmette-Guerin and adjuvant activity in vivo. Infect Immun. 2004;72(9):5235-46.

135. Van Rhijn I, Kasmar A, de Jong A, Gras S, Bhati M, Doorenspleet ME, et al. A conserved human T cell population targets mycobacterial antigens presented by CD1b. Nat Immunol. 2013;14(7):706-13.

136. Van Rhijn I, Gherardin NA, Kasmar A, de Jager W, Pellicci DG, Kostenko L, et al. TCR bias and affinity define two compartments of the CD1b-glycolipid-specific T Cell repertoire. J Immunol. 2014;192(9):4054-60.

137. DeWitt WS, Yu KKQ, Wilburn DB, Sherwood A, Vignali M, Day CL, et al. A Diverse Lipid Antigen-Specific TCR Repertoire Is Clonally Expanded during Active Tuberculosis. J Immunol. 2018;201(3):888-96.

138. Gras S, Van Rhijn I, Shahine A, Cheng TY, Bhati M, Tan LL, et al. T cell receptor recognition of CD1b presenting a mycobacterial glycolipid. Nature communications. 2016;7:13257.

139. Huang S, Cheng TY, Young DC, Layre E, Madigan CA, Shires J, et al. Discovery of deoxyceramides and diacylglycerols as CD1b scaffold lipids among diverse groove-blocking lipids of the human CD1 system. Proc Natl Acad Sci U S A. 2011;108(48):19335-40.

140. McCarthy C, Shepherd D, Fleire S, Stronge VS, Koch M, Illarionov PA, et al. The length of lipids bound to human CD1d molecules modulates the affinity of NKT cell TCR and the threshold of NKT cell activation. The Journal of experimental medicine. 2007;204(5):1131-44.

141. Rauch J, Gumperz J, Robinson C, Sköld M, Roy C, Young DC, et al. Structural features of the acyl chain determine self-phospholipid antigen recognition by a CD1d-restricted invariant NKT (iNKT) cell. Journal of Biological Chemistry. 2003;278(48):47508-15.

142. de Lalla C, Lepore M, Piccolo FM, Rinaldi A, Scelfo A, Garavaglia C, et al. High-frequency and adaptive-like dynamics of human CD1 self-reactive T cells. Eur J Immunol. 2011;41(3):602-10.

143. Vincent MS, Xiong X, Grant EP, Peng W, Brenner MB. CD1a-, b-, and c-restricted TCRs recognize both self and foreign antigens. The Journal of Immunology. 2005;175(10):6344-51.

144. Rossjohn J, Pellicci DG, Patel O, Gapin L, Godfrey DI. Recognition of CD1d-restricted antigens by natural killer T cells. Nature reviews Immunology. 2012;12(12):845-57.

145. Matsunaga I, Naka T, Talekar RS, McConnell MJ, Katoh K, Nakao H, et al. Mycolyltransferase-mediated glycolipid exchange in Mycobacteria. J Biol Chem. 2008;283(43):28835-41.

146. Horvath SE, Daum G. Lipids of mitochondria. Prog Lipid Res. 2013;52(4):590-614.

147. Sohlenkamp C, Geiger O. Bacterial membrane lipids: diversity in structures and pathways. FEMS Microbiol Rev. 2016;40(1):133-59.

148. Lepore M, de Lalla C, Gundimeda SR, Gsellinger H, Consonni M, Garavaglia C, et al. A novel self-lipid antigen targets human T cells against CD1c(+) leukemias. J Exp Med. 2014;211(7):1363-77.

149. Bagchi S, Li S, Wang CR. CD1b-autoreactive T cells recognize phospholipid antigens and contribute to antitumor immunity against a CD1b(+) T cell lymphoma. Oncoimmunology. 2016;5(9):e1213932.

150. Shahine A, Van Rhijn I, Cheng T-Y, Iwany S, Gras S, Moody DB, et al. A molecular basis of human T cell receptor autoreactivity toward self-phospholipids. Science immunology. 2017;2(16).

151. Zhao J, Siddiqui S, Shang S, Bian Y, Bagchi S, He Y, et al. Mycolic acid-specific T cells protect against Mycobacterium tuberculosis infection in a humanized transgenic mouse model. Elife. 2015;4:e08525.

152. Busch M, Herzmann C, Kallert S, Zimmermann A, Hofer C, Mayer D, et al. Lipoarabinomannan-Responsive Polycytotoxic T Cells Are Associated with Protection in Human Tuberculosis. Am J Respir Crit Care Med. 2016;194(3):345-55.

153. Bagchi S, He Y, Zhang H, Cao L, Van Rhijn I, Moody DB, et al. CD1b-autoreactive T cells contribute to hyperlipidemia-induced skin inflammation in mice. J Clin Invest. 2017;127(6):2339-52.

154. Brembilla NC, Senra L, Boehncke WH. The IL-17 Family of Cytokines in Psoriasis: IL-17A and Beyond. Front Immunol. 2018;9:1682.

155. Wasilewska A, Winiarska M, Olszewska M, Rudnicka L. Interleukin-17 inhibitors. A new era in treatment of psoriasis and other skin diseases. Postepy Dermatol Alergol. 2016;33(4):247-52.

156. Oliveira Mde F, Rocha Bde O, Duarte GV. Psoriasis: classical and emerging comorbidities. An Bras Dermatol. 2015;90(1):9-20.

157. Armstrong A, Harskamp C, Armstrong E. The association between psoriasis and obesity: a systematic review and meta-analysis of observational studies. Nutrition & diabetes. 2012;2(12):e54-e.

158. Ma C, Harskamp CT, Armstrong EJ, Armstrong AW. The association between psoriasis and dyslipidaemia: a systematic review. Br J Dermatol. 2013;168(3):486-95.

159. Kim JH, Hu Y, Yongqing T, Kim J, Hughes VA, Le Nours J, et al. CD1a on Langerhans cells controls inflammatory skin disease. Nat Immunol. 2016;17(10):1159-66.

160. Stenger S, Mazzaccaro RJ, Uyemura K, Cho S, Barnes PF, Rosat JP, et al. Differential effects of cytolytic T cell subsets on intracellular infection. Science. 1997;276(5319):1684-7.

161. Stenger S, Hanson DA, Teitelbaum R, Dewan P, Niazi KR, Froelich CJ, et al. An antimicrobial activity of cytolytic T cells mediated by granulysin. Science. 1998;282(5386):121-5.

162. Huang S, Gilfillan S, Cella M, Miley MJ, Lantz O, Lybarger L, et al. Evidence for MR1 antigen presentation to mucosal-associated invariant T cells. J Biol Chem. 2005;280(22):21183-93.

163. Reid SW, McAdam S, Smith KJ, Klenerman P, O'Callaghan CA, Harlos K, et al. Antagonist HIV-1 Gag peptides induce structural changes in HLA B8. J Exp Med. 1996;184(6):2279-86.

164. Clements CS, Kjer-Nielsen L, Kostenko L, Hoare HL, Dunstone MA, Moses E, et al. Crystal structure of HLA-G: a nonclassical MHC class I molecule expressed at the fetal-maternal interface. Proc Natl Acad Sci U S A. 2005;102(9):3360-5.

165. Garboczi DN, Hung DT, Wiley DC. HLA-A2-peptide complexes: refolding and crystallization of molecules expressed in Escherichia coli and complexed with single antigenic peptides. Proc Natl Acad Sci U S A. 1992;89(8):3429-33.

166. Mak JY, Xu W, Reid RC, Corbett AJ, Meehan BS, Wang H, et al. Stabilizing short-lived Schiff base derivatives of 5-aminouracils that activate mucosal-associated invariant T cells. Nature communications. 2017;8:14599.

167. Kim SM, Bhonsle L, Besgen P, Nickel J, Backes A, Held K, et al. Analysis of the paired TCR alpha- and beta-chains of single human T cells. PLoS One. 2012;7(5):e37338.

168. Picelli S, Bjorklund AK, Faridani OR, Sagasser S, Winberg G, Sandberg R. Smart-seq2 for sensitive full-length transcriptome profiling in single cells. Nat Methods. 2013;10(11):1096-8.

169. Porcelli S, Yockey CE, Brenner MB, Balk SP. Analysis of T cell antigen receptor (TCR) expression by human peripheral blood CD4-8- alpha/beta T cells demonstrates preferential use of several V beta genes and an invariant TCR alpha chain. J Exp Med. 1993;178(1):1-16.

170. Boudinot P, Mondot S, Jouneau L, Teyton L, Lefranc MP, Lantz O. Restricting nonclassical MHC genes coevolve with TRAV genes used by innate-like T cells in mammals. Proc Natl Acad Sci U S A. 2016;113(21):E2983-92.

171. Gherardin NA, Souter MN, Koay HF, Mangas KM, Seemann T, Stinear TP, et al. Human blood MAIT cell subsets defined using MR1 tetramers. Immunol Cell Biol. 2018;96(5):507-25.

172. Dusseaux M, Martin E, Serriari N, Peguillet I, Premel V, Louis D, et al. Human MAIT cells are xenobiotic-resistant, tissue-targeted, CD161hi IL-17-secreting T cells. Blood. 2011;117(4):1250-9.

173. Kurioka A, Ussher JE, Cosgrove C, Clough C, Fergusson JR, Smith K, et al. MAIT cells are licensed through granzyme exchange to kill bacterially sensitized targets. Mucosal Immunol. 2015;8(2):429-40.

174. Georgel P, Radosavljevic M, Macquin C, Bahram S. The non-conventional MHC class I MR1 molecule controls infection by Klebsiella pneumoniae in mice. Molecular immunology. 2011;48(5):769-75.

175. Wang H, D'Souza C, Lim XY, Kostenko L, Pediongco TJ, Eckle SBG, et al. MAIT cells protect against pulmonary Legionella longbeachae infection. Nature communications. 2018;9(1):3350.

176. Leahy DJ, Axel R, Hendrickson WA. Crystal structure of a soluble form of the human T cell coreceptor CD8 at 2.6 A resolution. Cell. 1992;68(6):1145-62.

177. Sewell AK, Gerth UC, Price DA, Purbhoo MA, Boulter JM, Gao GF, et al. Antagonism of cytotoxic T-lymphocyte activation by soluble CD8. Nat Med. 1999;5(4):399-404.

178. Wooldridge L, van den Berg HA, Glick M, Gostick E, Laugel B, Hutchinson SL, et al. Interaction between the CD8 coreceptor and major histocompatibility complex class I stabilizes T cell receptor-antigen complexes at the cell surface. J Biol Chem. 2005;280(30):27491-501.

179. Laugel B, van den Berg HA, Gostick E, Cole DK, Wooldridge L, Boulter J, et al. Different T cell receptor affinity thresholds and CD8 coreceptor dependence govern cytotoxic T lymphocyte activation and tetramer binding properties. J Biol Chem. 2007;282(33):23799-810.

180. Moebius U, Kober G, Griscelli AL, Hercend T, Meuer SC. Expression of different CD8 isoforms on distinct human lymphocyte subpopulations. Eur J Immunol. 1991;21(8):1793-800.

181. Kern P, Hussey RE, Spoerl R, Reinherz EL, Chang HC. Expression, purification, and functional analysis of murine ectodomain fragments of CD8alphaalpha and CD8alphabeta dimers. J Biol Chem. 1999;274(38):27237-43.

182. Bosselut R, Kubo S, Guinter T, Kopacz JL, Altman JD, Feigenbaum L, et al. Role of CD8beta domains in CD8 coreceptor function: importance for MHC I binding, signaling, and positive selection of CD8+ T cells in the thymus. Immunity. 2000;12(4):409-18.

183. Pang DJ, Hayday AC, Bijlmakers MJ. CD8 Raft localization is induced by its assembly into CD8alpha beta heterodimers, Not CD8alpha alpha homodimers. J Biol Chem. 2007;282(18):13884-94.

184. Wingren C, Crowley MP, Degano M, Chien Y, Wilson IA. Crystal structure of a gammadelta T cell receptor ligand T22: a truncated MHC-like fold. Science. 2000;287(5451):310-4.

185. Olivares-Villagomez D, Mendez-Fernandez YV, Parekh VV, Lalani S, Vincent TL, Cheroutre H, et al. Thymus leukemia antigen controls intraepithelial lymphocyte function and inflammatory bowel disease. Proc Natl Acad Sci U S A. 2008;105(46):17931-6.

186. Arase H, Arase N, Nakagawa K, Good RA, Onoe K. NK1.1+ CD4+ CD8- thymocytes with specific lymphokine secretion. Eur J Immunol. 1993;23(1):307-10.

187. Yoshimoto T, Paul WE. CD4pos, NK1.1pos T cells promptly produce interleukin 4 in response to in vivo challenge with anti-CD3. J Exp Med. 1994;179(4):1285-95.

188. Tang XZ, Jo J, Tan AT, Sandalova E, Chia A, Tan KC, et al. IL-7 licenses activation of human liver intrasinusoidal mucosal-associated invariant T cells. J Immunol. 2013;190(7):3142-52.

189. Shi Y, Qi J, Iwamoto A, Gao GF. Plasticity of human CD8alphaalpha binding to peptide-HLA-A*2402. Molecular immunology. 2011;48(15-16):2198-202.

190. Wang R, Natarajan K, Margulies DH. Structural basis of the CD8 alpha beta/MHC class I interaction: focused recognition orients CD8 beta to a T cell proximal position. J Immunol. 2009;183(4):2554-64.

191. Laskowski RA, Jablonska J, Pravda L, Varekova RS, Thornton JM. PDBsum: Structural summaries of PDB entries. Protein Sci. 2018;27(1):129-34.

192. Purbhoo MA, Boulter JM, Price DA, Vuidepot AL, Hourigan CS, Dunbar PR, et al. The human CD8 coreceptor effects cytotoxic T cell activation and antigen sensitivity primarily by mediating complete phosphorylation of the T cell receptor zeta chain. J Biol Chem. 2001;276(35):32786-92.

193. Choi EM, Chen JL, Wooldridge L, Salio M, Lissina A, Lissin N, et al. High avidity antigen-specific CTL identified by CD8-independent tetramer staining. J Immunol. 2003;171(10):5116-23.

194. Hutchinson SL, Wooldridge L, Tafuro S, Laugel B, Glick M, Boulter JM, et al. The CD8 T cell coreceptor exhibits disproportionate biological activity at extremely low binding affinities. J Biol Chem. 2003;278(27):24285-93.

195. Gao GF, Willcox BE, Wyer JR, Boulter JM, O'Callaghan CA, Maenaka K, et al. Classical and nonclassical class I major histocompatibility complex molecules exhibit subtle conformational differences that affect binding to CD8alphaalpha. J Biol Chem. 2000;275(20):15232-8.

196. Cole DK, Rizkallah PJ, Boulter JM, Sami M, Vuidepot AL, Glick M, et al. Computational design and crystal structure of an enhanced affinity mutant human CD8 alphaalpha coreceptor. Proteins. 2007;67(1):65-74.

197. Cole DK, Dunn SM, Sami M, Boulter JM, Jakobsen BK, Sewell AK. T cell receptor engagement of peptide-major histocompatibility complex class I does not modify CD8 binding. Molecular immunology. 2008;45(9):2700-9.

198. Iglesias MC, Almeida JR, Fastenackels S, van Bockel DJ, Hashimoto M, Venturi V, et al. Escape from highly effective public CD8+ T-cell clonotypes by HIV. Blood. 2011;118(8):2138-49.

199. Salio M, Gasser O, Gonzalez-Lopez C, Martens A, Veerapen N, Gileadi U, et al. Activation of human mucosal-associated invariant T cells induces CD40L-dependent maturation of monocyte-derived and primary dendritic cells. The Journal of Immunology. 2017;199(8):2631-8.

200. Tastan C, Karhan E, Zhou W, Fleming E, Voigt AY, Yao X, et al. Tuning of human MAIT cell activation by commensal bacteria species and MR1-dependent T-cell presentation. Mucosal immunology. 2018;11(6):1591-605.

201. Gherardin NA, Keller AN, Woolley RE, Le Nours J, Ritchie DS, Neeson PJ, et al. Diversity of T Cells Restricted by the MHC Class I-Related Molecule MR1 Facilitates Differential Antigen Recognition. Immunity. 2016;44(1):32-45.

202. Keller AN, Eckle SB, Xu W, Liu L, Hughes VA, Mak JY, et al. Drugs and drug-like molecules can modulate the function of mucosal-associated invariant T cells. Nat Immunol. 2017;18(4):402-11.

203. Lepore M, Kalinichenko A, Calogero S, Kumar P, Paleja B, Schmaler M, et al. Functionally diverse human T cells recognize non-microbial antigens presented by MR1. Elife. 2017;6:e24476.

204. Meermeier EW, Laugel BF, Sewell AK, Corbett AJ, Rossjohn J, McCluskey J, et al. Human TRAV1-2-negative MR1-reactive T cells detect S. pyogenes and alternatives to MAIT riboflavin-based antigens. Nature communications. 2016;7:12506.

205. Ma LJ, Acero LF, Zal T, Schluns KS. Trans-presentation of IL-15 by intestinal epithelial cells drives development of CD8alphaalpha IELs. J Immunol. 2009;183(2):1044-54.

206. Walker LJ, Marrinan E, Muenchhoff M, Ferguson J, Kloverpris H, Cheroutre H, et al. CD8alphaalpha Expression Marks Terminally Differentiated Human CD8+ T Cells Expanded in Chronic Viral Infection. Front Immunol. 2013;4:223.

207. Lee OJ, Cho YN, Kee SJ, Kim MJ, Jin HM, Lee SJ, et al. Circulating mucosal-associated invariant T cell levels and their cytokine levels in healthy adults. Exp Gerontol. 2014;49:47-54.

208. Kelly J, Minoda Y, Meredith T, Cameron G, Philipp MS, Pellicci DG, et al. Chronically stimulated human MAIT cells are unexpectedly potent IL-13 producers. Immunol Cell Biol. 2019;97(8):689-99.

209. Leeansyah E, Svard J, Dias J, Buggert M, Nystrom J, Quigley MF, et al. Arming of MAIT Cell Cytolytic Antimicrobial Activity Is Induced by IL-7 and Defective in HIV-1 Infection. PLoS Pathog. 2015;11(8):e1005072.

210. Booth JS, Salerno-Goncalves R, Blanchard TG, Patil SA, Kader HA, Safta AM, et al. Mucosal-Associated Invariant T Cells in the Human Gastric Mucosa and Blood: Role in Helicobacter pylori Infection. Front Immunol. 2015;6:466.

211. Reis BS, Rogoz A, Costa-Pinto FA, Taniuchi I, Mucida D. Mutual expression of the transcription factors Runx3 and ThPOK regulates intestinal CD4(+) T cell immunity. Nat Immunol. 2013;14(3):271-80.

212. Daniels MA, Jameson SC. Critical role for CD8 in T cell receptor binding and activation by peptide/major histocompatibility complex multimers. J Exp Med. 2000;191(2):335-46.

213. Harriff MJ, McMurtrey C, Froyd CA, Jin H, Cansler M, Null M, et al. MR1 displays the microbial metabolome driving selective MR1-reactive T cell receptor usage. Science immunology. 2018;3(25).

214. Sharma PK, Wong EB, Napier RJ, Bishai WR, Ndung'u T, Kasprowicz VO, et al. High expression of CD26 accurately identifies human bacteria-reactive MR1-reactive MAIT cells. Immunology. 2015;145(3):443-53.

215. Li S, Choi H-J, Felio K, Wang C-R. Autoreactive CD1b-restricted T cells: a new innate-like T-cell population that contributes to immunity against infection. Blood, The Journal of the American Society of Hematology. 2011;118(14):3870-8.

216. Shahine A, Reinink P, Reijneveld JF, Gras S, Holzheimer M, Cheng TY, et al. A T-cell receptor escape channel allows broad T-cell response to CD1b and membrane phospholipids. Nature communications. 2019;10(1):56.

217. Reeves PJ, Callewaert N, Contreras R, Khorana HG. Structure and function in rhodopsin: high-level expression of rhodopsin with restricted and homogeneous N-glycosylation by a tetracycline-inducible N-acetylglucosaminyltransferase I-negative HEK293S stable mammalian cell line. Proc Natl Acad Sci U S A. 2002;99(21):13419-24.

218. Kjer-Nielsen L, Borg NA, Pellicci DG, Beddoe T, Kostenko L, Clements CS, et al. A structural basis for selection and cross-species reactivity of the semi-invariant NKT cell receptor in CD1d/glycolipid recognition. J Exp Med. 2006;203(3):661-73.

219. Young MH, Gapin L. Group 1 CD1-restricted T cells take center stage. Eur J Immunol. 2011;41(3):592-4.

220. Wang GC, Dash P, McCullers JA, Doherty PC, Thomas PG. T cell receptor alphabeta diversity inversely correlates with pathogen-specific antibody levels in human cytomegalovirus infection. Sci Transl Med. 2012;4(128):128ra42.

221. Van Rhijn I, Godfrey DI, Rossjohn J, Moody DB. Lipid and small-molecule display by CD1 and MR1. Nat Rev Immunol. 2015;15(10):643-54.

222. Karadimitris A, Gadola S, Altamirano M, Brown D, Woolfson A, Klenerman P, et al. Human CD1d-glycolipid tetramers generated by in vitro oxidative refolding chromatography. Proc Natl Acad Sci U S A. 2001;98(6):3294-8.

223. Birkinshaw RW, Pellicci DG, Cheng TY, Keller AN, Sandoval-Romero M, Gras S, et al. alphabeta T cell antigen receptor recognition of CD1a presenting self lipid ligands. Nat Immunol. 2015;16(3):258-66.

224. Relloso M, Cheng TY, Im JS, Parisini E, Roura-Mir C, DeBono C, et al. pH-dependent interdomain tethers of CD1b regulate its antigen capture. Immunity. 2008;28(6):774-86.

225. Brennan PJ, Cheng T-Y, Pellicci DG, Watts GF, Veerapen N, Young DC, et al. Structural determination of lipid antigens captured at the CD1d–T-cell receptor interface. Proceedings of the National Academy of Sciences. 2017;114(31):8348-53.

226. Jakobsen B, Bell J, Gao G, Willcox B, Boulter J. Soluble T cell receptor. Google Patents; 2006.

227. Boulter JM, Glick M, Todorov PT, Baston E, Sami M, Rizkallah P, et al. Stable, soluble T-cell receptor molecules for crystallization and therapeutics. Protein Eng. 2003;16(9):707-11.

228. Borg NA, Wun KS, Kjer-Nielsen L, Wilce MC, Pellicci DG, Koh R, et al. CD1d-lipid-antigen recognition by the semi-invariant NKT T-cell receptor. Nature. 2007;448(7149):44-9.

229. Appel H, Gauthier L, Pyrdol J, Wucherpfennig KW. Kinetics of T-cell receptor binding by bivalent HLA-DR. Peptide complexes that activate antigen-specific human T-cells. J Biol Chem. 2000;275(1):312-21.

230. Li Y, Huang Y, Lue J, Quandt JA, Martin R, Mariuzza RA. Structure of a human autoimmune TCR bound to a myelin basic protein self-peptide and a multiple sclerosis-associated MHC class II molecule. EMBO J. 2005;24(17):2968-79.

231. Sato K, Kondo M, Sakuta K, Hosoi A, Noji S, Sugiura M, et al. Impact of culture medium on the expansion of T cells for immunotherapy. Cytotherapy. 2009;11(7):936-46.

232. Sieling PA, Ochoa MT, Jullien D, Leslie DS, Sabet S, Rosat JP, et al. Evidence for human CD4+ T cells in the CD1-restricted repertoire: derivation of mycobacteria-reactive T cells from leprosy lesions. J Immunol. 2000;164(9):4790-6.

233. Reinink P, Souter MNT, Cheng TY, van Gorkom T, Lenz S, Kubler-Kielb J, et al. CD1b presents self and Borrelia burgdorferi diacylglycerols to human T cells. Eur J Immunol. 2019;49(5):737-46.

234. Reiser JB, Darnault C, Gregoire C, Mosser T, Mazza G, Kearney A, et al. CDR3 loop flexibility contributes to the degeneracy of TCR recognition. Nat Immunol. 2003;4(3):241-7.

235. Patel O, Pellicci DG, Gras S, Sandoval-Romero ML, Uldrich AP, Mallevaey T, et al. Recognition of CD1d-sulfatide mediated by a type II natural killer T cell antigen receptor. Nat Immunol. 2012;13(9):857-63.

236. Zhang Y, Baycin-Hizal D, Kumar A, Priola J, Bahri M, Heffner KM, et al. High-throughput lipidomic and transcriptomic analysis to compare SP2/0, CHO, and HEK-293 mammalian cell lines. Analytical chemistry. 2017;89(3):1477-85.

237. van der Veen JN, Kennelly JP, Wan S, Vance JE, Vance DE, Jacobs RL. The critical role of phosphatidylcholine and phosphatidylethanolamine metabolism in health and disease. Biochim Biophys Acta Biomembr. 2017;1859(9 Pt B):1558-72.

238. Li Z, Vance DE. Phosphatidylcholine and choline homeostasis. J Lipid Res. 2008;49(6):1187-94.

239. Vance JE, Tasseva G. Formation and function of phosphatidylserine and phosphatidylethanolamine in mammalian cells. Biochim Biophys Acta. 2013;1831(3):543-54.

240. Mistry DAH, French PW. Circulating phospholipids as biomarkers of breast cancer: a review. Breast cancer: basic and clinical research. 2016;10:BCBCR. S40693.

241. Rolin J, Maghazachi AA. Effects of lysophospholipids on tumor microenvironment. Cancer Microenviron. 2011;4(3):393-403.

242. Lopez-Sagaseta J, Sibener LV, Kung JE, Gumperz J, Adams EJ. Lysophospholipid presentation by CD1d and recognition by a human Natural Killer T-cell receptor. EMBO J. 2012;31(8):2047-59.

243. Garcia-Alles LF, Versluis K, Maveyraud L, Vallina AT, Sansano S, Bello NF, et al. Endogenous phosphatidylcholine and a long spacer ligand stabilize the lipid-binding groove of CD1b. EMBO J. 2006;25(15):3684-92.

244. Sun GY, Shelat PB, Jensen MB, He Y, Sun AY, Simonyi A. Phospholipases A2 and inflammatory responses in the central nervous system. Neuromolecular Med. 2010;12(2):133-48.

245. Bourgeois EA, Subramaniam S, Cheng TY, De Jong A, Layre E, Ly D, et al. Bee venom processes human skin lipids for presentation by CD1a. J Exp Med. 2015;212(2):149-63.

246. Cheung KL, Jarrett R, Subramaniam S, Salimi M, Gutowska-Owsiak D, Chen YL, et al. Psoriatic T cells recognize neolipid antigens generated by mast cell phospholipase delivered by exosomes and presented by CD1a. J Exp Med. 2016;213(11):2399-412.

247. Lechevalier MP. Lipids in bacterial taxonomy - a taxonomist's view. CRC Crit Rev Microbiol. 1977;5(2):109-210.

248. Geiger O, Lopez-Lara IM, Sohlenkamp C. Phosphatidylcholine biosynthesis and function in bacteria. Biochim Biophys Acta. 2013;1831(3):503-13.

249. de Jong A, Pena-Cruz V, Cheng TY, Clark RA, Van Rhijn I, Moody DB. CD1a-autoreactive T cells are a normal component of the human alphabeta T cell repertoire. Nat Immunol. 2010;11(12):1102-9.

250. Cohen A, Mathiasen VD, Schon T, Wejse C. The global prevalence of latent tuberculosis: a systematic review and meta-analysis. Eur Respir J. 2019;54(3):1900655.

251. O'Garra A, Redford PS, McNab FW, Bloom CI, Wilkinson RJ, Berry MP. The immune response in tuberculosis. Annu Rev Immunol. 2013;31(1):475-527.

252. Dodd PJ, Yuen CM, Sismanidis C, Seddon JA, Jenkins HE. The global burden of tuberculosis mortality in children: a mathematical modelling study. Lancet Glob Health. 2017;5(9):e898-e906.

253. Glaziou P, Spring … S-C. Global epidemiology of tuberculosis. Cold Spring …. 2015.

254. Pawlowski A, Jansson M, Skold M, Rottenberg ME, Kallenius G. Tuberculosis and HIV co-infection. PLoS Pathog. 2012;8(2):e1002464.

255. Andersen P, Doherty TM. The success and failure of BCG - implications for a novel tuberculosis vaccine. Nat Rev Microbiol. 2005;3(8):656-62.

256. Rhoades ER, Geisel RE, Butcher BA, McDonough S, Russell DG. Cell wall lipids from Mycobacterium bovis BCG are inflammatory when inoculated within a gel matrix: characterization of a new model of the granulomatous response to mycobacterial components. Tuberculosis (Edinb). 2005;85(3):159-76.

257. Colditz GA, Berkey CS, Mosteller F, Brewer TF, Wilson ME, Burdick E, et al. The efficacy of bacillus Calmette-Guerin vaccination of newborns and infants in the

prevention of tuberculosis: meta-analyses of the published literature. Pediatrics. 1995;96(1 Pt 1):29-35.

258. Zodpey SP, Shrikhande SN, Maldhure BR, Vasudeo ND, Kulkarni SW. Effectiveness of Bacillus Calmette Guerin (BCG) vaccination in the prevention of childhood pulmonary tuberculosis: a case control study in Nagpur, India. Southeast Asian J Trop Med Public Health. 1998;29(2):285-8.

259. Sakai S, Mayer-Barber KD, Barber DL. Defining features of protective CD4 T cell responses to Mycobacterium tuberculosis. Curr Opin Immunol. 2014;29:137-42.

260. Derrick SC, Yabe IM, Yang A, Morris SL. Vaccine-induced anti-tuberculosis protective immunity in mice correlates with the magnitude and quality of multifunctional CD4 T cells. Vaccine. 2011;29(16):2902-9.

261. Lindenstrom T, Agger EM, Korsholm KS, Darrah PA, Aagaard C, Seder RA, et al. Tuberculosis subunit vaccination provides long-term protective immunity characterized by multifunctional CD4 memory T cells. J Immunol. 2009;182(12):8047-55.

262. Andersen P, Scriba TJ. Moving tuberculosis vaccines from theory to practice. Nat Rev Immunol. 2019;19(9):550-62.

263. Moody DB, Guy MR, Grant E, Cheng TY, Brenner MB, Besra GS, et al. CD1b-mediated T cell recognition of a glycolipid antigen generated from mycobacterial lipid and host carbohydrate during infection. J Exp Med. 2000;192(7):965-76.

264. Ernst WA, Maher J, Cho S, Niazi KR, Chatterjee D, Moody DB, et al. Molecular interaction of CD1b with lipoglycan antigens. Immunity. 1998;8(3):331-40.

265. Davis MM, Altman JD, Newell EW. Interrogating the repertoire: broadening the scope of peptide-MHC multimer analysis. Nat Rev Immunol. 2011;11(8):551-8.

266. D'Andrea A, Goux D, De Lalla C, Koezuka Y, Montagna D, Moretta A, et al. Neonatal invariant Valpha24+ NKT lymphocytes are activated memory cells. Eur J Immunol. 2000;30(6):1544-50.

267. Van Der Vliet HJ, Nishi N, De Gruijl TD, Von Blomberg BME, Van Den Eertwegh AJ, Pinedo HM, et al. Human natural killer T cells acquire a memory-activated phenotype before birth. Blood. 2000;95(7):2440-2.

268. Salio M, Silk JD, Yvonne Jones E, Cerundolo V. Biology of CD1-and MR1-reactive T cells. Annual review of immunology. 2014;32:323-66.

269. Koay HF, Gherardin NA, Enders A, Loh L, Mackay LK, Almeida CF, et al. A three-stage intrathymic development pathway for the mucosal-associated invariant T cell lineage. Nat Immunol. 2016;17(11):1300-11.

270. Kovalovsky D, Uche OU, Eladad S, Hobbs RM, Yi W, Alonzo E, et al. The BTB-zinc finger transcriptional regulator PLZF controls the development of invariant natural killer T cell effector functions. Nat Immunol. 2008;9(9):1055-64.

271. Savage AK, Constantinides MG, Han J, Picard D, Martin E, Li B, et al. The transcription factor PLZF directs the effector program of the NKT cell lineage. Immunity. 2008;29(3):391-403.

272. Pellicci DG, Patel O, Kjer-Nielsen L, Pang SS, Sullivan LC, Kyparissoudis K, et al. Differential recognition of CD1d-α-galactosyl ceramide by the Vβ8. 2 and Vβ7 semi-invariant NKT T cell receptors. Immunity. 2009;31(1):47-59.

273. Wun KS, Cameron G, Patel O, Pang SS, Pellicci DG, Sullivan LC, et al. A molecular basis for the exquisite CD1d-restricted antigen specificity and functional responses of natural killer T cells. Immunity. 2011;34(3):327-39.

274. Fritsch RD, Shen X, Sims GP, Hathcock KS, Hodes RJ, Lipsky PE. Stepwise differentiation of CD4 memory T cells defined by expression of CCR7 and CD27. J Immunol. 2005;175(10):6489-97.

275. Mahnke YD, Brodie TM, Sallusto F, Roederer M, Lugli E. The who's who of T-cell differentiation: human memory T-cell subsets. Eur J Immunol. 2013;43(11):2797-809.

276. Rizzetto S, Koppstein DNP, Samir J, Singh M, Reed JH, Cai CH, et al. B-cell receptor reconstruction from single-cell RNA-seq with VDJPuzzle. Bioinformatics. 2018;34(16):2846-7.

277. Godfrey DI, MacDonald HR, Kronenberg M, Smyth MJ, Van Kaer L. NKT cells: what's in a name? Nat Rev Immunol. 2004;4(3):231-7.

278. Le Nours J, Praveena T, Pellicci DG, Gherardin NA, Ross FJ, Lim RT, et al. Atypical natural killer T-cell receptor recognition of CD1d-lipid antigens. Nature communications. 2016;7:10570.

279. Shaulian E, Karin M. AP-1 as a regulator of cell life and death. Nature cell biology. 2002;4(5):E131-E6.

280. Mittelstadt PR, Ashwell JD. Inhibition of AP-1 by the glucocorticoid-inducible protein GILZ. J Biol Chem. 2001;276(31):29603-10.

281. Finak G, McDavid A, Yajima M, Deng J, Gersuk V, Shalek AK, et al. MAST: a flexible statistical framework for assessing transcriptional changes and characterizing heterogeneity in single-cell RNA sequencing data. Genome Biol. 2015;16(1):278.

282. Campbell JJ, Butcher EC. Chemokines in tissue-specific and microenvironment-specific lymphocyte homing. Curr Opin Immunol. 2000;12(3):336-41.

283. Contento RL, Molon B, Boularan C, Pozzan T, Manes S, Marullo S, et al. CXCR4-CCR5: a couple modulating T cell functions. Proc Natl Acad Sci U S A. 2008;105(29):10101-6.

284. Kumar A, Humphreys TD, Kremer KN, Bramati PS, Bradfield L, Edgar CE, et al. CXCR4 physically associates with the T cell receptor to signal in T cells. Immunity. 2006;25(2):213-24.

285. Kino T, Hurt DE, Ichijo T, Nader N, Chrousos GP. Noncoding RNA gas5 is a growth arrest–and starvation-associated repressor of the glucocorticoid receptor. Sci Signal. 2010;3(107):ra8-ra.

286. DeFrances MC, Debelius DR, Cheng J, Kane LP. Inhibition of T-cell activation by PIK 3 IP 1. European journal of immunology. 2012;42(10):2754-9.

287. Xiong Y, Hannon GJ, Zhang H, Casso D, Kobayashi R, Beach D. p21 is a universal inhibitor of cyclin kinases. Nature. 1993;366(6456):701.

288. Lin C-C, Bradstreet TR, Schwarzkopf EA, Sim J, Carrero JA, Chou C, et al. Bhlhe40 controls cytokine production by T cells and is essential for pathogenicity in autoimmune neuroinflammation. Nature communications. 2014;5:3551.

289. Yang XO, Pappu BP, Nurieva R, Akimzhanov A, Kang HS, Chung Y, et al. T helper 17 lineage differentiation is programmed by orphan nuclear receptors RORα and RORγ. Immunity. 2008;28(1):29-39.

290. Vereecke L, Beyaert R, van Loo G. The ubiquitin-editing enzyme A20 (TNFAIP3) is a central regulator of immunopathology. Trends in immunology. 2009;30(8):383-91.

291. Lu B, Ferrandino AF, Flavell RA. Gadd45β is important for perpetuating cognate and inflammatory signals in T cells. Nature immunology. 2004;5(1):38.

292. Leeansyah E, Loh L, Nixon DF, Sandberg JK. Acquisition of innate-like microbial reactivity in mucosal tissues during human fetal MAIT-cell development. Nature communications. 2014;5(1):3143.

293. Martin E, Treiner E, Duban L, Guerri L, Laude H, Toly C, et al. Stepwise development of MAIT cells in mouse and human. PLoS Biol. 2009;7(3):e54.

294. Constantinides MG, Link VM, Tamoutounour S, Wong AC, Perez-Chaparro PJ, Han SJ, et al. MAIT cells are imprinted by the microbiota in early life and promote tissue repair. Science. 2019;366(6464):eaax6624.

295. Legoux F, Bellet D, Daviaud C, El Morr Y, Darbois A, Niort K, et al. Microbial metabolites control the thymic development of mucosal-associated invariant T cells. Science. 2019;366(6464):494-9.

296. Dale KD, Trauer JM, Dodd PJ, Houben R, Denholm JT. Estimating the prevalence of latent tuberculosis in a low-incidence setting: Australia. Eur Respir J. 2018;52(6):1801218.

297. Deshayes C, Angala SK, Marion E, Brandli I, Babonneau J, Preisser L, et al. Regulation of mycolactone, the Mycobacterium ulcerans toxin, depends on nutrient source. PLoS Negl Trop Dis. 2013;7(11):e2502.

298. O'Brien DP, Jenkin G, Buntine J, Steffen CM, McDonald A, Horne S, et al. Treatment and prevention of Mycobacterium ulcerans infection (Buruli ulcer) in Australia: guideline update. Med J Aust. 2014;200(5):267-70.

299. Collins MD, Goodfellow M, Minnikin DE. A survey of the structures of mycolic acids in Corynebacterium and related taxa. J Gen Microbiol. 1982;128(1):129-49.

300. Grice EA, Kong HH, Conlan S, Deming CB, Davis J, Young AC, et al. Topographical and temporal diversity of the human skin microbiome. Science. 2009;324(5931):1190-2.

301. Man WH, de Steenhuijsen Piters WA, Bogaert D. The microbiota of the respiratory tract: gatekeeper to respiratory health. Nat Rev Microbiol. 2017;15(5):259-70.

302. Gibbs A, Leeansyah E, Introini A, Paquin-Proulx D, Hasselrot K, Andersson E, et al. MAIT cells reside in the female genital mucosa and are biased towards IL-17 and IL-22 production in response to bacterial stimulation. Mucosal Immunol. 2017;10(1):35-45.

303. Sobkowiak MJ, Davanian H, Heymann R, Gibbs A, Emgard J, Dias J, et al. Tissue-resident MAIT cell populations in human oral mucosa exhibit an activated profile and produce IL-17. Eur J Immunol. 2019;49(1):133-43.

304. Le Bourhis L, Dusseaux M, Bohineust A, Bessoles S, Martin E, Premel V, et al. MAIT cells detect and efficiently lyse bacterially-infected epithelial cells. PLoS Pathog. 2013;9(10):e1003681.

305. Eger KA, Sundrud MS, Motsinger AA, Tseng M, Van Kaer L, Unutmaz D. Human natural killer T cells are heterogeneous in their capacity to reprogram their effector functions. PLoS One. 2006;1(1):e50.

306. Metelitsa LS, Naidenko OV, Kant A, Wu HW, Loza MJ, Perussia B, et al. Human NKT cells mediate antitumor cytotoxicity directly by recognizing target cell CD1d with bound ligand or indirectly by producing IL-2 to activate NK cells. J Immunol. 2001;167(6):3114-22.

307. Segueni N, Tritto E, Bourigault ML, Rose S, Erard F, Le Bert M, et al. Controlled Mycobacterium tuberculosis infection in mice under treatment with anti-IL-17A or IL-17F antibodies, in contrast to TNFalpha neutralization. Sci Rep. 2016;6:36923.

308. Khader SA, Bell GK, Pearl JE, Fountain JJ, Rangel-Moreno J, Cilley GE, et al. IL-23 and IL-17 in the establishment of protective pulmonary CD4+ T cell responses after vaccination and during Mycobacterium tuberculosis challenge. Nat Immunol. 2007;8(4):369-77.

309. Yoshida YO, Umemura M, Yahagi A, O'Brien RL, Ikuta K, Kishihara K, et al. Essential role of IL-17A in the formation of a mycobacterial infection-induced granuloma in the lung. The Journal of Immunology. 2010;184(8):4414-22.

310. Scriba TJ, Kalsdorf B, Abrahams D-A, Isaacs F, Hofmeister J, Black G, et al. Distinct, specific IL-17-and IL-22-producing CD4+ T cell subsets contribute to the human anti-mycobacterial immune response. The Journal of Immunology. 2008;180(3):1962-70.

311. Basile JI, Geffner LJ, Romero MM, Balboa L, Sabio y García C, Ritacco V, et al. Outbreaks of Mycobacterium tuberculosis MDR strains induce high IL-17 T-cell response in patients with MDR tuberculosis that is closely associated with high antigen load. Journal of Infectious Diseases. 2011;204(7):1054-64.

312. Jurado JO, Pasquinelli V, Alvarez IB, Pena D, Rovetta AI, Tateosian NL, et al. IL-17 and IFN-gamma expression in lymphocytes from patients with active tuberculosis correlates with the severity of the disease. J Leukoc Biol. 2012;91(6):991-1002.

313. Coulter F, Parrish A, Manning D, Kampmann B, Mendy J, Garand M, et al. IL-17 Production from T Helper 17, Mucosal-Associated Invariant T, and gammadelta Cells in Tuberculosis Infection and Disease. Front Immunol. 2017;8:1252.

314. Alonzo ES, Sant'Angelo DB. Development of PLZF-expressing innate T cells. Curr Opin Immunol. 2011;23(2):220-7.

315. Kovalovsky D, Alonzo ES, Uche OU, Eidson M, Nichols KE, Sant'Angelo DB. PLZF induces the spontaneous acquisition of memory/effector functions in T cells independently of NKT cell-related signals. J Immunol. 2010;184(12):6746-55.

316. Savage AK, Constantinides MG, Bendelac A. Promyelocytic leukemia zinc finger turns on the effector T cell program without requirement for agonist TCR signaling. The Journal of Immunology. 2011;186(10):5801-6.

317. Gapin L. Development of invariant natural killer T cells. Curr Opin Immunol. 2016;39:68-74.

318. Hintzen RQ, Lens SM, Koopman G, Pals ST, Spits H, van Lier RA. CD70 represents the human ligand for CD27. Int Immunol. 1994;6(3):477-80.

319. De Jong R, Brouwer M, Hooibrink B, van der Pouw-Kraan T, Miedema F, van Lier RA. The CD27− subset of peripheral blood memory CD4+ lymphocytes contains functionally differentiated T lymphocytes that develop by persistent antigenic stimulation in vivo. European journal of immunology. 1992;22(4):993-9.

320. Tortorella C, Schulze-Koops H, Thomas R, Splawski JB, Davis LS, Picker LJ, et al. Expression of CD45RB and CD27 identifies subsets of CD4+ memory T cells with different capacities to induce B cell differentiation. J Immunol. 1995;155(1):149-62.

321. Ribot JC, Debarros A, Pang DJ, Neves JF, Peperzak V, Roberts SJ, et al. CD27 is a thymic determinant of the balance between interferon-γ-and interleukin 17–producing γδ T cell subsets. Nature immunology. 2009;10(4):427.

322. Bohmann D, Bos TJ, Admon A, Nishimura T, Vogt PK, Tjian R. Human proto-oncogene c-jun encodes a DNA binding protein with structural and functional properties of transcription factor AP-1. Science. 1987;238(4832):1386-92.

323. Fuchs SY, Dolan L, Davis RJ, Ronai Z. Phosphorylation-dependent targeting of c-Jun ubiquitination by Jun N-kinase. Oncogene. 1996;13(7):1531-5.

324. Foletta VC, Segal DH, Cohen DR. Transcriptional regulation in the immune system: all roads lead to AP-1. Journal of leukocyte biology. 1998;63(2):139-52.

325. Sabapathy K, Kallunki T, David J-P, Graef I, Karin M, Wagner EF. c-Jun NH2-terminal kinase (JNK) 1 and JNK2 have similar and stage-dependent roles in regulating T cell apoptosis and proliferation. Journal of Experimental Medicine. 2001;193(3):317-28.

326. Cannarile L, Delfino D, Riccardi C, Ayroldi E. Mini review: Implicating the role of GILZ in glucocorticoid modulation of T cell activation. Frontiers in Immunology. 2019;10:1823.

327. Cain DW, Cidlowski JA. Immune regulation by glucocorticoids. Nat Rev Immunol. 2017;17(4):233-47.

328. Ayroldi E, Migliorati G, Bruscoli S, Marchetti C, Zollo O, Cannarile L, et al. Modulation of T-cell activation by the glucocorticoid-induced leucine zipper factor via inhibition of nuclear factor kappaB. Blood. 2001;98(3):743-53.

329. Cannarile L, Fallarino F, Agostini M, Cuzzocrea S, Mazzon E, Vacca C, et al. Increased GILZ expression in transgenic mice up-regulates Th-2 lymphokines. Blood. 2006;107(3):1039-47.

330. Bereshchenko O, Coppo M, Bruscoli S, Biagioli M, Cimino M, Frammartino T, et al. GILZ promotes production of peripherally induced Treg cells and mediates the crosstalk between glucocorticoids and TGF-β signaling. Cell reports. 2014;7(2):464-75.

331. Yosef N, Shalek AK, Gaublomme JT, Jin H, Lee Y, Awasthi A, et al. Dynamic regulatory network controlling T H 17 cell differentiation. Nature. 2013;496(7446):461.

332. Jones SA, Perera DN, Fan H, Russ BE, Harris J, Morand EF. GILZ regulates Th17 responses and restrains IL-17-mediated skin inflammation. J Autoimmun. 2015;61:73-80.

333. Slavin DA, Koritschoner NP, Prieto CC, López-Díaz FJ, Chatton B, Bocco JL. A new role for the Krüppel-like transcription factor KLF6 as an inhibitor of c-Jun proto-oncoprotein function. Oncogene. 2004;23(50):8196.

334. Su B, Jacinto E, Hibi M, Kallunki T, Karin M, Ben-Neriah Y. JNK is involved in signal integration during costimulation of T lymphocytes. Cell. 1994;77(5):727-36.

335. Bettelli E, Korn T, Kuchroo VK. Th17: the third member of the effector T cell trilogy. Curr Opin Immunol. 2007;19(6):652-7.

336. Mangan PR, Harrington LE, O'Quinn DB, Helms WS, Bullard DC, Elson CO, et al. Transforming growth factor-beta induces development of the T(H)17 lineage. Nature. 2006;441(7090):231-4.

337. Veldhoen M, Hocking RJ, Atkins CJ, Locksley RM, Stockinger B. TGFbeta in the context of an inflammatory cytokine milieu supports de novo differentiation of IL-17-producing T cells. Immunity. 2006;24(2):179-89.

338. Manel N, Unutmaz D, Littman DR. The differentiation of human T(H)-17 cells requires transforming growth factor-beta and induction of the nuclear receptor RORgammat. Nat Immunol. 2008;9(6):641-9.

339. Miyazaki K, Miyazaki M, Guo Y, Yamasaki N, Kanno M, Honda Z, et al. The role of the basic helix-loop-helix transcription factor Dec1 in the regulatory T cells. J Immunol. 2010;185(12):7330-9.

340. Kanda M, Yamanaka H, Kojo S, Usui Y, Honda H, Sotomaru Y, et al. Transcriptional regulator Bhlhe40 works as a cofactor of T-bet in the regulation of IFN-γ production in iNKT cells. Proceedings of the National Academy of Sciences. 2016;113(24):E3394-E402.

341. Slauenwhite D, Johnston B. Regulation of NKT Cell Localization in Homeostasis and Infection. Front Immunol. 2015;6:255.

342. Feng Y, Broder CC, Kennedy PE, Berger EA. HIV-1 entry cofactor: functional cDNA cloning of a seven-transmembrane, G protein-coupled receptor. Science. 1996;272(5263):872-7.

343. Connor RI, Sheridan KE, Ceradini D, Choe S, Landau NR. Change in coreceptor use correlates with disease progression in HIV-1–infected individuals. Journal of Experimental Medicine. 1997;185(4):621-8.

344. Bell LCK, Noursadeghi M. Pathogenesis of HIV-1 and Mycobacterium tuberculosis co-infection. Nat Rev Microbiol. 2018;16(2):80-90.

345. Goletti D, Weissman D, Jackson RW, Graham NM, Vlahov D, Klein RS, et al. Effect of Mycobacterium tuberculosis on HIV replication. Role of immune activation. J Immunol. 1996;157(3):1271-8.

346. Kalsdorf B, Scriba TJ, Wood K, Day CL, Dheda K, Dawson R, et al. HIV-1 infection impairs the bronchoalveolar T-cell response to mycobacteria. Am J Respir Crit Care Med. 2009;180(12):1262-70.

347. Kinjo Y, Takatsuka S, Kitano N, Kawakubo S, Abe M, Ueno K, et al. Functions of CD1d-Restricted Invariant Natural Killer T Cells in Antimicrobial Immunity and Potential Applications for Infection Control. Front Immunol. 2018;9:1266.

348. Gaya M, Barral P, Burbage M, Aggarwal S, Montaner B, Warren Navia A, et al. Initiation of Antiviral B Cell Immunity Relies on Innate Signals from Spatially Positioned NKT Cells. Cell. 2018;172(3):517-33 e20.

349. Hartmann N, Harriff MJ, McMurtrey CP, Hildebrand WH, Lewinsohn DM, Kronenberg M. Role of MAIT cells in pulmonary bacterial infection. Molecular immunology. 2018;101:155-9.

350. Ussher JE, Willberg CB, Klenerman P. MAIT cells and viruses. Immunol Cell Biol. 2018;96(6):630-41.

351. Deroost K, Langhorne J. Gamma/delta T cells and their role in protection against malaria. Frontiers in immunology. 2018;9:2973.

352. Godfrey DI, Le Nours J, Andrews DM, Uldrich AP, Rossjohn J. Unconventional T Cell Targets for Cancer Immunotherapy. Immunity. 2018;48(3):453-73.

353. Bandyopadhyay K, Marrero I, Kumar V. NKT cell subsets as key participants in liver physiology and pathology. Cell Mol Immunol. 2016;13(3):337-46.

354. Kurioka A, Walker LJ, Klenerman P, Willberg CB. MAIT cells: new guardians of the liver. Clin Transl Immunology. 2016;5(8):e98.

355. Van Kaer L, Wu L. Therapeutic Potential of Invariant Natural Killer T Cells in Autoimmunity. Front Immunol. 2018;9:519.

356. Rouxel O, Lehuen A. Mucosal-associated invariant T cells in autoimmune and immune-mediated diseases. Immunol Cell Biol. 2018;96(6):618-29.

357. Malik S, Want MY, Awasthi A. The Emerging Roles of Gamma-Delta T Cells in Tissue Inflammation in Experimental Autoimmune Encephalomyelitis. Front Immunol. 2016;7:14.

358. Hammond KJ, Pellicci DG, Poulton LD, Naidenko OV, Scalzo AA, Baxter AG, et al. CD1d-restricted NKT cells: an interstrain comparison. J Immunol. 2001;167(3):1164-73.

359. Benlagha K, Weiss A, Beavis A, Teyton L, Bendelac A. In vivo identification of glycolipid antigen-specific T cells using fluorescent CD1d tetramers. J Exp Med. 2000;191(11):1895-903.

360. Sidobre S, Kronenberg M. CD1 tetramers: a powerful tool for the analysis of glycolipid-reactive T cells. J Immunol Methods. 2002;268(1):107-21.

361. Juno JA, Wragg KM, Amarasena T, Meehan BS, Mak JYW, Liu L, et al. MAIT Cells Upregulate alpha4beta7 in Response to Acute Simian Immunodeficiency Virus/Simian HIV Infection but Are Resistant to Peripheral Depletion in Pigtail Macaques. J Immunol. 2019;202(7):2105-20.

362. Lopez-Sagaseta J, Dulberger CL, McFedries A, Cushman M, Saghatelian A, Adams EJ. MAIT recognition of a stimulatory bacterial antigen bound to MR1. J Immunol. 2013;191(10):5268-77.

363. Xiao Z, Mescher MF, Jameson SC. Detuning CD8 T cells: down-regulation of CD8 expression, tetramer binding, and response during CTL activation. J Exp Med. 2007;204(11):2667-77.

364. Crooks ME, Littman DR. Disruption of T lymphocyte positive and negative selection in mice lacking the CD8 beta chain. Immunity. 1994;1(4):277-85.

365. Fung-Leung W-P, Schilham MW, Rahemtulla A, Kündig TM, Vollenweider M, Potter J, et al. CD8 is needed for development of cytotoxic T but not helper T cells. Cell. 1991;65(3):443-9.

366. Daniels MA, Devine L, Miller JD, Moser JM, Lukacher AE, Altman JD, et al. CD8 binding to MHC class I molecules is influenced by T cell maturation and glycosylation. Immunity. 2001;15(6):1051-61.

367. Moody AM, Chui D, Reche PA, Priatel JJ, Marth JD, Reinherz EL. Developmentally regulated glycosylation of the CD8alphabeta coreceptor stalk modulates ligand binding. Cell. 2001;107(4):501-12.

368. Walker LJ, Kang Y-H, Smith MO, Tharmalingham H, Ramamurthy N, Fleming VM, et al. Human MAIT and CD8αα cells develop from a pool of type-17 precommitted CD8+ T cells. Blood, The Journal of the American Society of Hematology. 2012;119(2):422-33.

369. Rahimpour A, Koay HF, Enders A, Clanchy R, Eckle SB, Meehan B, et al. Identification of phenotypically and functionally heterogeneous mouse mucosal-associated invariant T cells using MR1 tetramers. J Exp Med. 2015;212(7):1095-108.

370. Konig R, Huang LY, Germain RN. MHC class II interaction with CD4 mediated by a region analogous to the MHC class I binding site for CD8. Nature. 1992;356(6372):796-8.

371. Wang XX, Li Y, Yin Y, Mo M, Wang Q, Gao W, et al. Affinity maturation of human CD4 by yeast surface display and crystal structure of a CD4-HLA-DR1 complex. Proc Natl Acad Sci U S A. 2011;108(38):15960-5.

372. Burmeister WP, Gastinel LN, Simister NE, Blum ML, Bjorkman PJ. Crystal structure at 2.2 Å resolution of the MHC-related neonatal Fc receptor. Nature. 1994;372(6504):336.

373. Klein L, Robey EA, Hsieh CS. Central CD4(+) T cell tolerance: deletion versus regulatory T cell differentiation. Nat Rev Immunol. 2019;19(1):7-18.

374. Moran AE, Holzapfel KL, Xing Y, Cunningham NR, Maltzman JS, Punt J, et al. T cell receptor signal strength in Treg and iNKT cell development demonstrated by a novel fluorescent reporter mouse. J Exp Med. 2011;208(6):1279-89.

375. Pobezinsky LA, Angelov GS, Tai X, Jeurling S, Van Laethem F, Feigenbaum L, et al. Clonal deletion and the fate of autoreactive thymocytes that survive negative selection. Nature immunology. 2012;13(6):569.

376. Cameron G, Godfrey DI. Differential surface phenotype and context-dependent reactivity of functionally diverse NKT cells. Immunol Cell Biol. 2018.

377. Shevach EM. Mechanisms of foxp3+ T regulatory cell-mediated suppression. Immunity. 2009;30(5):636-45.

378. Krutzik SR, Tan B, Li H, Ochoa MT, Liu PT, Sharfstein SE, et al. TLR activation triggers the rapid differentiation of monocytes into macrophages and dendritic cells. Nature medicine. 2005;11(6):653-60.

379. Yakimchuk K, Roura-Mir C, Magalhaes KG, de Jong A, Kasmar AG, Granter SR, et al. Borrelia burgdorferi infection regulates CD1 expression in human cells and tissues via IL1-beta. Eur J Immunol. 2011;41(3):694-705.

380. Furlan R, Bergami A, Cantarella D, Brambilla E, Taniguchi M, Dellabona P, et al. Activation of invariant NKT cells by alphaGalCer administration protects mice from MOG35-55-induced EAE: critical roles for administration route and IFN-gamma. Eur J Immunol. 2003;33(7):1830-8.

381. Jahng AW, Maricic I, Pedersen B, Burdin N, Naidenko O, Kronenberg M, et al. Activation of natural killer T cells potentiates or prevents experimental autoimmune encephalomyelitis. J Exp Med. 2001;194(12):1789-99.

382. Zeng D, Liu Y, Sidobre S, Kronenberg M, Strober S. Activation of natural killer T cells in NZB/W mice induces Th1-type immune responses exacerbating lupus. J Clin Invest. 2003;112(8):1211-22.

383. Venken K, Jacques P, Mortier C, Labadia ME, Decruy T, Coudenys J, et al. RORgammat inhibition selectively targets IL-17 producing iNKT and gammadelta-T cells enriched in Spondyloarthritis patients. Nature communications. 2019;10(1):9.

384. Floyd K, Glaziou P, Zumla A, Raviglione M. The global tuberculosis epidemic and progress in care, prevention, and research: an overview in year 3 of the End TB era. Lancet Respir Med. 2018;6(4):299-314.

385. Fischer K, Scotet E, Niemeyer M, Koebernick H, Zerrahn J, Maillet S, et al. Mycobacterial phosphatidylinositol mannoside is a natural antigen for CD1d-restricted T cells. Proceedings of the National Academy of Sciences. 2004;101(29):10685-90.

386. Kasmar AG, Van Rhijn I, Magalhaes KG, Young DC, Cheng TY, Turner MT, et al. Cutting Edge: CD1a tetramers and dextramers identify human lipopeptide-specific T cells ex vivo. J Immunol. 2013;191(9):4499-503.

387. Ly D, Kasmar AG, Cheng TY, de Jong A, Huang S, Roy S, et al. CD1c tetramers detect ex vivo T cell responses to processed phosphomycoketide antigens. J Exp Med. 2013;210(4):729-41.

388. Fergusson JR, Smith KE, Fleming VM, Rajoriya N, Newell EW, Simmons R, et al. CD161 defines a transcriptional and functional phenotype across distinct human T cell lineages. Cell Rep. 2014;9(3):1075-88.

389. Reinink P, Van Rhijn I. Mammalian CD1 and MR1 genes. Immunogenetics. 2016;68(8):515-23.

390. Brigl M, Brenner MB. CD1: antigen presentation and T cell function. Annu Rev Immunol. 2004;22:817-90.

391. Morita D, Hattori Y, Nakamura T, Igarashi T, Harashima H, Sugita M. Major T cell response to a mycolyl glycolipid is mediated by CD1c molecules in rhesus macaques. Infect Immun. 2013;81(1):311-6.

392. Morita D, Katoh K, Harada T, Nakagawa Y, Matsunaga I, Miura T, et al. Trans-species activation of human T cells by rhesus macaque CD1b molecules. Biochem Biophys Res Commun. 2008;377(3):889-93.

393. Komori T, Nakamura T, Matsunaga I, Morita D, Hattori Y, Kuwata H, et al. A microbial glycolipid functions as a new class of target antigen for delayed-type hypersensitivity. J Biol Chem. 2011;286(19):16800-6.

Appendices

Appendix I: Soluble protein sequences

Table AI.1. Soluble human protein sequences and expression systems.

Protein	Expression system	Expression vector	Protein sequence
WT MR1	E. coli	pET30	MRTHSLRYFRLGVSDPIHGVPEFISVGYVDSHPITTYDSVTRQKEPRAPWMA ENLAPDHWERYTQLLRGWQQMFKVELKRLQRHYNHSGSHTYQRMIGCELLED GSTTGFLQYAYDGQDFLIFNKDTLSWLAVDNVAHTIKQAWEANQHELLYQKN WLEEECIAWLKRFLEYGKDTLQRTEPPLVRVNRKETFPGVTALFCKAHGFYP PEIYMTWMKNGEEIVQEIDYGDILPSGDGTYQAWASIELDPQSSNLYSCHVE HSGVHMVLQVPC
CD8-null MR1	E. coli	pET30	MRTHSLRYFRLGVSDPIHGVPEFISVGYVDSHPITTYDSVTRQKEPRAPWMA ENLAPDHWERYTQLLRGWQQMFKVELKRLQRHYNHSGSHTYQRMIGCELLED GSTTGFLQYAYDGQDFLIFNKDTLSWLAVDNVAHTIKQAWEANQHELLYQKN WLEEECIAWLKRFLEYGKDTLQRTEPPLVRVNRKETFPGVTALFCKAHGFYP PEIYMTWMKNGEEIVAKIDYGDILPSGDGTYQAWASIELDPQSSNLYSCHVE HSGVHMVLQVPC
WT HLA-A2	E. coli	pET30	MGSHSMRYFFTSVSRPGRGEPRFIAVGYVDDTQFVRFDSDAASQRMEPRAPW IEQEGPEYWDGETRKVKAHSQTHRVDLGTLRGYYNQSEAGSHTVQRMYGCDV GSDWRFLRGYHQYAYDGKDYIALKEDLRSWTAADMAAQTTKHKWEAAHVAEQ LRAYLEGTCVEWLRRYLENGKETLQRTDAPKTHMTHHAVSDHEATLRCWALS FYPAEITLTWQRDGEDQTQDTELVETRPAGDGTFQKWAAVVVPSGQEQRYTC HVQHEGLPKPLTLRWEPGSLHHILDAQKMVWNHR
CD8-null HLA-A2-BirA	E. coli	pET30	MGSHSMRYFFTSVSRPGRGEPRFIAVGYVDDTQFVRFDSDAASQRMEPRAPW IEQEGPEYWDGETRKVKAHSQTHRVDLGTLRGYYNQSEAGSHTVQRMYGCDV GSDWRFLRGYHQYAYDGKDYIALKEDLRSWTAADMAAQTTKHKWEAAHVAEQ LRAYLEGTCVEWLRRYLENGKETLQRTDAPKTHMTHHAVSDHEATLRCWALS FYPAEITLTWQRDGEDQTQKAELVETRPAGDGTFQKWAAVVVPSGQEQRYTC HVQHEGLPKPLTLRWEPGSGGGLNDIFEAQKIEWHE
CD8-enhancing HLA-A2-BirA	E. coli	pET30	MGSHSMRYFFTSVSRPGRGEPRFIAVGYVDDTQFVRFDSDAASQRMEPRAPW IEQEGPEYWDGETRKVKAHSQTHRVDLGTLRGYYNQSEAGSHTVQRMYGCDV GSDWRFLRGYHEYAYDGKDYIALKEDLRSWTAADMAAQTTKHKWEAAHVAEQ LRAYLEGTCVEWLRRYLENGKETLQRTDAPKTHMTHHAVSDHEATLRCWALS FYPAEITLTWQRDGEDQTQDTELVETRPAGDGTFQKWAAVVVPSGQEQRYTC HVQHEGLPKPLTLRWEPGSGGGLNDIFEAQKIEWHE
β_2m	E. coli	pET30	MIQRTPKIQVYSRHPAENGKSNFLNCYVSGFHPSDIEVDLLKNGERIEKVEH SDLSFSKDWSFYLLYYTEFTPTEKDEYACRVNHVTLSQPKIVKWDRDM

Table AI.1.(cont.)

Protein	Expression system	Expression vector	Protein sequence
1.27 TCRα	E. coli	pET30	MTQLLEQSPQFLSIQEGENLTVYCNSSSVFSSLQWYRQEPGEGPVLLVTVV TGGEVKKLKRLTFQFGDARKDSSLHITAAQPGDTGLYLCAGPRLSGGSNYK LTFGKGTLLTVNPNIQNPDPAVYQLRDSKSSDKSVCLFTDFDSQTNVSQSK DSDVYITDKCVLDMRSMDFKSNSAVAWSNKSDFACANAFNNSIIPEDTFFP SPESS
1.27 TCRβ	E. coli	pET30	MEAGVTQSPTHLIKTRGQQATLRCSPISGHTSVYWYQQALGLGLQFLLWYD EGEERNRGNFPPRFSGRQFPNYSSELNVNALELEDSALYLCASSSGHSTNE KLFFGSGTQLSVLEDLKNVFPPEVAVFEPSEAEISHTQKATLVCLATGFYP DHVELSWWVNGKEVHSGVCTDPQPLKEQPALNDSRYALSSRLRVSATFWQN PRNHFRCQVQFYGLSENDEWTQDRAKPVTQIVSAEAWGRAD
4.17 TCRβ	E. coli	pET30	MSMDTGITQTPKYLVTAMGSKRTMKREHLGHDSMYWYRQKAKKSLEFMFYY NCKEFIENKTVPNHFTPECPDSSRLYLHVVALQQEDSAAYLCASSQNRGRG DHYEQYFGPGTRLTVTDLKNVFPPEVAVFEPSEAEISHTQKATLVCLATGF YPDHVELSWWVNGKEVHSGVCTDPQPLKEQPALNDSRYALSSRLRVSATFW QNPRNHFRCQVQFYGLSENDEWTQDRAKPVTQIVSAEAWGRAD
CD8α	E. coli	pET30	MSQFRVSPLDRTWNLGETVELKCQVLLSNPTSGSSWLFQPRGAAASPTFLL YLSQNKPKAAEGLDTQRFSGKRLGDTFVLTLSDFRRENEGYYFCSALSNSI MYFSHFVPVFLPAKPTTTP
CD8α-His_6	E. coli	pET30	MSQFRVSPLDRTWNLGETVELKCQVLLSNPTSGSSWLFQPRGAAASPTFLL YLSQNKPKAAEGLDTQRFSGKRLGDTFVLTLSDFRRENEGYYFCSALSNSI MYFSHFVPVFLPAKPTTTPHHHHHH
CD1b-BirA	E. coli/ GNTI⁻ HEK 293S cells	pET30/ pHLsec	MGSEHAFQGPTSFHVIQTSSFTNSTWAQTQGSGWLDDLQIHGWDSDSGTAI FLKPWSKGNFSDKEVAELEEIFRVYIFGFAREVQDFAGDFQMKYPFEIQGI AGCELHSGGAIVSFLRGALGGLDFLSVKNASCVPSPEGGSRAQKFCALIIQ YQGIMETVRILLYETCPRYLLGVLNAGKADLQRQVKPEAWLSSGPSPGPGR LQLVCHVSGFYPKPVWVMWMRGEQEQQGTQLGDILPNANWTWYLRATLDVA DGEAAGLSCRVKHSSLEGQDIILYWGPGSGGGLNDIFEAQKIEWHEHHHHH H
CD8α-RLS	GNTI⁻ HEK 293S cells	pHLsec	TGSQFRVSPLDRTWNLGETVELKCQVLLSNPTSGSSWLFQPRGAAASPTFL LYLSQNKPKAAEGLDTQRFSGKRLGDTFVLTLSDFRRENEGYYFCSALSNS IMYFSHFVPVFLPAKPTTTKPVTRAPTPVPPPTGTPRPLRPEACRPGASGS VEGMGLGFACDIHHHHHH

Appendix II: Transfected protein sequences

Table AII.1. Sequences of human proteins transfected into cell lines.

Protein	Transfection vector	Protein sequence
WT MR1	pMIG-II	MGELMAFLLPLIIVLMVKHSDSRTHSLRYFRLGVSDPIHGVPEFISVGYVDSHPITTYDSV TRQKEPRAPWMAENLAPDHWERYTQLLRGWQQMFKVELKRLQRHYNHSGSHTYQRMIGCEL LEDGSTTGFLQYAYDGQDFLIFNKDTLSWLAVDNVAHTIKQAWEANQHELLYQKNWLEEEC IAWLKRFLEYGKDTLQRTEPPLVRVNRKETFPGVTALFCKAHGFYPPEIYMTWMKNGEEIV QEIDYGDILPSGDGTYQAWASIELDPQSSNLYSCHVEHCGVHMVLQVPQESETIPLVMKAV SGSIVLVIVLAGVGVLVWRRRPREQNGAIYLPTPDR
CD8-null MR1	pMIG-II	MGELMAFLLPLIIVLMVKHSDSRTHSLRYFRLGVSDPIHGVPEFISVGYVDSHPITTYDSV TRQKEPRAPWMAENLAPDHWERYTQLLRGWQQMFKVELKRLQRHYNHSGSHTYQRMIGCEL LEDGSTTGFLQYAYDGQDFLIFNKDTLSWLAVDNVAHTIKQAWEANQHELLYQKNWLEEEC IAWLKRFLEYGKDTLQRTEPPLVRVNRKETFPGVTALFCKAHGFYPPEIYMTWMKNGEEIV AKIDYGDILPSGDGTYQAWASIELDPQSSNLYSCHVEHCGVHMVLQVPQESETIPLVMKAV SGSIVLVIVLAGVGVLVWRRRPREQNGAIYLPTPDR
CD3-P2A	pMIG-II	MEHSTFLSGLVLATLLSQVSPFKIPIEELEDRVFVNCNTSITWVEGTVGTLLSDITRLDLG KRILDPRGIYRCNGTDIYKDKESTVQVHYRMCQSCVELDPATVAGIIVTDVIATLLLALGV FCFAGHETGRLSGAADTQALLRNDQVYQPLRDRDDAQYSHLGGNWARNKVKQTLNFDLLKL AGDVESNPGPMEQGKGLAVLILAIILLQGTLAQSIKGNHLVKVYDYQEDGSVLLTCDAEAK NITWFKDGKMIGFLTEDKKKWNLGSNAKDPRGMYQCKGSQNKSKPLQVYYRMCQNCIELNA ATISGFLFAEIVSIFVLAVGVYFIAGQDGVRQSRASDKQTLLPNDQLYQPLKDREDDQYSH LQGNQLRRNEGRGSLLTCGDVEENPGPMQSGTHWRVLGLCLLSVGVWGQDGNEEMGGITQT PYKVSISGTTVILTCPQYPGSEILWQHNDKNIGGDEDDKNIGSDEDHLSLKEFSELEQSGY YVCYPRGSKPEDANFYLYLRARVCENCMEMDVMSVATIVIVDICITGGLLLLVYYWSKNRK AKAKPVTRGAGAGGRQRGQNKERPPPVPNPDYEPIRKGQRDLYSGLNQRRIQCTNYALLKL AGDVESNPGPMKWKALFTAAILQAQLPITEAQSFGLLDPKLCYLLDGILFIYGVILTALFL RVKFSRSADAPAYQQGQNQLYNELNLGRREEYDVLDKRRGRDPEMGGKPQRRKNPQEGLYN ELQKDKMAEAYSEIGMKGERRRGKGHDGLYQGLSTATKDTYDALHMQALPPR
WT CD1b	pMIG-II	MLLLPFQLLAVLFPGGNSEHAFQGPTSFHVIQTSSFTNSTWAQTQGSGWLDDLQIHGWDSD SGTAIFLKPWSKGNFSDKEVAELEEIFRVYIFGFAREVQDFAGDFQMKYPFEIQGIAGCEL HSGGAIVSFLRGALGGLDFLSVKNASCVPSPEGGSRAQKFCALIIQYQGIMETVRILLYET CPRYLLGVLNAGKADLQRQVKPEAWLSSGPSPGPGRLQLVCHVSGFYPKPVWVMWMRGEQE QQGTQLGDILPNANWTWYLRATLDVADGEAAGLSCRVKHSSLEGQDIILYWRNPTSIGSIV LAIIVPSLLLLLCLALWYMRRRSYQNIP
PG10 TCR	pMIG-II	MTSIRAVFIFLWLQLDLVNGENVEQHPSTLSVQEGDSAVIKCTYSDSASNYFPWYKQELGK GPQLIIDIRSNVGEKKDQRIAVTLNKTAKHFSLHITETQPEDSAVYFCAASKRGFQKLVFG TGTRLLVSPNIQNPDPAVYQLRDSKSSDKSVCLFTDFDSQTNVSQSKDSDVYITDKTVLDM RSMDFKSNSAVAWSNKSDFACANAFNNSIIPEDTFFPSPESSCDVKLVEKSFETDTNLNFQ NLSVIGFRILLLKVAGFNLLMTLRLWSSGSGATNFSLLKQAGDVEENPGPMGCRLLCCAVL CLLGAVPIDTEVTQTPKHLVMGMTNKKSLKCEQHMGHRAMYWYKQKAKKPPELMFVYSYEK LSINESVPSRFSPECPNSSLLNLHLHALQPEDSALYLCASSQPPLGVGTDTQYFGPGTRLT VLEDLKNVFPPEVAVFEPSEAEISHTQKATLVCLATGFYPDHVELSWWVNGKEVHSGVSTD PQPLKEQPALNDSRYCLSSRLRVSATFWQNPRNHFRCQVQFYGLSENDEWTQDRAKPVTQI VSAEAWGRADCGFTSESYQQGVLSATILYEILLGKATLYAVLVSALVLMAMVKRKDSRG

Table AII.1. (cont.).

Protein	Transfection vector	Protein sequence
PG90 TCR	pMIG-II	MRLVARVTVFLTFGTIIDAKTTQPPSMDCAEGRAANLPCNHSTISGNEYVYWYRQIHSQGP QYIIHGLKNNETNEMASLIITEDRKSSTLILPHATLRDTAVYYCIVRVAYRQKVTFGTGTK LQVIPNIQNPDPAVYQLRDSKSSDKSVCLFTDFDSQTNVSQSKDSDVYITDKTVLDMRSMD FKSNSAVAWSNKSDFACANAFNNSIIPEDTFFPSPESSCDVKLVEKSFETDTNLNFQNLSV IGFRILLLKVAGFNLLMTLRLWSSGSGATNFSLLKQAGDVEENPGPMGTRLLCWVVLGFLG TDHTGAGVSQSPRYKVAKRGQDVALRCDPISGHVSLFWYQQALGQGPEFLTYFQNEAQLDK SGLPSDRFFAERPEGSVSTLKIQRTQQEDSAVYLCASSLARAQGASNTGELFFGEGSRLTV LEDLKNVFPPEVAVFEPSEAEISHTQKATLVCLATGFYPDHVELSWWVNGKEVHSGVSTDP QPLKEQPALNDSRYCLSSRLRVSATFWQNPRNHFRCQVQFYGLSENDEWTQDRAKPVTQIV SAEAWGRADCGFTSESYQQGVLSATILYEILLGKATLYAVLVSALVLMAMVKRKDSRG
1.27 TCR	pMIG-II	MVLKFSVSILWIQLAWVSTQLLEQSPQFLSIQEGENLTVYCNSSSVFSSLQWYRQEPGEGP VLLVTVVTGGEVKKLKRLTFQFGDARKDSSLHITAAQPGDTGLYLCAGPRLSGGSNYKLTF GKGTLLTVNPNIQNPDPAVYQLRDSKSSDKSVCLFTDFDSQTNVSQSKDSDVYITDKTVLD MRSMDFKSNSAVAWSNKSDFACANAFNNSIIPEDTFFPSPESSCDVKLVEKSFETDTNLNF QNLSVIGFRILLLKVAGFNLLMTLRLWSSGSGATNFSLLKQAGDVEENPGPMGPRLLFWAL LCLLGTGPVEAGVTQSPTHLIKTRGQQATLRCSPISGHTSVYWYQQALGLGLQFLLWYDEG EERNRGNFPPRFSGRQFPNYSSELNVNALELEDSALYLCASSSGHSTNEKLFFGSGTQLSV LEDLKNVFPPEVAVFEPSEAEISHTQKATLVCLATGFYPDHVELSWWVNGKEVHSGVSTDP QPLKEQPALNDSRYCLSSRLRVSATFWQNPRNHFRCQVQFYGLSENDEWTQDRAKPVTQIV SAEAWGRADCGFTSESYQQGVLSATILYEILLGKATLYAVLVSALVLMAMVKRKDSRG
4.17 TCR	pMIG-II	METLLGVSLVILWLQLARVNSQQGEEDPQALSIQEGENATMNCSYKTSINNLQWYRQNSGR GLVHLILIRSNEREKHSGRLRVTLDTSKKSSSLLITASRAADTASYFCAAQMGYSTLTFGK GTMLLVSPDIQNPDPAVYQLRDSKSSDKSVCLFTDFDSQTNVSQSKDSDVYITDKTVLDMR SMDFKSNSAVAWSNKSDFACANAFNNSIIPEDTFFPSPESSCDVKLVEKSFETDTNLNFQN LSVIGFRILLLKVAGFNLLMTLRLWSSGSGATNFSLLKQAGDVEENPGMSISLLCCAAFPL LWAGPVNAGVTQTPKFRILKIGQSMTLQCTQDMNHNYMYWYRQDPGMGLKLIYYSVGAGIT DKGEVPNGYNVSRSTTEDFPLRLELAAPSQTSVYFCASSQNRGRGDHYEQYFGPGTRLTVT EDLKNVFPPEVAVFEPSEAEISHTQKATLVCLATGFYPDHVELSWWVNGKEVHSGVSTDPQ PLKEQPALNDSRYCLSSRLRVSATFWQNPRNHFRCQVQFYGLSENDEWTQDRAKPVTQIVS AEAWGRADCGFTSESYQQGVLSATILYEILLGKATLYAVLVSALVLMAMVKRKDSRG
4.13-2 TCR	pMIG-II	MAGIRALFMYLWLQLDWVSRGESVGLHLPTLSVQEGDNSIINCAYSNSASDYFIWYKQESG KGPQFIIDIRSNMDKRQGQRVTVLLNKTVKHLSLQIAATQPGDSAVYFCAENRYAGGTSYG KLTFGQGTILTVHPNIQNPDPAVYQLRDSKSSDKSVCLFTDFDSQTNVSQSKDSDVYITDK TVLDMRSMDFKSNSAVAWSNKSDFACANAFNNSIIPEDTFFPSPESSCDVKLVEKSFETDT NLNFQNLSVIGFRILLLKVAGFNLLMTLRLWSSGSGATNFSLLKQAGDVEENPGPMSNQVL CCVVLCFLGANTVDGGITQSPKYLFRKEGQNVTLSCEQNLNHDAMYWYRQDPGQGLRLIYY SQIVNDFQKGDIAEGYSVSREKKESFPLTVTSAQKNPTAFYLCASSLTSVAKNIQYFGAGT RLSVLEDLKNVFPPEVAVFEPSEAEISHTQKATLVCLATGFYPDHVELSWWVNGKEVHSGV STDPQPLKEQPALNDSRYCLSSRLRVSATFWQNPRNHFRCQVQFYGLSENDEWTQDRAKPV TQIVSAEAWGRADCGFTSESYQQGVLSATILYEILLGKATLYAVLVSALVLMAMVKRKDSR G

Table AII.1. (cont.).

Protein	Transfection vector	Protein sequence
4.27 TCR	pMIG-II	MVLKFSVSILWIQLAWVSTQLLEQSPQFLSIQEGENLTVYCNSSSVFSSLQWYRQEPGEGP VLLVTVVTGGEVKKLKRLTFQFGDARKDSSLHITAAQPGDTGLYLCAGPRYSGGSNYKLTF GKGTLLTVNPNIQNPDPAVYQLRDSKSSDKSVCLFTDFDSQTNVSQSKDSDVYITDKTVLD MRSMDFKSNSAVAWSNKSDFACANAFNNSIIPEDTFFPSPESSCDVKLVEKSFETDTNLNF QNLSVIGFRILLLKVAGFNLLMTLRLWSSGSGATNFSLLKQAGDVEENPGPMGPGLLCWVL LCLLGAGSVETGVTQSPTHLIKTRGQQVTLRCSSQSGHNTVSWYQQALGQGPQFIFQYYRE EENGRGNFPPRFSGLQFPNYSSELNVNALELDDSALYLCASSDRDIAKNIQYFGAGTRLSV LEDLKNVFPPEVAVFEPSEAEISHTQKATLVCLATGFYPDHVELSWWVNGKEVHSGVSTDP QPLKEQPALNDSRYCLSSRLRVSATFWQNPRNHFRCQVQFYGLSENDEWTQDRAKPVTQIV SAEAWGRADCGFTSESYQQGVLSATILYEILLGKATLYAVLVSALVLMAMVKRKDSRG
4.41 TCR	pMIG-II	MVKIRQFLLAILWLQLSCVSAAKNEVEQSPQNLTAQEGEFITINCSYSVGISALHWLQQHP GGGIVSLFMLSSGKKKHGRLIATINIQEKHSSLHITASHPRDSAVYICAVLSGSARQLTFF GSGTQLTVLPNIQNPDPAVYQLRDSKSSDKSVCLFTDFDSQTNVSQSKDSDVYITDKTVLD MRSMDFKSNSAVAWSNKSDFACANAFNNSIIPEDTFFPSPESSCDVKLVEKSFETDTNLNF QNLSVIGFRILLLKVAGFNLLMTLRLWSSGSGATNFSLLKQAGDVEENPGPMSLGLLCCGA FSLLWAGPVNAGVTQTPKFRVLKTGQSMTLLCAQDMNHEYMYWYRQDPGMGLRLIHYSVGE GTTAKGEVPDGYNVSRLKKQNFLLGLESAAPSQTSVYFCASSYLRGRSYEQYFGPGTRLTV TEDLKNVFPPEVAVFEPSEAEISHTQKATLVCLATGFYPDHVELSWWVNGKEVHSGVSTDP QPLKEQPALNDSRYCLSSRLRVSATFWQNPRNHFRCQVQFYGLSENDEWTQDRAKPVTQIV SAEAWGRADCGFTSESYQQGVLSATILYEILLGKATLYAVLVSALVLMAMVKRKDSRG
TCR42 **(135)**	pMIG-II	MWGVFLLYVSMKMGGTTGQNIDQPTEMTATEGAIVQINCTYQTSGFNGLFWYQQHAGEAPT FLSYNVLDGLEEKGRFSSFLSRSKGYSYLLLKELQMKDSASYLCAVRNTGGFKTIFGAGTR LFVKANIQNPDPAVYQLRDSKSSDKSVCLFTDFDSQTNVSQSKDSDVYITDKTVLDMRSMD FKSNSAVAWSNKSDFACANAFNNSIIPEDTFFPSPESSCDVKLVEKSFETDTNLNFQNLSV IGFRILLLKVAGFNLLMTLRLWSSGSGATNFSLLKQAGDVEENPGPMSLGLLCCGAFSLLW AGPVNAGVTQTPKFRVLKTGQSMTLLCAQDMNHEYMYWYRQDPGMGLRLIHYSVGEGTTAK GEVPDGYNVSRLKKQNFLLGLESAAPSQTSVYFCASSPRLAGDEQFFGPGTRLTVLEDLKN VFPPEVAVFEPSEAEISHTQKATLVCLATGFYPDHVELSWWVNGKEVHSGVSTDPQPLKEQ PALNDSRYCLSSRLRVSATFWQNPRNHFRCQVQFYGLSENDEWTQDRAKPVTQIVSAEAWG RADCGFTSESYQQGVLSATILYEILLGKATLYAVLVSALVLMAMVKRKDSRG
CD8α	pMIG-II	MALPVTALLLPLALLLHAARPSQFRVSPLDRTWNLGETVELKCQVLLSNPTSGCSWLFQPR GAAASPTFLLYLSQNKPKAAEGLDTQRFSGKRLGDTFVLTLSDFRRENEGYYFCSALSNSI MYFSHFVPVFLPAKPTTTPAPRPPTPAPTIASQPLSLRPEACRPAAGGAVHTRGLDFACDI YIWAPLAGTCGVLLLSLVITLYCNHRNRRRVCKCPRPVVKSGDKPSLSARYV
CD8αβ	pMI-II (GFP replaced with CD8α)	MRPRLWLLLAAQLTVLHGNSVLQQTPAYIKVQTNKMVMLSCEAKISLSNMRIYWLRQRQAP SSDSHHEFLALWDSAKGTIHGEEVEQEKIAVFRDASRFILNLTSVKPEDSGIYFCMIVGSP ELTFGKGTQLSVVDFLPTTAQPTKKSTLKKRVCRLPRPETQKGPLCSPITLGLLVAGVLVL LVSLGVAIHLCCRRRRARLRFMKQFYK----IRES---- MALPVTALLLPLALLLHAARPSQFRVSPLDRTWNLGETVELKCQVLLSNPTSGCSWLFQPR GAAASPTFLLYLSQNKPKAAEGLDTQRFSGKRLGDTFVLTLSDFRRENEGYYFCSALSNSI MYFSHFVPVFLPAKPTTTPAPRPPTPAPTIASQPLSLRPEACRPAAGGAVHTRGLDFACDI YIWAPLAGTCGVLLLSLVITLYCNHRNRRRVCKCPRPVVKSGDKPSLSARYV

Table AII.1. (cont.).

Protein	Transfection vector	Protein sequence
MAIT TCR (AF-7**(58)**)	pMIG-II	MWGVFLLYVSMKMGGTTGQNIDQPTEMTATEGAIVQINCTYQTSGFNGLFWYQQHAGEAPT FLSYNVLDGLEEKGRFSSFLSRSKGYSYLLLKELQMKDSASYLCAVKDSNYQLIWGAGTKL IIKPDIQNPDPAVYQLRDSKSSDKSVCLFTDFDSQTNVSQSKDSDVYITDKTVLDMRSMDF KSNSAVAWSNKSDFACANAFNNSIIPEDTFFPSPESSCDVKLVEKSFETDTNLNFQNLSVI GFRILLLKVAGFNLLMTLRLWSSGSGATNFSLLKQAGDVEENPGPMSIGLLCCVAFSLLWA SPVNAGVTQTPKFQVLKTGQSMTLQCAQDMNHNSMYWYRQDPGMGLRLIYYSASEGTTDKG EVPNGYNVSRLNKREFSLRLESAAPSQTSVYFCASSVWTGEGSGELFFGEGSRLTVLEDLK NVFPPEVAVFEPSEAEISHTQKATLVCLATGFYPDHVELSWWVNGKEVHSGVSTDPQPLKE QPALNDSRYCLSSRLRVSATFWQNPRNHFRCQVQFYGLSENDEWTQDRAKPVTQIVSAEAW GRADCGFTSESYQQGVLSATILYEILLGKATLYAVLVSALVLMAMVKRKDSRG

Appendix III: Unpaired TCR sequences

Table AIII.1. TCRα sequences derived from TCR-sequencing of GMM-reactive T cells.

Donor	TRAV	TRAJ	CDR3	CDR3 length	Count
A1	TRAV1-2*01	TRAJ9*01	CAVRLTGGFKTIF	13	1
A1	TRAV1-2*01	TRAJ9*01	CAVRALGGFKTIF	13	4
A1	TRAV1-2*01	TRAJ9*01	CAVRATGGFKTIF	13	1
A1	TRAV12-2*01	TRAJ48*01	CAVKNFGNEKLTF	13	1
A1	TRAV1-2*01	TRAJ9*01	CAVRRTGGFKTIF	13	1
A1	TRAV17*01	TRAJ9*01	CATPYTGGFKTIF	13	1
A2	TRAV26-1*01	TRAJ45*01	CIVRGRGGADGLTF	14	1
A2	TRAV1-2*01	TRAJ9*01	CAVRETGGFKTIF	13	1
A2	TRAV1-2*01	TRAJ9*01	CAVRNTGGFKTIF	13	4
A3	TRAV3*01	TRAJ10*01	CAVRDLRHKLTF	12	2
A4	TRAV1-2*01	TRAJ9*01	CAVRGAGGFKTIF	13	1
A4/5	TRAV1-2*01	TRAJ9*01	CAVRSTGGFKTIF	13	5
A5	TRAV8-2*01	TRAJ40*01	CVVSGWAGTYKYIF	14	1
A5	TRAV1-2*01	TRAJ9*01	CAVRKTGGFKTIF	13	1
A6	TRAV1-2*01	TRAJ9*01	CAVRRTGGFKTIF	13	2
A6	TRAV6*01	TRAJ10*01	CALDRVTGGGNKLTF	15	1
A6	TRAV17*01	TRAJ9*01	CATAPTGGFKTIF	13	1

Table AIII.2. TCRβ sequences derived from TCR-sequencing of GMM-reactive T cells.

Donor	TRBV	TRBJ	CDR3	CDR3 length	Count
A1	TRBV4-1*01	TRBJ2-1*01	CASSHVGLAGGHYYNEQFF	19	1
A1	TRBV30*01	TRBJ1-4*01	CAWSYSGLTTNEKLFF	16	1
A1	TRBV6-2*01	TRBJ1-1*01	CASSSRVGGDEAFF	14	1
A1	TRBV30*01	TRBJ2-3*01	CAWSKTGLGADTQYF	15	3
A1	TRBV6-2*01	TRBJ1-1*01	CASSSRVGGDEAFS	14	1
A1	TRBV4-1*01	TRBJ2-1*01	CASSHVGLAGGHYYNEQFF	19	1
A2	TRBV12-4*02	TRBJ1-5*01	CASSFRQTYSNQPQHF	16	1
A3	TRBV4-1*01	TRBJ2-3*01	CASSQPGLARPQDDPDTQYF	20	1
A4	TRBV6-2*01	TRBJ2-1*01	CASTPRLGGDEQFF	14	1
A4	TRBV6-2*01	TRBJ2-3*01	CASSPRLGGDTQYF	14	1
A5	TRBV4-1*01	TRBJ2-1*01	CASSQGGLAGGPRNNEQFF	19	3
A5	TRBV5-4*01	TRBJ1-2*01	CASTRTGGDGYTF	13	1
A5	TRBV28*01	TRBJ2-4*01	CASNKPRGKNIQYF	14	1
A6	TRBV6-2*01	TRBJ1-4*01	CASSFRVGGEKLFF	14	1
A6	TRBV6-2*01	TRBJ2-3*01	CASSRRTGGDTQYF	14	1
A6	TRBV4-1*01	TRBJ2-3*01	CASSQPSFRLAGNTDTQYF	19	1
A6	TRBV30*01	TRBJ2-1*01	CAWRPGGLGGDEQFF	15	2
A6	TRBV4-1*01	TRBJ2-3*01	CASSQPSFRLAGNTDTQYF	19	1

Table AIII.3. TCRα sequences derived from RNA-sequencing of GMM-reactive T cells.

Donor	TRAV	TRAJ	CDR3	CDR3 length	Count
42	TRAV17*01	TRAJ9*01	CATPGTGGFKTIF	13	2
42	TRAV1-2*01	TRAJ9*01	CAVRVTGGFKTIF	13	6
42	TRAV8-1*01	TRAJ49*01	CAVHGAGNQFYF	12	1
42	TRAV1-2*01	TRAJ9*01	CAVRNTGGFKTIF	13	3
42	TRAV1-2*01	TRAJ9*01	CAVYSTGGFKTIF	13	7
42	TRAV38-1*01	TRAJ54*01	CAFMNWRFQGAQKLVF	16	1
42	TRAV17*01	TRAJ10*01	CATLPGGGNKLTF	13	1
42	TRAV8-1*01	TRAJ3*01	CAVSRYSSASKIIF	14	1
42	TRAV1-2*01	TRAJ9*01	CAVRKTGGFKTIF	13	2
42	TRAV8-2*01	TRAJ4*01	CVVSRGGYNKLIF	13	1
44	TRAV35*01	TRAJ17*01	CARRSAGNKLTF	12	2
44	TRAV35*01	TRAJ17*01	CARMGAAGNKLTF	13	9
44	TRAV1-2*01	TRAJ9*01	CAVRLTGGFKTIF	13	1
44	TRAV35*01	TRAJ56*01	CALLGANSKLTF	12	1
44	TRAV2*01	TRAJ30*01	CAVNRDDKIIF	11	1

Table AIII.4. TCRβ sequences derived from RNA-sequencing of GMM-reactive T cells.

Donor	TRBV	TRBJ	CDR3	CDR3 length	Count
42	TRBV6-2*01	TRBJ2-3*01	CASSFRVGGDTQYF	14	9
42	TRBV5-4*01	TRBJ1-6*01	CASRRTPGDSYNSPLHF	17	1
42	TRBV6-2*01	TRBJ1-2*01	CASTRRLSNYGYTF	14	5
42	TRBV4-1*01	TRBJ2-5*01	CASTGLAIETQYF	13	1
42	TRBV14*01	TRBJ1-2*01	CASSPPWLRGWSGYTF	16	1
42	TRBV6-2*01	TRBJ2-5*01	CASSSRLGGETQYF	14	4
42	TRBV7-2*01	TRBJ1-1*01	CASGEQGLRQNTEAFF	16	1
42	TRBV6-2*01	TRBJ2-7*01	CASTLRKGGDEQYF	14	1
42	TRBV20-1*01	TRBJ1-1*01	CSAATWNTEAFF	12	4
42	TRBV6-2*01	TRBJ2-3*01	CASSFRVGGDTQFF	14	1
44	TRBV5-4*01	TRBJ1-3*01	CASSSPGISSSGNTIYF	17	4
44	TRBV6-2*01	TRBJ2-5*01	CASSPRLGGETQYF	14	1

Table AIII.5. TCRα sequences derived from RNA-sequencing of NKT cells.

Donor	TRAV	TRAJ	CDR3	CDR3 length	Count
63	TRAV10*01	TRAJ18*01	CVVSDRGSTLGRLYF	15	23
63	TRAV8-2*01	TRAJ29*01	CVVSGGSGNTPLVF	14	1
63	TRAV12-1*01	TRAJ20*01	CVVNLENDYKLSF	13	1
63	TRAV10*01	TRAJ18*01	CVVSDRGSTLGKLYF	15	1
63	TRAV10*01	TRAJ18*01	CVVIDRGSTLGRLYF	15	1
63	TRAV21*01	TRAJ18*01	CAPDRGSTLGRLYF	14	1
8	TRAV26-1*01	TRAJ45*01	CIVNGYSGGGADGLTF	16	1
8	TRAV2*01	TRAJ5*01	CAVEDRGTGRRALTF	15	1
8	TRAV9-2*01	TRAJ13*01	CALNSGGYQKVTF	13	1
8	TRAV23/DV6*01	TRAJ58*01	CAASKVTSGSRLTF	14	1
8	TRAV3*01	TRAJ6*01	CAVRGSSGGSYIPTF	15	1
8	TRAV10*01	TRAJ18*01	CVVGDRGSTLGRLYF	15	1
8	TRAV9-2*01	TRAJ13*01	CALISGGYQKVTF	13	1
8	TRAV12-3*01	TRAJ34*01	CAMSAPRNTDKLIF	14	1

Table AIII.5. (cont.).

Donor	TRAV	TRAJ	CDR3	CDR3 length	Count
8	TRAV2*01	TRAJ6*01	CAVAPGGGSYIPTF	14	1
8	TRAV9-2*01	TRAJ54*01	CALKGQGAQKLVF	13	1
8	TRAV2*01	TRAJ20*01	CAPRKRDDYKLSF	13	1
8	TRAV17*01	TRAJ20*01	CATAAGDYKLSF	12	1
8	TRAV2*01	TRAJ27*01	CAVGTNAGKSTF	12	1
8	TRAV12-2*01	TRAJ10*01	CAVNIEGGGNKLTF	14	1
8	TRAV29/DV5*01	TRAJ56*01	CAASATPGANSKLTF	15	1

Table AIII.6. TCRβ sequences derived from RNA-sequencing of NKT cells.

Donor	TRBV	TRBJ	CDR3	CDR3 length	Count
63	TRBV25-1*01	TRBJ1-1*01	CASSEYNTGDTEAFF	15	1
63	TRBV25-1*01	TRBJ2-1*01	CASSDQRPSGGPGEQFF	17	1
63	TRBV25-1*01	TRBJ2-5*01	CASSESRGTQYF	12	1
63	TRBV25-1*01	TRBJ2-2*01	CASSEELRTGELFF	14	1
63	TRBV25-1*01	TRBJ1-1*01	CASSVTGQVTEAFF	14	1
63	TRBV25-1*01	TRBJ2-7*01	CASSLTGGGRPNYEQYF	17	1
63	TRBV25-1*01	TRBJ1-3*01	CASSESGGSGNTIYF	15	1
63	TRBV25-1*01	TRBJ2-5*01	CASSEKRSTRGTGPKTQYF	19	1
63	TRBV25-1*01	TRBJ1-5*01	CASSGPDNQPQHF	13	1
63	TRBV25-1*01	TRBJ1-5*01	CASSDGNWDRGPAEGAQHF	19	1
63	TRBV20-1*01	TRBJ2-5*01	CSARVRLAGTQETQYF	16	1
8	TRBV20-1*01	TRBJ2-7*01	CSARDRGRGHEQYF	14	1
8	TRBV25-1*01	TRBJ2-7*01	CASTPRGGRADEQYF	15	1
8	TRBV25-1*01	TRBJ2-2*01	CASSPSGQGLITGELFF	17	1
8	TRBV11-2*01	TRBJ2-1*01	CASSFSGSLHNEQFF	15	1
8	TRBV12-3*01	TRBJ1-1*01	CASSPPKNTEAFF	13	1
8	TRBV7-3*01	TRBJ1-1*01	CASSLVAGVTEAFF	14	1
8	TRBV5-1*01	TRBJ2-7*01	CASSPGSGTVYEQYF	15	1
8	TRBV25-1*01	TRBJ2-1*01	CASSESNEQFF	11	1
8	TRBV5-1*01	TRBJ2-2*01	CASSLPGGAGTGELFF	16	1
8	TRBV12-3*01	TRBJ2-5*01	CASSRRAGEEETQYF	15	1
63	TRBV25-1*01	TRBJ2-2*01	CASDTGGLGTGELFF	15	1
63	TRBV25-1*01	TRBJ2-5*01	CASSEHGTSGGETQYF	16	1
63	TRBV25-1*01	TRBJ1-3*01	CASSEDGGPVYF	12	1
63	TRBV25-1*01	TRBJ2-1*01	CASSPRLGTSGVSEQFF	17	1
63	TRBV25-1*01	TRBJ1-5*01	CASSESGQGEEARGNQPQHF	20	1
63	TRBV25-1*01	TRBJ2-5*01	CASSVSTETQYF	12	1
63	TRBV25-1*01	TRBJ1-5*01	CASSGDGDHSNQPQHF	16	1
63	TRBV25-1*01	TRBJ1-5*01	CASSEWGTTDSNQPQHF	17	1
63	TRBV25-1*01	TRBJ2-4*01	CASSESSDSPKNIQYF	16	1
63	TRBV25-1*01	TRBJ2-1*01	CASSEPGSVRGTYQGGNEQFF	21	1
63	TRBV25-1*01	TRBJ2-6*01	CASSGSGANVLTF	13	1
63	TRBV25-1*01	TRBJ1-5*01	CASSETGGQPQHF	13	1
63	TRBV25-1*01	TRBJ1-3*01	CASSDPTGVGGNTIYF	16	1
63	TRBV25-1*01	TRBJ1-5*01	CASSGGNQPQHF	12	1
63	TRBV25-1*01	TRBJ1-5*01	CASSEGKLQHF	11	1
63	TRBV25-1*01	TRBJ2-1*01	CASSDRGERGISSYNEQFF	19	1
63	TRBV25-1*01	TRBJ2-1*01	CASSDLTGTGPNEQFF	16	1
63	TRBV25-1*01	TRBJ2-7*01	CASSDPGPPRGSEQYF	16	1
63	TRBV25-1*01	TRBJ2-7*01	CASSPPGQAYEQYF	14	1
63	TRBV25-1*01	TRBJ1-4*01	CASSEPISQENEKLFF	16	1

Table AIII.6. (cont.).

Donor	TRBV	TRBJ	CDR3	CDR3 length	Frequency
63	TRBV25-1*01	TRBJ2-3*01	CASSEPLPRRTDTQYF	16	1
63	TRBV25-1*01	TRBJ1-2*01	CASSEYGRGRSVPNYGYTF	19	1
63	TRBV25-1*01	TRBJ1-5*01	CASSGDSNQPQHF	13	1
63	TRBV25-1*01	TRBJ2-3*01	CASSSRDRVPGGPGTDTQYF	20	1
8	TRBV19*01	TRBJ2-7*01	CASSPRDRGGEQYF	14	1
8	TRBV25-1*01	TRBJ1-1*01	CASSGGTGGTEAFF	14	1
8	TRBV18*01	TRBJ2-7*01	CASSPVPGGQGLYEQYF	17	1
8	TRBV25-1*01	TRBJ2-7*01	CASSESEREIYEQYF	15	1
8	TRBV25-1*01	TRBJ2-1*01	CASSARNLNEQFF	13	1
8	TRBV25-1*01	TRBJ2-2*01	CASSDSNRVGTGELFF	16	1
8	TRBV7-7*01	TRBJ2-5*01	CASSLRGRSSFGETQYF	17	1
8	TRBV19*01	TRBJ1-1*01	CASSFIGGTTEAFF	14	1
8	TRBV6-5*01	TRBJ1-2*01	CASSSQGGTYGYTF	14	1
8	TRBV28*01	TRBJ1-5*01	CASSLQGVNQPQHF	14	1
8	TRBV28*01	TRBJ1-5*01	CASRKVGQGARQPQHF	16	1
8	TRBV3-1*01	TRBJ2-1*01	CASSQDLYTLPYNEQFF	17	1
8	TRBV25-1*01	TRBJ2-7*01	CASSESRTSGSKGEQYF	17	1
8	TRBV5-6*01	TRBJ1-2*01	CASSLGWDTGSGYTF	15	1
8	TRBV10-3*01	TRBJ2-7*01	CAISESKAGGISYEQYF	17	1
8	TRBV25-1*01	TRBJ2-7*01	CASSELGTDYTSYEQYF	17	1
8	TRBV20-1*01	TRBJ2-5*01	CSASEREETQYF	12	1
8	TRBV25-1*01	TRBJ1-2*01	CASSDPGQSYDYTF	14	1
8	TRBV25-1*01	TRBJ2-7*01	CASSTEGTGGHEQYF	15	1
8	TRBV25-1*01	TRBJ1-1*01	CASSSLETSTPAFF	14	1
8	TRBV25-1*01	TRBJ1-2*01	CASSELARGYTF	12	1
8	TRBV7-9*01	TRBJ2-5*01	CASSPRGIQETQYF	14	1
8	TRBV29-1*01	TRBJ2-1*01	CSVTPGGRSYNEQFF	15	1

Table AIII.7. TCRα sequences derived from RNA-sequencing of CD4$^+$ cells.

Donor	TRAV	TRAJ	CDR3	CDR3 length	Frequency
63	TRAV38-2/DV8*01	TRAJ57*01	CAYRFGGSEKLVF	13	1
63	TRAV4*01	TRAJ27*01	CLVGSEVDTNAGKSTF	16	1
63	TRAV8-3*01	TRAJ45*01	CAVGARYSGGGADGLTF	17	1
63	TRAV13-1*01	TRAJ41*01	CAASKGRSGYALNF	14	1
63	TRAV17*01	TRAJ37*01	CATAGLPSNTGKLIF	15	1
63	TRAV8-3*01	TRAJ39*01	CAVGAANAGNMLTF	14	1
63	TRAV2*01	TRAJ29*01	CAVERNTPLVF	11	1
63	TRAV8-4*01	TRAJ43*01	CAVSVGNNDMRF	12	1
63	TRAV3*01	TRAJ42*01	CAVRAQGNLIF	11	1
63	TRAV26-2*01	TRAJ17*01	CILAMIKAAGNKLTF	15	1
63	TRAV8-6*01	TRAJ36*01	CAVSRQGGANNLFF	14	1
63	TRAV8-6*01	TRAJ3*01	CAVSSYSSASKIIF	14	1
63	TRAV12-3*01	TRAJ4*01	CAMTFSGGYNKLIF	14	1
63	TRAV2*01	TRAJ29*01	CAVDSNSGNTPLVF	14	1
63	TRAV21*01	TRAJ37*01	CAVKGSSNTGKLIF	14	1

Table AIII.8. TCRβ sequences derived from RNA-sequencing of CD4⁺ cells.

Donor	TRBV	TRBJ	CDR3	CDR3 length	Frequency
63	TRBV4-1*01	TRBJ2-1*01	CASSQGTSEWYNEQFF	16	1
63	TRBV10-3*01	TRBJ2-3*01	CAIRSQGTDTQYF	13	1
63	TRBV30*01	TRBJ2-7*01	CAWRRDSTPYEQYF	14	1
63	TRBV20-1*01	TRBJ1-1*01	CSARGQRDTEAFF	13	1
63	TRBV6-1*01	TRBJ1-1*01	CASSLDRGMNTEAFF	15	1
63	TRBV24/OR9-2*01	TRBJ1-2*01	CATNDGIGGYTF	12	1
63	TRBV30*01	TRBJ1-1*01	CASNSDTGPEAFF	13	1
63	TRBV7-2*01	TRBJ1-2*01	CASSLGTADGYTF	13	1
63	TRBV20-1*01	TRBJ1-2*01	CSAPGQGVKYGYTF	14	1
63	TRBV2*01	TRBJ1-3*01	CASRGRDRNTIYF	13	1
63	TRBV21-1*01	TRBJ1-3*01	CASSVRTGNTIYF	13	1
63	TRBV9*01	TRBJ1-6*01	CASSTSTGASNSPLHF	16	1
63	TRBV5-6*01	TRBJ2-1*01	CASSSGGYEQFF	12	1
63	TRBV20-1*01	TRBJ1-6*01	CSASPQGDNSPLHF	14	1
63	TRBV4-1*01	TRBJ2-3*01	CASSQGWTGGTDTQYF	16	1
63	TRBV12-4*01	TRBJ2-1*01	CASSPTGTGGRGEQFF	16	1
63	TRBV5-6*01	TRBJ2-7*01	CASSGDTFYSYEQYF	15	1
63	TRBV28*01	TRBJ2-2*01	CASRGELMLFF	11	1
63	TRBV5-1*01	TRBJ1-1*01	CASSLGTTWDTEAFF	15	1
63	TRBV29-1*01	TRBJ2-7*01	CSASKERRSYEQYF	14	1
63	TRBV4-1*01	TRBJ2-5*01	CASSQDPGLAGGQETQYF	18	1
63	TRBV20-1*01	TRBJ2-7*01	CSPSGLSYEQYF	12	1